

UC San Diego

UC San Diego Electronic Theses and Dissertations

Title

Amino acid biosignatures : implications for the detection of extinct or extant microbial communities on Mars

Permalink

<https://escholarship.org/uc/item/9c3794nr>

Author

Aubrey, Andrew D.

Publication Date

2008

Peer reviewed|Thesis/dissertation

UNIVERSITY OF CALIFORNIA, SAN DIEGO

Amino Acid Biosignatures –

Implications for the Detection of Extinct or Extant Microbial Communities on Mars

A dissertation submitted in partial satisfaction of the
requirements for the degree Doctor of Philosophy

in

Oceanography

by

Andrew D. Aubrey

Committee in charge:

Professor Jeffrey L. Bada, Chair
Professor Douglass Bartlett
Professor Miriam Kastner
Professor Devendra Lal
Professor Mark Thiemens

2008

Copyright

Andrew D. Aubrey, 2008

All rights reserved.

The dissertation of Andrew D. Aubrey is approved, and it is acceptable in quality and form for publication on microfilm:

Chair

University of California, San Diego

2008

To my wife, Megan, and my entire family who have supported and motivated me throughout my studies.

TABLE OF CONTENTS

SIGNATURE PAGE	iii
DEDICATION	iv
TABLE OF CONTENTS	v
LIST OF SYMBOLS AND ABBREVIATIONS	viii
LIST OF FIGURES	ix
LIST OF TABLES & APPENDICES	xii
ACKNOWLEDGEMENTS	xiii
VITA	xiv
ABSTRACT OF DISSERTATION	xvi
CHAPTER I. Introduction	
1.1 Life in our Universe - The Study of Astrobiology.....	1
1.2 The Search for Extraterrestrial Life	3
1.3 Amino Acids as Biosignatures for Life Detection	4
1.4 Stability & Diagenesis of Amino Acids on Mars	9
1.5 Scope of Dissertation	14
1.6 Conclusion	16
References.....	17
CHAPTER II. Amino Acids as Organic Biomarkers	
Abstract.....	20
2.1 Introduction.....	20
2.2 Experimental Section	23
2.3 Results and Discussion	25
2.4 Conclusion	30
References.....	31
CHAPTER III. Sulfate Minerals and Organic Compound Preservation on Mars	
Abstract.....	33
3.1 Introduction.....	33
3.2 Methods.....	34
3.3 Results.....	36
3.4 Discussion	40
3.5 Conclusion	45
References.....	47
CHAPTER IV. Southern Australian Saline Lake Sulfates	
Abstract.....	50
4.1 Introduction.....	50
4.2 Materials & Methods	52
4.3 Results & Discussion	55
4.4 Conclusion	68

References.....	70
Supplementary Information 4.A1	72
Supplementary Information 4.A2	73
Supplementary Information 4.B.....	74
CHAPTER V. San Diego County Ironstones as Mars Analogs	
Abstract	75
5.1 Introduction.....	75
5.2 Materials & Methods	80
5.3 Results & Discussion	83
5.4 Conclusions.....	107
References.....	109
Supplementary Information 5.A	114
CHAPTER VI. South African Gold Mines - Low Biodensity Microbial Communities	
Abstract	115
6.1 Introduction.....	115
6.2 Materials & Methods	118
6.3 Results & Discussion	120
6.4 Conclusions.....	132
References.....	134
CHAPTER VII. Chemical Biosignatures from Antarctic Dry Valley Microbial Life	
Abstract	138
7.1 Introduction.....	138
7.2 Experimental Section	140
7.3 Results & Discussion	145
7.4 Conclusion	154
References.....	156
Supplementary Information 7.A	159
Supplementary Information 7.B.....	160
CHAPTER VIII. Atacama Desert Surface Soils as Mars Analogs	
Abstract	161
8.1 Introduction.....	161
8.2 Materials & Methods	162
8.3 Results.....	165
8.4 Biochemical Indicators of Diagenetic Alteration	178
8.5 Conclusion	186
References.....	187

CHAPTER IX. Instrumentation to Detect Life on Mars - The <i>Urey</i> Instrument	
Abstract	190
9.1 Introduction - Instrumentation	191
9.2 Analytical procedures	192
9.3 SCWE Instrument	193
9.4 MOD Instrument	197
9.5 SCWE and MOD coupling	201
9.6 Discussion and evaluation of results	206
9.7 Conclusion	207
References	209
CHAPTER X. The Future Search for Evidence of Extinct or Extant Life on Mars	
Abstract	211
10.1 Martian Exploration	211
10.2 Thesis Conclusions	216
10.3 Final Dissertation Conclusions	220
References	221
APPENDICES	
Appendix A - Australian Sulfate Heating Experiments	223
Appendix B - San Diego Ironstone Heating Experiments	228

LIST OF SYMBOLS AND ABBREVIATIONS

°C	degrees centigrade
ABA	Amino- <i>n</i> -butyric acid
AIB	α -aminoisobutyric acid
APXS	Alpha-Particle-X-ray Spectrometer (MER)
CO	carbon monoxide
CO ₂	carbon dioxide
CRISM	Compact Reconnaissance Imaging Spectrometer for Mars (MRO)
CTX	Context Camera (MRO)
$\delta^{13}\text{C}$	delta carbon-13
$\delta^{15}\text{N}$	delta nitrogen-15
dd	doubly-distilled
<i>E. coli</i>	<i>Escherichia coli</i>
EA	ethylamine
ESA	European Space Agency
GCMS	gas chromatography mass spectrometry
γ -aba	gamma-amino-n-butyric acid
H ₂ O	water
HCl	hydrochloric acid
IBA	isobutylamine
IPA	isopropylamine
JPL	NASA/CalTech Jet Propulsion Laboratory
λ_{em}	emission wavelength
λ_{ex}	excitation wavelength
MA	methylamine
MER	Mars Exploration Rover
MI	Microscopic Imager (MER)
μ -CE	micro-capillary electrophoresis
NaOAc	Sodium Acetate
NASA	National Aeronautics and Space Administration
NH ₃	ammonia
NH ₄ OH	ammonium hydroxide
PAH	polycyclic aromatic hydrocarbons
ppb	parts-per-billion
ppm	parts-per-million
RAT	Rock Abrasion Tool (MER)
RP-HPLC	Reverse-Phase High performance Liquid Chromatography
SEM	Scanning Electron Microscopy
TOC	Total Organic Carbon
TON	Total Organic Nitrogen
XRD	X-Ray Diffraction

LIST OF FIGURES

Figure 1.1: Major Molecular Classes in <i>E. coli</i>	4
Figure 1.2: The 20 canonical proteinaceous amino acids at neutral pH	5
Figure 1.3: Mirror-image configurations of amino acids called L- or D-enantiomers ...	6
Figure 1.4: Racemization of amino acids as a function of time and temperature.....	7
Figure 1.5: Common extraterrestrial amino acids	9
Figure 1.6: Trends of amino acid diagenesis over time	10
Figure 1.7: Properties of Earth and Mars.....	11
Figure 1.8: Amine degradation compounds.....	12
Figure 1.9: Mars' geological and mineralogical histories	13
Figure 2.1: Degradation mechanism of glutamine and asparagines	21
Figure 2.2: Reaction of <i>o</i> -phthaldialdehyde (OPA) and N-acetyl-L-cysteine (NAC) ...	22
Figure 2.3: Reaction of OPA/NAC with a primary amine	22
Figure 2.4: HPLC buffer-methanol gradients A and B.....	25
Figure 2.5: Chromatograms of amino acid separations (0-40 mins)	26
Figure 2.6: Plot of <i>E. coli</i> amino acid compositions	29
Figure 3.1 North American sample origin locations.....	34
Figure 3.2 Combined RP-HPLC chromatograms of amino acids and amines.....	39
Figure 3.3 Plots of Z-ratios versus age	41
Figure 3.4 Glycine and alanine half-lives extrapolated to Mars' temperatures	44
Figure 4.1 Proposed formation model for acid saline lake bottom grown minerals	52
Figure 4.2 Photographs of gypsum samples and sampling map	53
Figure 4.3 Total amino acid abundances and D/L-enantiomeric ratios	58
Figure 4.4 Amino acid decarboxylation products	59
Figure 4.5 Amines plotted against parent amino acid concentrations	62
Figure 4.6 Amines plotted against total amino acids	63
Figure 4.7 Plot of gypsum sample Z-ratios.....	65
Figure 4.8 Plot of enzymatic degradation products β -ala and γ -aba.....	67
Supplementary Information 4.A1 RP-HPLC amino acid chromatograms, gypsum....	72
Supplementary Information 4.A2 RP-HPLC amino acid chromatograms, jarosite....	73
Supplementary Information 4.B RP-HPLC volatile amine chromatograms.....	74
Figure 5.1 Comparison between Mars “blueberries” and San Diego ironstones.....	78
Figure 5.2 San Diego county ironstone deposits.....	79
Figure 5.3 Flowchart of amino acid sample processing.....	80
Figure 5.4 60x magnified Sunset Cliffs ironstone SEM 18-image mosaic.....	85
Figure 5.5 SEM EDS composition data compared to APXS data	86
Figure 5.6 BSE and SE magnified images of Convoy ironstones	88
Figure 5.7 SEM BS images of evidence of life in ironstones	89
Figure 5.8 Averages of measured TOC and TON in ironstone samples and isotopes....	91
Figure 5.9 TOC plotted against TON for all ironstones	92

Figure 5.10 Summary of ironstone fraction analyses	94
Figure 5.11 Summary of measured median and high enantiomeric ratios.....	96
Figure 5.12 Average amino acid DL-ratios	98
Figure 5.13 Approximate Ages of San Diego county ironstones	101
Figure 5.14 Ironstone formation model	103
Supplementary Information 5.A Mossbauer spectrometry data	114
Figure 6.1 Location of South African sampling sites	116
Figure 6.2 Amino acid chromatograms of the low-level filtrate samples.....	122
Figure 6.3 Amino acid abundances measured from deep fracture sample filtrates	123
Figure 6.4 Amino acid D/L ratios measured from deep fracture sample filtrates	124
Figure 6.5 Schematic for steady-state amino acid racemization box model.....	126
Figure 6.6 Amino acid derived cell counts and turnover times	130
Figure 6.7 Model sensitivity of fraction of viable cells compared to total cells.....	131
Figure 7.1 Sampling locations of Antarctic dry valley rock samples	141
Figure 7.2 Images of rock samples with sampling depths designated.....	143
Figure 7.3 Representative chromatograms (0-35 mins) of a subsurface sample	144
Figure 7.4 Plot of total amino acids as a function of sample depth	148
Figure 7.5 Amino acid enantiomeric ratios representative of various rock samples	150
Figure 7.6 Amino acids measured in sample COM-120.....	152
Figure 7.7 Degradation of glutamic and aspartic acids.....	153
Figure 7.8 Plots of diagenetic indicators.....	154
Supplementary Information 7.A	159
Supplementary Information 7.B	160
Figure 8.1 Location of Atacama Desert sampling locations	163
Figure 8.2 HPLC chromatograms of N-S transect total amino acid concentrations.....	166
Figure 8.3 TOC/TON and stable isotope labels for the Atacama Desert.....	167
Figure 8.4 RP-HPLC chromatograms of 10uL concentrated extract.....	171
Figure 8.5 RP-HPLC chromatograms of 30uL concentrated extract.....	173
Figure 8.6 RP-HPLC chromatograms of 30uL concentrated extract.....	175
Figure 8.7 RP-HPLC chromatograms of 30uL concentrated extract.....	177
Figure 8.8 Depth profiles of diagenetic indicators for sample sites 54 and 57	179
Figure 8.9 Potential diagenetic pathways of amino acid interconversion.....	181
Figure 8.10 RP-HPLC chromatograms of amino acid degradation products	182
Figure 8.11 Plot of amino acid decarboxylation age dating for sites 54 and 57	185
Figure 9.1 SCWE Batch-type reactor	192
Figure 9.2 Conceptual schematic of energy associated SCW treatment.....	193
Figure 9.3 Properties of water at 200-300 bar	194
Figure 9.4 Graphical representation of the optimization of the South Bay SCWE	196
Figure 9.5 Analytical protocol and sublimation apparatus schematic	197
Figure 9.6 HPLC results and tabulated sublimation recoveries.....	198
Figure 9.7 Formation of degradation products.....	199

Figure 9.8 Methods of cell enumeration via sublimation	200
Figure 9.9 Comparison of treated TOC vs. bulk SCWE-extracted TOC.....	202
Figure 9.10 HPLC chromatograms from sublimed SCWE Atacama Desert extracts	205
Figure 10.1 Near-future planned missions to Mars.....	213
Figure 10.2 Cross-section of Mars	214
Figure 10.3 Predicted amino acid racemization over time at Mars Temperatures	217
Figure 10.4 Predicted amino acid degradation over time at Mars Temperatures	218
Figure A.1 Amino acid Arrhenius degradation plots within gypsum/jarosite	225
Figure A.2 Amino acid Arrhenius racemization plots within gypsum/jarosite	226
Figure A.3 Comparison of amino acid degradation and racemization rates	227
Figure B.1 Pseudo 1 st -order Arrhenius plots for amino acid degradation.....	230
Figure B.2 Pseudo 1 st -order Arrhenius plots for amino acid racemization	232

LIST OF TABLES

Table 2.1: Amino acid abundances from hydrolyzed/desalted <i>E. coli</i>	27
Table 3.1: TOC, TON, and stable isotope analyses	37
Table 3.2: Amino acid concentrations of various sulfate minerals	38
Table 3.3: Estimated rates of decarboxylation in gypsum	43
Table 4.1: Sample Descriptions for Australian Saline Lake minerals	53
Table 4.2: TOC, TON, and stable isotope data	55
Table 4.3: Blank and recovery corrected amino acid concentrations (ppm)	56
Table 4.4: Calculations of Z-ratios from various decarboxylation schemes.....	61
Table 5.1 Total hydrolyzable amino acid concentrations (ppb) for ironstones.....	95
Table 5.2 Racemization rate constants determined by the calibration method	99
Table 5.3 Sunset Cliffs amino acid racemization rate determination	105
Table 6.1 Filter samples sent to SIO for analyses	119
Table 6.2 Amino acid measurements on South African mine filtrates	121
Table 7.1 Descriptions and locations of samples investigated in this study	142
Table 7.2 Major amino acid concentrations in Antarctic Dry Valley samples	146
Table 8.1 Descriptions of Atacama soil samples collected from YUN1122	164
Table 8.2 Hydrolyzed and desalted blank-corrected amino acid concentrations	169
Table 8.3 Concentrations of amino acid decarboxylation products	184
Table 9.1 Amino acid concentrations (ppb) from SCWE extracts.....	203
Table 9.2 Amino acid D/L-ratios from SCWE extracts	203
Table 10.1 List of Urey target compounds and mass percentages of <i>E. coli</i> cell	215
Table A.1 E_a and $\ln(k)$ values for amino acid degradation within Australian samples...	224

LIST OF APPENDICES

Appendix A Racemization and Degradation Heating Experiment Data (Chapter 4)	223
Appendix B Racemization and Degradation Heating Experiment Data (Chapter 5)	228

ACKNOWLEDGEMENTS

I would like to thank my advisor, Jeffrey L. Bada, for his support from the moment that I arrived at Scripps. His dedication to geochemistry and its recent application to future exploration of Mars has motivated and inspired me through the course of my thesis. I give great thanks to my thesis committee, especially Devendra Lal and Miriam Kastner, for providing their support throughout my research at Scripps.

Jim Cleaves, Evan Solomon, and John Chalmers were stalwart colleagues during the course of my Ph.D. and I learned such a great deal from all of them during our overlap at Scripps. Danny Glavin, Gerhard Kminek, and Oliver Botta offered me so much leadership and helped educate me with a planetary science background during our time together working in the Bada laboratory. Danny was especially stellar in helping me learn about publishing and good laboratory practice through our work together in Danny's expertise, low-level meteorite amino acid analyses. Lois Lane also provided much guidance and support for the course of my time at Scripps.

The Unified Laboratory Facility (ULF) at Scripps headed by Dr. Bruce Deck was invaluable in running our geological samples for TOC, TON, $\delta^{13}\text{C}$, and $\delta^{15}\text{N}$. The whole analytical facility provided expertise and skilled training that allowed for the throughput of large batches of low level samples with fast turn around time. They also provided the XRD, ICP-OES, and SEM instruments which we used on many occasions.

I am grateful to our collaborators on the *Urey* instrument from whom I have learned a great deal. These include Frank Grunthaner and Peter Willis from JPL, Richard Mathies from Berkeley, and Pascale Ehrenfreund from University of Leiden.

I am extremely grateful to my family and close friends who kept me confident through my whole Ph.D. tenure and convinced me to stay the course. Most of all, I am grateful to my loving wife, Megan Beth. Her love and confidence in me mean more than anything in the world.

VITA

1979	Born, Falmouth, Massachusetts
2001	B.S. Chemical Engineering, Tufts University, Medford, MA
2001-2003	NASA Specialized Center of Research and Training (NSCORT) Graduate Student Research Fellow
2004-2005	Teaching Assistant, Department of Earth Sciences University of California, San Diego
2006	M.S. Oceanography, University of California, San Diego
2008	Ph.D., Scripps Institution of Oceanography – UCSD

PUBLICATIONS

Aubrey, A.D., Cleaves H.J., and Bada, J.L. Organic Synthesis in Submarine Hydrothermal Systems I: Amino Acids. Submitted to *Earth Planet. Sci. Lett.*

Cleaves, H.J., **Aubrey, A.D.**, and Bada, J.L. Organic Synthesis in Submarine Hydrothermal Systems II: Peptides. Submitted to *Geochim. Cosmochim. Acta.*

Aubrey, A.D., Chalmers, J.H., Bada, J.L., Grunthaner, F.J., Amashukeli, X., Willis, P., Skelley, A.M., Mathies, R.A., Quinn, R.C., Zent, A.P., Ehrenfreund, P., Amundson, R., Glavin, D.P., Botta, O., Barron, L., Blaney, D.L., Clark, B.C., Coleman, M., Hofmann, B.E., Josset, J.-L., Rettberg, P., Ride, S., Robert, F., Sephton, M.A., and Yen, A. The Urey Instrument: An Advanced in situ Organic and Oxidant Detector for Mars Exploration. *Astrobiology*, in press.

Glavin, D.P., Cleaves, H.J., Schubert, M., **Aubrey, A.**, and Bada, J.L. (2004) New Method for Estimating Bacterial Cell Abundances in Natural Samples by Use of Sublimation. *Appl. Environ. Microbiol.* **70**, 5923-5928.

Skelley, A.M., Scherer, J.R., **Aubrey, A.D.**, Grover, W.H., Ivester, R.H.C., Ehrenfreund, P., Grunthaner, F.J., Bada, J.L., and Mathies, R.A. (2005) Development and evaluation of a microdevice for amino acid biomarker detection and analysis on Mars. *Proc. Natl. Acad. Sci. U.S.A.* **102**, 1041-1046.

Glavin, D.P., Cleaves, H.J., Buch, A., Schubert, M., **Aubrey, A.**, Bada, J.L., and Mahaffy, P.R. (2006) Sublimation extraction coupled with gas chromatography-mass spectrometry: A new technique for future in situ analyses of purines and pyrimidines on Mars. *Planet. Space Sci.* **54**, 1584-1591.

Glavin, D.P., Dworkin, J.P., **Aubrey, A.**, Botta, O., Doty, J.H., Martins, Z., and Bada, J.L. (2006) Amino acid analyses of Antarctic CM2 meteorites using liquid chromatography-time of flight-mass spectrometry. *Meteorit. Planet. Sci.* **41**, 889-902.

Aubrey, A.D., Cleaves, H.J., Chalmers, J.H., Skelley, A.M., Mathies, R.A., Grunthaner, F.J., Ehrenfreund, P., and Bada, J.L. (2006) Sulfate minerals and organic compounds on Mars. *Geology* **34**, 357-360.

Skelley, A.M., **Aubrey, A.D.**, Willis, P.A., Amashukeli, X., Ehrenfreund, P., Bada, J.L., Grunthaner, F.J., and Mathies, R.A. (2007) Organic Amine Biomarker Detection in the Yungay Region of the Atacama Desert with the Urey Instrument. *J. Geophys. Res.* **112**, G04S11.

FIELDS OF STUDY

Major Field: Oceanography

Studies in Geochemistry and Marine Chemistry

Professors Jeffrey Bada, Miriam Kastner, Devendra Lal, and Mark Thiemens

Studies in Marine Chemistry

Professors Andrew Dickson, Joris Gieskes, Lihini Aluwihare, and Kathy Barbeau

Studies in Geology and Marine Geology

Professors David Hilton, Peter Lonsdale, James Hawkins, and Steven Cande

Studies in Biological Oceanography

Professors Peter Franks and Douglas Bartlett

Studies in Physical Oceanography

Professors Myrl Hendershott and Paul Robbins

ABSTRACT OF THE DISSERTATION

Amino Acid Biosignatures –
Implications for the Detection of Extinct or Extant Microbial Communities on Mars

by

Andrew D. Aubrey

Doctor of Philosophy in Oceanography

University of California, San Diego, 2008

Professor Jeffrey L. Bada, Chair

Investigations of Mars have recently found strong geochemical evidence for the presence of standing bodies of water early in the planet's history. It still remains to be discovered whether organic compounds exist on Mars, a question which concurrent international scientific efforts are focused on for future *in situ* planetary missions. Amino acids are at the core of terrestrial biochemistry, ubiquitous in terrestrial life, and are easily detectable via highly advanced instrumentation with parts-per-trillion sensitivity making them an ideal biomolecular class to target during planetary exploration. Furthermore, amino acid chirality allows for the discrimination between compounds produced abiotically and those formed by biological processes, and these measurements can provide unequivocal evidence of extinct or extant life.

The studies herein investigate organic components within Mars analog environmental samples and specifically characterize the concentrations and distributions of amino acids and their diagenetic products. Kinetic modeling of degradation reactions within ancient Mars analog minerals allows for the lifetimes of these bioorganic compounds to be estimated. The degree of amino acid preservation from an extinct biota

will be much greater within Mars' near-surface environments due to the characteristic cold temperatures and dry climates. Extrapolations of terrestrial amino acid stability models show the potential for preservation within sulfate minerals over billions of years on Mars.

High degrees of microscale variability, with respect to amino acid concentrations and distributions, are observed within the surface and immediate subsurface of Atacama Desert Soils and Antarctic rock samples which result from exposure to harsh surface conditions. All of these studies support the necessity of subsurface sampling procedures during future *in situ* robotic missions to Mars in order to detect and characterize well-preserved organic matter. Sulfate minerals appear to be prime targets for the search for evidence of extinct or extant life on Mars because of their high degrees of organic inclusion and observed persistence of amino acids within these minerals. The integration of advanced flight instrumentation such as the *Urey* instrument in future *in situ* mission payloads will offer the best chance of success in detecting biomolecular evidence of extinct or extant life on Mars.

CHAPTER I. Introduction

“If it's true that our species is alone in the universe, then I'd have to say
that the universe aimed rather low and settled for very little.”

-George Carlin

1.1 LIFE IN OUR UNIVERSE – THE STUDY OF ASTROBIOLOGY

The possible presence of life elsewhere in our universe is a subject of investigation still riddled with speculation. Although prebiotic chemistry has developed drastically and evolved over the last 60 years into the current field of astrobiology, there is still not a thorough understanding of the series of chemical reactions that first created living entities or even the most probable location for them to have occurred. Early theories about the origin of life can be traced back to Oparin (1924) and Haldane (1929) and have been since referred to as the Oparin-Haldane hypothesis. They proposed that the origin of life necessarily involved a rich broth of biomolecules that proceeded to form life as we know it after a series of chemical reactions. Many experiments have promoted this early theory, however, debate still exists about the most plausible time and location for life's origin on Earth.

Stanley Miller's empirical synthesis of amino acids from water, hydrogen, methane, and ammonia (1953) helped begin a new field of origin of life chemistry. His experiments demonstrated that the most plausible model for the synthesis of biomolecules was under reducing atmospheric conditions on the early earth. Miller's experiments validated the early 20th century theories of Oparin (1924) and Haldane (1928). Similar experiments have recently shown that these syntheses are also successful in neutral atmospheres, although not with as high of yields (Cleaves et al., 2008). Submarine hydrothermal systems (SHSs) vents have been proposed as the location for the origin of life (Corliss et al., 1981) and this theory persists despite little empirical evidence. These debates regarding these central questions regarding life's origin are not surprising. There are vast unknowns about the early Earth during the prebiotic epoch approximately 3.5 billion years ago and a slim geological record from this epoch makes it inherently difficult to study. Among the major uncertainties are the composition of the atmosphere and chemistry of the early oceans. The only principles that the scientific community seems to agree upon is that water and organic compounds were essential for the origin of life

(Bada, 2004). The synthesis of organic compounds has thus become a central theme for origin of life chemistry, and the search for life on other planets has focused on detecting these necessary ingredients for life's formation (Bada, 2004). 'Follow the water' is a moniker used by NASA for extraterrestrial exploration which implies how important the presence of water is deemed in the search for extraterrestrial life.

The field of Astrobiology has emerged within the last 10 years and represents a concert of disciplines working together towards specific scientific goals. Astrobiology specifically addresses the question of whether or not extraterrestrial life exists, and assuming it does, what its origin, occurrence, distribution, and evolution might be. These can be categorized into 4 major fields of study:

- *Prebiotic chemistry* – defining the conditions and pathways suitable for chemical reactions involving the creation or alteration of simple organic molecules; origin of life chemistry.
- *Extraterrestrial Exploration* – Searching for habitats that may be hospitable to life elsewhere in the universe, either by remote sensing techniques or *in situ* studies including robotic exploration (and eventually manned exploration) of other planets, such as Mars.
- *Habitability* – Defining the conditions under which terrestrial life can exist or withstand and applying this to possible extraterrestrial life by expanding the known constraints associated with habitability.
- *Analog Studies* – Studying similar environmental or mineralogical analogs compared to what has been defined for extraterrestrial locations; applying the understanding of these analog environments including constraints on microbial life (including extremophilic life) to what may exist on other planets.

These broad groupings represent the central disciplines of astrobiology, an inherently multidisciplinary science which combines the expertise of many fields. Astrobiology provides the forum to address questions about the origin of life and assess the probability of life having arisen on other planets within our solar system and universe. The more we learn regarding the surface and subsurface chemistry of other planets seems to indicate that life may be much more widespread than previously thought. This increased knowledge of our solar system coupled with the expanding limits of habitability in extreme environments continues to show the adaptability and tolerance of terrestrial life.

It is now widely believed that microbiological life in the deep ocean and deep biosphere are far greater a reservoir of carbon than all terrestrial life combined (Whitman et al., 1998). Included in this large reservoir are all of the sea dwellers and microbial life that inhabit the seafloor, making their living in the oceanic crust or at hydrothermal vent systems. As life is recognized to be more and more ubiquitous on our planet, this leads one to think how improbable it would be if Earth were the only planet that life had originated on.

1.2 THE SEARCH FOR EXTRATERRESTRIAL LIFE

The Mars exploration program has been successful as of late with a number of important achievements including the robotic exploration of Mars' surface by twin landed Mars Exploration Rovers (MERs), Spirit and Opportunity. These two Mars rovers have achieved great success in confirming an aqueous history of the planet through detection of minerals deposited by standing water bodies on Mars. Although the timescales of these deposits are not fully known, the detection of evaporitic mineral assemblages confirms that Mars was once a wet planet, similar to the Earth in many respects, most likely very early in the planet's history. Deposits of ice still remain in the polar regions of Mars and within the deep subsurface where water is stable, however, the most accessible regions of the planet appear to be very inhospitable not only to life, but to the preservation of any biosignatures from the past.

In the next few years, robotic missions to Mars will include instruments specifically designed to detect organic compounds and evidence of life on our neighboring planet (Bada, 2001). These planetary life detection missions have the potential to not only find out if there was ever life on Mars, but it might also aid in answering some of the fundamental unknowns associated with the origin of terrestrial life. For instance, if evidence of extinct or extant microbiological life on Mars were detected, and it was determined to have a similar biochemistry to terrestrial life, this could be interpreted in many ways. It could be evidence of similar independent chemical processes that led to independent origins on neighboring planets, or this could imply that there could have been exchange of organic compounds or other material between planets that would have helped the spread a common origin of life. Regardless, these are the questions that should be anticipated if we are successful in the next 10 years in detecting life on Mars.

If the Mars community focuses on the detection of biomolecules that offer unequivocal evidence of life, then we may be successful detecting traces of life that once existed on Mars. Any success in this field through in situ studies via robotic exploration, future sample return mission, or far distant manned missions to Mars must target environments that offer high degrees of preservation of organics within the harsh and extreme Martian surface.

1.3 AMINO ACIDS AS BIOSIGNATURES FOR LIFE DETECTION

Biosignatures are defined as any type of physical or chemical record that show evidence of the presence of extinct or extant life. These can be remnants of a microbial community that existed in the planet's early history or the detection of active microbial life. The best biosignatures to target are biomolecules that are ubiquitous components of microbial life, constitute a significant portion of their cellular mass, offer good preservation over geological time, and can be detected at trace levels with current technologies.

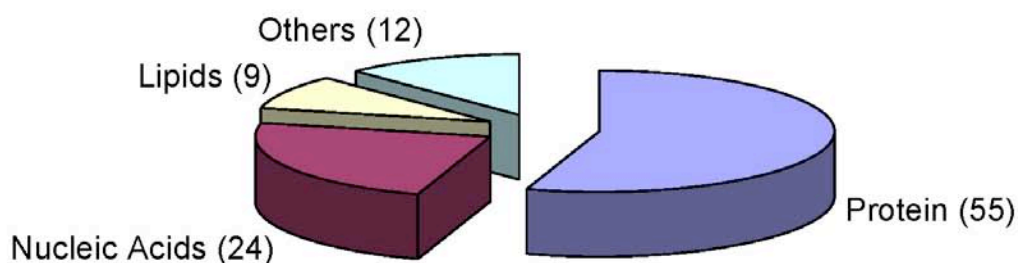


Figure 1.1 Major molecular classes in *E. coli* (Neidhardt et al., 1996).

The two largest classes of biomolecules are Nucleic acids and proteins (Figure 1.1). Proteins, composed of individual amino acid residues linked by peptide bonds, comprise ~55% of the mass of bacterial cells and have a mean length of ~315 residues (Zhang, 2000). Only 20 amino acids are utilized in terrestrial proteins (Figure 1.2) except for the rare cases of selenocysteine (Diamond, 2004) and pyrrolysine (Atkins & Gesteland, 2002), however, due to the rare occurrence of these amino acids, they are not considered important. Total amino acids within environmental samples can be used to estimate biodensities in microbial communities associated with extinct or extant life. The total hydrolyzed amino acids (THAA) give an idea of the mass of total protein and can be extrapolated to estimated equivalent cell counts (cells/g) by

comparing them to the protein dry weight composition of prokaryotes. Chapter II below discusses this method of bacterial cell enumeration.

There is no reason to expect that extraterrestrial life utilizes completely different biochemistry than here on Earth. The best chance at detecting evidence of life on Mars is to focus on the major terrestrial biomolecular classes such as amino acids which have been defined as prime targets in the search for biosignatures on Mars. The drawback of amino acids (and likewise other simple organic molecules) is that they might be degraded on Mars if inadequately protected from harsh surface conditions such as ionizing radiation from space (Kminek & Bada, 2006). However, certain secondary minerals that sequester organics could allow for some degree of protection from these extreme conditions.

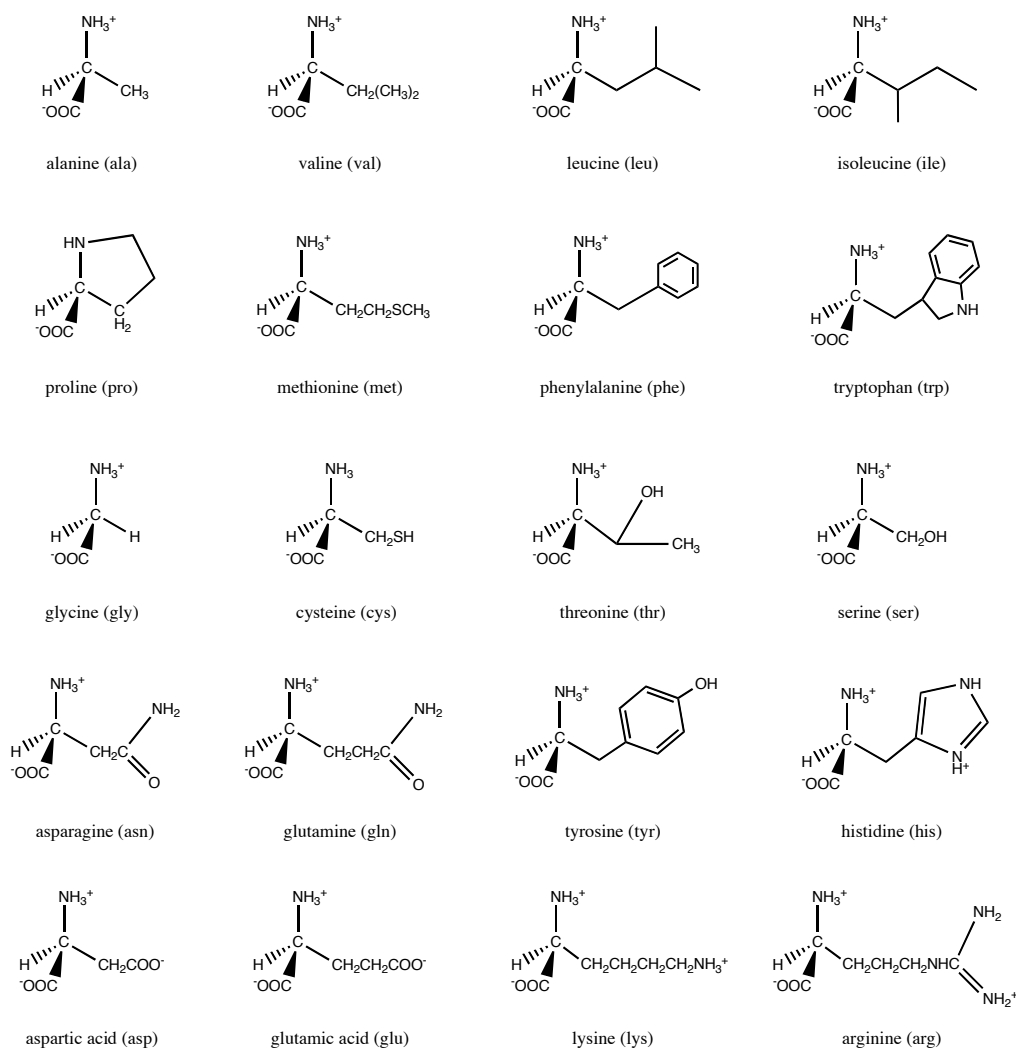


Figure 1.2 The 20 canonical proteinaceous amino acids at neutral pH.

One fundamental property of amino acids other than glycine is their chirality. The amino acid α -carbon provides for two mirror image configurations based on the relative orientation of the side group (Figure 1.3). Terrestrial biological amino acids consist of only one configuration (the L-enantiomer), however, there is no reason why proteins in extraterrestrial life would need to be based on L-amino acids as on Earth. Proteins as catalytically active as their natural biological L-amino acid counterparts have been synthesized of entirely D-amino acids (Milton et al., 1992), thus it is assumed that life elsewhere could be based on either L- or D-amino acids.

Amino acid homochirality associated with extant terrestrial life changes over time after the bacterial community becomes deceased due to racemization. When living, the protein turnover time is sufficient to preserve the homochiral protein composition, however after death, the amino acids interconvert from the biological L-enantiomer to the abiological D-enantiomer. This interconversion is a natural process that becomes significant over geological timescales and continues until they are present in equal abundances, that is a D/L-ratio equal to 1.

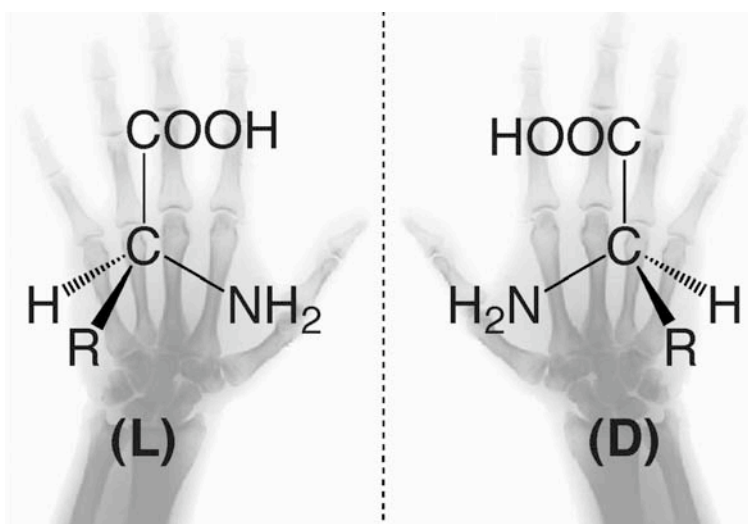


Figure 1.3 Mirror-image configurations of amino acids called L- or D-enantiomers.

The D/L-enantiomer ratio along with known rates of racemization has been useful in determining the geological age of terrestrial samples up to hundreds of millions of years old (Figure 1.4). Although racemization compromises the microbial signature of terrestrial proteins over geological timescales, the determination of amino acid chirality still offers a powerful

biosignature for the presence of microbial life. The detection of amino acids alone is not unequivocal evidence of life, rather a homochiral signature is necessary to confirm a biological amino acid source. Although sufficiently old biological samples may show racemic signatures similar to those derived from abiotic syntheses, well preserved amino acids from extinct bacterial communities at extremely cold temperatures would still show good chirality preservation for hundreds of millions of years. In future life detection experiments, the chirality of amino acids should easily discriminate between biological amino acids and those which may have formed abiotically or derived from meteorite influx.

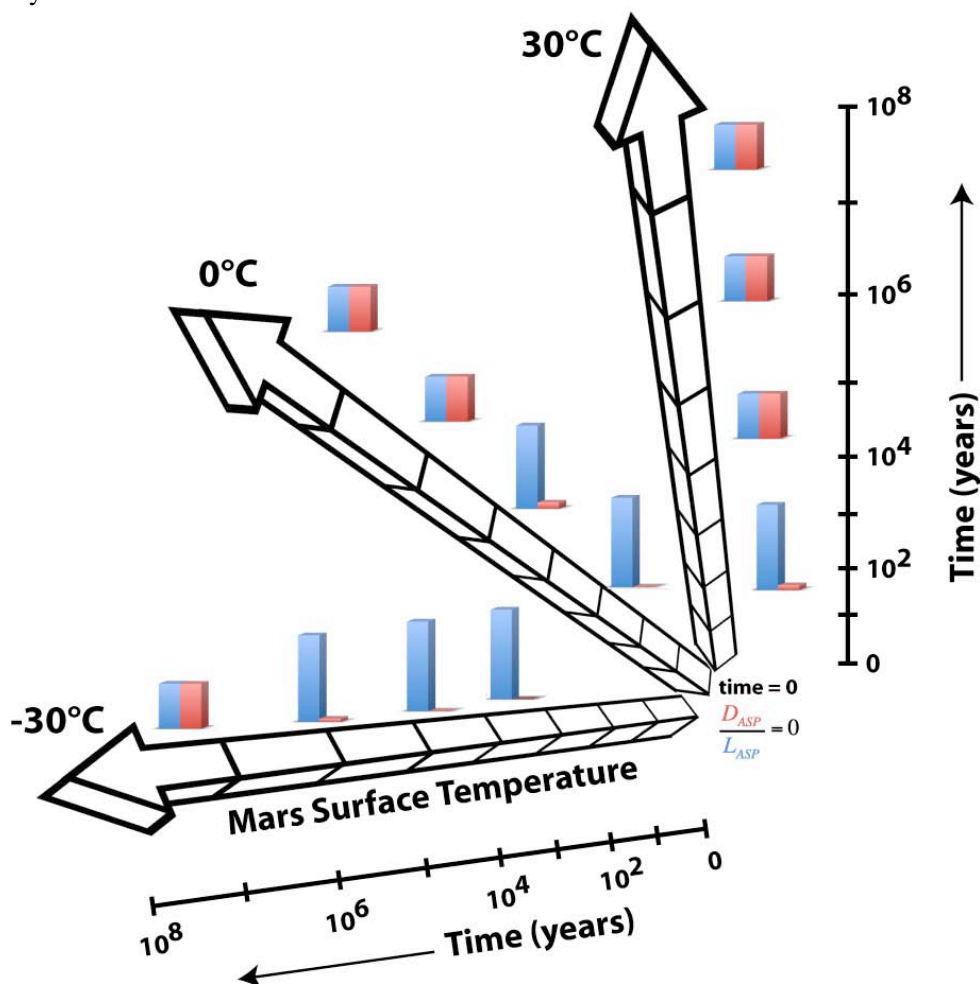


Figure 1.4 Graphical representation of aspartic acid racemization as a function of time at three different temperatures (30°, 0°, -30°C). Arrows show time progressing up to 100 Ma and the relative amounts of the biological L-enantiomer (blue) and D-enantiomer (red) are shown to illustrate the effect of temperature on chirality retention over geological timescales. Rates were extrapolated to the three temperatures using aspartic acid *in vivo* racemization rates (Masters et al., 1978) assuming an activation energy of 23.5 kcal/mole (Bada, 1972).

Known abiotic pathways exist for the formation of amino acids such as spark discharge experiments and laboratory hydrothermal syntheses, however they are all known to produce equal amounts of D- and L- amino acids (racemic mixtures) in low concentrations. This marked difference between homochiral biological and racemic abiotic composition permits the discrimination of the source of the detected amino acids by resolving their enantiomeric abundances (Kvenvolden, 1973). Also important is that abiotic amino acid syntheses tend to form a relatively small suite of amino acids compared to those utilized in bacterial proteins. The suite of protein amino acids utilized in the bacterium *E. coli* is evaluated in Chapter II and compared to previous empirical studies. If detected amino acids are too old or degraded for any chiral signature to be deduced, the distribution can be used to definitively decide the source of the amino acids as microbially or abiotically derived.

A variety of amino acids have been detected in meteorites as well, but these are interpreted as having formed during parent-body processes. The fact that amino acids within meteorites are all racemic (Kvenvolden et al., 1971), and that they show a suite of amino acids similar to those formed in abiotic syntheses, makes them easy to distinguish from biologically sourced amino acids again based on chirality or distribution. Any preferential dominance of L-amino acids detected in meteorites is assumed to be due to terrestrial contamination (Kvenvolden et al., 1970).

Certain amino acids within the large suite of amino acids detected in meteorites are not components of terrestrial proteins, rather they are known to be indigenous because they are unique to meteorites and reflect formation during parent-body processes (Ehrenfreund et al., 2001). The two most abundant extra-terrestrial amino acids are isovaline (ival) and amino-isobutyric acid (AIB), however there are a variety of others that are recognized as a indicative of an extraterrestrial signature (Figure 1.5). The presence of these amino acids in geological samples (Zhao & Bada, 1989) is suggested to reflect deposition by during a period of high meteoritic influx.

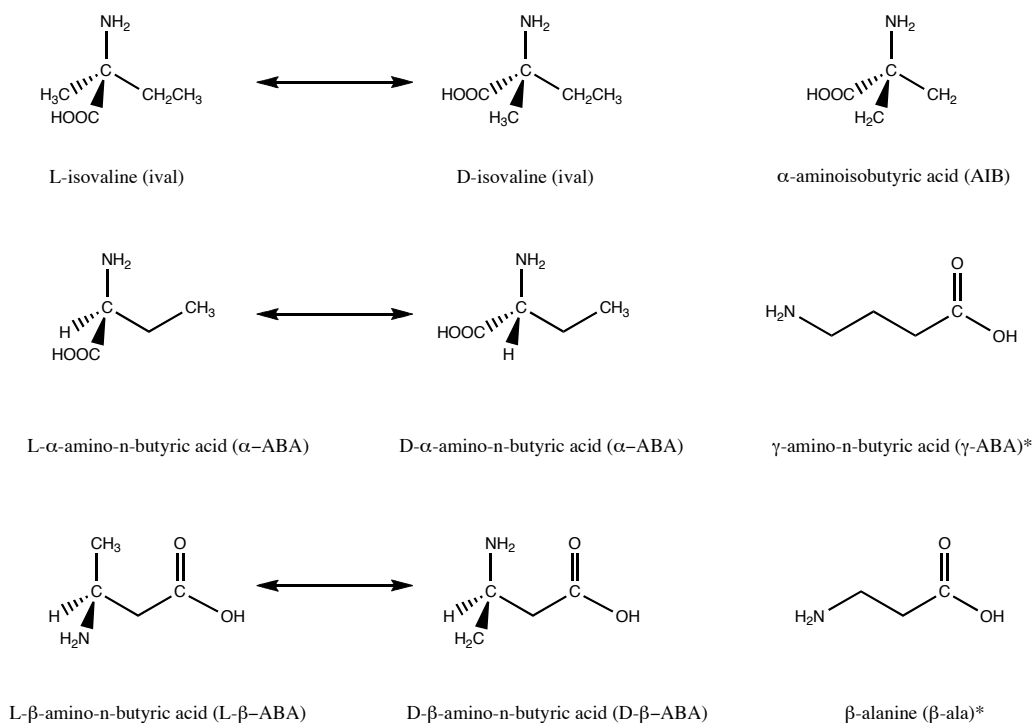


Figure 1.5 Common extraterrestrial amino acids (* = formed by protein amino acid degradation).

1.4 STABILITY & DIAGENESIS OF AMINO ACIDS ON MARS

The most relevant amino acid biomarkers depend on their relative abundances in bacterial proteins and the stability of the individual residues. There are two major amino acid diagenetic pathways, degradation and racemization (Figure 1.6). The rates associated with degradation are slower than racemization by at least a factor of 100 in most cases. The most stable protein amino acids will persist through geological time and allow for the quantification of long extinct bacterial communities. Amino acids degrade primarily by decarboxylation (gly, leu, ile, val, ala) or deamination (asp, asn, cys, gln) but other processes like dehydration (glu, gln) and aldol cleavage (ser, thr) can also be significant (Li & Brill, 2003).

The relative aqueous decarboxylation rates of 5 protein amino acids, from fastest to slowest, are Gly > Leu ~ Ile ~ Val > Ala (Li & Brill, 2003). The amino acid decarboxylation rates show roughly the inverse trend as the racemization rates Asp > Ala ~ glu ~ gly > ile ~ leu > Phe > Leu > Ala > Val (Li & Brill, 2003; Kawamura and Yukioka, 2001). These data were determined for aqueous-phase amino acids and these rates are highly dependent on the mineralogy of natural samples.

The most commonly occurring amino acids in ancient and degraded microbial communities are glycine and alanine (Kvenvolden, 1973), a finding corroborated by the analyses of natural samples of anoxic sediments (Rosenfeld, 1979). Glycine (~10.1% of *E. coli* protein) and alanine (~16.7% *E. coli* protein) are both present in bacterial communities in very high abundances, however, only alanine shows degradation rates among the slowest of the amino acids (Li & Brill, 2003). This implies that glycine may be better preserved in geological settings or that diagenetic pathways lead to its secondary formation from other compounds. Regardless, both alanine and glycine remain among the most important amino acids to assay for in geological samples as well as asp, glu, and ser. Valine, present in lower abundances than these other amino acids, shows slow racemization kinetics (Li & Brill, 2003) and degradation kinetics (Cohen & Chyba, 2000) and should show good preservation in environmental samples despite composing only ~5% of total bacterial protein.

The plots in Figure 1.6 show the evolution of aspartic acid concentration and D/L-ratio versus time. Aqueous rates of aspartic acid degradation ($7.2 \times 10^{-5} \text{ yr}^{-1}$) and racemization ($1.54 \times 10^{-4} \text{ yr}^{-1}$) were used in these models and therefore represent the fastest rates of these reactions. Racemization is a much faster process which results in a racemization half-life ($D/L = 0.33$) of ~2,200 years whereas the half-life of aspartic acid degradation is ~10,000 years. Environmental samples always show slower degradation and racemization in colder and dryer conditions.

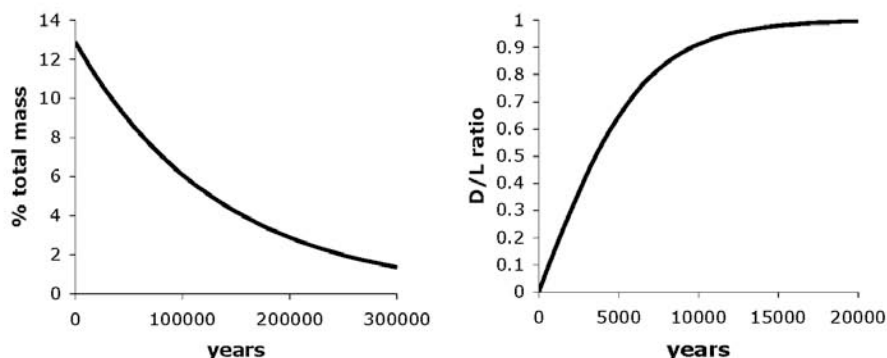


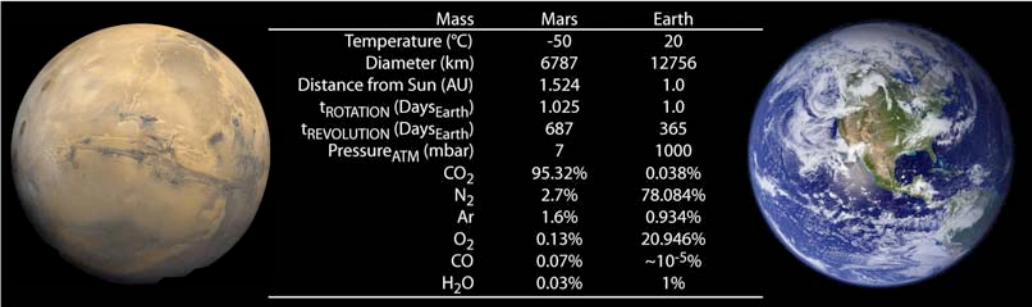
Figure 1.6 Trends of amino acid diagenesis over time. The half-life of amino acid degradation is ~10,000 years and the half-life for racemization ($D/L = 0.33$) is ~2,200 years.

The aspartic acid racemization rates in dry environmental conditions have been reported to be as slow as $1.20 \times 10^{-6} \text{ yr}^{-1}$ (Collins et al., 1999) and $6.93 \times 10^{-7} \text{ yr}^{-1}$ (Bada & Mann, 1980), equivalent to half-lives of ~600,000 and 1,000,000 years, and therefore must be evaluated

carefully for each geological sample for the purposes of amino acid racemization age dating (Bada & Schroeder, 1975; Williams & Smith, 1977). Likewise, any degradation reactions are equally dependent on the mineralogy of the environmental sample and may be accelerated by the presence of metal ion catalysts (Ikawa & Snell, 1954). Racemization age dating has been suggested to be applicable to amino acids from hundreds of thousands to millions of years old (Bada & Mann, 1980) at low temperatures, but this range can be extended to older samples under colder conditions. Likewise, amino acids from hundreds of millions of years old up to billions of years could be well preserved under the appropriate environmental conditions (Aubrey et al., 2006).

Target biomolecules in the search for evidence of life on Mars must be stable enough to persist for geological timescales so that evidence of life on Mars does not go undetected. The fate of amino acids includes racemization, degradation, and bacterial uptake. In the absence of biological processing (recycling), racemization is faster than degradation by at least 100x. Racemization involves a planar carbocation intermediate formed by the loss of a proton on the α -carbon and subsequent attack on the top or bottom by another proton (Bada, 1982). The reactions for the destruction of amino acids include decarboxylation to amine compounds (Figure 1.8) or deamination. These rates are highly matrix and temperature dependent and therefore must be evaluated for the specific environmental conditions.

Although the prevailing cold and dry conditions on Mars (Figure 1.7) tend to drastically increase the lifetimes of organic degradation and amino acid racemization (Bada & McDonald, 1995), there are other effects that must be considered. For instance, the surrounding mineral matrix can catalyze amino acid diagenetic reactions, especially degradation in the presence of metallic ions (Ikawa and Snell, 1954). Therefore, the specific preservation of organic material will be strongly a function of chemical environment.



Mass	Mars	Earth
Temperature (°C)	-50	20
Diameter (km)	6787	12756
Distance from Sun (AU)	1.524	1.0
t_{ROTATION} (Days _{Earth})	1.025	1.0
$t_{\text{REVOLUTION}}$ (Days _{Earth})	687	365
Pressure _{ATM} (mbar)	7	1000
CO ₂	95.32%	0.038%
N ₂	2.7%	78.084%
Ar	1.6%	0.934%
O ₂	0.13%	20.946%
CO	0.07%	~10 ⁻⁵ %
H ₂ O	0.03%	1%

Figure 1.7 Properties of Earth and Mars (Owen et al., 1977)

If intact amino acids are detected and show an abundance of one enantiomer over the other, this would unequivocally show that the source of these amino acids was biological. If these biomarkers from extinct life on Mars were to have been degraded over geological timescales, there are certain classes of compounds that we would expect to be diagenetic endproducts or intermediates. Compounds such as humic acids and kerogen are products of the diagenesis of organic matter over time, however there may be generation of other diagenetic products due to the slow degradation of amino acids over time that might indicate what might be favored on Mars in terms of diagenetic products. For instance, decarboxylation is known to be a the primary degradation reaction amino acids such as glycine, alanine, and valine and form their corresponding amine degradation products (Figure 1.8).

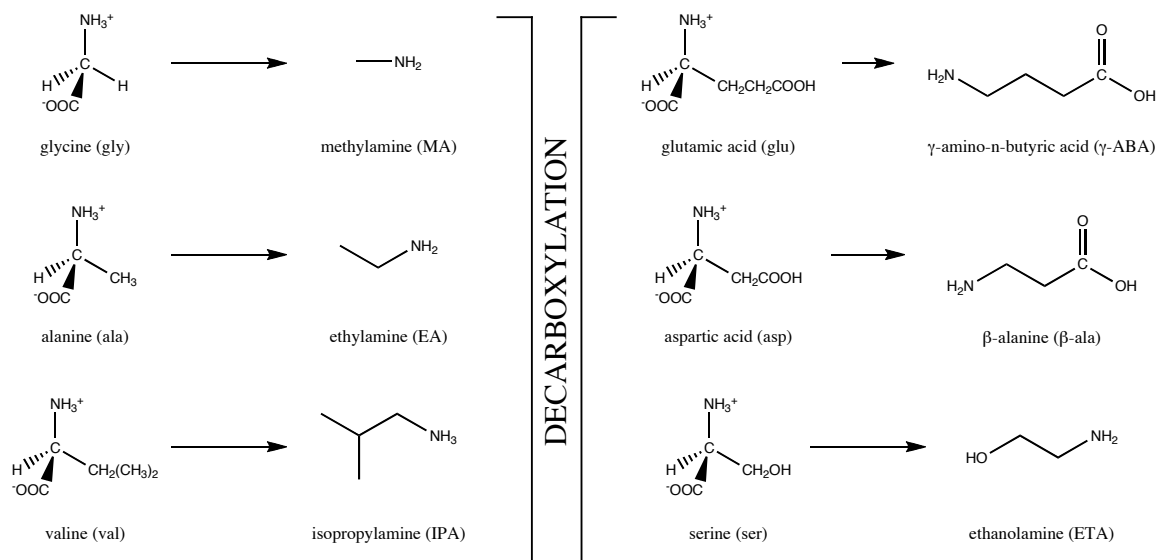


Figure 1.8 Amine degradation compounds from amino acid decarboxylation. Other common degradation reactions not shown are the deamination, dehydration, and reverse aldol cleavage.

The study of organic inclusion in terrestrial Martian analogs allows for the characterization of similar types of environments on Earth as detected on Mars so that we can understand some of the processes that might be important on Mars. The study of organics in Mars analog minerals can offer an idea of the sequestration potential and stability of these deposits on Earth. Indeed if Mars really experienced warm and wet climate early in its history (Figure 1.9), it may have been more similar than we realize to Earth and may have a lot in common with many of the proposed Mars analog locations. The determination of the stability

within terrestrial Mars analog minerals can help to approximate biochemical stability that might be expected on Mars. It turns out that low levels of amino acid degradation products that indicate diagenetic processes can often be used to determine the stabilities or diagenetic state of the included amino acids.

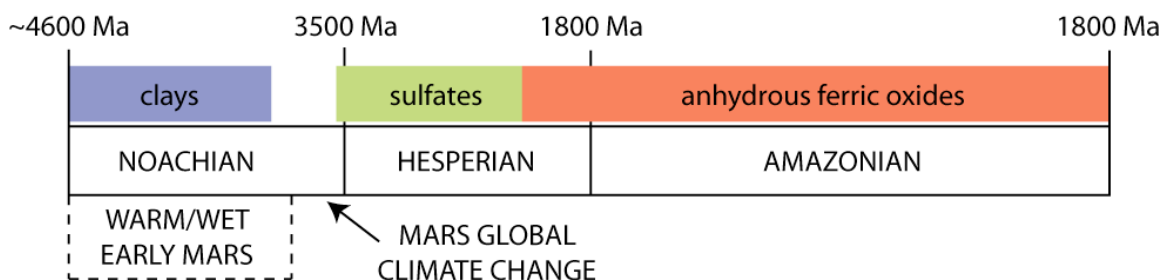


Figure 1.9 Mars' geological and mineralogical histories (modified from Bibring et al., 2006). The geological timescale boundaries (Noachian/Hesperian/Amazonian) are defined by analyses of impact crater densities. The widespread global climate change precedes the Hesperian era and may have been caused by widespread catastrophic volcanism.

Figure 1.9 shows the general geological history of Mars dominated by an early wet era in which clays were formed by water alteration. There was a catastrophic climate change around ~3.5 billion years ago. Water on Mars has always been of interest for physical and chemical reasons. Water is a medium for interesting chemistry to occur, it provides a location for the origin of life, and geologists can use water abundance to explain many of the erosive features on Mars. Therefore, preservation becomes the key issue when talking about finding evidence of life on Mars. The evidence of an extinct Martian biota might be from a biological community billions of years old and must show good preservation over the history of the samples.

The idea of using chirality as a biosignature was first proposed by Halpern (1968) to search for evidence of life on Mars. This idea has resurfaced in the current strategies for life detection recognizing for over 30 years the strength of amino acid chirality as a biosignature and discrimination versus abiotic amino acid signatures (Kvenvolden, 1973). On Mars, racemization kinetics are expected to be extremely slow because of the cold, dry conditions, and any chiral signature of extinct life should be preserved for billions of years (Bada and McDonald, 1995).

The harsh surface conditions on Mars may limit the survival of some organics within the host regolith (Benner et al., 2000). Because amino acid diagenesis is so intimately linked with matrix effects, the study of amino acid preservation and diagenesis in terrestrial Mars analogs is

necessary to make predictions on the best locations to search for biosignatures on Mars. Extrapolation of these diagenetic reaction rates to Mars' surface temperatures can allow for estimates of amino acid stability and rates of diagenetic reactions on Mars.

1.5 SCOPE OF DISSERTATION

This dissertation covers my investigations of organic inclusion and sequestration within various Mars analog minerals. Throughout these studies, amino acids are investigated for their applicability as biomarkers for the detection of extinct or extant microbial communities on Mars. A variety of environments that have been suggested as analogous to Mars for mineralogical or climatic conditions are profiled and in some cases, rate data is gleaned from the coupling of amino acid degradation reactions and extrapolated to predicted rates on Mars. The stabilities of amino acids in analog minerals essentially sequesters them and offers some degree of protection from harsh surface conditions, allowing for enhanced preservation in some cases. Specifically, these studies investigate amino acid diagenetic reactions including racemization and degradation to try and predict the degree of survival of these biosignatures over geological timescales upon the surface of Mars.

Chapter 2 characterizes the amino acid composition in bacteria and verifies our methods of analysis used in these studies. The amino acid distributions and concentrations are so markedly different from any type of abiotic formation process that discrimination between these processes should be possible even over very long timescales.

Chapter 3 introduces a new chemical chronometer based on the detection of amino acid degradation products within ancient geological samples. Methylamine and ethylamine, the degradation products of glycine and alanine, are detected in increasingly high abundances with age in ancient sulfate samples up to ~40Ma. The comparison of these concentrations to their parent amino acids allow for the calculation of glycine and alanine decarboxylation rates and are assumed to be indicative of these rates in sulfate matrices. Because sulfate minerals have been detected in high abundance on Mars, these rates are extrapolated to Mars' average surface temperatures to offer an estimate of the rates that might be expected on Mars. Chapter 4 analyzes modern sulfate samples from Southern Australia for amino acids and extrapolates these concentrations to equivalent bacterial concentrations (Chapter 2). The low abundances of

methylamine and ethylamine in these modern samples show consistency with previous findings (Chapter 3).

Chapter 5 focuses on a new analog to the Martian hematite blueberries that have been detected on Mars in the Meridiani Planum region. These ironstones are ubiquitous in San Diego county, and by analyzing samples from various deposits, they are dated using amino acid racemization based on the measured D/L-ratios and a sample calibration method. Similar concretions on Mars would show good preservation in such environments despite the fact that they're iron rich. The ironstone formation seems to be mediated by enhanced precipitation as well as the possibility of bacterially induced mineralization (BIM) within these deposits.

Chapter 6 investigate an extreme environment deep within a South African subterranean gold mine. These filtrates show extremely low biodensities and is of interest because it might represent the extremely low levels of biomass and extremely slow turnover times that push the limits of analytical sensitivity. A simple steady-state model corroborates the long turnover times that have been reported for these samples.

Two well known Mars analog sites comprise the next two chapters, rock samples from the Antarctic dry valley Deserts (Chapter 7) and surface soils from the Atacama Desert, Chile (Chapter 8), which have been suggested to be the best terrestrial Mars soil analog (Banin, 2005). The fact that life can persist in these extreme climates is impressive enough, however the extremely cold samples from Antarctica show amazing preservation while the opposite is observed in the Atacama Desert surface and near-surface samples. The inferred cell counts based on total amino acid abundances within cryptoendolithic microbial life agree well with previous biodensity enumerations in similar environments. The Atacama Desert shows extremely degraded organic material at the surface and shows drastic variations in amino acid distributions and diagenetic state as a function of depth and surface microenvironment habitability.

One of the premier instruments for advanced in situ Mars life detection experiments is the *Urey* - Mars Organic and Oxidant detector. Chapter 9 focuses on research and development of the instrument over the past 3 years, specifically the optimization of the extraction system for Mars exploration. Both laboratory and field experiment data is discussed in detail and exhibits efficient extraction of target biomolecules, specifically amino acids and total organic carbon. The use of sublimation as a second-stage extraction method for extract purification and concentration is evaluated for recoveries using various mineral matrices.

1.6 CONCLUSION

The astrobiological studies have broad implications for the search for life on Mars over the next decade. Two missions will be launched within the next 6 years: NASA's Mars Science Laboratory (2009) and the ESA's ExoMars (2013). The studies herein validate the importance of targeting amino acids in life detection studies, emphasize their importance as an indicator of biodensity, and demonstrate the potential for sequestration within Mars mineral deposits. Not to be dismissed is the fact that the detection limits of the *Urey* Mars Organic Detector are many orders of magnitude greater than necessary for the detection of amino acid biomarkers in some of the most uninhabitable places in the world such as the Atacama Desert. Sulfate minerals are highly abundant on Mars and our studies suggest that they can offer enhanced preservation on the Martian surface based on the estimated rates observed for in situ diagenetic reactions.

REFERENCES

- Aubrey, A.D., Cleaves, H.J., Chalmers, J.H., Skelley, A.M., Mathies, R.A., Grunthaner, F.J., Ehrenfreund, P., and Bada, J.L. (2006) Sulfate minerals and organic compounds on Mars. *Geology* 34(5), 357-360.
- Atkins, J.F., and Gesteland, R. (2002) The 22nd Amino Acid. *Science* 296, 1409-1411.
- Bada, J.L. (2004) How life began on Earth: a status report. *Earth Planet. Sci. Lett.* 226, 1-15.
- Bada, J.L. (2001) State-of-the-art instruments for detecting extraterrestrial life. *Proc. Natl. Acad. Sci. U.S.A.* 98(3), 797-800.
- Bada, J.L., and McDonald, G.D. (1995) Amino Acid Racemization on Mars: Implications for the Preservation of Biomolecules from an Extinct Martian Biota. *Icarus* 114, 139-143.
- Bada, J.L., and Mann, E.H. (1980) Amino acid diagenesis in deep sea drilling project cores: Kinetics and mechanisms of some reactions and their applications in geochronology and in paleotemperature and heat flow determinations. *Earth-Science Reviews* 16, 21-55.
- Bada, J.L., and Schroeder, R.A. (1975) Amino Acid Racemization Reactions and their Geochemical Implications. *Naturwissenschaften* 62, 71-79.
- Bada, J.L. (1982) Racemization of Amino Acids in Nature. *Interdisciplinary Science Reviews* 7, 30-46.
- Bada, J.L. (1972) Kinetics of Racemization of Amino Acids as a Function of pH. *J. Am. Chem. Soc.* 94(4), 1371-1373.
- Banin, A. (2005) The Enigma of the Martian Soil. *Science* 309, 888-890.
- Benner, S.A., Devine, K.G., Matveeva, L.N., and Powell, D.H. (2000) The Missing organic molecules on Mars. *Proc. Natl. Acad. Sci. U.S.A.* 97(6), 2425-2430.
- Bibring, J.P., Langevin, Y., Mustard, J.F., Poulet, F., Arvidson, R., Gendrin, A., Gondet, B., Mangold, N., Pinet, P., Forget, F., and the OMEGA team (2006) Global Mineralogical and Aqueous Mars History Derived from OMEGA/Mars Express Data. *Science* 312, 400-404.
- Cleaves, H.J., Chalmers, J.H., Lazcano, A., Miller, S.L., and Bada, J.L. (2008) A Reassessment of Prebiotic Organic Synthesis in Neutral Planetary Atmospheres. *Orig. Life Evol. Biosph.* 38(2), 105-115.
- Cohen, B.A., and Chyba, C.F. (2000) Racemization of Meteoric Amino Acids. *Icarus* 145, 272-281.
- Collins, M.J., Waite, E.R., and van Duin, A.C.T. (1999) Prediction protein decomposition: the case of aspartic acid racemization kinetics. *Phil. Trans. R. Soc. Lond. B* 354, 51-64.

Corliss, J.B., Baross, J.A., and Hoffman, S.E. (1981) An hypothesis concerning the relationship between submarine hot springs and the origin of life on Earth. *Oceanologica Acta No. Sp.*, 59.

Diamond A.M. (2004) On the Road to Selenocysteine. *Proc. Natl. Acad. Sci. U.S.A.* 101, 13395-13396.

Ehrenfreund, P., Glavin, D.P., Botta, O., Cooper, G., and Bada, J.L. (2001) Extraterrestrial amino acids in Orgueil and Ivuna: Tracing the parent body of CI type carbonaceous chondrites. *Proc. Natl. Acad. Sci. U.S.A.* 98 2138-2141.

Haldane, J.B.S. (1929) The origin of life. *Rationalist Ann.* 148, 3-10.

Halpern, B. (1968) Optical Activity for Exobiology and the Exploration of Mars. *Applied Optics* 8, 1349-1353.

Ikawa, M., and Snell, E.E. (1954) Oxidative Deamination of Amino Acids by Pyridoxal and Metal Salts. *J. Am. Chem. Soc.* 76, 4900.

Kawamura, K., and Yukioka, M. (2001) Kinetics of the racemization of amino acids at 225-275°C using a real-time monitoring method of hydrothermal reactions. *Thermochimica Acta* 375, 9-16.

Kminek, G., and Bada, J.L. (2006) The effect of ionizing radiation on the preservation of amino acids on Mars. *Earth Planet. Sci. Lett.* 245, 1-5.

Kvenvolden, K., Lawless, J., Pering, K., Peterson, E., Flores, J., Pnnamperuma, C., Kalpan, I.R., and Moore, C. (1970) Evidence for Extraterrestrial Amino-acids and Hydrocarbons in the Murchison Meteorite. *Nature* 228, 923-926.

Kvenvolden, K.A., Lawless, J.G., and Ponnampereuma, C. (1971) Nonprotein Amino Acids in the Murchison Meteorite. *Proc. Natl. Acad. Sci. U.S.A.* 68, 486-490.

Kvenvolden, K.A. (1973) Criterion for Distinguishing Biogenic and Abiogenic Amino Acids – Preliminary Considerations. *Space Life Sciences* 4, 60-68.

Li, J., and Brill, T.B. (2003) Spectroscopy of Hydrothermal Reactions Part 26: Kinetics of Decarboxylation of Aliphatic Amino Acids and Comparison with the Rates of Racemization. *Int. J. Chem. Kinet.* 35(11), 602-610.

Masters, P.M., Bada, J.L., and Zigler, J.S. (1978) Aspartic acid racemization in heavy molecular weight crystallins and water-insoluble protein from normal human lenses and cataracts. *Proc. Natl. Acad. Sci. U.S.A.* 75, 1204-1208.

Miller, S.L. (1953) A production of Amino Acids Under Possible Primitive Earth Conditions. *Science* 117, 528-529.

Milton, R.C., Milton, S.C.F., and Kent, S.B.H. (1992) The Enantiomers of HIV-1 Protease Show Demonstration of Reciprocal Chiral Substrate Specificity. *Science* 256, 1445-1448.

Neidhardt, F.C., et al. (eds.) (1996) *Escherichia coli* and *Salmonella typhimurium*-Cellular and Molecular Biology, 2nd edition. American Society for Microbiology, Washington, DC.

Oparin, A.I. (1924) *Proischozhenie zhizni*. Izd. Moscovsky Rabochii, Moscow.

Owen, T., Biemann, K., Rushneck, D.R., Biller, J.E., Howarth, D.W., and Lafleur, A.L. (1977) The composition of the atmosphere at the surface of Mars. *J. Geophys. Res.* 82, 4635-4639.

Rosenfeld, J.K. (1979) Amino Acid Diagenesis and Adsorption in Nearshore Anoxic Sediments. *Limnol. Oceanogr.* 24(6), 1014-1021.

Whitman, W.B., Coleman, D.C., and Wiebe, W.J. (1998) Prokaryotes: The unseen majority, *Proc. Natl. Acad. Sci. U.S.A.* 95, 6578-6583.

Williams, K.M., and Smith, G.G. (1977) A Critical Evaluation of the Application of Amino Acid Racemization to Geochronology and Geothermometry. *Origins Life Evol. Biosph.* 8, 91-144.

Zhang, J. (2000) Protein-length distributions for the three domains of life. *Trends in Genetics* 16, 107-109.

Zhao, M., and Bada, J.L. (1989) Extraterrestrial amino acids in Cretaceous/Tertiary boundary sediments at Stevns Klint, Denmark. *Nature* 339, 463-465.

CHAPTER II. Amino Acids as Organic Biomarkers

ABSTRACT

Amino acid biosignatures from extinct or extant life can be differentiated due to their distributions and chiralities of the detected amino acid monomers after hydrolysis. We have determined the protein amino acid abundances of serpentine inoculated with living *E. coli* cells by traditional laboratory extractions to determine the most useful targets for amino acid biosignatures. Half of the protein amino acids (10 of 20) account for ~92% of the total amino acids and six of these (aspartic acid, glutamic acid, serine, glycine, alanine, and valine) account for ~70%, in agreement with previous studies. The residues with detectable D-amino acid enantiomers show very low D/L-ratios (~0.02), the minor amounts presumably caused by acid hydrolysis treatment. D-alanine showed the only appreciable enantiomeric ratio (~0.05) due to D-enantiomers derived from bacterial cell walls.

2.1 INTRODUCTION

Bacterial biodensity can be quantified by a number of traditional cell staining methods. Many of these methods target intact DNA, such as 4',6-diamidino-2-phenylindole (DAPI), acridine orange (DNA/RNA), or ethidium bromide. These methods target only intact nucleoid-containing cells (NUCC). Other staining methods, such as trypan blue, target cell membranes and will react with both living and dead cells. Cell staining can lead to erroneous biodensity calculation due to human error and interfering medium (Schallenberg et al., 1989).

Analyses of individual cellular molecular components can be used to accurately determine cell concentrations in natural samples. Two of these methods are cell enumerations based on total adenosine triphosphate (ATP) and phospholipid fatty acid (PLFA) analyses, and these have been shown to be accurate at determining cell concentrations in natural samples (Balkwill et al., 1988). ATP is a nucleotide and a ubiquitous component of bacterial life while the majority of phospholipids and fatty acids are present as components within microbial cell walls. One unique aspect of PLFA analyses is that they can distinguish between different types of bacteria (gram-positive or gram-negative) depending on the distribution of the target molecules. Similarly, any biomarker can be used to quantify bacteria such as amino acids or nucleobases.

Quantifying total hydrolyzable amino acids (THAA) yields accurate determination of the total protein content in bacterial colonies. Traditional wet chemistry extraction and analytical methods for amino acid quantification involve acid hydrolysis followed by desalting, pre-column derivatization using a fluorescent chiral adduct, separation by reverse-phase high performance liquid chromatography (RP-HPLC), and quantification by fluorescence detection against standards of known concentration (Zhao & Bada, 1995).

Most amino acids are stable during traditional acid-hydrolysis methods (6N HCl, 24 hours) as only the peptide bonds within proteins are cleaved during this treatment. The exception is tryptophan which is completely destroyed during acid hydrolysis while arginine, tyrosine, threonine, serine, methionine, and cysteine are degraded to a small degree during longer hydrolysis times (Fountoulakis and Lahm, 1998). Asparagine and glutamine are converted to aspartic and glutamic acids during liquid hydrolysis. These degradation mechanisms (Figure 2.1) involve the conversion of the carboxamide side groups to carboxyl groups through the incorporation of water and liberation of ammonia.

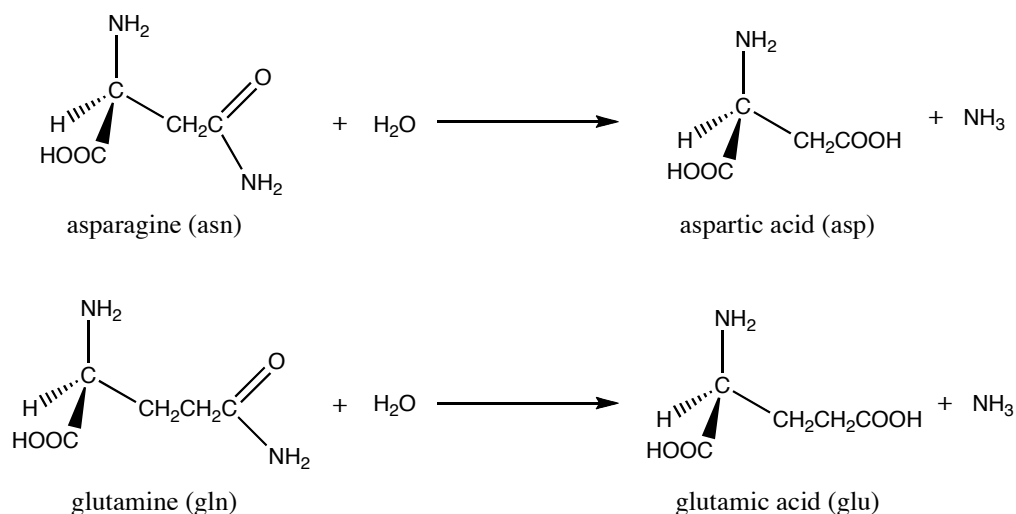


Figure 2.1 Degradation mechanism of glutamine and asparagine to glutamic acid and aspartic acid, respectively, during acid hydrolysis.

Ortho-phthaldialdehyde/*N*-acetyl-L-cysteine (OPA/NAC) was first used to derivatize amino acids by Aswad (1984) and later applied to amino acid quantification in geological samples (Zhao and Bada, 1995). The fluorescent derivatizing chiral adduct is made by combining

OPA and NAC into an alkaline borate buffered solution to form a cyclic fluorescent derivative (Figure 2.2).

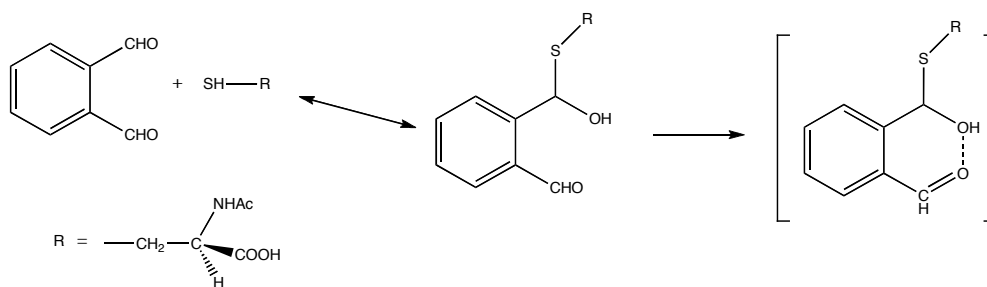


Figure 2.2 Reaction of *o*-phthalaldehyde (OPA) and N-acetyl-L-cysteine (NAC) to form OPA/NAC.

This fluorescent chiral adduct reacts with primary amines to form fluorescent derivatives (Figure 2.3). The fluorogen reacts with all primary amines, so it targets all 20 protein amino acids except for proline. Highly specific fluorescence detection is accomplished at an excitation wavelength of 340 nm and an emission wavelength of 450 nm. This highly specific derivatization allows for low interference during quantification.

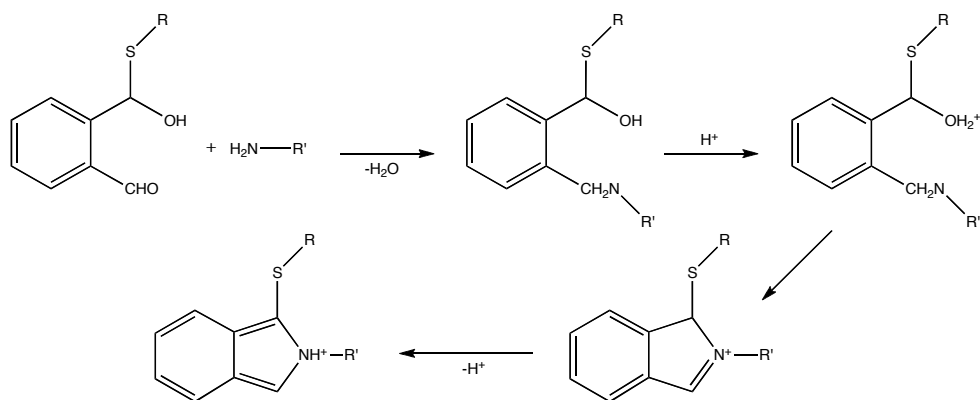


Figure 2.3 Reaction of OPA/NAC with a primary amine to form a fluorescent derivative (R' = an amino acid or amine alkyl group).

In order to determine the amino acid composition and distribution of a typical bacterial culture, and to test the THAA method for cell enumeration, samples of cultured *E. coli* cells (assumed to be good representative bacteria) were run through traditional wet chemistry extraction and analytical protocols. This allowed for determination of the most important targets

for the search for amino acid biosignatures derived from bacterial proteins in the study of geological samples and for the purposes of life detection.

2.2 EXPERIMENTAL SECTION

Cultured *E. coli* cells (strain MG1655) were obtained and added to a sterilized crushed serpentine medium. Cell biodensities were measured by traditional methods on the inoculated sample and a procedural blank growth medium that did not contain *E. coli* cells. The OD₄₆₀ of the *E. coli* growth medium was measured to be 0.65 which corresponded to 6.5×10^9 *E. coli* cells in 10 ml of LB growth medium with a 5% measurement error. Because physiological variation may changes in cell size, capsule formation, or aggregation, small differences in the conversion between OD and total cell counts may be observed. For this reason, the total number of *E. coli* cells as determined from the OD reading was independently confirmed by measuring the mass of a solid *E. coli* pellet generated by overnight growth and centrifugation of a volume of LB medium identical to that used to inoculate the serpentine. If it is assumed that the *E. coli* cells were homogenously mixed into the 0.5-g crushed serpentine sample, a concentration of 1.3×10^{10} cells/g ($\pm 5\%$) for the serpentine inoculated with *E. coli* was inferred.

~200 mg of the inoculated serpentine cell media and a serpentine growth medium blank (with no *E. coli* cells present) were hydrolyzed and desalted according to the procedures of Zhao and Bada (1995). The sample was vapor-phase hydrolyzed under 6M doubly-distilled HCl (ddHCl) for 24 hours in a flame-sealed test tube after flushing with nitrogen. The hydrolyzed residue was loaded onto an equilibrated desalting column (Amelung & Zhang, 2001) of ~2.5 mL of BioRad AG50W-X8 resin in a pasteur pipette. The sample was rinsed with ~6 column volumes of doubly-distilled water (ddH₂O) before eluting the amino acid fraction with 3mL of ~3M doubly-distilled ammonium hydroxide (NH₄OH). These fractions were concentrated on a vacuum centrifuge under 60°C heat into 1.5mL mini-ependorf vials. These residues were resuspended into 100μL of ddH₂O for derivatization and analysis by RP-HPLC.

The OPA/NAC fluorescent derivative was prepared with chemicals purchased from Sigma. 4 mg of OPA was first dissolved into 300μL of methanol, and 250μL of borate buffer was added to the solution, followed by the addition of 435μL of double-distilled water. The last step is the addition of 15μL of 1M NAC solution (adjusted to pH 5.5 with NaOH). This derivatizing solution has a final concentration of ~0.03M OPA (M.W. 134.1) and ~0.015M NAC

before they react. The final concentration of the cyclical derivative in the OPA/NAC solution is 0.015M OPA/NAC. The reaction between OPA/NAC and primary amines has been demonstrated to be linear over large concentration ranges for reaction with amino acids (Molnár-Perl & Bozor, 1998) and biogenic amines (Busto et al., 1997).

10 μ L aliquots of diluted fractions (1:10-1:100) of the desalted hydrolyzed *E. coli* extracts and procedural blanks were first dried down on a vacuum centrifuge at room temperature with 10 μ L of borate buffer to remove any residual ammonia from the NH₄OH carried through from the desalting stage. These residues were brought up in 20 μ L of ddH₂O and derivatized for 1 minute with 5 μ L of the 0.015M OPA/NAC solution. After this pre-column derivatization, the samples were separated by RP-HPLC and quantified with a fluorescence detector. The RP-HPLC setup utilizes an Hitachi L6200 Intelligent HPLC pumps, rheodyne sample injectors, coupled with a Phenomenex Luna-C18(2) RP-HPLC column and a Shimadzu fluorescence detector (model RF-535). Data sampling and analysis, including automatic and manual Gaussian peak integrations, were performed using Thermo Scientific Grams/AI software. Sample peak intensities were quantified against 100-1000x diluted commercial standards of known concentration (Pierce Amino Acid Standard H, protein hydrolysate 16 amino acid standard, #20088), and the trace amounts of D-enantiomers ratio-normalized against racemic laboratory standards of similar concentration.

The HPLC conditions included a stationary-phase buffer, 50mM sodium acetate solution with 8% methanol, with methanol as the mobile phase. Two gradient protocols were necessary to resolve the 16 amino acids extracted and purified by these methods (Figure 2.4). The traditional amino acid separation protocol developed over the last 20 years (gradient A) has been used in a variety of studies including those on natural samples (Aubrey et al., 2006), meteorites (Glavin et al., 1999), and hydrolyzed bacteria (Glavin et al., 2001). This RP-HPLC protocol was primarily developed to well separate the primary amino acids present in geological samples as well as their enantiomers. A slower methanol elution gradient (gradient B) was developed that was necessary to resolve the coeluting peaks of glycine and arginine, and to better resolve threonine as a shoulder of glycine and tyrosine from alanine. The trace amounts of D-enantiomers did not interfere with the peak separation as the D/L-enantiomer ratios were too small to be significant. This is expected of any extant bacterial community and the hydrolysis not harsh enough to cause a significant degree of racemization.

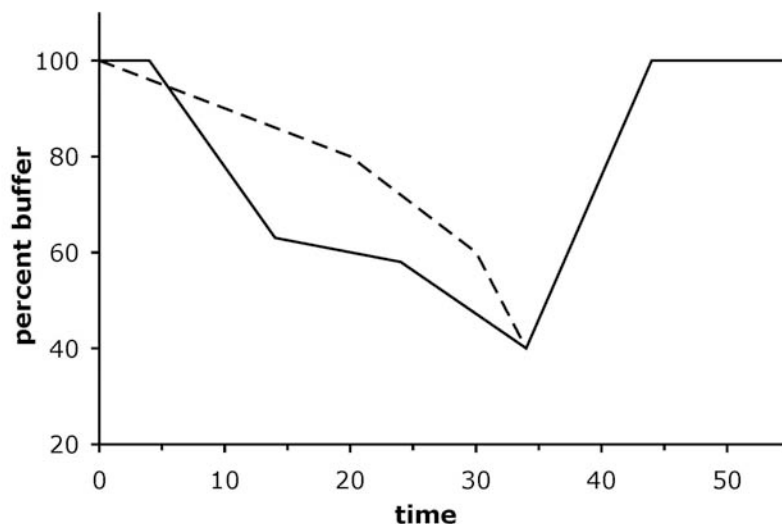


Figure 2.4 HPLC buffer/methanol gradients (A) from meteorite separation gradient (–), and (B) slow elution gradient B (---). Buffer is 50mM sodium acetate with methanol (92:8) and mobile phase is pure methanol.

The OPA/NAC fluorescent derivatizing reagent tags only primary amines, so proline does not react, tryptophan is completely destroyed during hydrolysis in 6N HCl for 24 hours, and asparagine and glutamine degrade to aspartic acid and glutamic acid during acid-catalyzed hydrolysis, respectively. This results in the derivatization of 16 of 20 total protein amino acids.

2.3 RESULTS AND DISCUSSION

Aspects of this study have been investigated before. Similar procedures were utilized by Glavin et al. (2001) to determine the amino acid composition in similarly treated fraction of hydrolyzed *E. coli* cultures, however they analyzed a more limited set of amino acids during their experiments. More recently, the recoveries of adenine from sublimed *E. coli* colonies were used to enumerate bacterial biodensity (Glavin et al., 2004), so this study provides verification of procedures for THAA determination and accurate enumeration of cell biodensity. Sixteen of twenty protein amino acids were separated and quantified by these methods using two separate RP-HPLC protocols (Figure 2.5). The *E. coli* cells were easily detectable at the concentrations examined in this study.

The amino acid separations were successful using the traditional laboratory protocol developed over the last 15 years (Figure 2.5A). Gradient B was necessary to better resolve the

coeluting peaks of glycine and arginine. The second gradient also showed much better separation of threonine from a shoulder of glycine and tyrosine from alanine (Figure 2.5 B). The traditional gradient A showed much better overall separation of the amino acids, especially in the amino acids which coeluted further downfield.

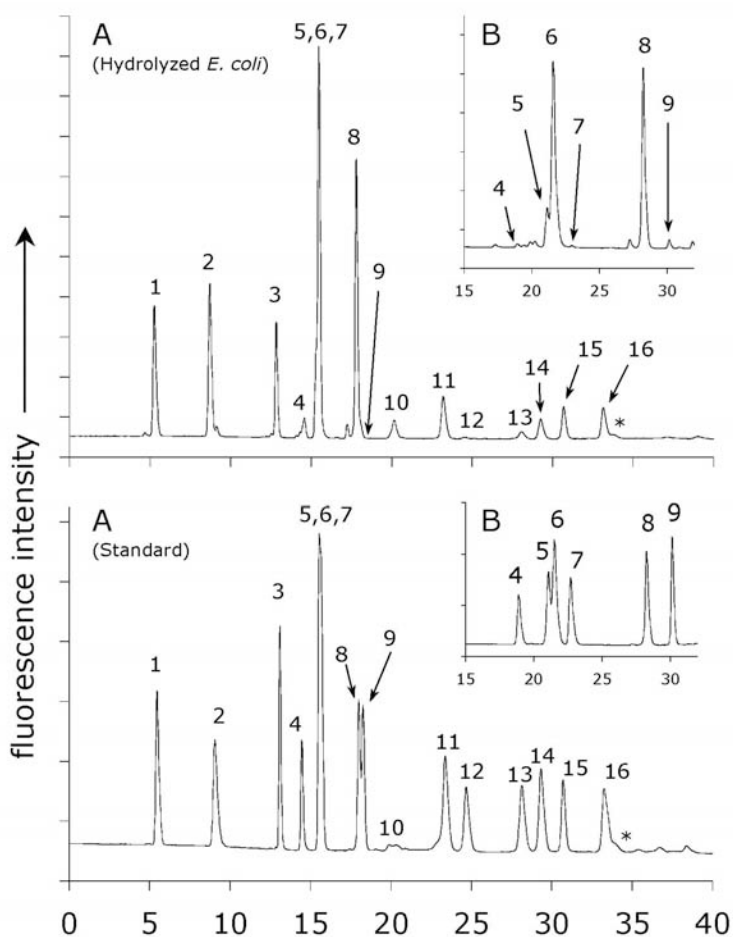


Figure 2.5 Chromatograms of amino acid separations (0-40 mins) of hydrolyzed/desalted *E. coli* sample extract (top) against a standard (bottom). Gradient A showed good overall resolution, but gradient B was necessary to separate histidine/glycine/threonine and to better resolve alanine and tyrosine. 1=aspartic acid, 2=glutamic acid, 3=serine, 4=histidine, 5=threonine, 6=glycine, 7=arginine, 8=alanine, 9=tyrosine, 10=cysteine, 11=valine, 12=methionine, 13=phenylalanine, 14=Isoleucine, 15=lysine (*=secondary peak), 16=leucine.

The 16 amino acids shown in figure 2.5 were quantified and compared to the data from Glavin et al. (2001), showing good overall agreement (Table 2.1).

Table 2.1 Amino acid abundances from hydrolyzed/desalted *E. coli* inoculated serpentine (this study) compared to hydrolyzed/desalted *E. coli* inoculated palagonite (Glavin et al., 2001). The deviation showed for glycine for the reported data reflects the magnitude of threonine plus arginine which partially separate in the standard amino acid RP-HPLC protocol (gradient A). Reported concentrations (ppm) are procedural blank corrected.

	Concentration		
	percent total	$\mu\text{g/g}$ serpentine	
Asx	12.9	155 ± 2	
Glx	16.1	194 ± 4	
Ser	6.7	81.2 ± 5.2	
His	4.8	57.4 ± 2.9	
Thr	5.2	62.1	
Gly	11.1	134	
Arg	0.2	2.67	
Ala	19.3	233 ± 9	
Tyr	0.3	3.78	
Cys	5.7*	68.3	
Val	4.6	55.7 ± 22	
Met	0.4	5.06	
Phe	1.4	17.0 ± 3.5	
Ile	2.4	29.5 ± 2.2	
Lys	3.5	42.5 ± 10.7	
Leu	5.4	64.6 ± 15.0	
TOTAL	100.0	1206	
Σ major 6 ¹	70.7	853	
Cells/gram ²	NA	1.4×10^{-10}	
Cells/gram ³	NA	1.3×10^{-10}	

NOTE: Average of 5 separate HPLC runs for asx, glx, ser, ala, val, phe, and leu. His, ile, and lys were each averages of 3 runs while the samples without uncertainties represent an average of only 2 runs (thr, gly, arg, tyr, cys, met better average of 2 runs which better separated using gradient B).

¹Major 6 amino acids are aspartic acid, glutamic acid, serine, glycine, alanine, and valine.

²Total protein calculated assuming that the quantified amino acids represent 100% of the total amino acids and that a typical *E. coli* cell weighs contains 1.55×10^{-13} grams of protein (55% of 2.55×10^{-13} grams dry weight; Neidhardt et al., 1990).

³Cells per gram as measured by traditional cell counting methods (Glavin et al., 2004).

The only major differences between the two datasets (Table 2.1) are the magnitudes of the glycine and alanine peaks. The distinct difference in the alanine concentrations between these data reflects different amino acid compositions of the analyzed bacterial colonies. The large difference (~5%) in the glycine peak can be explained by assuming that threonine, which constitutes ~5% of the total mass of *E. coli*, coeluted and was quantified with glycine in the previous study (Glavin et al., 2001). The error bar over glycine for the data gathered in this study (Table 2.1) shows the magnitude of threonine plus glycine if they coeluted, explaining the

disagreement between the two datasets. Threonine, present in gradient A as a shoulder of glycine, better separates using gradient B (insets, Figure 2.5) and was more accurately determined with this program. However, using gradient A, any significant concentration of threonine present in natural samples may still be determined as it shows up as a shoulder of glycine.

The cellular biodensity may be enumerated by estimating the mass of each *E. coli* cell to be 1.55×10^{-13} grams/cell, the protein content of each cell to be 55% (Neidhardt et al., 1990), and the quantified amino acids (16) to be ~100% of the total protein mass. Extrapolation of the total amino acid concentrations to an equivalent cell count shows that the total biodensity is on the order of 1.4×10^{10} cells per gram of serpentine. This is in close agreement to the cell staining methods utilized in this study which showed approximately 1.3×10^{10} cells per gram of serpentine. Assuming a 5% error in each approximation, these data agree within the error limits.

Data from this study show that the 10 amino acids quantified with the highest concentrations account for approximately 92% of the total mass. In agreement with data from Glavin et al. (2001), six of these amino acids (asp, glu, ser, gly, ala, val) account for 70.7% of the total amino acids present in *E. coli*. Quantification of these 6 amino acids represents the majority of the protein amino acids and is sufficient to accurately enumerate the cell biodensities of geological samples. Also of importance is that these six amino acids and their enantiomers all elute before 25 minutes and show good chiral resolution between D- and L-configurations using the established RP-HPLC gradient protocol (gradient A). The coelution of glycine and arginine in gradient A is a non-issue because arginine is present in such low concentrations (0.2%) in bacterial communities (Table 2.1).

One of the most important confirmations of this study was the deficiency of D-amino acids detected in these analyses. The optimum hydrolysis procedures preserve the integrities of the amino acids as well as their chiralities. The average D/L-ratios of the amino acids asp, glu, ser, gly, and val was approximately 0.02 while alanine showed a slightly higher average D/L-ratio of 0.05. This means that the racemization percentage is well under 1% and does a good job of preserving the enantiomer signature of geological samples. Figure 2.6 shows the results from this study against data from previous studies. The distributions are very similar for all of the amino acids and show good agreement.

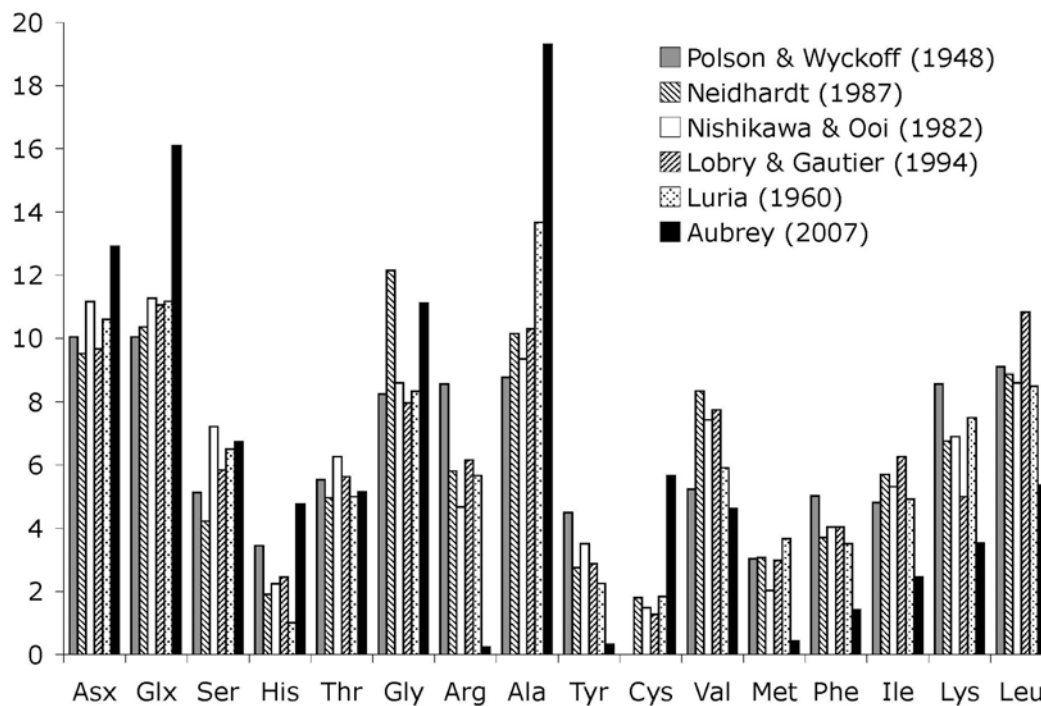


Figure 2.6 Plot of *E. coli* amino acid compositions from this study compared to those from other studies. Proline is not reported because it is undetected by the derivatization methods used in this study. Asparagine and glutamine are converted to Asp (Asx) and Glu (Glx) during hydrolysis, and Trp is destroyed during hydrolysis.

The major differences appear to be in the amino acids asx, glx, ala, and cys. The differences in asx and glx must represent a difference in the protein content of the *E. coli* strains analyzed or may be explained by different methods of quantification. As these numbers agree well with the data from Glavin et al. (2001), this is unexplainable and may reflect the superior methods of quantification utilized in this study. The difference in ala concentrations, also observed compared to the data from Glavin et al. (2001), perhaps shows a higher percentage in this strain of *E. coli* compared to others studied. Finally, the differences in cysteine concentration can be explained by the effect of hydrolysis on recovery (Fountoulakis and Lahn, 1998) and peak coelution. The cysteine peak overlapped with trace amounts of ammonia in the standard and hydrolyzed samples. The borate drydown step did not completely remove all of the residual ammonia left over from the desalting stage (elution with NH_4OH), resulting in trace amounts of ammonia coeluting with cysteine.

2.4 CONCLUSION

The distribution of amino acids from microbial life has been reinvestigated in this study and found to agree fairly well with previous results. Amino acids derived from extant microbial communities are homochiral (L-enantiomers) with very low abundances of D-amino acids. The distributions show the major amino acids components as alanine, glutamic acid, aspartic acid, glycine, and serine. Any detected abiotic enantiomer abundance from purely extant bacteria is due to sample processing during hydrolysis ($D/L < 0.05$) or the presence of a small amount of racemized microbial remnants present in the overall community. In the case of alanine, the D-enantiomer is prevalent in low concentrations within peptidoglycan and should normally show the highest D/L-ratio.

The distribution of amino acids within *E. coli* is assumed to be representative of a wide variety of microbial life. Merely six of the twenty amino acids account for ~70.7% of the total amino acids (Σ asp, glu, ser, gly, ala, val). These are the most important amino acids to detect in the search for biomarkers within geological samples or during future astrobiological missions. The chirality of the detected amino acids is the key to the unequivocal determination of the presence of biological material.

ACKNOWLEDGEMENTS

The *E. coli* cell cultures were prepared by Michael Schubert from Prof. Bartlett's laboratory. Cell enumerations were calculated by cell staining with DAPI and adenine quantification with the help of Alex Purdy. I also would like to thank Daniel P. Glavin and Jim Cleaves for helping with much of the experimental work. This chapter based in part on the following paper:

Glavin, D.P., Cleaves, H.J., Schubert, M., Aubrey, A., and Bada, J.L. (2004) New Method for Estimating Bacterial Cell Abundances in Natural Samples by Use of Sublimation. *App. Environ. Microbiol.* **70**, 5923-5928.

REFERENCES

- Amelung, W., and Zhang, X. (2001) Determination of amino acid enantiomers in soils. *Soil Biology & Biochemistry* 33, 553-562.
- Aswad, D.W. (1984) Determination of D- and L-Aspartate in Amino Acid Mixtures by High-Performance Liquid Chromatography after Derivatization with a Chiral Adduct of o-Phthaldialdehyde. *Anal. Biochem.* 137, 405-409.
- Aubrey, A.D., Cleaves, H.J., Chalmers, J.H., Skelley, A.M., Mathies, R.A., Grunthaner, F.J., Ehrenfreund, P., and Bada, J.L. (2006) Sulfate minerals and organic compounds on Mars. *Geology* 34, 357-360.
- Balkwill, D.L., Leach, F.R., Wilson, J.T., McNabb, J.F., and White, D.C. (1988) Equivalence of Microbial Biomass Measures Based on Membrane Lipid and Cell Wall Components, Adenosine Triphosphate, and Direct Counts in Subsurface Aquifer Sediments. *Microb. Ecol.* 16, 73-84.
- Busto, O., Miracle, M., Guasch, J., and Borrull, F. (1997) Determination of biogenic amines in wines by high-performance liquid chromatography with on-column fluorescence derivatization. *J. Chromatogr. A* 757, 311-318.
- Fountoulakis, M., Lahn, H.-W. (1998) Hydrolysis and amino acid composition analysis of proteins. *J. Chromatogr. A* 826, 109-134.
- Glavin, D.P., Schubert, M., Botta, O., Kminek, G., and Bada, J. L. (2001) Detecting Pyrolysis Products from Bacteria on Mars. *Earth Planet. Sci. Lett.* 185, 1-5.
- Glavin, D.P., Cleaves, H.J., Schubert, M., Aubrey, A., and Bada, J.L. (2004) New Method for Estimating Bacterial Cell Abundances in Natural Samples by Use of Sublimation. *App. Environ. Microbiol.* 70, 5923-5928.
- Glavin, D.P., Bada, J.L., Brinton, K.L.F., and McDonald, G.D. (1999) Amino acids in the Martian meteorite Nakhla. *Proc. Natl. Acad. Sci. U.S.A.* 96, 8835-8838.
- Lobry, J.R., and Gautier, C. (1994) Hydrophobicity, expressivity and aromaticity are the major trends of amino-acid usage in 999 *Escherichia coli* chromosome-encoded genes. *Nucleic Acids Research* 22, 3174-3180.
- Luria, S. E. (1960) in I. C. Gunsalus and R. Y. Stanier (eds.), *The Bacteria - A Treatise on Structure and Function*, Vol. 1, Academic Press, New York, p. 1.
- Molnár-Perl, I., and Bozor, I. (1998) Comparison of the stability and UV and fluorescence characteristics of the o-phthaldialdehyde/N-acetyl-L-cysteine reagents and those of their amino acid derivatives. *J. Chromatogr. A*, 798, 37-46.
- Neidhardt, F.C., Ingraham, J.L., and Schaechter, M. (1990) *In Physiology of the bacterial cell: a molecular approach*. Sunderland, Massachusetts: Sinauer Associates, 506 pp.

Neidhardt, F.C. (1987) In Neidhardt, F.C. (ed.) *Escherichia coli and Salmonella typhimurium, cellular and molecular biology*, American Society for Microbiology, Washington, pp. 3-6.

Nishikawa, K., and Ooi, T. (1982) Correlation of the Amino Acid Composition of a Protein to Its Structural and Biological Characters. *J. Biochem.* 91, 1821-1824.

Polson, A., and Wyckoff, R.W.G. (1948) The Amino Acid Content of Bacteriophage. *Science* 108, 501.

Schallenberg, M., Kalff, J., and Rasmussen, J.B. (1989) Solutions to Problems in Enumerating Sediment Bacteria by Direct Counts. *Appl. Environ. Microbio.* 55, 1214-1219.

Zhao, M., and Bada, J.L. (1995) Determination of alpha-dialkylamino acids and their enantiomers in geological samples by high-performance liquid chromatography after derivatization with a chiral adduct. *J. Chromatogr. A* 690, 55-63.

CHAPTER III. Sulfate Minerals and Organic Compound Preservation on Mars

ABSTRACT

The presence of evaporitic sulfate minerals such as gypsum and anhydrite has recently been confirmed on the surface of Mars. Although organic molecules are often co-deposited with evaporitic minerals in terrestrial environments, there have been no systematic investigations of organic components in sulfate minerals. The detection of organic material within ancient and terrestrial sulfate minerals in these samples is reported herein, including amino acids and their amine degradation products. Amino acids and amines appear to be preserved for geologically long periods in gypsum mineral matrices. This suggests that sulfate minerals should be prime targets in the search for organic compounds on Mars, including those of biological origin, during future *in situ* missions.

3.1 INTRODUCTION

The search for evidence of water and organic compounds, including those of possible biological origin, is one of the major goals of both the NASA and European Space Agency (ESA) Mars exploration programs. The NASA Mars Exploration Rovers and the ESA OMEGA/Mars Express have provided the best evidence to date that liquid water was once present on Mars. Abundant sulfate minerals such as gypsum and jarosite suggest that large acidic water basins were once present and that as they evaporated sulfate minerals were precipitated (Squyres et al., 2004; Langevin et al., 2005; Gendrin et al., 2005). Although it is unknown when these standing bodies of water existed or for what duration, they could potentially have provided an environment capable of supporting life.

On the other hand, it remains uncertain whether organic compounds are present on Mars. While the Viking missions in 1976 detected no organic compounds above a threshold level of a few parts per billion in near surface Martian soils (Biemann et al., 1976). However, it is now known that key biomolecules such as amino acids would not have been detected by the Viking GCMS even if several million bacterial cells per gram were present (Glavin et al., 2001). In addition, oxidation reactions involving organic compounds on the Martian surface would likely produce non-volatile products such as mellitic acid salts that also would not have been detected

by Viking (Benner et al., 2000). Thus, the Viking results did not conclusively disprove that there are organic compounds present on the surface of Mars. The only other opportunity to analyze samples from Mars has been provided by meteorites ejected from its surface and delivered to Earth. However, contamination of these meteorites by terrestrial organic material during their residence times on Earth (ranging from 10^2 to 10^4 years) compromises their use in assessing whether organic compounds are present on Mars (Jull et al., 1998).

Organic matter is often co-deposited in terrestrial evaporites, and similar deposition processes should occur on Mars if organic molecules were present in the early oceans (Mancinelli et al., 2004). To our knowledge, there have been no systemic investigations of organic compounds in sulfate minerals on Earth. The concentrations of organic carbon and nitrogen of several sulfate minerals are reported herein, as well as the abundance of amino acids and their degradation products.

3.2 METHODS

The samples investigated included gypsum-rich soil from the Atacama Desert, Chile (~2 Ma), gypsum from the Anza-Borrego Desert, CA (~4 Ma), anhydrite sample from a DSDP Red Sea core (~5 Ma), gypsum from the Haughton impact crater, Canada (~23 Ma) and gypsum from Panoche Valley, CA (~40 Ma). A modern gypsum sample from a saltworks pond in South Bay San Diego, CA was also analyzed. Sample ages were estimated based on the geology of their respective localities (Figure 3.1).

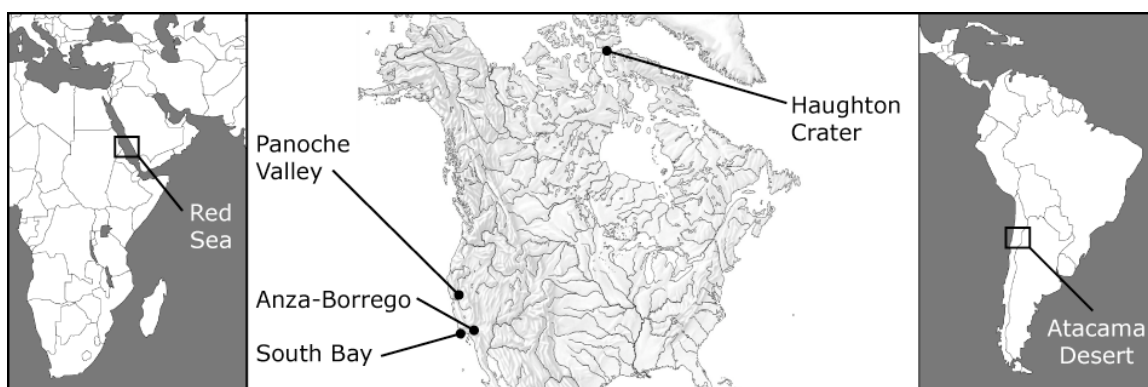


Figure 3.1 Sample origin locations.

Atacama Desert gypsum deposits have been reported to be late Pliocene in age, so this near-surface soil sample, composed of a high mass percent gypsum, was assumed to be ~2 Ma (Hartley & Chong, 2002). The evaporite formations from the Anza-Borrego Desert have been extensively studied. The gypsum investigated here was collected from the Fish Creek area and has been dated at 3-5 Ma (Remeika and Lindsay, 1992). Gypsum from the Haughton impact crater, Canada, was donated by John Parnell and is assumed to date from the time of the impact crater at 23 Ma (Parnell et al., 2004). The age of the host rock of the Panoche Valley samples is 75-65 Ma (Presser and Ohlendorf, 1987) but the ages of the sulfate minerals are estimated at 40 Ma (middle Tertiary) because this is when the coastal ranges were raised in this area during the Sierra Nevada uplift, which caused ocean water to withdraw and deposit evaporitic minerals in California's Central Valley. In order to verify the geologically deduced ages of the Panoche Valley samples, strontium isotope analyses were conducted. Celestite, SrSO₄, is often included in gypsum mineral matrices as a minor component, and because the Panoche Valley gypsum formed evaporitically, the Sr isotopes should be indicative of the seawater ratio at the time of formation. The Panoche Valley gypsum ^{87/86}Sr ratio was 0.707745 (±0.000005). Comparing this ^{87/86}Sr ratio to the strontium isotope history of seawater (Hess et al., 1986), gives an age 40 Ma, consistent with the inferred geologic age. The modern gypsum sample is from the South Bay salt works in South Bay San Diego, California. The area is rich in marshes and tidal flats and experiences continuous evaporite formation during tidal fluctuations. Because of the poor water quality in this region of San Diego Bay, the salts typically include significant amounts of organic material.

The surface of each sample was thoroughly rinsed with doubly-distilled water (ddH₂O) followed by doubly-distilled 1M HCl, then again with ddH₂O. The identity of each mineral was verified by XRD analyses using a Scintag XDS-2000 powder diffractometer. Samples were analyzed for total organic carbon and nitrogen using a Costech elemental combustion C-N analyzer. Carbon and nitrogen isotopic ratios were determined with a Thermofinnigan Delta-XP Plus stable isotope ratio mass spectrometer on ~30 mg of each sample. In order to remove carbonate from the samples, they were pre-treated with an excess of 3N double-distilled HCl and dried down on a vacuum centrifuge at 45°C for 1 hour before analyses for total organic carbon (TOC) and nitrogen (TON).

Amino acids were isolated by vapor-phase acid hydrolysis (6 N HCl, 24 hours, 100°C) of ground samples followed by desalting (Amelung and Zhang, 2001). Amines were isolated by micro-diffusion from the powdered mineral treated with 1N NaOH, into a 0.01N HCl solution at 40°C for 6 days (Conway, 1963). Extracts were analyzed for amino acids and amines by RP-HPLC using pre-column derivatization with *o*-phthaldialdehyde/*N*-acetyl L-cysteine using a Shimadzu RF-530 fluorescence detector (Zhao and Bada, 1995) and a Phenomenex Synergi Hydro-RP column (250 x 4.6 mm). Quantification of amino acids and amines included background level correction using a serpentine procedural blank and a comparison of the peak areas with those of an amino acid standard. A D/L-norleucine internal standard was added to normalize amino acid recoveries from desalting and derivatization. The recovery of the amines carried through the extraction procedure was found to be near 100% using spiked procedural samples.

To investigate the possible presence of modern bacterial contamination in the various minerals, total adenine concentrations were measured. Both a liquid extraction involving treatment of 1 gram of sample with 2 ml of 95% formic acid solution for 24 hours at 100°C and a sublimation extraction method at 500°C for 5 minutes were performed. Adenine concentrations were quantified by HPLC with UV absorption detection (260 nm) and converted to bacterial cell densities (*E. coli* equivalents/g) as described in Glavin et al. (2004).

3.3 RESULTS

The XRD results verified each mineral's identity. The gypsum samples that were obtained from Anza-Borrego, Panoche Valley, and Haughton crater were selenite, pure gypsum in discrete layers. The South Bay gypsum sample was the most impure. The Atacama Desert soils have previously been characterized as having high gypsum content (Hartley & Chong, 2002) and were not characterized by XRD analysis.

The organic carbon and nitrogen data are tabulated in Table 3.1. The organic carbon contents ranged from 0.12 – 0.77 mg·C/g in the 3 gypsum samples, the Atacama Desert was fairly low at 0.16 mg·C/g, while the contemporary gypsum from South Bay showed significantly higher percent organic carbon (6.91 mg·C/g) due to the sample's origin in a highly organic included region. The nitrogen trends were similar in that the ancient gypsum and anhydrite samples ranged from 0.01-0.03 mg·N/g. The high nitrogen content of the Atacama Desert sample reflects

the high nitrate content of these surface soils while the South Bay sample showed elevated levels of TOC, 1.01 mg-N/g.

Table 3.1 Total Organic Carbon (TOC), Total Organic Nitrogen (TON), and stable isotopes.

Location (Ma)	TOC (mg/g)	TON (mg/g)	$\delta^{13}\text{C}$ (‰)	$\delta^{15}\text{N}$ (‰)	$\frac{\Sigma\text{AA} + \text{AMINES}}{\text{TOC}}$ (%)	$\frac{\Sigma\text{AA} + \text{AMINES}}{\text{TON}}$ (%)
South Bay Gypsum (0)	6.91	1.01	-17.3	+11.0	0.041	0.117
Atacama Desert Soil (2)*	0.16	0.13	-32.3	+1.1	0.052	0.018
Anza-Borrego Gypsum (4) [†]	0.29	0.02	-34.9	+1.7	0.042	0.265
Red Sea Anhydrite (5) [§]	0.41	0.01	-24.6	+2.8	0.007	0.091
Houghton Crater Gypsum (23) [#]	0.77	0.03	-31.3	+0.1	0.007	0.105
Panoche Gypsum (40) ^{††}	0.12	0.01	-30.0	+13.1	0.110	0.399

Note: The last two columns represent the mass percent of the TOC and TON accounted for by amino acids and amines. The uncertainties are roughly $\pm 5\%$ for TOC, $\pm 10\%$ for TON and $\pm 0.5\text{-}1.0\text{‰}$ for the isotopic values.

*24°04'S, 69°52'W; (Hartley & Chong, 2002)

[†]33°00'N, 116°10'W; (Remeika and Lindsay, 1992)

[§]21°20'N, 38°08'E; (Whitmarsh et al., 1974)

[#]75°22'N, 89°41'W; (Cockell and Lee, 2002)

^{††}36°35'N, 120°42'W; (Presser and Ohlendorf, 1987)

The organic C/N ratios in the ancient gypsum and anhydrite samples ranged from 12 – 41, indicating that the major organic component present in these sulfates is likely a humic acid/kerogen-like material (Ertel and Hedges, 1983), a conclusion that is consistent with the depleted carbon and nitrogen isotopic values associated with organic material. The exceptions are the Atacama Desert Sample, C/N ~ 1.2, and the South Bay gypsum with a C/N ratio of ~7. These numbers are more indicative of recent biological material, however the Atacama result is skewed because of the high nitrate content.

The detected levels of amino acids and their enantiomers, as well as methylamine (MA) and ethylamine (EA), the decarboxylation products of glycine and alanine, on average account for ~0.04 % of the total organic carbon and ~0.17 % of the total organic nitrogen for the six samples (the Panoche gypsum and Atacama Desert soils showed unknown peaks that eluted near valine and decrease the average percents). Even though amino acids and amines constitute only a fraction of the total organic carbon and nitrogen present in the sulfate minerals (Table 3.1), they are readily detected and characterized (Figure 3.2; Table 3.2).

Table 3.2 Amino acid concentrations of various sulfate minerals.

Location (Ma)	Asp	Ser	Glu	Gly	Ala	Val	MA	Z _{MA}	EA	Z _{EA}
S.B. Gypsum (0)	77.7 [†]	1495 [†]	176	1591	3172 [†]	731	37.2	0.02	173	0.01
A.D. Soil (2)	6.0	15.8	98.1	57.5	169	??	14.9	0.26	19.9	0.12
A.B. Gypsum (4)	137 [†]	8.3 [†]	116	10.3	30.0 [†]	Trace	10.2	0.99	8.8	0.29
R.S. Anhydrite (5)	ND	16.9	30.9	<1	1.2	ND	ND	ND	0.5	0.42
H.C. Gypsum (23)	21.7	65.9	13.5	~1	6.7 [†]	Trace	17.7	17.7	18.7	2.79
P.V. Gypsum (40)	5.6 [†]	3.3 [†]	234	~1	2.9 [†]	??	40.3	40.3	21.2	7.31

Note: All values are blank-corrected and reported in mass ppb. Uncertainties in the measurements are ±10%.

$$* Z_{MA} = \frac{[MA]}{[gly]} \quad ; \quad Z_{EA} = \frac{[EA]}{[ala]}$$

[†]D-enantiomer detected.

N.D. – Not detected above blank level.

?? – Valine is not possible to evaluate because of interference from an unknown component.

Adenine was detected in every sample except the Anza-Borrego gypsum. The adenine levels detected (2-6 ppb) indicate that the E. coli equivalents per gram of sample (ECE/g) are in the range of 10⁶-10⁷ cells/gram. With the exception of the Anza-Borrego gypsum, which is the most pristine, the various samples all have low cell counts indicating that some of the organic matter is likely associated with bacterial remains.

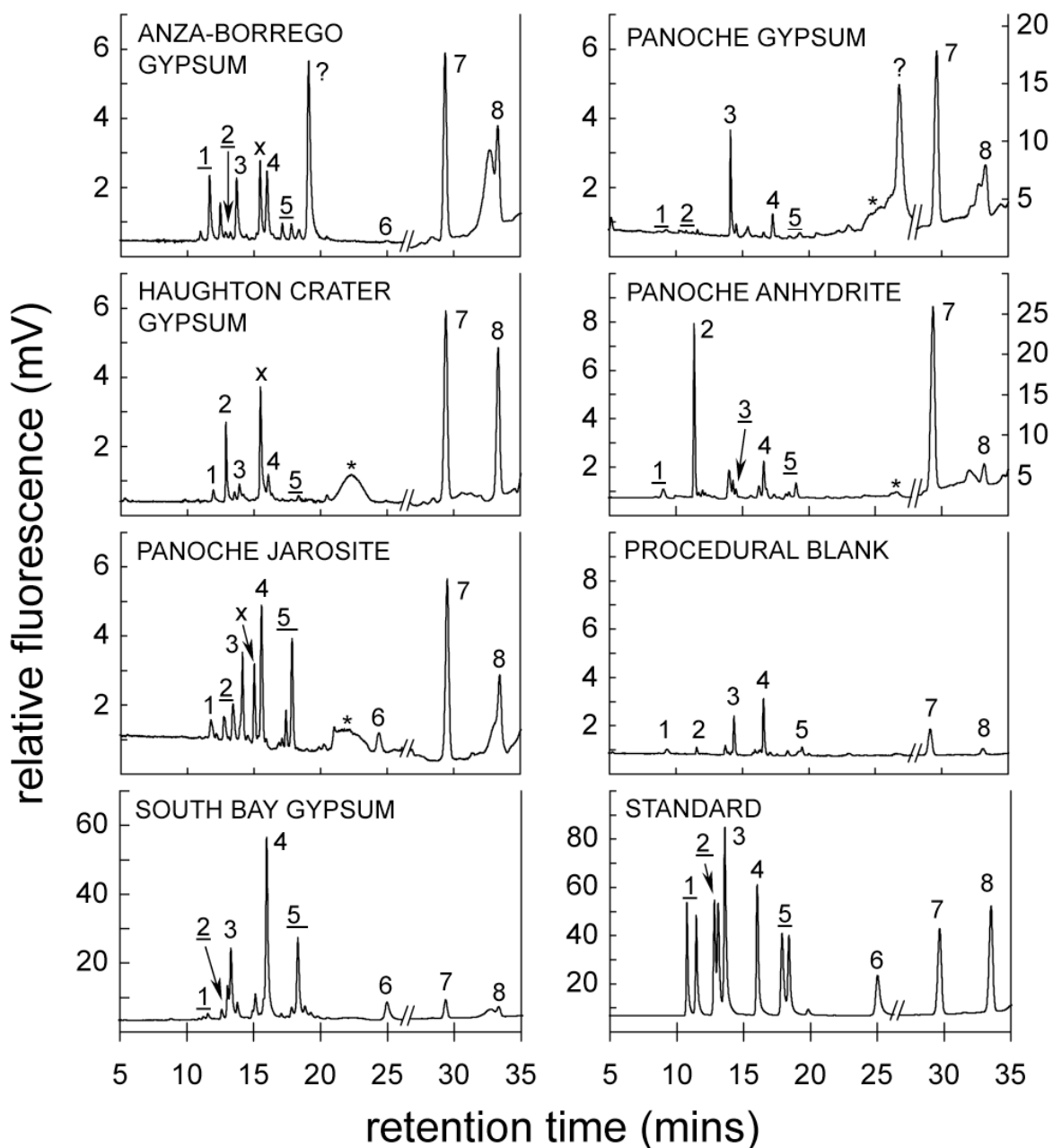


Figure 3.2 RP-HPLC chromatograms of recovery-corrected amino acids (5-25 minutes) and amines (27-35 minutes) in sulfate minerals. The chromatograms are a combination of two runs and represent elutions with identical gradients. The chromatograms on the left and the standard have later retention times because they were separated with a different buffer than the samples on the right. Detection limits were ~ 1 ppb for amino acids and ~ 0.5 ppb for amines. 1=(D+L)-aspartic acid, 2=(D+L)-serine, 3=glutamic acid, 4=glycine, 5=(D+L)-alanine, 6=L-valine, 7=methylamine, 8=ethylamine, *=residual ammonia from extraction process, x=resin impurity. Underlined numbers indicate resolution of the L- and D-enantiomers for that respective amino acid. The peaks labeled '?' are currently unidentified. The y-axis scales are listed on the left for each separation. The right axis has been labeled accordingly if the amine data is at a different attenuation.

3.4 DISCUSSION

The majority of organic matter detected in these sulfate minerals is likely ancient organic matter trapped within the matrix, along with a minor component derived from the remnants of more recent sulfate-reducing microbial communities. The presence of the D-enantiomers (produced by racemization) of several amino acids in the gypsum samples suggest that these compounds are mostly original components of the depositional environment and not recent contaminants, however in the case of alanine, their presence could partially be due to bacterial cell wall material. The correlation between the ratios of the amino acids glycine and alanine and their degradation products, methylamine and ethylamine respectively, also suggests the organic material is a component of the original evaporite. Amines are not typically detected in ancient terrestrial carbonate minerals (Glavin and Bada, 1998), presumably because they are volatile and lost from the mineral matrices because they tend to form in alkaline environments. However, they appear to be retained in sulfate minerals, perhaps as their non-volatile sulfate salts.

The amino acids should be racemic ($D/L = 1$) in the ancient samples because they have ages in excess of several million years (Bada et al. 1999), but this was found not to be the case in all of the samples. The Anza-Borrego gypsum is the only sample in which the D/L alanine ratio is close to unity and this sample therefore appears to be the most pristine. Anza-Borrego also has no detectable adenine, so these amino acids appear to be from extinct life as ancient biosignature.

The ratio Z , the concentrations of methylamine divided by the concentrations of glycine and the concentration of ethylamine divided by the concentrations of alanine can be used as a diagenetic indicator for these samples. The Z -ratios for these two degradation systems are shown in Equations 3.1 and 3.2.

$$\text{Equation 3.1} \quad Z_{MA} = \frac{[MA]}{[gly]} \quad (\text{glycine} \rightarrow \text{methylamine})$$

$$\text{Equation 3.2} \quad Z_{EA} = \frac{[EA]}{[ala]} \quad (\text{alanine} \rightarrow \text{ethylamine})$$

Plots of the relative amounts of amine degradation products in each sample appear to increase with age in the sulfate samples (Figure 3.3).

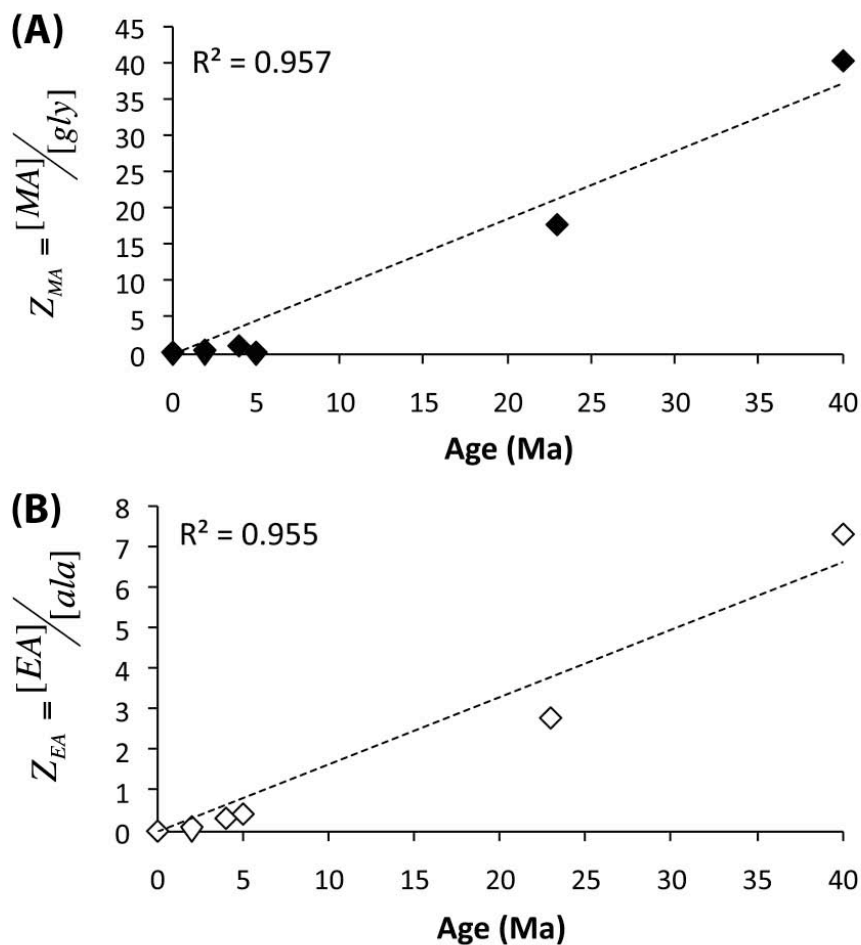


Figure 3.3 Plots of Z-ratios versus age for the samples analyzed in this study for (A) Z_{MA} and (B) Z_{EA} . The red sea anhydrite had no detectable concentrations of methylamine.

Assuming that the change in the relative amounts of methylamine and ethylamine compared to glycine and alanine in the various sulfates over time are entirely due to decarboxylation, then the data in Figure 3.3 would be expected to obey the following irreversible first order kinetic relationship:

Equation 3.3
$$\ln\left(\frac{AA_t}{AA_0}\right) = -k_{DC} \cdot t$$

where AA_t = glycine or alanine concentration at time t , AA_0 is the original glycine or alanine concentration in the sample, and k_{DC} is the rate of decarboxylation of glycine and alanine.

Assuming amines are retained in gypsum and that the major sources of methylamine and ethylamine are glycine and alanine decarboxylation, respectively, then:

$$\text{Equation 3.4} \quad AA_0 = AA_t + AMINES_t$$

where $AMINES_t$ is the methylamine or ethylamine concentration at time t . This also assumes that only trace levels of amines were present in the original gypsum samples which is observed for the modern South Bay gypsum ($Z_{MA} = 0.02$; $Z_{EA} = 0.01$). Substituting Equation 3.4 into Equation 3.3 yields:

$$\text{Equation 3.5} \quad \ln(1 + Z) = k_{DC} \cdot t$$

Equation 3.5 was used to estimate the rates of decarboxylation (k_{DC}) in gypsum from the various sample localities and these values were used to calculate the half lives ($t_{1/2}$) for glycine and alanine decarboxylation (Table 3.3).

The calculated kinetic decarboxylation rate constants and half-lives are shown in Table 3.3 for all of the samples, along with the estimated average exposure temperatures. The Atacama Desert is assumed to have been climatically stable for the past 2 Ma (Hartley et al., 2005), so its average exposure temperature is assumed to be $\sim 20^\circ\text{C}$. At the Anza-Borrego site, present average temperatures are $\sim 23^\circ\text{C}$ (Remeika and Lindsay, 1992) although average temperatures over the last 5 million years have likely been somewhat cooler especially during Pleistocene ice ages. The temperature of the Red Sea sediment sample was estimated to have ranged from the present day bottom water temperatures of 22°C to $\sim 48^\circ\text{C}$ at 230 m depth where the sample was obtained (Whitmarsh et al., 1974). Although, the present temperatures at Haughton Crater are very cold (average annual temperature of -16°C), when the crater and sulfate minerals were formed there was an extended period of high temperature hydrothermal activity (Parnell et al., 2005). Even 2-3 Ma, temperatures in this region were likely significantly warmer than today (Brigham-Grette and Crater, 1992), so the average exposure temperature is assumed to be 0°C . The modern Panoche Valley average temperature is $\sim 17^\circ\text{C}$, but over the past 40 Ma depositional history of the region, the average exposure temperature was likely higher (Park and Downing, 2001). Using these

estimated average exposure temperatures, the calculated kinetic decarboxylation rate constants and half-lives were calculated (Table 3.3).

Table 3.3 Estimated rates of glycine and alanine decarboxylation and half-lives in calcium sulfate samples at estimated exposure temperatures.

Location	T (°C)	glycine → methylamine		alanine → ethylamine	
		$k_{DC, gly}$ (yrs ⁻¹)	$t_{1/2, gly}$ (yrs)	$k_{DC, ala}$ (yrs ⁻¹)	$t_{1/2, ala}$ (yrs)
Atacama Desert	20	1.2×10^{-7}	6.0×10^6	5.6×10^{-8}	1.2×10^7
Anza-Borrego	20	1.7×10^{-7}	4.0×10^6	6.4×10^{-8}	1.1×10^7
Red Sea	22	NA	NA	7.0×10^{-8}	9.9×10^6
Haughton Crater	0	1.3×10^{-7}	5.4×10^6	5.8×10^{-8}	1.2×10^7
Panoche Valley	20	9.3×10^{-8}	7.5×10^6	5.3×10^{-8}	1.3×10^7

Note: Half-lives calculated using the formula: $t_{1/2} = \frac{0.693}{k_{DC}}$

The calculated $t_{1/2}$ values show consistency between the samples for both degradation systems (Table 3.3) with k_{DC} values $\sim 10^{-7}$ yr⁻¹. Most notably, the decarboxylation rate constants for alanine are approximately one order of magnitude slower than for glycine. Glycine is known to be more stable to degradation than glycine (Li & Brill, 2003), so this result is expected. The outlier is the Haughton Crater sample which shows similar rates ($\sim 10^{-7}$ yr⁻¹ for glycine and $\sim 10^{-8}$ yr⁻¹ for alanine decarboxylation reactions) although the temperature in this region is significantly colder. This sample has been reported to contain extant sulfate-reducing bacterial communities, so the signals may be diluted for both degradation systems with more recent organic material.

The values in Table 3.3 can be used to estimate the half-life to decarboxylation in gypsum at the temperatures characteristic of Mars using the Arrhenius equation:

$$\text{Equation 3.6} \quad \ln \left[\frac{t_{1/2(T_2)}}{t_{1/2(T_1)}} \right] = \frac{E_A \cdot (T_2 - T_1)}{R \cdot T_1 \cdot T_2}$$

where $t_{1/2}(T_1)$ and $t_{1/2}(T_2)$ are the half-lives of decarboxylation at T_1 and T_2 , respectively, E_A is the activation energy, and R is the universal gas constant ($8.314 \text{ J} \cdot \text{mole}^{-1} \cdot \text{K}^{-1}$). Assuming a mean exposure temperature of $\sim 0^\circ\text{C}$ for Haughton Crater and $\sim 20^\circ\text{C}$ for the Atacama Desert, Anza Borrego, and Panoche Valley, and using the average of the aqueous Arrhenius activation energies for glycine (138.4 kJ/mole) and alanine (~ 190.6 kJ/mole) determined in Li and Brill (2003), the

half-lives of glycine and alanine decarboxylation in sulfate minerals at Martian temperatures can be estimated (Figure 3.4).

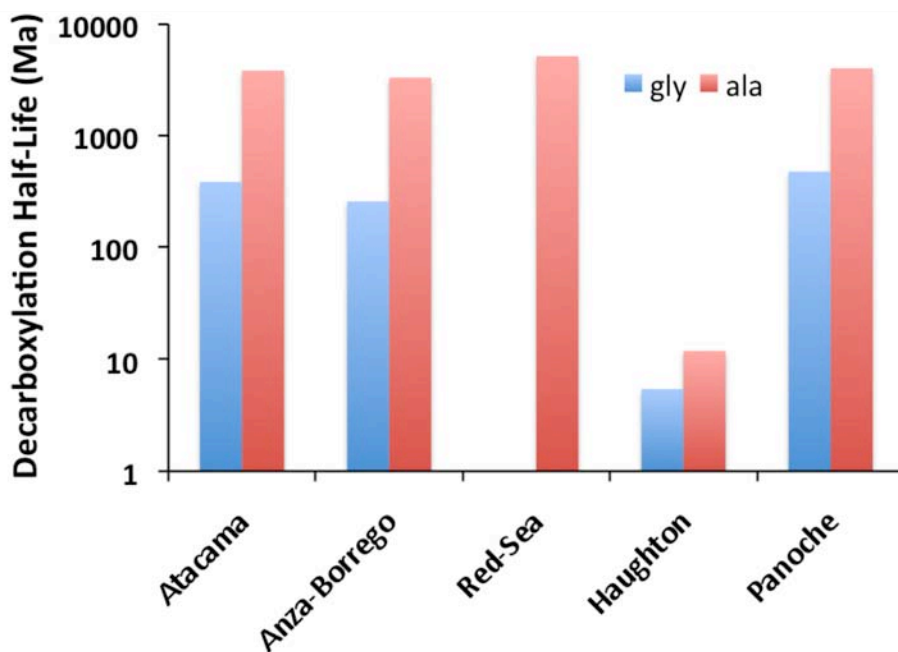


Figure 3.4 Glycine and alanine half-lives extrapolated to Martian surface temperatures ($T \sim 0^\circ\text{C}$) using kinetics determined for decarboxylation from various sample locations. The red sea sample showed no detectable ethylamine, so the kinetics for glycine decarboxylation could not be reported.

Temperatures on Mars over the last 4 billion years are considered to be similar to the cold ($< 0^\circ\text{C}$) that prevail today (Shuster and Weiss, 2005). If the surface paleotemperature on Mars has averaged 0°C , then $t_{1/2}$ for decarboxylation of glycine in gypsum is estimated to be $\sim 4 \times 10^8$ years based on the Atacama Desert data, $\sim 3 \times 10^8$ years for the Anza-Borrego results, and $\sim 5 \times 10^8$ using the Panoche sample. The Haughton Crater sample indicates significantly faster kinetics with a half-life at 0°C of $\sim 5 \times 10^6$ years. The alanine decarboxylation system yields kinetic half-lives approximately one order of magnitude greater in all samples, $\sim 5 \times 10^9$ years (Red Sea sample), in accord with previous studies (Li & Brill, 2003). If the surface temperature on Mars has averaged -20°C , then the calculated glycine and alanine decarboxylation $t_{1/2}$ values would be much longer, resulting in much greater preservation over billion-year timescales. The apparently shorter half-lives predicted using the Haughton Crater gypsum may be explained by its exposure to either a warmer climate over its history, hydrothermal conditions after deposition, or this may

be the result of more recent amino acid contamination diluting the Z-values. Because of the pristine nature of the Anza-Borrego gypsum, the $t_{1/2}$ values based on this sample are considered the most accurate, although the results from the Atacama Desert, Red Sea, and Panoche Valley agree well with these results. These calculations imply that at modern Martian surface temperatures, amino acids in gypsum should be preserved for periods in excess of several billion years.

The estimated decarboxylation rates in sulfate minerals on Mars are so slow that the limiting factor in the survival of amino acids is likely to be radiolysis in the upper 1-2 meters of the regolith by galactic cosmic radiation (Kminek & Bada, 2006) and UV-induced (Benner et al., 2000) or metal-catalyzed oxidation (Sumner, 2004). The Martian iron-oxide rich soils may provide a barrier against cosmic radiation, and organic material preservation may be increased at greater depths in the regolith. If jarosite is present at these locations, then its high iron content might assist preservation by offering further shielding against radiolysis. While pure crystalline gypsum is transparent to visible and UV light (Parnell et al., 2004), impure Antarctic gypsum crusts are essentially opaque to radiation below 400 nm (Hughes and Lawley, 2003), and a few millimeters of a similar mineral on Mars should be able to shield gypsum from UV penetration. In the absence of UV-light, the contribution of metal-catalyzed oxidation should be minimal. Therefore, amino acids and other organic compounds should be extremely persistent in sulfate minerals at the low temperatures on Mars.

3.5 CONCLUSION

These results demonstrate that amino acids and other organic compounds are well preserved in terrestrial sulfate minerals. Based on these results, it is predicted that organic matter should be preserved over timescales of billions of years on Mars. Amino acids are excellent indicators for the presence of other organic material because they can be detected at very low levels using modern analytical techniques, including those that potentially can be used to carry out space-craft based *in situ* analyses (Skelley et al., 2005). Their structural diversity and chirality may also provide a unique biological signature, making amino acids excellent targets in the search for evidence of life on Mars (Bada, 2001). Investigations of sulfate rich evaporite deposits, such as those seen at Meridiani Planum, should be potential targets for organic compounds on Mars.

ACKNOWLEDGEMENTS

NASA Grant NAG5-12851 supported this work. The authors collected the various samples, with the exception of the Haughton crater sample, which was generously provided by Drs. John Parnell and Pascal Lee. Dr. Bruce Deck determined the isotope and total carbon and nitrogen data at SIO. Tabitha Hensley carried out the strontium isotope analyses and Dr. Ron Amundson shared his extensive knowledge of California's Panoche Valley during this study. This chapter based in part on the following paper:

Aubrey, A.D., Cleaves, H.J., Chalmers, J.H., Skelley, A.M., Mathies, R.A., Grunthaner, F.J., Ehrenfreund, P., and Bada, J.L. (2006) Sulfate minerals and organic compounds on Mars. *Geology* **34(5)**, 357-360.

REFERENCES

- Amelung, W., and Zhang, X. (2001) Determination of Amino Acid Enantiomers in Soil: Soil Biology & Biochemistry, v. 33, p. 553–562.
- Bada, J.L. (2001) State-of-the-art instruments for detecting extraterrestrial life. Proc. Natl. Acad. Sci. U.S.A. 98, 797–800.
- Bada, J.L., Wang, X.S., and Hamilton, H. (1999) Preservation of key biomolecules in the fossil record: current knowledge and future challenges. Philos. Trans. R. Soc. Lond., B, Biol. Sci. 354(1379), 77–87.
- Benner, S.A., Devine, K.G., Matveeva, L.N., and Powell, D.H. (2000) The missing organic molecules on Mars. Proc. Natl. Acad. Sci. U.S.A. 97, 2425–2430.
- Biemann, K., Oró, J., Toulmin, P., III, Orgel, L.E., Nier, A.O., Anderson, D.M., Simmonds, P.G., Flory, D., Diaz, A.V., Rushneck, D.R., and Biller, J.A. (1976) Search for organic and volatile inorganic compounds in two surface samples from the Chryse Planitia region of Mars. Science 194, 72–76.
- Brigham-Grette, J., and Crater, L.D. (1992) Pliocene marine transgressions of Northern Alaska: Circumarctic correlations and paleoclimatic interpretations. Arctic 45, 74–89.
- Cockell, C.S., and Lee, P. (2002) The biology of impact craters – A review. Biological Reviews 77, 279–310.
- Conway, E.J. (1963) Microdiffusion analysis and volumetric error: New York, Chemical Pub. Co., pp. 195–200.
- Ertel, R.E., and Hedges, J.I. (1983) Bulk chemical and spectroscopic properties of marine and terrestrial humic acids, melanoidins and catechol-based synthetic polymers: Aquatic and Terrestrial Humic Materials, *in* Christman, R.F., and Gjessing, E.T., eds., Aquatic and Terrestrial Humic Materials: Collingwood, Ann Arbor Science Publishers, pp. 143–163.
- Gendrin, A., Mangold, N., Bibring, J.P., Langevin, Y., Gondet, B., Poulet, F., Bonello, G., Quantin, C., Mustard, J., Arvidson, R., and LeMouelic, S. (2005) Sulfates in Martian Layered Terrains: The OMEGA/Mars Express View. Science, 307, 1587–1591.
- Glavin, D.P., and Bada, J.L. (1998) Isolation of amino acids from natural samples using sublimation. Anal. Chem. 70, 3119–3122.
- Glavin, D.P., Cleaves, H.J., Schubert, M., Aubrey, A.D., and Bada, J.L. (2004) New method for estimating bacterial cell abundances in natural samples by use of sublimation. Appl. Environ. Microbiol. 70, 5923–5928.
- Glavin, D.P., Schubert, M., Botta, O., Kminek, G., and Bada, J.L. (2001) Detecting pyrolysis products from bacteria on Mars. Earth Planet. Sci. Lett. 185, 1–5.

- Hartley, A.J., and Chong, G. (2002) Late Pliocene age for the Atacama Desert: Implications for the desertification of western South America. *Geology* 30(1), 43-46.
- Hartley, A.J., Chong, G., Houston, J., and Mather, A.E. (2005) 150 million years of climatic stability: evidence from the Atacama Desert, Northern Chile. *Journal of the Geological Society of London* 162, 421-424.
- Hess, J., Stott, L.D., Bender, M.L., and Schilling, J.G. (1986) The Oligocene marine microfossil record: Age assessments using strontium isotopes. *Paleoceanography* 4, 655–679.
- Hughes, K.A., and Lawley, B. (2003) A novel Antarctic microbial endolithic community within gypsum crusts. *Environ. Microbiol.* 5, 555–565.
- Jull, A.J.T., Courtney, C., Jeffrey, D.A., and Beck, J.W. (1998) Isotopic evidence for a terrestrial source of organic compounds found in Martian Meteorites Allan Hills 84001 and Elephant Moraine 79001. *Science* 279, 366–369.
- Kminek, G., and Bada, J.L. (2006) The effect of ionizing radiation on the preservation of amino acids on Mars. *Earth Planet. Sci. Lett.* 245, 1-5.
- Langevin, Y., Poulet, F., Bibring, J.-P., and Gondet, B. (2005) Sulfates in the North Polar region of Mars detected by OMEGA/Mars Express. *Science* 307, 1584–1586.
- Li, J., and Brill, T.B. (2003) Spectroscopy of hydrothermal reactions, part 26: Kinetics of decarboxylation of aliphatic amino acids and comparison with the rates of racemization. *Int. J. Chem. Kinet.* 35(11), 602–610.
- Mancinelli, R.L., Fahlen, T.F., Landheim, R., and Klovstad, M.R. (2004) Brines and evaporites: analogs for Martian life. *Adv. Space Res.* 33(8), 1244–1246.
- Park, L.E., and Downing, K.F. (2001) Paleoecology of an exceptionally preserved arthropod fauna from lake deposits of the Miocene Barstow Formation, Southern California, U.S.A. *Palaios* 16, 175–184.
- Parnell, J., Lee, P., Cockell, C.S., and Osinski, G.R. (2004) Microbial colonization in impact-generated hydrothermal sulphate deposits, Haughton impact structure, and implications for sulphates on Mars. *Int. J. Astrobiology* 3, 247–256.
- Parnell, J., Osinski, G.R., Lee, P., Green, P.F., and Baron, M.J. (2005) Thermal alteration of organic matter in an impact crater and the duration of postimpact heating. *Geology* 33, 373–376.
- Presser, T.S., and Ohlendorf, H.M. (1987) Biogeochemical cycling of selenium in the San Joaquin Valley, California, USA. *Environ. Manage.* 11, 805–821.
- Remeika, P., and Lindsay, L. (1992) *Geology of Anza-Borrego: edge of creation*: Sunbelt Publications Inc., San Diego.
- Shuster, D.L., and Weiss, B.P. (2005) Martian surface paleotemperatures from thermochronology of meteorites. *Science* 309, 594–597.

Skelley, A.M., Scherer, J.R., Aubrey, A.D., Grover, W.H., Isvester, R.H.C., Ehrenfreund, P., Grunthaner, F.G., Bada, J.L., and Mathies, R.A. (2005) Development and evaluation of a microdevice for amino acid biomarker detection and analysis on Mars. *Proc. Natl. Acad. Sci. U.S.A.* 102, 1041–1046.

Squyres, S.W., Grotzinger, J.P., Arvidson, R.E., Bell, J.F., III, Calvin, W., Christensen, P.R., Clark, B.C., Crisp, J.A., Farrand, W.H., Herkenhoff, K.E., Johnson, J.R., Klingelhöfer, G., Knoll, A.H., McLennan, S.M., McSween, H.Y., Jr., Morris, R.V., Rice, J.W., Jr., Rieder, R., and Soderblom, L.A. (2004) In situ evidence for an aqueous environment at Meridiani Planum, Mars. *Science* 306, 1709–1714.

Sumner, D.Y. (2004) Poor preservation potential of organics in Meridiani Planum hematite-bearing sedimentary rocks. *J. Geophys. Res.* 109, E12007.

Whitmarsh, R.B., Weser, O.E., Ross, D.A., et al. (1974) Initial Reports of the Deep Sea Drilling Project, Volume 23, Washington (U.S. Government Printing Office) pp. 601-615; 879-886.

Zhao, M., and Bada, J.L. (1995) Determination of α -dialkylamino acids and their enantiomers in geological samples by high-performance liquid chromatography after derivatization with a chiral adduct of *o*-phthalaldehyde. *J. Chromatogr. A* 690, 55–63.

CHAPTER IV. Southern Australian Saline Lake Sulfates

ABSTRACT

Hypersaline lakes located in Southern Australia contain complex evaporitic mineral assemblages that form as modern deposits. The lakes are set in shallow depressions and form evaporitic deposits due to mineral precipitation during evaporation processes. These systems have recently been suggested as analogs to Martian environments (Benison and Bowen, 2006) and could help to explain the abundant sulfates, jarosite, and high abundance of hydrated minerals detected within the Martian regolith. Although these formations have been geologically profiled elsewhere (Benison and LaClair, 2003), organic inclusions and amino acid stability within these sulfate minerals have not been previously studied and are thus investigated herein. Rates of amino acid racemization are determined through heating experiments for gypsum and jarosite samples and major differences are discussed. Degradation rates are estimated through the quantification of amino acid degradation products and a model to estimate the contribution of protein from extant life and extinct life. Extrapolation of these rates to temperatures characteristic of Mars agree with previous estimates and show that the cold and dry conditions might preserve amino acids well within similar mineral matrices for long geological timescales. The rates of degradation and racemization predicted for Mars are used to predict the evolution of biosignatures over time and lower limit preservation limits.

4.1 INTRODUCTION

Understanding of the geological history of Mars has evolved drastically in the last 10 years due to extensive spectral imaging of the planet's surface from orbit and from landed robotic exploration. It has long been known that Mars experienced some degree of aqueous activity evident by the sulfur isotopes within Martian meteorites, which show fractionation consistent with hydrothermal systems (Farquhar et al., 1998). In situ investigation by the MER rovers has found massive salt deposits within the surface regolith. The presence of abundant gypsum, hematite, jarosite, and salts is compelling evidence that much of Mars was once overlaid with water. This evidence of a warm and wet early Mars, perhaps over 3 billion years ago (Bibring et al., 2006), is apparent by in situ investigation (Squyres et al., 2004) and remote sensing of

erosional features that may be indicative of extensive seas and river and valley networks (Malin & Edgett, 2003).

However, large unknowns still exist such as the reason for the lack of carbonates on Mars and how widespread or long-lasting the aqueous history of Mars actually was. Abundant sulfates and hematite have been remotely sensed for years, both of which have known aqueous deposition formation processes, but the lack of spectral identification of carbonates on Mars was problematic (Blaney and McCord, 1989; Christensen et al., 2000). Carbonates such as siderite should be deposited by the reaction of CO₂ gas and water (Kahn, 1985) and this was suggested to be a major blockade to the warm wet early Mars theory. This may be explained by acidic oceans on a wet early Mars under 0.8-4 bar of CO₂ with high sulfate and iron species concentrations, creating conditions under which carbonates would not have been deposited (Fairén et al., 2004).

The surface mineralogy of Mars as investigated by the exploration Rovers (MER) Spirit and Opportunity have revealed a lot about the geological history of Mars. Abundant salts and gypsum are widespread in many areas of the regolith, presumably deposited by aqueous processes. The existence of gypsum and jarosite, sulfate minerals, along with the lack of carbonates upon the surface of Mars, have led to the propagation of early theories about acidic early oceans which expelled any CO₂ into the atmosphere instead of forming carbonates during evaporation.

The uncertain aqueous history of Mars happened sometime in the ancient past (billions of years ago) and makes it essential to try and predict the stabilities of organic inclusions within these types of mineral deposits. This can be estimated by the analysis of natural samples here on Earth. Samples of gypsum and jarosite from Australian hypersaline lakes offers the chance to examine minerals possibly formed by identical processes on Mars.

The samples from these areas have been suggested to be analogous to Mars in papers by Benison and LaClair (2003) and Benison and Bowen (2006). The primary reason why these samples give clues to past environments on Mars is that the mineralogy is similar and may represent a process whereby evaporitic minerals are precipitated in situ by acidic lakewater or groundwater. These formation processes can be applied to a possible formation on Mars. The Southern Australian saline lakes have deposits of calcium sulfates, magnesium sulfates, jarosite, hematite, chloride, hematite concretions, and gypsum (Benison & Bowen, 2006). The presence

of this diverse suite of minerals shows some degree of similarity to what is contained on Mars and may reflect similar formation mechanisms (Figure 4.1).

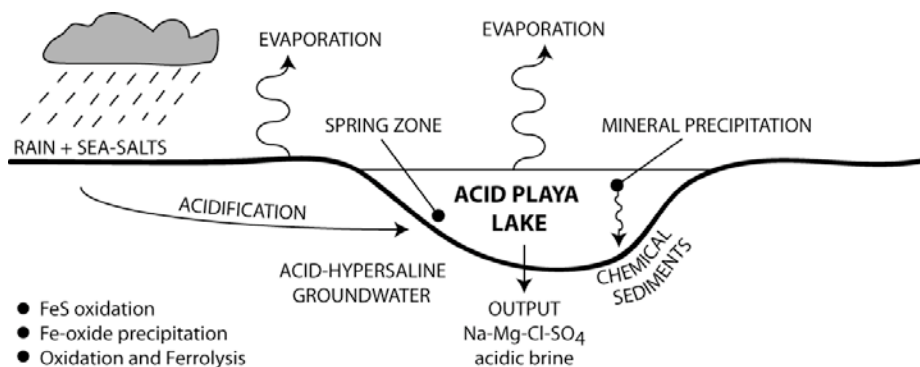


Figure 4.1 Proposed formation model for acid saline lake bottom growth mineral deposits and groundwater flow (after Benison and LaClair, 2003).

The most well studied area is the Tyrrell Basin in Southeastern Australia and is well profiled hydrologically (Macumber, 1992) and geochemically with respect to the formation of evaporite deposits (Long et al., 1992a) and alunite, jarosite, and hydrous iron oxides (Long et al., 1992b). Similar processes have also been observed in acid saline lakes in Southwestern Australia (Alpers et al., 1992).

4.2 MATERIALS & METHODS

Sample Acquisition. Samples were collected in 2001 by Professor Kathy Benison during an expedition to saline lakes in Southeastern and Southwestern Australia. A sample set of 10 samples, listed in Table 4.1, was delivered to Scripps Institution of Oceanography in 2004. Sampling locations are shown in Figure 4.2 along with images of the individual samples analyzed in this study.

Sample Preparation. The samples were surface sterilized with an excess of doubly-distilled H_2O (dd H_2O), then with doubly-distilled 1N HCl (ddHCl), followed by a final rinse with dd H_2O . The samples were allowed to dry overnight in an oven at $60^\circ C$ and then powdered using annealed mortars and pestles. The samples were catalogued in sterile sample vials.

Table 4.1 Southern Australia mineral descriptions of gypsum samples (1, 2, 3, and 7) and mud or sediment samples (4, 5, 6, and 8) delivered to SIO from Kathy Benison.

Sample	pH	Description
1A	2-3	Shallow lake water bottom growth gypsum crystals (2) from Aerodrome Lake near Norseman, Western Australia.
1B		
1C		
1D		
2A	2-3	Shallow lake water bottom growth gypsum crystals (2) from Walker Lake in Narembeen, Western Australia.
2B		
3	2.5	Displacive gypsum crystal from Cumulate Raceway near Norseman, Western Australia
4	2.5	Shallow groundwater precipitated yellow jarosite mud from Twin Lake West near Salmon Gums, Western Australia.
5	2.5	Shallow groundwater precipitated pale yellow jarosite and alunite mud from Twin Lake West near Salmon Gums, Western Australia.
6	acid	Precipitated white alunite mud from Peak Charles Road Lake near Salmon Gums, Western Australia.
7	5.5-6	Shallow groundwater bottom growth displacive gypsum crystals from Cheetham Salt Works at north end of Lake Tyrrell near Sea Lake, Victoria.
8	3.5	Groundwater-precipitate red jarosite-containing subsurface sediment from sandflat at south end of Lake Tyrrell near Sea Lake, Victoria

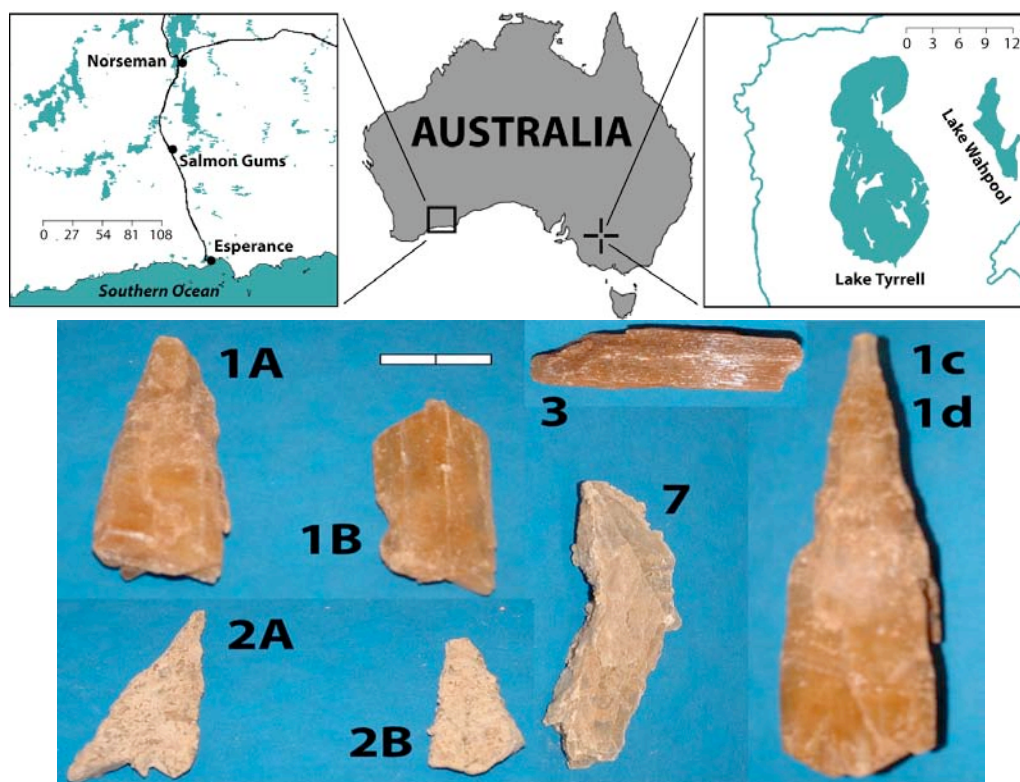


Figure 4.2 Photographs of gypsum samples (scale bar ~ 2 cm) and map of sampling locations below the descriptions of all the samples (Table 4.1). Samples not shown in the picture are samples of mud or sediment (4, 5, 6, and 8).

Amino Acid Analyses. Approximately 250mg of each sample was weighed out into 20 x 150 mm sterile test tubes. 1mL of 6N HCl was added to each sample, the tubes evacuated with nitrogen, and flame-sealed. They were treated at 100°C for 24 hours in order to hydrolyze any proteins and liberate free amino acids from the bound state. The hydrolyzed samples were removed from heat, transferred to 10 x 70 mm test tubes and brought to dryness on a vacuum centrifuge. These dried residues were loaded onto equilibrated desalting columns, flushed with 5 column volumes of water to remove any anions not bound by the desalting columns, and eluted with ~3M NH₄OH. These desalted fractions were collected and brought to dryness in 1.5mL mini-ependorf vials. They were resuspended in 100uL of ddH₂O, of which 10uL aliquots were analyzed by RP-HPLC after pre-column derivatization with OPA/NAC.

Amine Quantification. In order to detect volatile amine compounds, samples were exposed to vapor-phase transfer at 60°C for 6 days. The outer test tube (20 x 150 mm) contained ~1g of sample in 1M doubly distilled NaOH (ddNaOH) while the inner test tube (10 x 12 mm) contained 1mL 0.1M HCl. Over time at these low temperatures, the volatile amines, which are stable in dilute acid, transfer into the small test tube after being liberated from the solid sample at basic pH. These were run by the identical amino acid protocol against standards of methylamine and ethylamine.

Organic fraction analyses. Samples were analyzed for TOC, TON, and stable isotopes after treatment with 2mL of 3M HCl to remove carbonates. ~30mg samples were analyzed using a Thermofinnigan Delta XP-Plus.

Heating Experiments. Heating experiments were conducted on jarosite sediment (Sample 8) and gypsum (Sample 1c) samples with abundant amino acid concentrations. Although heating experiments often do not adequately approximate the rate of racemization or degradation within mineral matrices due to the advanced diagenetic state of the organic material (Williams & Smith, 1977), the samples show abundant fresh organic material with low D/L enantiomeric ratios and should be fairly close to the actual *in situ* rates of degradation and racemization (Heating Experiment results in Appendix A).

4.3 RESULTS & DISCUSSION

All of the samples show light stable carbon isotopes (-24.3 to -39.1) demonstrating minimal carbonate influence due to the acid pretreatment. The pure mineral samples showed low amounts of both TOC (0.0868 – 0.752 mg/g) and TON (<0.024 mg/g) while the sediments and mud showed high values.

Table 4.2 TOC, TON, and stable isotope data for Australian Saline Lake minerals.

	Sample	TOC (mg/g)	$\delta^{13}\text{C}$ (‰)	TON (mg/g)	$\delta^{15}\text{N}$ (‰)
Gypsum	1A	0.311	-27.9	0.020	+1.86
	1B	0.166	-29.3	ND	+1.53
	C / D	0.211	-29.3	ND	+1.633
	2A	0.402	-27.8	0.024	-0.414
	2B	0.752	-26.3	ND	+1.27
	3	0.0868	-39.1	0.018	+0.404
	7	0.553	-26.3	ND	+1.94
Mud/Sediment	Jarosite (4)	1.17	-24.3	0.017	+0.937
	Jarosite (5)	4.82	-27.2	0.104	+0.288
	Jarosite (8)	2.06	-26.0	0.075	+1.97
	Alunite (6)	1.12	-24.8	0.051	+0.436

Note: Samples are reported from a single run after acid treatment.
 ND = <0.01 mg/g (used for TOC/TON ratio)

The sediment samples generally show higher values for both TOC and TON, indicative of organic rich sedimentary deposits. The gypsum TOC values are all consistently low (~0.10-0.311 mg/g) with TON values below the detection limit (0.001 mg/g) in 4 of 7 gypsum samples. These modern gypsum samples show lower carbon and nitrogen abundances than the South Bay modern gypsum, which showed 6.91 mg-C/g and 1.01 mg-N/g (Aubrey et al., 2006), however, the heavy isotopic carbon signature ($\delta^{13}\text{C} = -17.3\text{‰}$) shows that some sediment may have been included.

Table 4.3 Blank and recovery corrected amino acid concentrations (ppm) and amine concentrations (ppb) in Australian saline lake deposits. Some of gypsum sample 3 was lost during sample workup and is not reported. RP-HPLC chromatograms for amino acids and amines in all samples are in Supplementary Information A.

SAMPLE		AMINO ACIDS (ppm)							DEG. (ppm)			AMINES (ppb)		
Matrix	Sample	Asp	Glu	Ser	Gly	Ala	Val	Σ AA	β-Ala	γ-ABA	MA	EA		
Gypsum	1A	20.9	20.6	9.86	16.3	12.7	2.31	82.66	0.451	1.36	78.7	128		
	1B	9.34	9.18	4.51	7.46	5.95	0.728	37.17	0.225	0.589	68.1	95.4		
	1C	14.3	13.8	6.35	8.43	8.89	8.88	60.66	0.0169	0.842	76.0	107		
	1D	14.7	14.3	6.38	8.56	9.18	9.18	62.29	0.0951	0.867	127	94.6		
	2A	8.40	9.47	4.90	11.0	5.97	0.462	40.21	0.215	0.457	88.6	101		
	2B	17.2	20.1	8.81	15.5	11.9	0.599	74.15	0.420	1.058	82.2	171		
Jarosite	7	17.9	18.8	4.88	8.50	10.8	9.38	70.21	0.0497	0.448	257	233		
	4	1.89	4.33	1.22	4.32	3.42	ND	15.18	0.854	3.92	7.28	ND		
	5	13.7	29.8	14.5	36.3	25.7	22.8	142.72	12.8	27.9	ND	ND		
	8	19.7	28.4	12.8	26.3	21.5	21.9	130.51	1.64	3.81	96.6	356		
Alunite	6	0.780	3.69	2.02	5.20	2.66	2.20	16.55	0.848	2.97	ND	32.8		

Note: Modern South Bay gypsum showed glycine and alanine levels of ~1.6 and ~3.2 ppm, respectively. ND = Not Detected above blank levels.

The gypsum samples look to be highly included with bacteria as the amino acid distributions are similar to that of extant bacteria (Chapter 2; Glavin et al., 2001). Further evidence of extant bacterial colonies is the fact that other amino acids that do not tend to persist over geological timescales such as phe, met, lys, and leu are present, showing that the source of the amino acids is most likely thriving bacteria. This is to be expected in these gypsum samples, as these minerals are often highly included with sulfate reducing bacteria (SRBs) in similar lacustrine environments within sediments and the water column (Paskauskas et al., 2005) as well as in gypsum crusts in Antarctica (Hughes & Lawley, 2003) and the high arctic (Parnell et al., 2004). Bacteria have also been suggested to mediate the formation of organosedimentary gypsum minerals (Kobluk & Crawford, 1990).

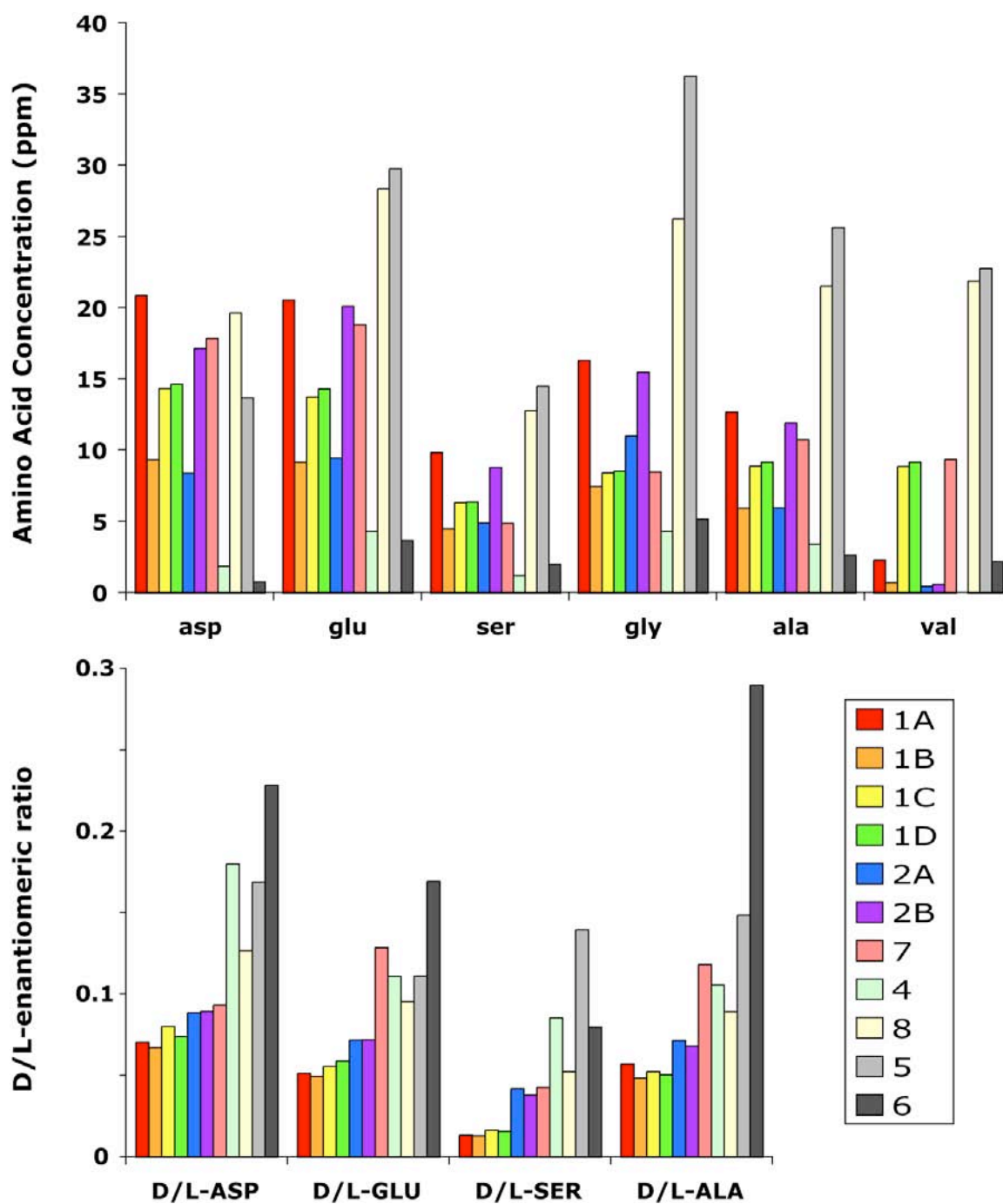


Figure 4.3 Total amino acid abundances (ppm) and D/L-enantiomeric ratios for each sample. Low levels imply well-preserved organic material or the influence of an extant microbial community. Samples 1, 2, and 7 are the gypsum samples while 4, 8, 5, and 6 are jarosite or alunite mud or sediment samples.

4.3.1 Amine abundance as an indicator of diagenetic state

The detection of the degradation products of 4 amino acids (Table 4.4) makes it possible that these formed from the decarboxylation of parent amino acids (Figure 4.4). Methylamine and ethylamine form from the decarboxylation of glycine and alanine, respectively, when heated and are the lowest energy degradation pathway for these amino acids (Li & Brill, 2003). β -Ala and γ -ABA, the decarboxylation products of aspartic acid and glutamic acid, however, are not preferably formed during degradation. Their presence has instead been used as an indicator of biologically mediated decarboxylation (Bada, 1991; Perry et al., 2003). The presence of β -Ala and γ -ABA are well detailed within marine sediments where their abundances increase rapidly with depth (Whelan, 1977) and has been used as a diagenetic indicator and shows the reverse trend with depth of the parent amino acid mole fractions (Cowie & Hedges, 1994).

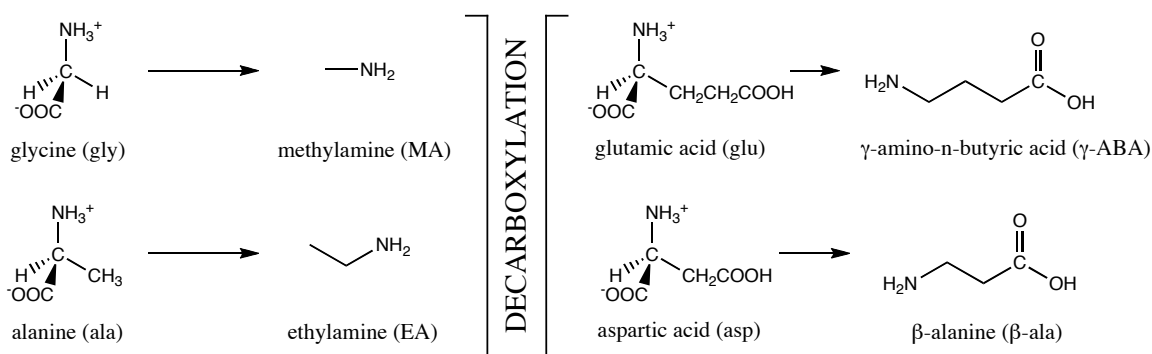


Figure 4.4 Amino acid decarboxylation products (modified from Chapter 1).

Therefore, it seems probable that microbial activity within sediments most likely degrades old organic matter, causing the decarboxylation of aspartic and glutamic acids to form β -Ala and γ -ABA, respectively.

The low abundances of amine products (low ppb) compared to glycine and alanine concentrations (low ppm) indicates that these samples are very young. If we assume that the samples are all ~ 100 years old (modern) and that all the methylamine and ethylamine detected are all from the decarboxylation of alanine and glycine, then the rates of degradation for glycine and alanine are $\sim 1.0 \times 10^{-6} \text{ yr}^{-1}$ and $2.0 \times 10^{-7} \text{ yr}^{-1}$, respectively. These estimates correspond to a lower limit of the rates of degradation because the samples were probably formed more recently than in

the last decade, however, these give ballpark rates of amino acid degradation in various mineral matrices.

The Z-ratio has been used to characterize the relative amounts of amine degradation products to parent amino acid (Aubrey et al., 2006) and can be defined for individual amino acid and degradation product systems as follows:

$$\text{Equation 4.1} \quad Z_{MA+EA} = \frac{[MA + EA]}{[gly + ala]} \quad (\text{Aubrey et al., 2006})$$

$$\text{Equation 4.2} \quad Z_{MA} = \frac{[MA]}{[gly]} \quad (\text{glycine} \rightarrow \text{methylamine})$$

$$\text{Equation 4.3} \quad Z_{EA} = \frac{[EA]}{[ala]} \quad (\text{alanine} \rightarrow \text{ethylamine})$$

$$\text{Equation 4.4} \quad Z_{\beta-ala} = \frac{[\beta-ala]}{[asp]} \quad (\text{aspartic acid} \rightarrow \beta\text{-Ala})$$

$$\text{Equation 4.5} \quad Z_{\gamma-ABA} = \frac{[\gamma-ABA]}{[glu]} \quad (\text{glutamic acid} \rightarrow \gamma\text{-ABA})$$

These designations offer more specific analyses of the relative rates of degradation for each amine and amino acid system. These values are all extremely low for the gypsum samples analyzed (Table 4.4).

Table 4.4 Calculations of Z-ratios from various decarboxylation schemes. All concentrations are in ppm.

	aspartic acid \rightarrow β -Ala			glutamic acid \rightarrow γ -ABA			glycine \rightarrow methylamine			Alanine \rightarrow ethylamine			Aubrey et al. (2006)		
	Asp	β -Ala	$Z_{\beta\text{-ala}}$	Glu	γ -ABA	$Z_{\gamma\text{-ABA}}$	Gly	MA	Z_{MA}	Ala	EA	Z_{EA}	Gly+Ala	MA+EA	$Z_{\text{MA+EA}}$
<u>1A</u>	20.9	0.451	0.022	20.6	1.36	0.066	16.3	0.0787	0.0048	12.7	0.128	0.010	29.0	0.206	0.007
<u>1B</u>	9.34	0.225	0.024	9.18	0.589	0.064	7.46	0.0681	0.0091	5.95	0.0954	0.016	13.4	0.164	0.012
<u>1C</u>	14.3	0.0169	0.001	13.8	0.842	0.061	8.43	0.0760	0.0090	8.89	0.107	0.012	17.3	0.183	0.011
<u>1D</u>	14.7	0.0951	0.007	14.3	0.867	0.061	8.56	0.127	0.0148	9.18	0.0946	0.010	17.7	0.222	0.013
<u>2A</u>	8.40	0.215	0.026	9.47	0.457	0.048	11.0	0.0886	0.0081	5.97	0.101	0.017	17.0	0.190	0.011
<u>2B</u>	17.2	0.420	0.024	20.1	1.058	0.053	15.5	0.0822	0.0053	11.9	0.171	0.014	27.4	0.253	0.009
<u>7</u>	17.9	0.0497	0.003	18.8	0.448	0.024	8.50	0.257	0.0302	10.8	0.233	0.022	19.3	0.490	0.025
<u>4</u>	1.89	0.854	0.452	4.33	3.92	0.905	4.32	0.00728	0.0017	3.42	ND	0	7.74	0.00728	0.001
<u>5</u>	13.7	12.8	0.934	29.8	27.9	0.936	36.3	ND	0.0000	25.7	ND	0	62.0	0	0
<u>8</u>	19.7	1.64	0.083	28.4	3.81	0.134	26.3	0.0966	0.0037	21.5	0.356	0.017	47.8	0.453	0.009
<u>6</u>	0.780	0.848	1.087	3.69	2.97	0.805	5.20	ND	0.0000	2.66	0.0328	0.012	7.86	0.0328	0.004

NOTE: gypsum samples are underlined in the left hand column.

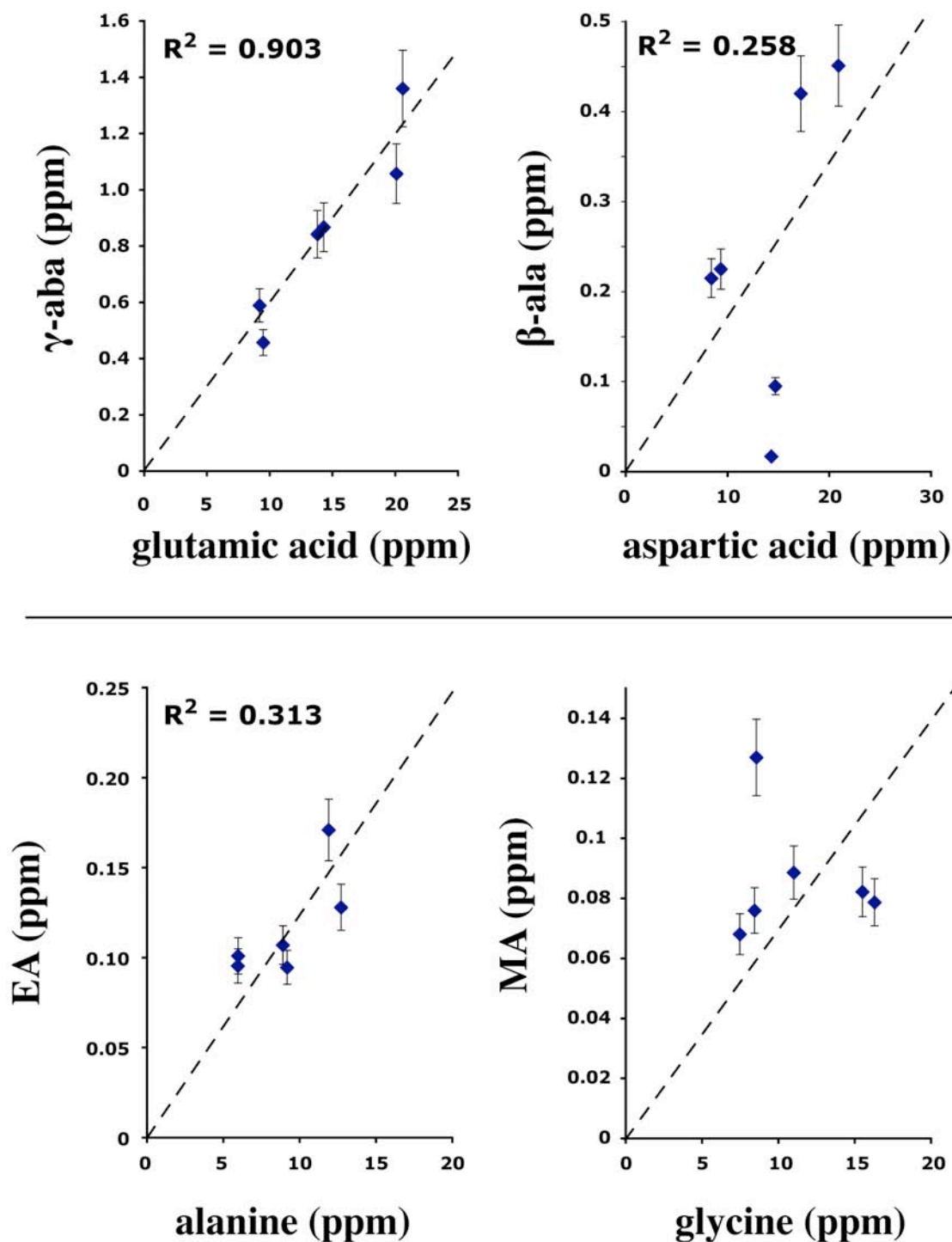


Figure 4.5 Plots of decarboxylation systems (A) β -ala vs. asp, (B) γ -aba vs glu, (C) MA vs. gly, and (D) EA vs. ala. The total amino acids are used in these calculations for asp, glu, and ala. However, this should not make a drastic difference because the D/L-enantiomer ratios are all so low (<0.1 for gypsum samples; Figure 4.3) and the amounts of methylamine and ethylamine decarboxylation products are so low. Error bars represent 10% uncertainty associated with the amine quantifications. Amine chromatograms are shown in Supplementary Information B.

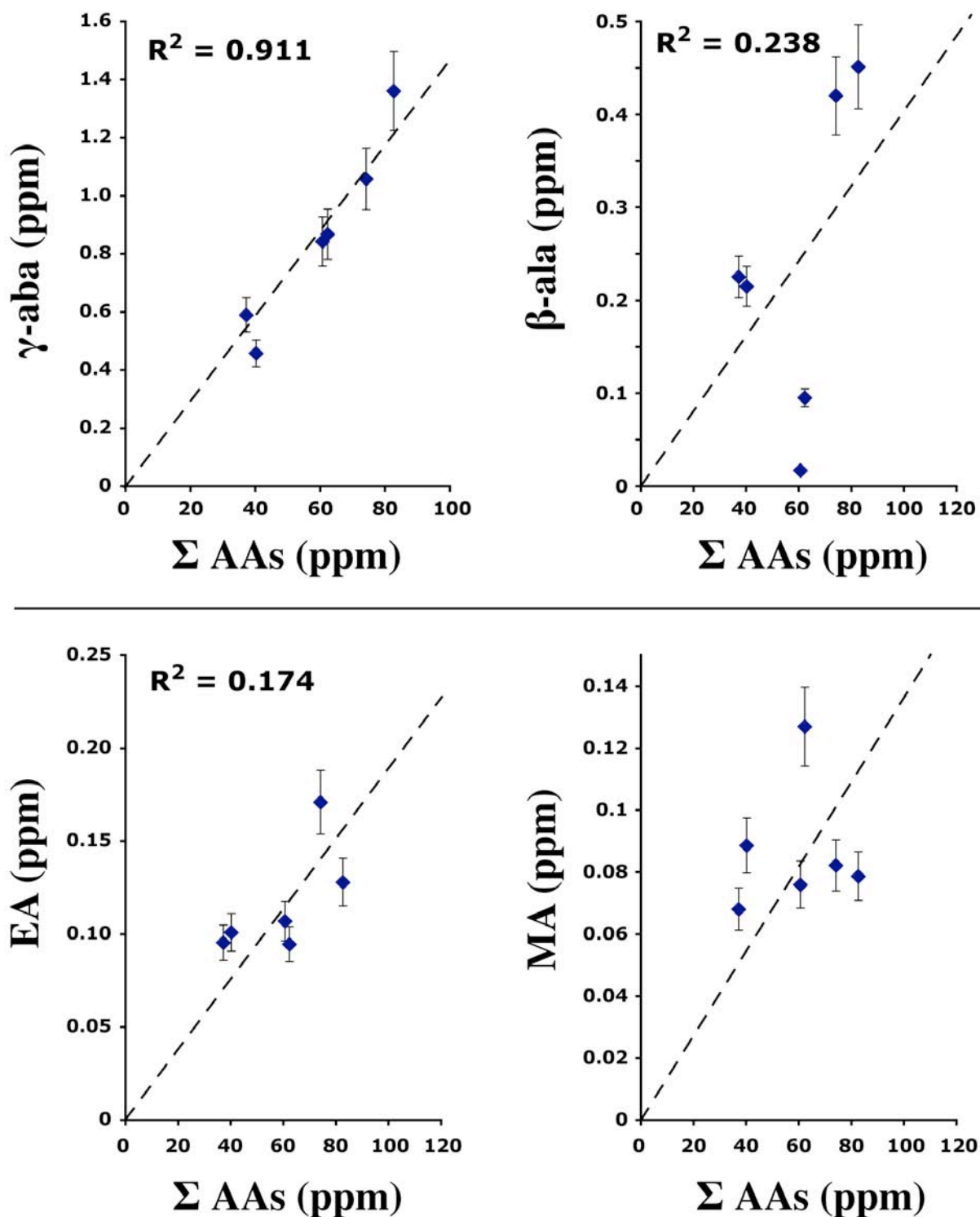


Figure 4.6 Plots of amino acid decarboxylation products versus total amino acids (~biomass) for (A) β -ala, (B) γ -aba, (C) MA, and (D) EA. Alanine is observed to plot linearly with total amino acids, and it also plots linearly with D-alanine. Error bars represent 10% uncertainty associated with the amine quantifications. Amine chromatograms are shown in Supplementary Information B.

The plots of the amine-amino acid degradation products do not show strong linear correlation, but it does appear that the greater parent amino acid concentrations correspond with high amine degradation products generally (Figure 4.5). Plots of the amine products versus total amino acids (roughly equivalent to total cell counts) show similar trends (Figure 4.6). The most consistent system looks to be the glutamic acid and γ -aba trends (figure 4.5) and the γ -aba versus total amino acid trend (Figure 4.6) which plot linearly in both cases. The second most consistent trends are the β -ala trends plotted against the concentration of aspartic acid and total amino acids (Figure 4.6). These show a general trend with parent amino acid and also against the total amino acids. The strong linear trend of this degradation product corresponds to an extant biological community and suggests that the microbial life catalyzes greater amounts of γ -aba formation when cell counts are high.

These trends are all consistent with an extant microbial community with high biodiversity. The microbial activity is approximated by the relative amount of γ -aba and β -alanine. The amine decarboxylation products look more like a cluster and don't plot compared to the parent amino acid or total amino acids. What this shows is that these modern gypsum samples are still too young to have accumulated any appreciable amounts of degradation products because they are highly stable in this environment.

These trends probably reflect the background concentrations of amine degradation products (MA and EA) for a modern sample. Subsequent aging of the microbial community would most likely result in an increase in the amine degradation products relative to the source amino acids. Similarly, the plots versus total amino acids (Figure 4.6) look to cluster in the same areas. The plots of glycine versus methylamine concentrations (Figure 6-A) should show linear trends in a while, 10s or hundreds of years. There is insufficient time for any of this product to accumulate, so the time zero ratios are observed, consistent with low Z-ratios for these modern environments.

If it assumed that the rates of degradation and racemization are fairly similar in these a sample matrices and that the samples formed relatively coincidentally (i.e. modern times), the samples should all plot linearly. The non-linearity of these trendlines suggests that the amines are not proportional to the total parent amino acids.

The Z-ratios have previously been used to determine the decarboxylation rate constant of an ancient sample with a well constrained age (Equation 4.6).

Equation 4.6 $\ln(1 + Z) = k_{DC} \cdot t$

We are assuming that all of the gypsum samples are modern as they are continually forming during evaporation cycles. Therefore, if the samples are all the same age, the Z-ratios should be relatively consistent and the amine degradation products versus the parent amino acids should plot linearly, however they do not appear to show the good correlation of linear trends associated with the total amino acids (Figure 4.6). Likewise, if the Z-ratios are all consistent, then their ages must be identical.

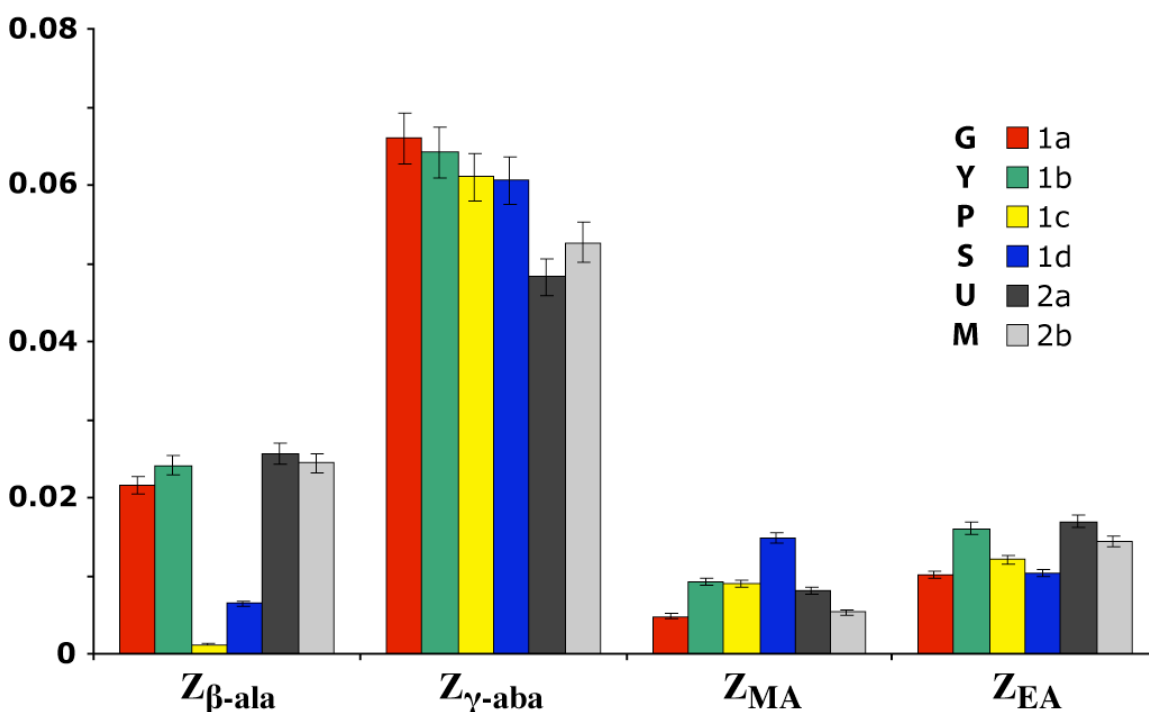


Figure 4.7 Plot of gypsum sample Z-ratios showing the consistency between these samples for all of the decarboxylation systems.

This better shows the consistency between gypsum samples with low to background levels of these decarboxylation products. The average Z-ratios are clustered towards low values in all the samples, however, the much greater concentration⁵ The only significant deviations seem to be in samples 1c and 1d for $Z_{\beta\text{-ala}}$. This could likely be an effect of uncertainty due to

partial coelution with glycine. This seems likely because the other Z-ratios for samples 1c and 1d are so consistent with the others.

Essentially, these samples show the background amine to amino acid ratios present in modern samples. This has been estimated as ~ 0.04 in a modern gypsum sample from South Bay, San Diego (Aubrey et al., 2006) for the Z-ratio in Equation 1, that is the sum of the amine products over glycine plus alanine. The component Z-ratios for the South Bay sample are $Z_{MA} = 0.023$ and $Z_{EA} = 0.055$. This agrees better with the average for Z_{MA} in these modern Southern Australian samples, however both of the time zero ratios are still a factor of 2-3 higher in the South Bay sample.

These multiple modern samples solidify a number of the same order, around 0.01 for Z_{MA} and Z_{EA} at time zero. This will allow for better calibration of the background amines within an extant microbial community and assure for greater accuracy using the relative amine concentrations as a diagenetic indicator.

A qualitative estimate of the relative production of the degradation products β -Ala and γ -ABA compared to methylamine and ethylamine show greater concentrations of the products formed by enzymatic decarboxylation. This can be expected in samples with high concentrations of extant microbial life as they would tend to degrade aspartic and glutamic acids over time within these environments.

It must be mentioned that the alunite (6) and jarosite (4, 5, 8) samples show incredibly high Z-ratios for the enzymatic decarboxylation products. The total amino acids are all highly similar in these microbial communities (Figure 4.3), equivalent to biodensities of $\sim 10^8$ cells/gram (ECE), so it must not be an issue of greater biodiversity causing greater production of these enzymatic decarboxylation products. Rather, this difference might reflect a greater availability of organic matter for the bacteria to degrade.

Another rough estimate to the amount of microbial activity can be gleaned by plotting the diagenetic indicators (β -ala and γ -aba) versus total concentration of organic carbon. These plot amazing well for all the samples with linear trends with fits over 0.7.

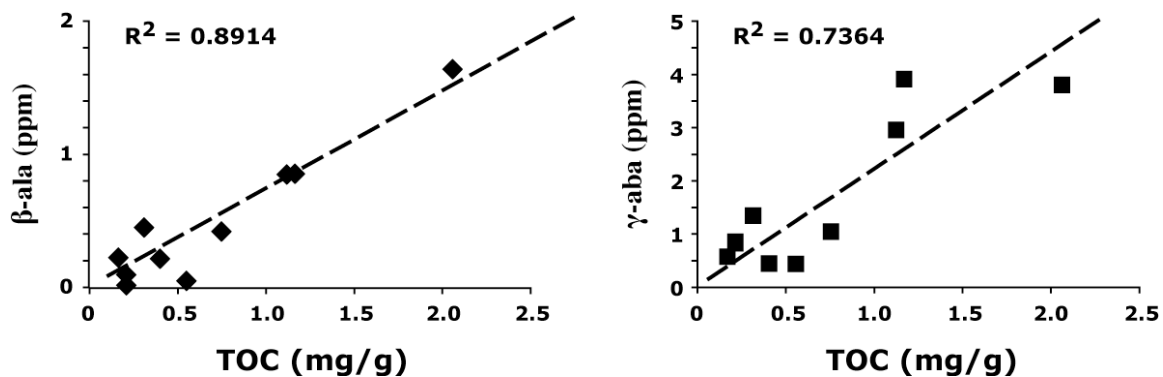


Figure 4.8 Plot of enzymatic degradation products β -ala (\blacklozenge) and γ -ABA (\blacksquare) versus total organic carbon (TOC). The data shows good fit with linear trends. The most organic rich sample, jarosite sample 5 (TOC = 4.82‰) also plotted on these trends (β -ala = 12.8 ppm; γ -aba = 27.9 ppm), but was not included because it was so organic rich.

The plots of β -ala and γ -ABA versus total organic carbon show good correlation with linear trends. Clearly this is showing evidence of a very dense microbial community whose cell count appears to scale with the amount of microbially catalyzed degradation products, β -ala and γ -ABA. These appear to be highly accurate gauges of the biodensity of a sample, especially for the formation of γ -ABA from glutamic acid. The fact that these products also correlate linearly with the total organic carbon supports the idea that these are real trends indicative of biological activity for both the β -ala and γ -ABA systems. In sediments where this correlation has been studied (marine sediments), the amount of β -ala and γ -aba increase with depth very predictably (Cowie & Hedges, 1994). These samples more or less show similar trends for the amino acids, with respect to the increases of the diagenetic indicators β -ala and γ -ABA, similar to previous studies (Cowie & Hedges, 1994). However, with such closed systems like evaporitic gypsum deposits, there may be a limited input after crystal growth, therefore the production of β -ala and γ -ABA may slow eventually, but over significantly long geological timescales.

The wide range of biodensity within similar environments has been reported as 10^3 - 10^7 cells/dm³ within sediments (Paskauskas et al., 2005). Our data fits into this wide range on the upper end of the scale, however, the gypsum itself is host to these microbes, not just the sediments. Therefore, there is the possibility that the gypsum is a product of microbial mediation, similar to previous suggestions (Kobluk & Crawford, 1990), although this cannot be confirmed.

4.4 CONCLUSION

The samples studied herein all show extremely high levels of amino acids. The linear trends against the microbially-catalyzed amino acid products show that these might be a good proxy for bacterial activity indicator of a diagenetic indicator.

These samples show great amino acid preservation overall because all the samples they show very low D/L-ratios and a lack of any appreciable amino acid MA and EA degradation products. The majority of these compounds are consistent with the occurrence of a massive portion of these, may be derived from extant microbial communities as they show low D/L-enantiomer ratios and appear to support extant life. Amino acid in situ degradation rates could be estimated, but there are no known racemization or degradation compounds have been estimated by two independent methods 1) through the detection of amine degradation products and comparison to the levels of amino acids, and 2) through heating experiments determination of Arrhenius parameters and subsequent extrapolation of degradation at ambient temperature. These rates seem to agree fairly well, although the heating experiments offer greater accuracy of degradation rates.

Shortcomings of heating studies to produce accurate rate data, at least for decarboxylation. These should be evaluated against other literature estimates and determined based on their merit. Amino acid degradation may not be as much of a function of mineral type as mentioned before in these types of environments. Degradation might be more strongly a function of the environmental setting and the presence of catalysts, possibly readily available cationic salts in such a highly saline system. The degradation trends observed in both jarosite and sulfate matrices show that this may be the case and the fact that heating experiments show pseudo-first order behavior, the catalyst is shown to be readily available and not limiting in any way.

The stability of amino acids in minerals has been shown to be strongly a function of mineralogy through a series of heating experiments. The estimated rates of degradation are reasonable and compare well to literature estimates. Assuming that the high-temperature heating studies are indicative of the stability of amino acids in natural environments at ambient temperature, the stability of amino acids in general is greater in jarosite sediments than gypsum.

The rates of racemization, however, show a correlation with mineral matrix as gypsum shows slower rates of racemization. The extrapolation of these rates of amino acid degradation in

jarosite and gypsum matrices (Mars T ~ -20°C) lead to degradation rates of $\sim 10^{-12}$ yr⁻¹. This is equivalent to a half-life of degradation around 100 Ma and might preserve amino acids for billions of years in similar matrices on Mars if similar degradation rates were in effect on Mars.

The implication of the formation of gypsum and jarosite precipitated from lacustrine environments shows that similar lake systems would lead to similar physical mineral precipitation. Past environments on Mars may have been similar to these and may have also had organic-rich signatures locked in and perhaps preserved since the time of their formation. Similar gypsum deposits on Mars would offer good targets for organic detection and a high probability of success in detecting chemical biosignatures and may have preserved them for billions of years. Because marine sediments have high concentrations of divalent cations, this may cause many problems for *in situ* instrumentation if these regions are chosen as target sites. Although the organic levels are observed to be high in the mud and sediment samples analyzed in this study, these types of samples, any processing may result in catalytic degradation, as has been observed before in samples with high concentration of divalent cations (Bada, 1971).

ACKNOWLEDGEMENTS

We would like to thank Kathleen Benison and Brenda Bowen for providing us with these samples from the saline lakes of Australia. Also, John H. Chalmers performed the nucleobase quantification and Eric Parker treated and weighed out the samples for TOC/TON analyses. Bruce Deck performed the TOC/TON analyses in the SIO Unified Laboratory Facility.

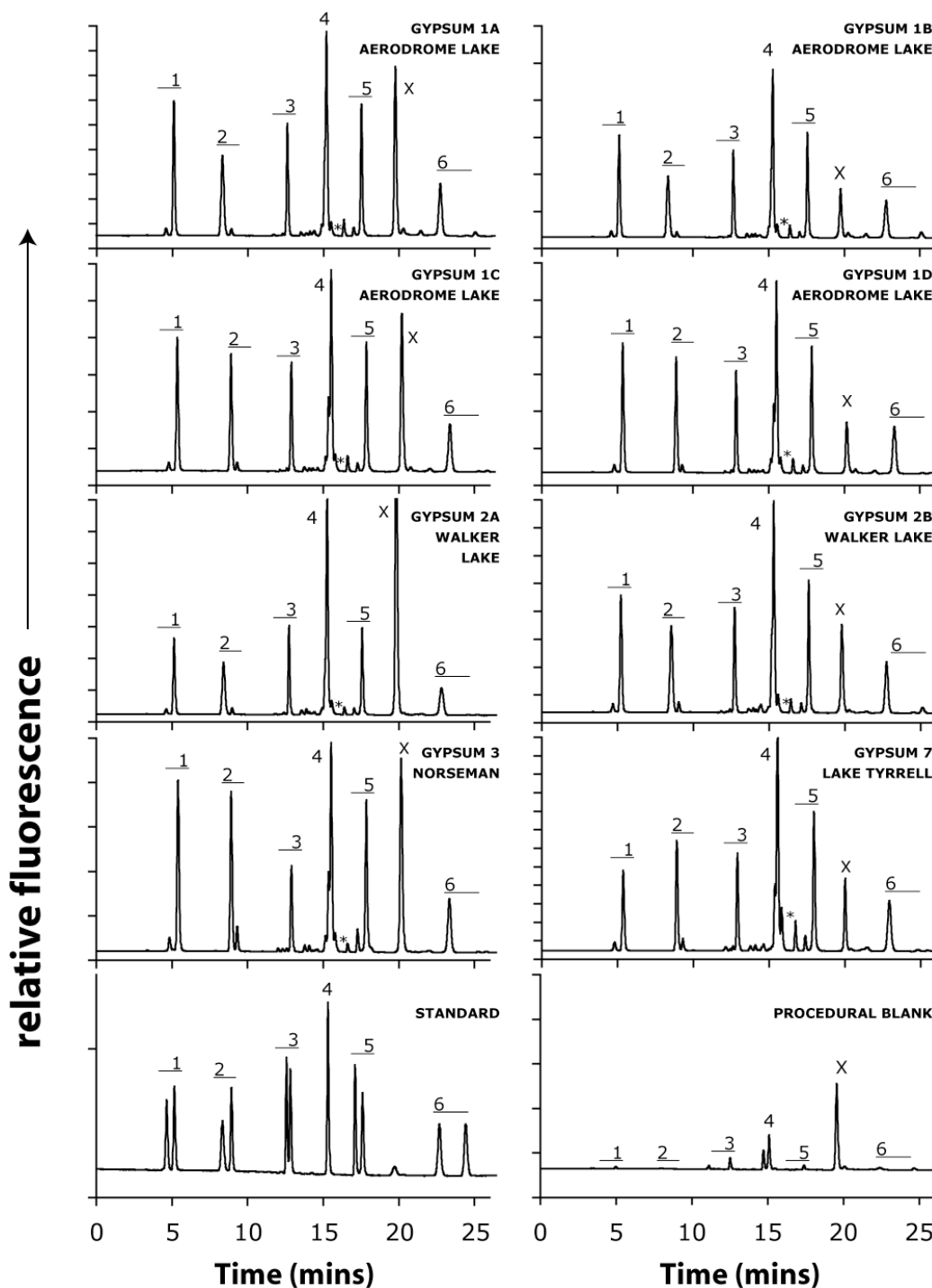
REFERENCES

- Alpers, C.N., Rye, R.O., Nordstrom, D.K., White, L.D., and King, B.S. (1992) Chemical, crystallographic and stable isotopic properties of alunite and jarosite from acid-hypersaline Australian lakes. *Chem. Geol.* 96, 203-226.
- Aubrey, A.D., Cleaves, H.J., Chalmers, J.H., Skelley, A.M., Mathies, R.A., Grunthaner, F.J., Ehrenfreund, P., and Bada, J.L. (2006) Sulfate minerals and organic compounds on Mars. *Geology* 34(5), 357-360.
- Bada, J.L. (1991) Amino Acid Cosmochemistry. *Phil. Trans. Roy. Soc. B Biol. Sci.* 333(1268), 349-358.
- Bada, J.L. (1971) Kinetics of the Nonbiological Decomposition and Racemization of Amino Acids in Natural Waters. *Adv. Chem. Ser.* 106, 309-331.
- Benison, K.C., and LaClair, D.A. (2003) Modern and Ancient Extremely Acid Saline Deposits: Terrestrial Analogs for Martian Environments? *Astrobiology* 3, 609-618.
- Benison, K.C., and Bowen, B.B. (2006) Acid saline lake systems give clues about past environments and the search for life on Mars. *Icarus* 183, 225-229.
- Bibring, J-P., Langevin, Y., Mustard, J.F., Poulet, F., Arvidson, R., Gendrin, A., Gondet, B., Mangold, N., Pinet, P., Forget, F., and the OMEGA team (2006) Global Mineralogical and Aqueous Mars History Derived from OMEGA/Mars Express Data. *Science* 312, 400-404.
- Blaney, D.L., and McCord, T.B. (1989) An observational search for carbonates on Mars. *J. Geophys. Res.*, 94, 10,159– 10,166.
- Christensen, P.R., Bandfield, J.L., Smith, M.D., Hamilton, V.E., and Clark, R.N. (2000) Identification of a basaltic component on the martian surface from Thermal Emission Spectrometer data, *J. Geophys. Res.* 105, 9609–9621.
- Cowie, G.L., and Hedges, J.I. (1994) Biochemical indicators of diagenetic alteration in natural organic matter mixtures. *Nature* 369, 304-307.
- Fairén, A.G., Fernández-Remolar, D., Dohm, J.M., Baker, V.R., and Amils, R. (2004) Inhibition of carbonate synthesis in acidic oceans on early Mars. *Nature* 431, 423-426.
- Farquhar, J., Thiemens, M.H., and Jackson, T. (1998) Atmosphere-Surface Interactions on Mars: $\Delta^{17}\text{O}$ Measurements of Carbonate from ALH 84001. *Science* 280, 1580-1582.
- Glavin, D. P., Schubert, M., Botta, O., Kminek, G., and Bada, J. L. (2001) Detecting Pyrolysis Products from Bacteria on Mars. *Earth Planet. Sci. Lett.* 185, 1–5.
- Hughes, K.A., and Lawley, B. (2003) A novel Antarctic microbial endolithic community within gypsum crusts. *Environmental Microbiology* 5, 555-565.

- Kahn, R. (1985) The evolution of CO₂ on Mars. *Icarus* 62, 175-190.
- Kobluk, D.R., and Crawford, D.R. (1990) A Modern Hypersaline Organic Mud- and Gypsum-Dominated Basin and Associated Microbialites. *Palaios* 5(2), 134-148.
- Li, J., and Brill, T.B. (2003) Spectroscopy of hydrothermal reactions, part 26: Kinetics of decarboxylation of aliphatic amino acids and comparison with the rates of racemization. *Int. J. Chem. Kinet.* 35(11), 602-610.
- Long, D.T., Fegan, N.E., Lyons, W.B., Hines, M.E., Macumber, P.G., and Giblin, A.M. (1992a) Geochemistry of acid brines: Lake Tyrrell, Victoria, Australia. *Chemical Geology* 96, 33-52.
- Long, D.T., Fegan, N.E., McKee, J.D., Lyons, W.B., Hines, M.E., and Macumber, P.G. (1992b) Formation of alunite, jarosite and hydrous iron oxides in a hypersaline system: Lake Tyrrell, Victoria, Australia. *Chemical Geology* 96, 183-202.
- Macumber, P.G. (1992) Hydrological processes in the Tyrrell Basin, southeastern Australia. *Chem. Geol.* 96, 1-18.
- Malin, M.C., and Edgett, K.S. (2003) Evidence for Persistent Flow and Aqueous Sedimentation on Early Mars. *Science* 302, 1931-1934.
- Parnell, J., Lee, P., Cockell, C.S., and Osinski, G.R. (2004) Microbial colonization in impact-generated hydrothermal sulphate deposits, Haughton impact structure, and implications for sulphates on Mars. *International Journal of Astrobiology* 3(3), 247-256.
- Paskauskas, R., Kucinskiene, A., and Zvikas, A. (2005) Sulfate-Reducing Bacteria in Gypsum Karst Lakes of Northern Lithuania. *Microbiol.* 74(6), 715-721.
- Perry, R.S., Engel, M.H., Botta, O., and Staley, J.T. (2003) Amino acid analyses of desert varnish from the Sonoran and Mojave Deserts. *Geomicrobiology Journal* 20(5), 427-438.
- Squyres, S.W., Grotzinger, J.P., Arvidson, R.E., Bell III, J.F., Calvin, W., Christensen, P.R., Clark, B.C., Crisp, J.A., Farrand, W.H., Herkenhoff, K.E., Johnson, J.R., Klingelhöfer, G., Knoll, A.H., McLennan, S.M., McSween Jr., H.Y., Morris, R.V., Rice Jr., J.W., Rieder, R., and Soderblom, L.A. (2004) In Situ Evidence for an Ancient Aqueous Environment at Meridiani Planum, Mars. *Science* 306, 1709-1714.
- Whelan, J.K. (1977) Amino acids in a surface sediment core of the Atlantic abyssal plain. *Geochimica et Cosmochimica Acta* 41, 803-810.
- Williams, K.M., and Smith, G.G. (1977) A critical evaluation of the application of amino acid racemization to geochronology and geothermometry. *Orig. Life Evol. Biosph.* 8, 91-144.

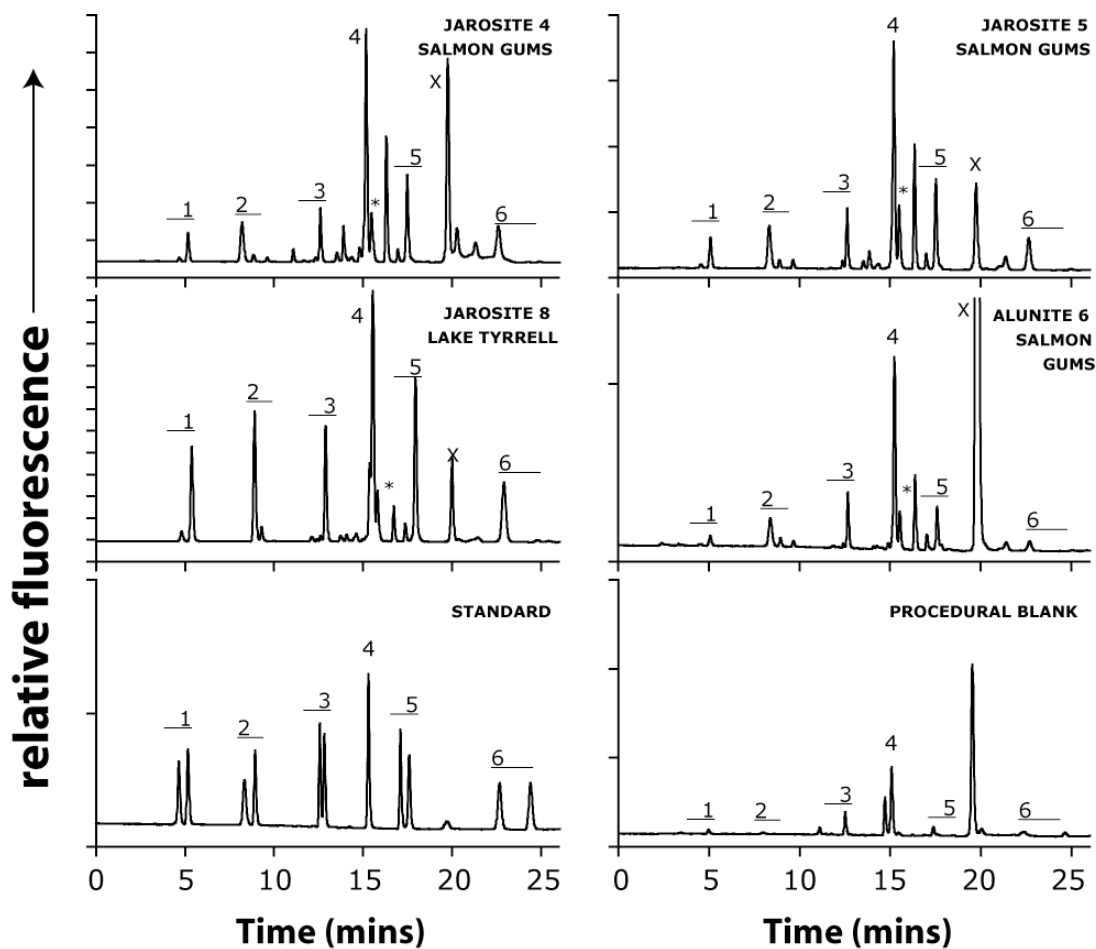
SUPPLEMENTARY INFORMATION 4.A1

0-26 minute RP-HPLC amino acid chromatograms of Southern Australian gypsum samples. 1=D/L-asp, 2=L/D-glu, 3=D/L-ser, 4=gly, 5=D/L-ala, 6=L/D-val, *= β -ala/ γ -ABA, X=residual ammonia peak. Small peaks downfield were also observed corresponding with concentrations of other amino acids (e.g.: phe, met, leu, lys) but were not quantified due to the fact that they were minor compared to other amino acids.



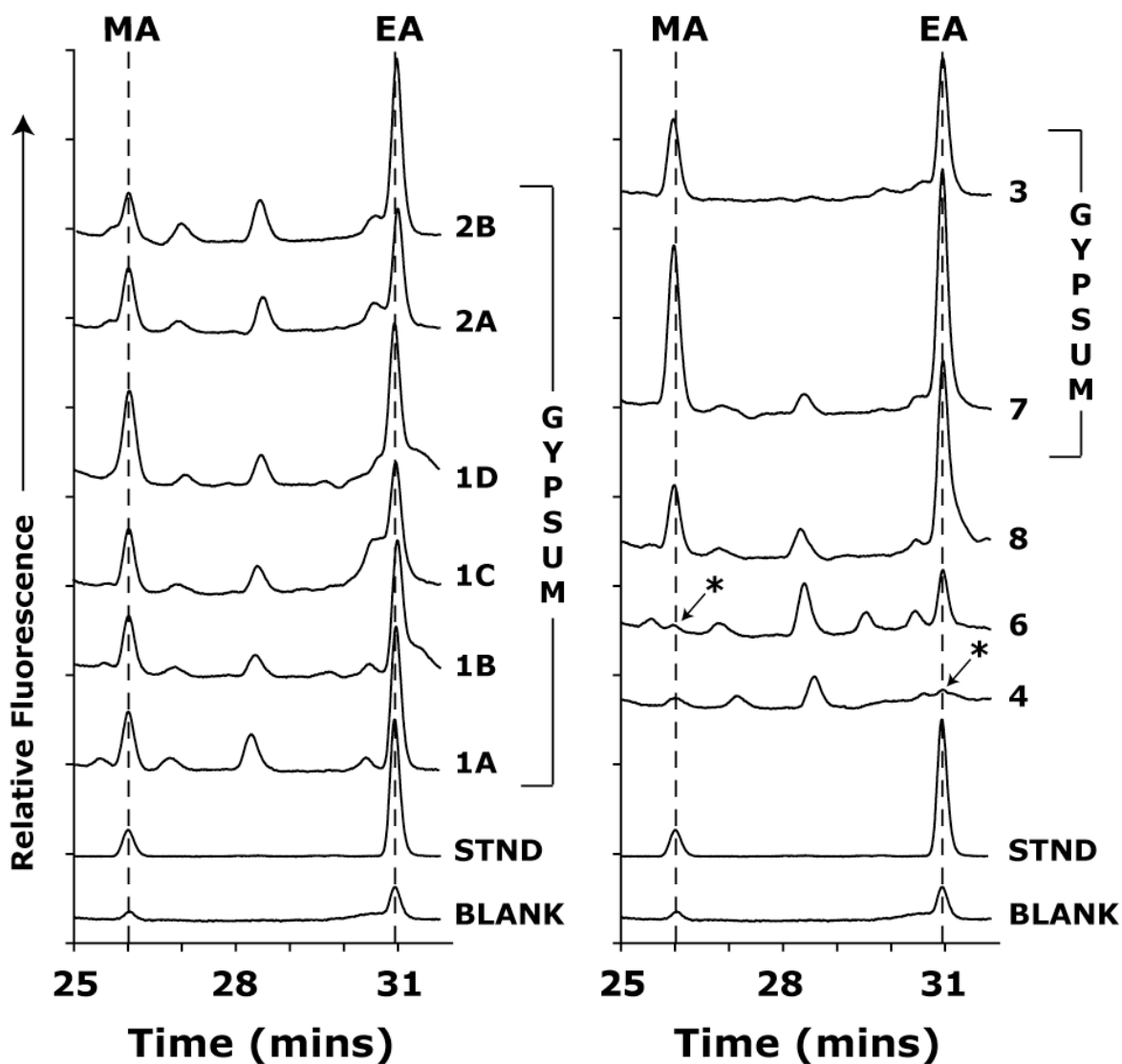
SUPPLEMENTARY INFORMATION 4.A2

0-26 minute RP-HPLC amino acid chromatograms of Southern Australian jarosite and alunite samples. 1=D/L-asp, 2=L/D-glu, 3=D/L-ser, 4=gly, 5=D/L-ala, 6=L/D-val, *= β -ala/ γ -ABA, X=residual ammonia peak. Small peaks downfield were also observed corresponding with concentrations of other amino acids (e.g.: phe, met, leu, lys) but were not quantified due to the fact that they were minor compared to other amino acids.



SUPPLEMENTARY INFORMATION 4.B

25-32 minute RP-HPLC amine chromatograms of Southern Australia gypsum, jarosite, and alunite samples showing peaks for methylamine (MA) and ethylamine (EA). Unidentified peaks represent other amine products (none are known amino acid degradation products) that are volatile under the treatment conditions. Multiple peaks in the target areas were deconvolved using Gaussian distribution fits and only two peaks in non-gypsum samples were below blank levels (*). Amine transfer recoveries based on spiked amine standards for MA and EA were 81% and 68%, respectively, and reported values were recovery corrected (Table 4.4).



CHAPTER V. San Diego County Ironstones as Mars Analogs

ABSTRACT

Many discoveries on Mars have received attention recently due to the influx of geochemical and mineralogical data from the Mars Exploration rovers (MER), however the hematite-rich concretions imaged by the MER Opportunity remain one of the most interesting and perplexing mission discoveries. We report herein new terrestrial analogs to Martian hematite concretions that are found in coastal marine terraces throughout San Diego County. Their geological formation setting is much different than what has been observed elsewhere and perhaps represents a unique sedimentary diagenetic process that may have occurred on the early Martian surface. Similarities between the concretions exposed throughout San Diego County to those found on the surface of Mars are physically and chemically profiled. The presence of organic compounds and visual biological microfossils give strong evidence that they are remnants of an extant microbial community, biosignatures perhaps from the time of the ironstone formation. High degrees of similarity between concretions from six deposits in San Diego county in amino acid concentrations, distributions, enantiomeric ratios, and organic carbon and nitrogen suggests that their formations were coincident over geological timescales. The estimated average age of the ironstone cores of 100 ± 20 ka places their formation during a period in the quaternary of enhanced precipitation and emphasizes the importance of prevailing climatic conditions on the formation process. Organic components within these concretions are emphasized because they have been suggested as geological targets for both the 2009 NASA MSL and 2013 ESA ExoMars missions in the search for life on Mars.

5.1 INTRODUCTION

The Meridiani Planum region of Mars has been identified as an area extremely rich in crystalline hematite *via* remote sensing by the Mars Global Surveyor (Christensen et al., 2000). The unique mineralogical signature and evidence of recent aqueous activity made it a primary target as a landing site for the MER Opportunity (Golombek et al., 2003). The presence of hematite alone may indicate aqueous processes because most formation mechanisms require water (e.g. Christensen & Ruff, 2004), however, there are known non-aqueous deposition mechanisms (Christensen et al., 2000) that must be considered.

One of the most interesting finds by Opportunity in the Meridiani Planum region were millimeter-scale iron-rich concretions called ‘blueberries’ scattered upon the Martian surface and within the surface soil (Squyres et al., 2004a; Squyres et al., 2004b, Soderblum et al., 2004). These features were investigated with the alpha-particle x-ray spectrometer (APXS), pancam, and Mössbauer spectrometer to determine their distribution and composition. The concretions were determined to be extremely high in iron oxide through APXS measurements (Rieder et al., 2004). The Mössbauer spectrometer characterized hematite as the primary iron phase with minor amounts of olivine, pyroxene, and jarosite and was determined as the major source of the region’s ubiquitous hematite signature (Klingelhöfer et al., 2004). Investigation of these concretions with the rock-abrasion tool (RAT) revealed relatively homogeneous concretion interiors.

Terrestrial iron concretions, formed via the flow of groundwater through porous rock and subsequent exit along cracks and fissures, have recently been suggested as analogs to the Martian ‘blueberries’ (Chan et al., 2004; Morris et al., 2005). Precipitated iron oxides mobilized by groundwater flow constitute a significant portion of these concretions, often in the form of hematite. The discovery of hematite concretions upon Mars may therefore be strong evidence of aqueous processes as water is thought to be necessary for their diagenetic formation (Squyres et al., 2004a). Further evidence of past aqueous activity includes the presence of abundant salts and sulfates via *in situ* (Klingelhöfer et al., 2004) and remote sensing (Gendrin et al., 2005).

Southern California contains a variety of raised marine shorelines formed in the late Quaternary due to fluctuations of sea level and climate (Kern & Rockwell, 1992). Unique features within these terraces are small millimeter-scale concretions within the host paleosol (Emery, 1950). These concretions, called ironstones, are similar in size and morphology to the Martian ‘blueberries’ and are ubiquitous throughout San Diego County (Abbott, 1981). Exposed outcrops throughout San Diego County offer perfect locations to observe and sample these concretions within beach ridges of varying geological age.

A comparison between the Martian blueberries and the proposed ironstone concretion analogs show a high degree of visual similarity to the images taken by the MER Opportunity (Figure 5.1). Images of the Martian concretions within the Burns Cliff sedimentary formation (1A) indicate that they form as diagenetic products and are subsequently exposed after weathering and subsequent erosion (McLennan et al., 2005). The largest two blueberries in the bottom half of the image show a perfectly spherical deposit (RHS) adjacent to an eccentric

shaped concretion (LHS). Terrestrial ironstones hosted within silicate sandstone cliffs occur in dense distributions around San Diego County (1B).

After the formation of blueberries within sedimentary deposits at Meridiani Planum, these spherules are weathered out and become scattered on the ground (1C), and the same is observed after erosion of ironstone concretions (1D). The weathering of the old concretions from the sedimentary cliffs leave ‘vugs’ where they were formed in situ (1E), and similar cavities are observed at Sunset Cliffs, San Diego (1F). A minor difference between the Martian blueberries and the San Diego ironstones are their interiors. The Martian blueberries show completely homogeneous interiors (1G) while the ironstones show evidence of light layering (1H). Another physical difference involves the more indurated Martian host matrix compared to the loosely consolidated ironstone host paleosol. This difference can be explained by the evolution of a sedimentary cliff in a more desiccated environment like Mars’ cold and dry climate where water is unstable at the surface. A rapid desiccation of the terrestrial soil matrix, similar to petrification or silicification, could possibly cause more induration. Both of these differences are discussed in more detail in the formation section.

The San Diego County ironstones are found within beach ridges located on San Diego’s marine terraces of varying formation age and products of a previous era (Abbott, 1981). The ironstones are ubiquitously present within a discrete paleosol horizon below finely granulated loamy sand, cemented by iron oxides (Emery, 1950), and are best developed within Pleistocene sandstone that formed as ridges atop the marine terraces of San Diego. These concretions are present above a sandy silt and clay layer atop an iron and silica-cemented hardpan (Abbott, 1981), which may have significantly limited drainage during precipitation events and allowed water to persist in the upper soil horizon for long periods.

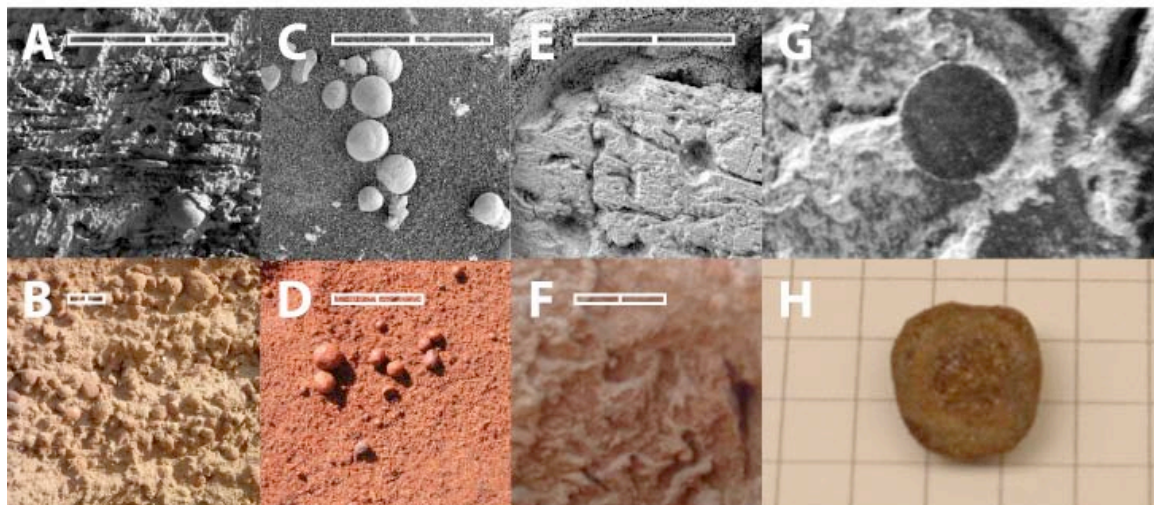


Figure 5.1 Comparison between Mars ‘blueberries’ and San Diego ironstones. Scale bars represent 2cm (A=Sol 152 Image ID# 1M141691232, B=Sunset Cliffs ironstones, C=Sol 257 Image ID# 1M150998322, D=UCSD Canyon ironstones, E=Sol 152 Image ID# 1M141690116, F=Sunset Cliffs matrix, G=Sol 34 Image ID# 1M131212713, H=Interior of large Sunset Cliffs ironstone).

The source of the iron was most likely iron-rich groundwater which led to the formation of the ironstones and an iron-rich subsurface horizon, ~ 1 m below surface containing the ironstone concretions. Exposed locations of these ironstones (Figure 5.2) have been mapped by Emery (1950), including his interpretation that these concretions are *in situ* formations based on three lines of evidence: 1) the even thickness of the concretionary layer, 2) ironstones observed at variable stages of formation, and 3) sand grains from the host marine terraces are included within the concretions. The major components of included sand from the Linda Vista Terrace and Mount Soledad ironstones are magnetite, hornblende, and epidote (Emery, 1950), the surfaces of which are iron-stained. Another observation supporting *in situ* ironstone formation is the lack of any sorted distribution, as any physical transport process would have resulted. They were probably formed very soon after the deposition of the host sedimentary layer because the ironstones never occur within slopes and valleys cut within the beach ridges and the fact that only small amounts of silt and clay (weathering products) are included in the ironstones (Emery, 1950).

Because of the geologic and climatic importance of the evolutionary history of the terraces (Lal, 2004), several attempts have been made to put them in a chronological framework within historical climatic variation and sea-level changes. Based largely on the amino-acid

racemization ratios in fossil mollusks from the marine sand deposits, Kern and Rockwell (1992) give a chronology of 16 shorelines in the San Diego County ranging from 80 ka to 1.29 Ma. The only radiometric chronology is for the upper Pleistocene Nestor terrace (Ku and Kern, 1974), one of the younger marine terraces, based on $^{230}\text{Th}/^{234}\text{U}$ ratios in fossil mollusks; the age estimated is 120 ± 10 ka. These age estimates place upper limits on the ages of the ironstones assuming that they formed sometime after the host soil deposition.

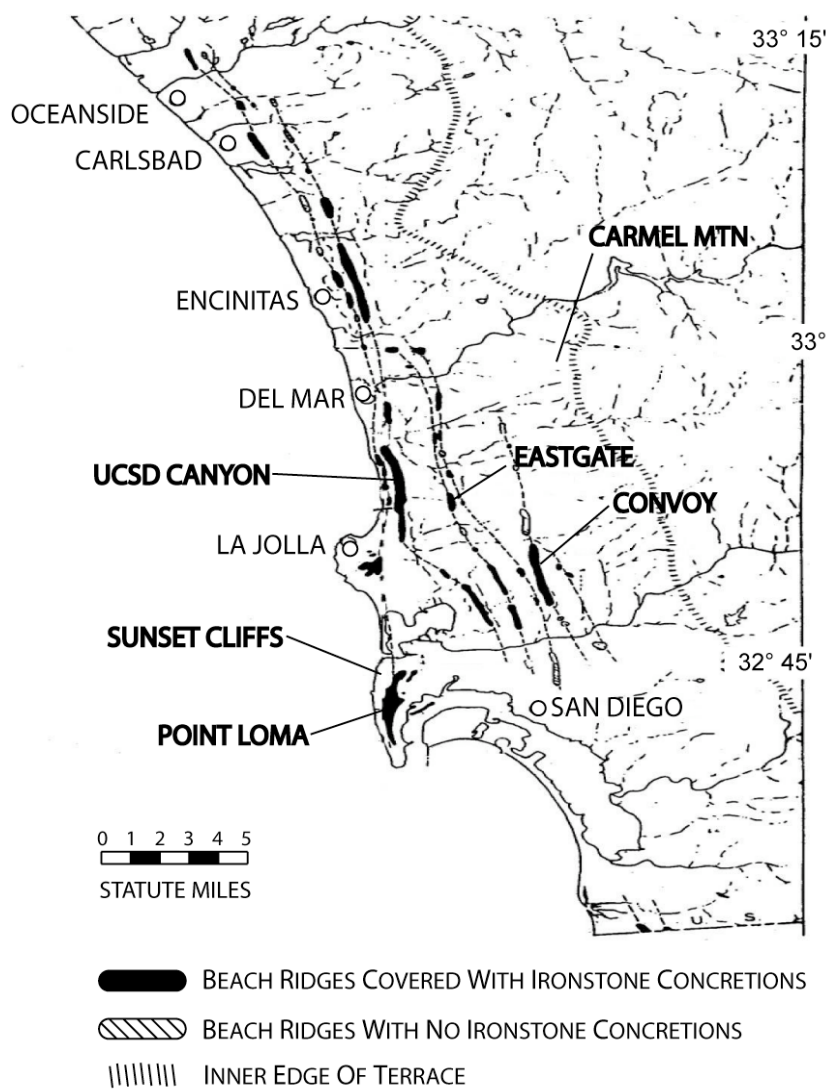


Figure 5.2 San Diego county ironstone deposits and Sunset Cliffs sampling location (modified from Emery et al., 1950).

5.2 MATERIALS & METHODS

The ironstones were collected from 6 known deposits of exposed beach ridges: Point Loma, Sunset Cliffs, UCSD Canyon, Eastgate, Convoy, and Carmel Mountain (Figure 5.2). These samples were catalogued in the laboratory, after which the ironstone deposits were physically and geochemically characterized with a rigorous analytical approach (Figure 5.3).

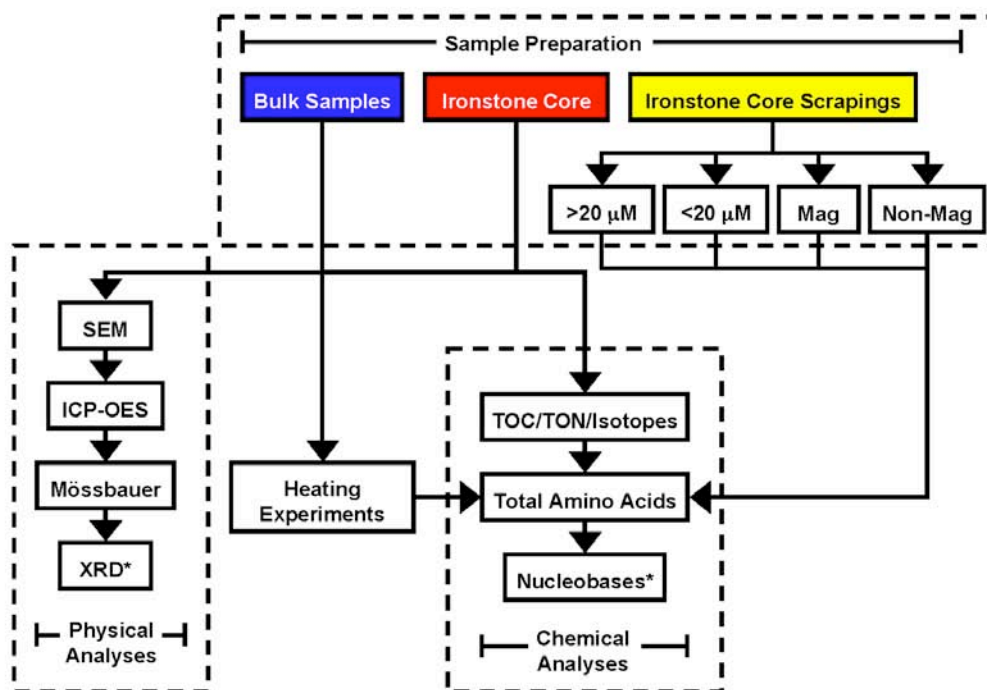


Figure 5.3 Flowchart of amino acid sample processing. Asterisks (*) represent inconclusive results for XRD and nucleobase analyses.

5.2.1 Sample Preparation

The collected ironstones were each surface rinsed with doubly distilled water (ddH₂O), 1M ddHCl, and a final rinse with ddH₂O. After surface cleansing, each ironstone was crushed with sterile annealed mortars and pestles (500°C, 24 hours), placed in a sterile vial, and catalogued as small (~2mm), medium (~5mm), or large (~1cm) ironstone bulk samples.

Studies were conducted on three different portions of the ironstones. Initial measurements were made on the bulk samples after surface cleansing as detailed above. The second measurements were conducted on the inner core of the ironstone samples which were prepared with a small diamond-bladed rock saw by cutting large concretions in half (catalog other

half) and isolating the core by trimming away the outer portions. This preparation effectively isolates the innermost core samples in order to eliminate any modern surficial contamination and to probe the older biological material. After surface cleaning each core samples as outlined above, they were powdered using sterile mortars and pestles, during which any remaining remnants of the outer layers, such as large sand grains, were separated and disposed of at this point. Scrapings isolated from the innermost core of UCSD Canyon ironstones were separated based on grain size into two fractions (<20 μM and >20 μM). Another interior core scraping was taken from Sunset Cliffs, San Diego, isolated into magnetic and non-magnetic fractions, presumably based on the presence of magnetite as an iron phase.

5.2.2 Physical Characterization

Bulk Composition Analyses. Characterization of San Diego ironstone samples was conducted at the Scripps Institution of Oceanography's Unified Laboratory Facility using the X-ray diffractometer (XRD) and scanning electron microscope (SEM). Bulk and interior powdered samples were analyzed by X-ray diffraction (XRD) using a Scintag XDS-2000 powder diffractometer to attempt identification of primary crystalline mineral phases. Wide scanning ranges were used ($\sigma = 0-90^\circ$) in order to cover a wide range of unknown phases, especially in the iron oxide region(s). High-resolution scanning electron (SE) and backscatter electron (BSE) pictures were imaged with the SEM and analyzed for composition using energy dispersive X-ray spectroscopy (EDS). Using these methods, 2 large ironstone halves were compared to 3 standard samples during SEM investigations. Ironstone halves were prepared as SEM targets by first smoothing stepwise from 400 to 1200 grit sandpaper. Treatment with a fine diamond polish (5 μm) smoothed the surface to a luster. These ironstone surfaces were targeted at 50-60x magnification for the SE, BSE, and EDS surface mapping of the interior Sunset Cliffs ironstone. Only the core of the Convoy ironstone was analyzed, however these compositions are assumed to be generally indicative of the compositions of the various ironstone deposits. A limited number of SEM analyses of the ironstone halves were analyzed at magnifications from 300-2400x to analyze the composition of individual iron grains. In order to characterize the purities of individual grains, they were compared to standards purchased from Wards of micaceous gray hematite (46E3876), red hematite (46E0946), and oolitic hematite (46E3866).

Mössbauer Spectrometry. Analyses for the primary iron phases via Mössbauer spectrometry were conducted on ironstone samples at the Department of Geology and Geography at Mount Holyoke College in South Hadley Massachusetts. A small set of ironstone (6 samples) interior powdered samples was analyzed using this technique and compared to Mössbauer spectra from the MER Opportunity. These results, methods, and brief analysis are summarized at the end of this chapter (Supplementary Information 5.A).

Microfossil Analysis. Thin sections of ironstones (0.22µM width) were analyzed at University of California Los Angeles using Scanning Electron Microscopy (SEM) at magnifications from 500-2000x to look for visual bacterial remnants and the presence of carbon. Most of this data appear elsewhere (Lal et al., submitted).

5.2.3 *Chemical Characterization*

Organic Reservoir Characterization. Bulk chemical characterization of total organic carbon (TOC), total organic nitrogen (TON), stable isotopes ($\delta^{13}\text{C}$, $\delta^{15}\text{N}$), amino acids, and nucleobases was conducted at Scripps Institution of Oceanography on bulk and interior ironstone samples. The bulk sample set analysis was conducted on an equal size distribution of 18 ironstones from Sunset Cliffs, San Diego (6 each small, medium, large). The entire interior ironstone sample set consisting of 45 samples from each of the 6 sample deposit sites were also analyzed by these methods ($n \geq 3$ for each locale). Analyses for amino acids were conducted on the various size fractions from the UCSD sampling location and on Sunset Cliffs magnetic and non-magnetic fractions.

TOC and TON were determined using a Costech elemental combustion C-N analyzer on approximately ~50mg of sample. Carbon and nitrogen isotopic ratios were determined on the identical sample with a Thermofinnigan Delta-XP Plus stable isotope ratio mass spectrometer. In order to remove any carbon contribution from carbonate, ~200mg of each sample was pre-treated with an excess of 2N doubly-distilled HCl (~2mL) and dried down on a vacuum centrifuge before analyses (~50 mg) for total organic carbon (TOC) and nitrogen (TON).

Amino acids were extracted by direct acid hydrolysis (6 N HCl, 24 hours, 100°C) on ~250mg of each powdered sample after evacuating with nitrogen. The supernatant fractions were desalted by methods similar to Amelung and Zhang (2001) after evaporation of the 6N HCl from the liquid fractions on a vacuum centrifuge. Extracts were analyzed for amino acids by reverse-

phase high performance liquid chromatography (RP-HPLC) after pre-column derivatization with *o*-phthaldialdehyde/*N*-acetyl L-cysteine using a Shimadzu RF-530 or RF-535 fluorescence detector (Zhao and Bada, 1995) and a Phenomenex Luna C-18(2) column (250 x 4.6 mm). Quantification of amino acids included background level correction using a procedural blank and a comparison of the peak areas with those of amino acid standards (asp, glu, ser, gly, ala, val), including the quantification of 5 enantiomeric (D/L) pairs. Ironstone water extracts (24-hour, 100°C) were analyzed by identical HPLC methods following vapor-phase hydrolysis in 6N ddHCl for 24-hours. No amino acids were detected by this technique. Heating experiments were also conducted to determine the approximate degradation rates of amino acids within ironstone matrices, however, oxidation at high temperatures was observed (Appendix B).

Nucleobase Determination. In order to investigate the possible presence of bacterially derived material in the various minerals, determinations of nucleobase concentrations were carried out. 250mg samples were extracted by treatment with 1 ml of 95% formic acid solution for 24 hours at 100°C. Sample extracts were run using RP-HPLC with UV-absorbance detection ($\lambda = 260\text{nm}$) against known standards (AGCTU) and evaluated based on enumerated bacterial cell densities (*E. coli* equivalents/g) as described in Glavin et al. (2004). Nucleobase analyses were also conducted on a 24-hour formic acid hydrolyzed fraction of the 24-hour water extract. No nucleobases were detected by either of these methods.

5.3 RESULTS & DISCUSSION

The diameters of the Sunset Cliffs ironstones vary from small (~2-5mm) to medium (~5-10 mm) to large (~10-30 mm) with a median 5-10 mm diameter. A previous size distribution study of ironstones from the Linda Vista locality showed the average concretion size to be ~9mm up to a maximum of 30mm (Emery, 1950). This size distribution agreement between two well-profiled sites is generally similar at all deposits throughout San Diego County. The exception are ironstones from the UCSD Canyon locale, where size distributions are biased towards larger diameter concretions, ~10-15 mm on average. The majority of the ironstones are spherical with even interior layering. SEM images of polished interior ironstone surfaces (Figure 5.1) show darker nuclei, representing zones of initial growth surrounded by lighter toned coloring, however. Although the ironstones do show signs of layering, with darker nuclei surrounded by lighter toning, however the ironstones still show high similarity to the Martian blueberries. The slightly

oblate ironstones are always oriented with the layering heaviest layering on the bottom (extracted from in situ layers), suggesting that the direction of maximum growth was vertically downwards.

5.3.1 *Physical Analyses*

X-ray diffraction (XRD) studies on the Sunset Cliffs ironstones were inconclusive in regards to the mineral phases present, as these concretions are host to a variety of oxidized elements including Fe, Ti, Si, and Mn. Strong bands for magnetite and hematite (Fe_2O_3) were expected as primary iron phases, but they were either masked by interference from a mixed-mineral matrix or revealed the amorphous nature of the iron oxides. Emery (1950) attributed the majority of the oxidized iron-phases to hematite (Fe_2O_3) based on iron-phase analyses (up to 15% by weight).

Mössbauer spectrometry analyses of powdered bulk ironstone samples show spectral similarities to the Mars Berry Bowl analyses (Supplementary Information 5.A). The MER Opportunity Mössbauer data analyses on localized areas of Meridiani Planum are the primary reason that the region's abundant surface hematite signature is attributed to the presence of Martian blueberries (Klingelhöfer et al., 2004). The hematite detected within San Diego ironstones by Mössbauer spectrometry as a primary iron phase and possible detections of jarosite and goethite are indicative of the mixed iron phase, similar to the mineralogy detected in situ on Mars.

A SEM mosaic of a bulk Sunset Cliffs ironstone (Figure 5.4) shows major element composition of oxygen (39.8%), silicon (26.2%), and iron (19.3%). The average EDS element compositions (18 spectra total) have standard deviations less than 5% for silicon and oxygen while the iron standard deviation is around 13%. The large percentage of silicon is due to the inclusion of sand grains during the ironstone concretions. The iron signature is due to precipitated iron oxides primarily in the form of Fe_2O_3 , and inclusion of magnetite grains during accretion, which are primary heavy minerals in the ironstone host matrices (Emery, 1950). There seems to be no compositional trend between the interior of the ironstones and the exterior portions for the Sunset Cliffs sample suggesting that the ironstone formation resulted in homogeneous accretion. Each of the 18 SEM analyses revealed sand grains included within the ironstone matrix (Figure 5.4 – Red). The iron concentrations (Figure 5.4 – Green) are more difficult to discern but are composed of smaller groupings of iron-enriched areas.

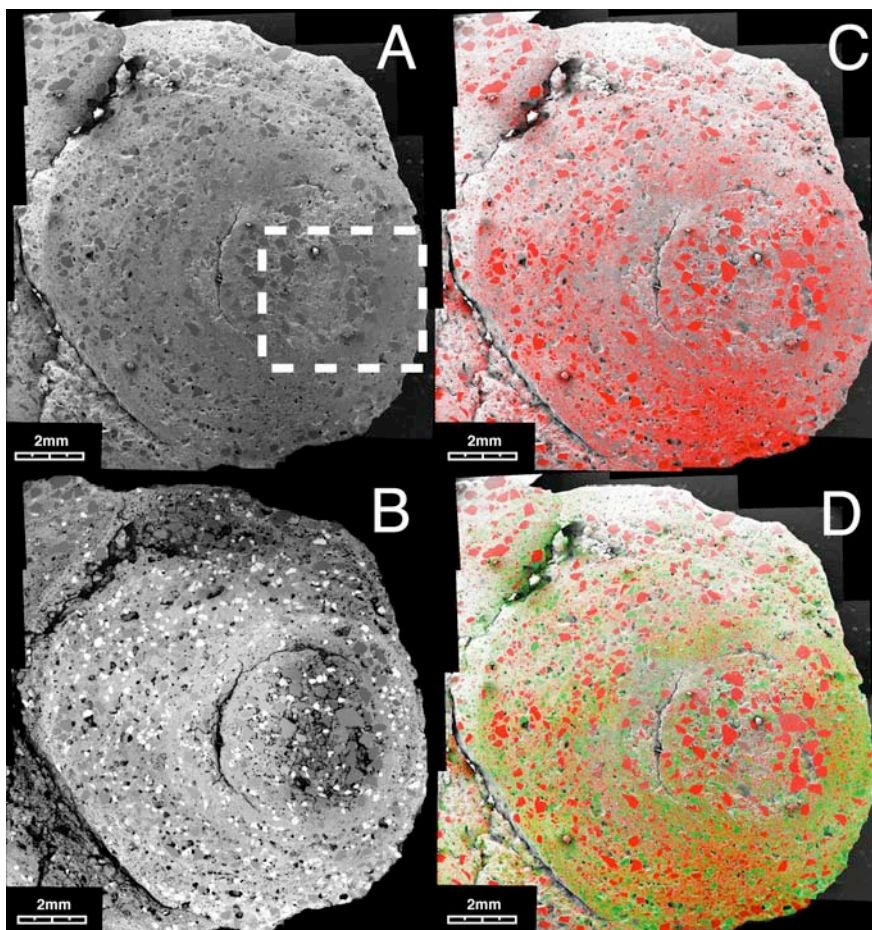


Figure 5.4 60x magnified Sunset Cliffs ironstone SEM 18-image mosaic showing (A) scanning electron image, SE, (B) backscatter electron image, BSE, and ADX color mapping images of (C) silicon concentrations in red, and (D) iron concentrations in green overlaid on silicon. The outline in (A) shows the size of each of the 18 mapped areas and a high degree of overlap was utilized to gain high-resolution and consistent data.

The composition of various SEM-EDS analyses of Sunset Cliffs ironstone compositions (Figure 5.5) shows good comparison to APXS data from Mars (Rieder et al., 2004). The average composition at 50x looks very similar to the Full Berry Bowl measurement by the APXS aboard the Opportunity MER rover. The ironstone levels of the cation salt components sodium, magnesium, and calcium are depleted, but the potassium levels are elevated. This could be due to the enhanced deposition of potassium salts in the ironstone matrix due to mobilization during ironstone nucleation. Titanium is elevated in the ironstone samples while the biologically labile element manganese is depleted in the ironstones compared to the Mars concretions. The SEM

analyses at 160x and 600x give compositions that agree fairly well to the overall bulk Sunset Cliffs composition with oxygen, silicon, and iron as the major elements present at levels close to the Mars blueberries. It is important to note that carbon is not present in any of the Sunset Cliffs EDS spectra, however, analyses at greater magnification and of a Convoy ironstone at the same scale (~50x) show small carbon concentrations (5-7%), possibly derived from biological activity.

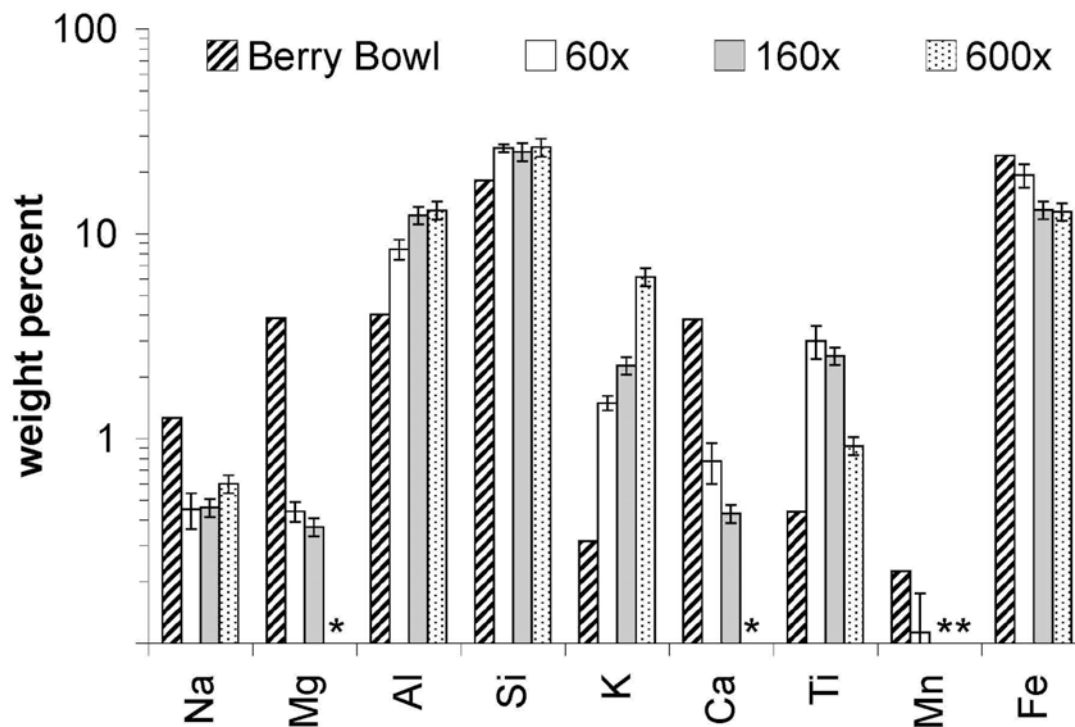
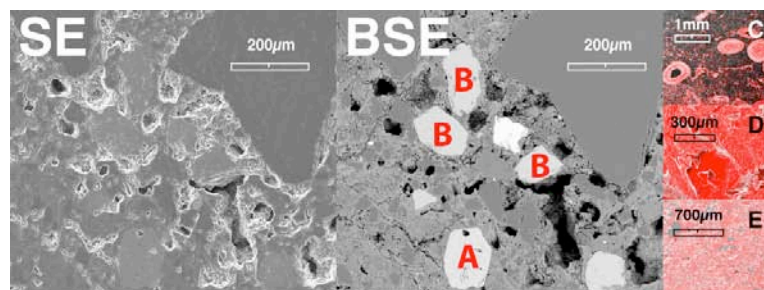


Figure 5.5 SEM EDS composition data compared to APXS data from Rieder et al. (2004). SEM Data A represents the average EDS composition from the 18-image mosaic shown in Figure 5.4 while the 160x and 600x measurements are single composition measurements at closer scale. Note that the * symbols represent concentrations <0.1% and that no carbon was detected in any of these SEM EDS images.

In order to better investigate the dominant iron phases present in these ironstones, they were investigated at a closer scale. Figure 5.6 shows a 300x magnification of an area rich in iron grains. Four of these discrete iron grains were analyzed and compared to hematite standards of micaceous gray hematite, red hematite, and oolitic hematite purchased from Wards. The purity of the red oolitic hematite standard was low and showed high concentrations of impurities such as Ca, Mg, and Al and a trace of K. The gray and red hematite standards were 71.2% and 54.7%

iron, respective, and these standards showed high purity for hematite (69.9% iron). In grains 1-3, there were significant concentrations of titanium, and this may be indicative that these grains are included ilmenite or its alteration product leucoxene. Grain 4 (72.3% iron) appears to be a relatively pure hematite grain, as it was absent of significant titanium concentrations (0.26%) and low in silicon (1.47%). These data are consistent with the iron within the ironstones as pure crystalline hematite, in agreement with previous studies (Emery, 1950). It is also interesting to note that all of these ironstone analyses at 300x magnification showed the presence of carbon (4.58-7.56%) and all but one showed the presence of manganese (1.94-2.77%). The source of some of this carbon could be microbially derived, especially given its presence located within iron-rich grains. If indeed these analyses represent some type of microbial carbon, the coincident concentrations of iron and manganese deposits may have been deposited by bacterial action. The SEM EDS analyses on the ironstone samples show strong qualitative similarities to standards of pure hematite (Figure 5.6) with iron as a primary phase with large amount of silicon (similar to the red hematite standard, Figure 5.6-D).

The presence of crystalline magnetite hematite, ilmenite, or manganese oxide could be present from Biologically Induced Mineralization (BIM) or Biologically Controlled Mineralization (BCM), as these are the major oxides formed by microbial action (Weiner and Dove, 2003). Iron biominerals comprise almost 40% of all minerals formed by organisms (Bazylinski & Frankel, 2003). If these concretions were formed as a byproduct of bacterial action, as has previously been suggested (Lal et al., submitted), the presence of iron oxides (including unquantified amorphous phases) may be remnants from microbial activity. The inconclusive results of iron minerals via XRD analyses may be indicative of significant amorphous iron oxide phases.



Energy Dispersive X-ray Spectroscopy (EDS) Plot

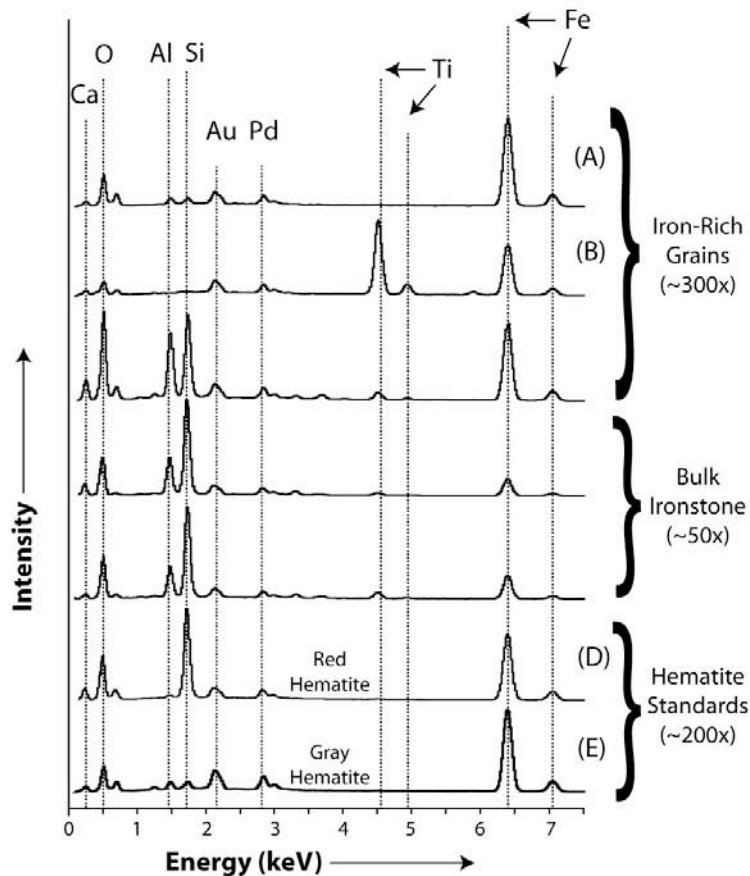


Figure 5.6 BSE and SE magnified images of Convoy ironstones ($\sim 300\times$) and iron crystal EDS spectra compared to standards of oolitic (C), red (D), and gray hematite (D) with iron colored in red. The EDS spectra are shown for the individual crystal analyses, standards, and bulk ironstone analyses ($\sim 50\times$ magnification). The major element EDS analyses on San Diego Ironstones at high ($\sim 300\times$) and low ($\sim 50\times$) magnifications show good agreement compared to standards of red ($\sim 55\%$ Fe) and gray hematite ($\sim 71\%$ Fe) with iron concentrations of $\sim 72\%$ (A) and $\sim 42\%$ (B) by mass. The bulk ironstone analyses ($50\times$) show high concentrations of oxidized iron ($\sim 20\%$) and silicon ($\sim 26\%$), evidenced by high oxygen contents ($\sim 40\%$). High titanium in the iron-rich grains (B $\sim 32\%$ Si) are characteristic of included material, such as ilmenite, and indicative of impure iron oxide phases. Oolitic hematite was omitted because of high degrees of detected calcium impurities.

The presence of microbial life within these ironstones has been verified by SEM images of biological microfossils (Figure 5.7A). These biosignatures show good preservation and represent colonies of iron-stained spheroidal cells (each of 6-10 microns in diameter) with each of the colonies composed of 30-50 closely packed cells. These structures are similar to some members of the genus *Siderocapsa* (iron/manganese precipitating bacteria), for their presence would explain the high enrichments of iron and trace manganese detected within the ironstone concretions (Figure 5.5). The presence of these colonial coccoids indicates that cellular microorganism structures are preserved in the ironstones and these unknown spheroidal bacteria, or other microbes, may have mediated the ironstone formation.

In one of the SEM-EDS images, carbon is shown to be closely associated with a pure deposit of iron and manganese traces (Figure 5.7B, BSE image). The EDS maps show carbon (Figure 5.7C, green) clustered around the interior and exterior of iron-rich grains (Figure 5.7D, red), and has a bulk composition of 8.9% C, 17.8% O, 34.3% Ti, 0.558% Mn, and 37.9% iron. The high percentages of both iron and titanium may again indicate the presence of included ilmenite ($\text{Fe}^{2+}\text{TiO}_3$) or leucoxene. The most interesting aspects of this SEM analysis, however, are the elevated levels of carbon and manganese clustered around an iron-rich grain, with trace carbon also detected in the interior (Figure 5.7C).

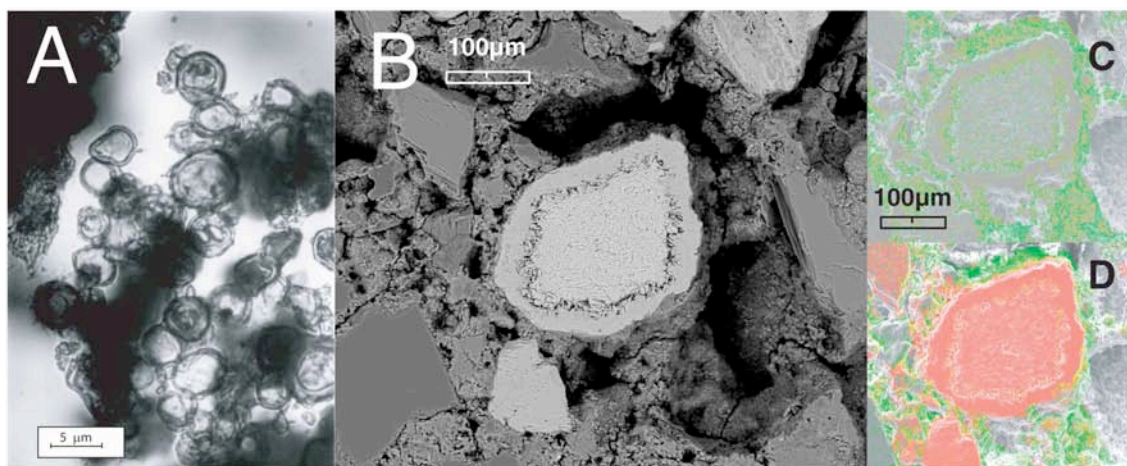
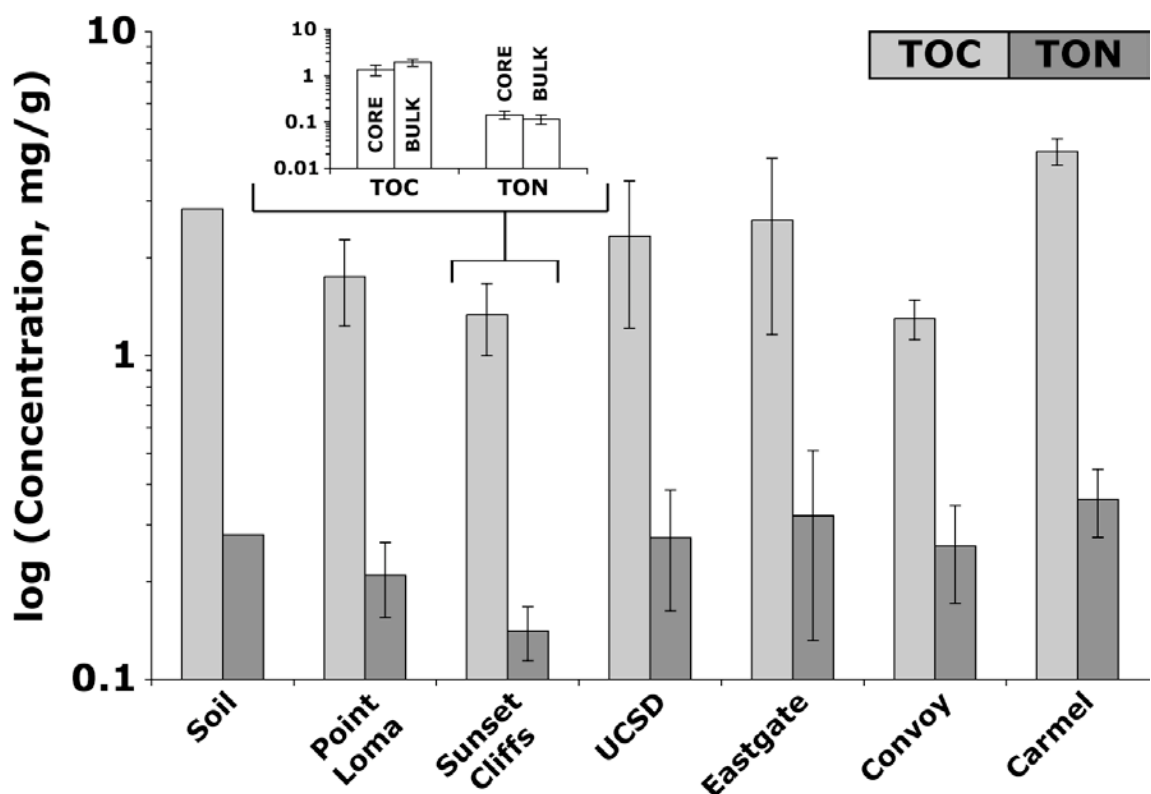


Figure 5.7 SEM BS images of (A) iron-stained colonial coccoidal cells imaged from ironstone thin sections (Image courtesy D. Lal) and (B) BSE of pure ironstone grain showing (C) carbon colored in green, and (D) carbon with iron colored in red.

5.3.2 *Chemical Analyses*

Despite the presence of visual biosignatures within the ironstones, quantitative chemical evidence of life must supplement these observations in order to provide stronger evidence of extinct life in the Sunset Cliffs ironstones, especially evidence of older, degraded organic material from an extinct microbial community. The first analyses were carried out on bulk ironstone samples from the Sunset Cliffs and Convoy locations. Small, medium, and large concretions from Sunset Cliffs were compared to bulk samples from the Convoy location. The next analyses were on the separated inner cores of ironstones from all the locations. The TOC, TON, $\delta^{13}\text{C}$, $\delta^{15}\text{N}$, and amino acid abundances for these samples (Figure 5.8) show consistent values for all Ironstone samples independent of location. The TOC and TON concentrations are all within a factor of ~ 2 for all locations and the comparison between the bulk and core Sunset Cliffs ironstone fractions (Figure 5.8, inset) show very similar values. These values for TOC and TON are relatively consistent with similar iron-rich quaternary paleosol deposits (Choi, 2005) and microbial activity has previously been observed to be high in similar environments (Kieft et al., 1993). Isotopically depleted carbon isotope signatures ($-23.8 - -29.1\%$) were detected in the ironstones and reveal that the source carbon is from a fractionated pool, which is strong evidence of extinct or extant microbial life (Craig, 1953).

All of the samples show elevated ratios of TOC to TON, indicating more refractory organic material which has undergone diagenesis and may represent materials such as humic acids which older organic material. The average ratios of TOC/TON for the bulk ironstone samples ($n=6$) are between 15-18, the soil is ~ 10 , and the core TOC/TON ratios fall between 5 and 10. This implies that more degraded organic matter is present within the bulk concretions compared to the soils, as the TOC/TON ratio tends to increase with time (Ertel & Hedges, 1983). The lower ratio of TOC/TON in the soil can be explained by contamination with more modern biological matter, possibly supplied by groundwater flow. The fact that the core samples show values lower than both the soil and bulk ironstone measurements can only be explained by better preservation within the ironstone interiors as it is uniquely stands out from the soil and bulk measurements.



	Location	Subset	n	TOC (mg/g)	$\delta^{13}\text{C}$ (‰)	TON (mg/g)	$\delta^{15}\text{N}$ (‰)	$\frac{\text{TOC}}{\text{TON}}$
Bulk	Sunset Cliffs	Soil	1	2.84	-23.2	0.28	+3.83	10.1
		SCS	6	2.04	-25.7	0.117	+3.11	17.4
		SCM	6	2.17	-25.5	0.141	+3.08	15.4
		SCL	6	1.54	-27.0	0.088	+3.44	17.5
		AVG	18	1.92	-26.1	0.115	+3.21	16.7
Core	Sunset Cliffs	CORE	11	1.33	-22.7	0.14	+3.13	9.5
	Point Loma	CORE	5	1.76	-23.3	0.21	+2.03	8.4
	UCSD Canyon	CORE	11	2.34	-24.2	0.27	+2.68	8.6
	Eastgate	CORE	7	2.61	-24.5	0.32	+3.91	8.2
	Convoy	CORE	4	1.30	-22.9	0.26	+2.74	5.1
	Carmel Mtn.	CORE	3	4.27	-24.6	0.36	+2.94	11.9

Figure 5.8 Averages of measured TOC and TON measured in ironstone samples and stable carbon and nitrogen isotope measurements. Error bars represent 1 standard deviation ($\pm\sigma$).

A plot of TOC versus TON for all of the samples analyzed reveals a general trend (Figure 5.9) and similarity of the TOC/TON sample ratios. The series representing the bulk fraction Sunset Cliffs measurements (\diamond) fall above the general trendline showing either older material or some type of preferential carbon enrichment over the soil and core samples.

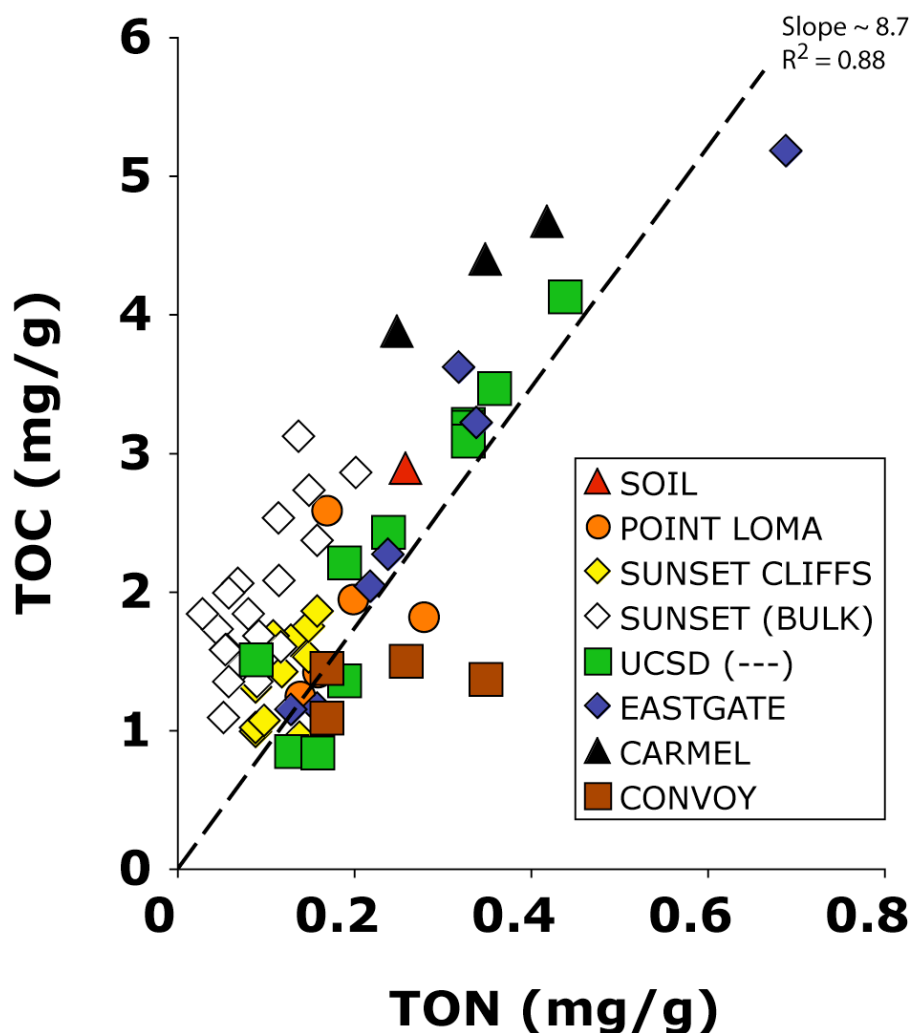


Figure 5.9 TOC plotted against TON for all ironstones. Trendline is plotted against UCSD samples (green squares) and shows a good fit ($R^2 \sim 0.88$) for the TOC relation to TON in this sample series and shows a general trend for the overall sample set. The slope of the line represents the average TOC/TON ratio for this series (~ 8.7).

Concentrations of total hydrolyzable amino acids for soil and average Sunset Cliffs and UCSD bulk sample measurements are compared to core samples from the various research sites (Table 5.1). The average amino acid abundances look similar for all of the core samples from various sites, which implies that these distributions are from similar microbial community concentrations. The bulk samples show lower concentrations than the Sunset Cliffs core samples by a factor of ~ 5 , and the UCSD canyon bulk samples show much greater paucity of amino acids. This indicates that the interior portions of the ironstones contain the bulk of the organic material. This finding is supported by elevated levels of amino acids within the interior core ironstone

scrapings in both the small (<20 μ M) and large (>20 μ M) fractions. The small scrapings showed much higher levels of total amino acids by a factor of ~ 2 compared to the core samples (Table 5.1; Figure 5.10). These observed differences in amino acid distributions in different ironstone fractions would support the hypothesis of microbial mediation as necessary for the formation of these ironstone deposits along with higher biodensities located in the ironstone cores or better preservation of these materials.

The relative amino acid distributions in the San Diego Ironstone cores look dissimilar to extant bacterial distributions (Glavin et al., 2001) and show evidence of degradation over long timescales. Mainly, glycine is present in lower relative concentrations than would be expected for extant microbial life, indicated by the relative amount detected in the soil (Figure 5.10). The fact that the TOC/TON ratios in these samples are elevated (~ 9) compared to fresh organic matter and that the amino acids are markedly different from an extant microbial distribution are consistent with the premise that the organic matter is degraded and from an extinct microbial community. It must also be mentioned that no nucleobases were detected in the ironstones implies that these communities lack intact nucleic acids, which are known to degrade much faster than amino acids (Miller & Bada, 1988). These results agree with the detection of β -alanine (β -Ala) and γ -aminobutyric acid (γ -ABA), possibly generated from the microbially mediated degradation of aspartic and glutamic acids (Bada, 1991) in the geological past. Hydrolyzable amino acids were not present in a 24-hour acid hydrolyzed water extract, implying that the amino acids are present in a non-soluble diagenetic material such as a kerogen matrix or humic acid substance.

If the amino acid abundances are extrapolated to bacterial counts assuming that the quantified amino acids represent $\sim 75\%$ of the total protein (Glavin et al., 2004) and a typical *E. coli* cell is 55% protein and the mass of an *E. coli* cell is 9.5×10^{-13} g/cell (Neidhardt et al., 1990), then $\sim 10^7$ bacterial cells/gram are present in the ironstone concretions if they represent a coincident community. If these cells were from recent contamination from extant bacteria, the enantiomeric excesses and degradation compounds (β -Ala and γ -ABA) would be negligible, and nucleobases from the extant communities would be detected. If the extrapolated cell counts are accurate, then there would have been at least 10^{-10} moles of nucleobases in the formic acid extracts, well above our detection limit of 10^{-11} moles of nucleobases. Therefore, the idea of

preferential degradation of more labile nucleobases while amino acids persist is favored in the interpretation of the mineralogical biosignatures.

The analyses of the magnetized and non-magnetized separated samples from Sunset Cliffs show similar amino acid concentrations (~16% difference in total amino acids), however, the acidic amino acids are elevated in the non-magnetic fraction which cannot be explained easily.

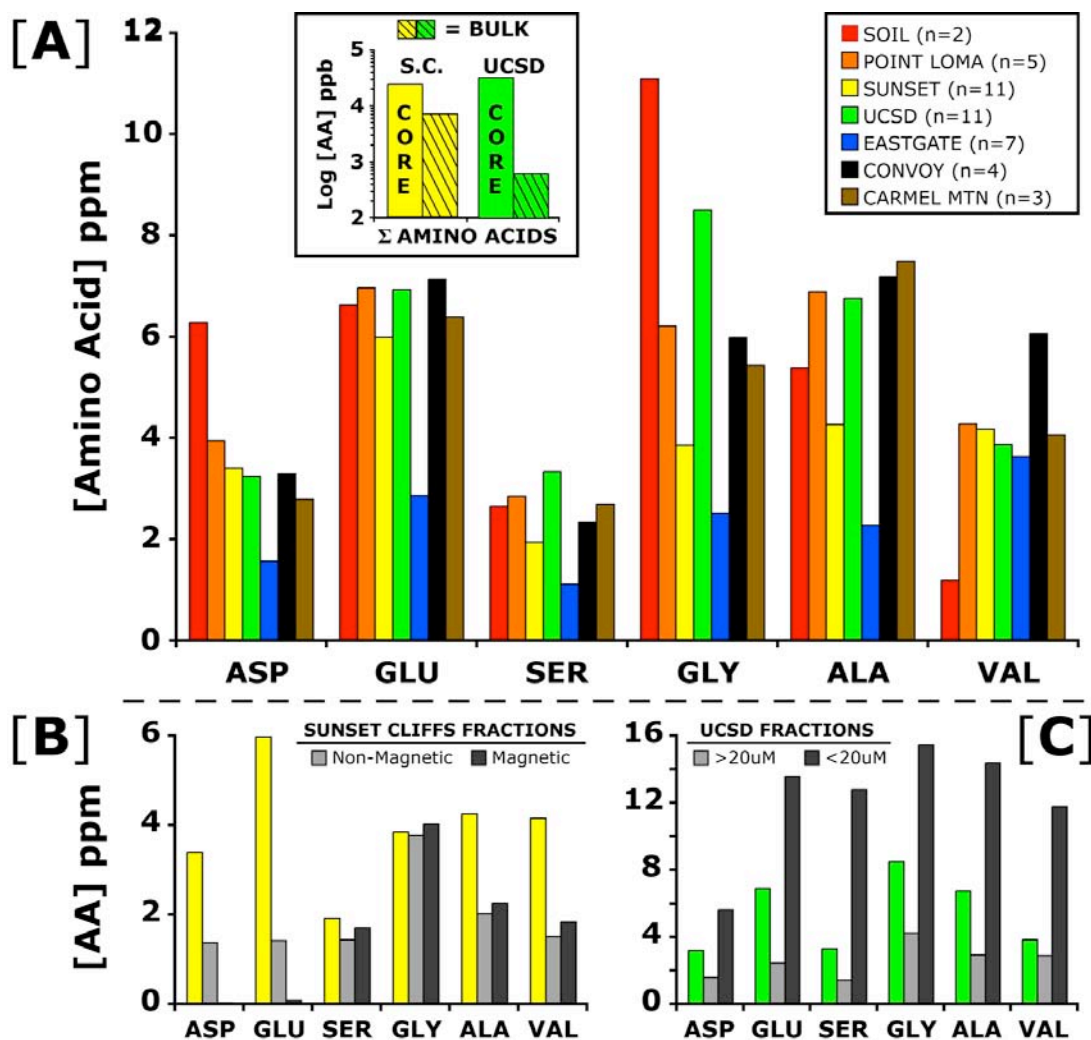


Figure 5.10 Summary of the various ironstone fraction analyses showing (A) relative total amino acid values from ironstone core analyses from various locations (Σ asp, glu, ser, gly, ala, val) with inset comparing the bulk ironstone analyses from Sunset Cliffs and UCSD compared to core samples, (B) relative amino acid values from Sunset Cliffs bulk magnetic fractions compared to core samples, and (C) UCSD Canyon small (< 20 μ M) and large (> 20 μ M) core scrapings compared to core sample analyses.

Table 5.1 Total hydrolyzable amino acid concentrations (ppb) for ironstone concretions. β -Ala and γ -ABA also detected in low ppb quantities.

Fraction	Location	Subset	n	Asp	Glu	Ser	Gly	Ala	Val	Total
Soil	Sunset Cliffs	Loose	2	6,279	6,630	2,640	11,100	5,383	1,183	33,200
Bulk Ironstone	Sunset Cliffs	2 mm	3	749	1,017	439	1,830	2,023	1,212	7,520
		5 mm	3	1,150	1,701	362	2,380	2,719	1,423	9,900
		10 mm	3	519	562	138	674	865	362	3,190
		AVG	9	805	1,090	313	1,630	1,870	999	6,870
	UCSD Canyon	SCS	3	186	98.0	64.0	119	91.2	56.2	615
Core	Sunset Cliffs ¹	-	11	3,400	5,988	1,934	3,854	4,268	4,167	23,609
	Point Loma	-	5	3,943	6,960	2,850	6,210	6,888	4,272	31,100
	UCSD Canyon	-	11	3,235	6,930	3,330	8,502	6,755	3,868	32,600
	Eastgate	-	7	1,564	2,860	1,110	2,510	2,274	3,634	14,000
	Convoy	-	4	3,294	7,130	2,330	5,980	7,180	6,049	32,000
	Carmel Mountain	-	3	2,785	6,380	2,690	5,430	7,486	4,063	28,800
	UCSD Canyon	> 20 μ M	3	1,620	2,480	1,450	4,260	2,960	2,910	15,700
Scrapings	UCSD Canyon	< 20 μ M	3	5,650	13,600	12,810	15,500	14,400	11,790	73,700
	Sunset Cliffs	Mag	1	40.1	94.6	1,720	4,030	2,270	1,850	10,000
		Non-Mag	1	1,380	1,430	1,450	3,790	2,030	1,520	11,600

Another indicator of the age of the detected amino acids are the enantiomeric ratios, shown in Figure 5.11 for all samples. The amino acid D/L enantiomeric ratios at all sample sites are enriched in the D-enantiomer which cannot be due to contamination, rather must be due to racemization over geological timescales. Bacterial remnants that existed in the past as almost completely L-amino acids ($D/L \sim 0$) and began to racemize over time after the microbial community became deceased. D/L-ratios can be used to determine the average age of the inner core of the samples. However, the fact that the enantiomeric abundances seem fairly consistent among the various sampling sites (mean D/L-ratios ~ 0.2 except for serine) suggest that these amino acids have undergone racemization for similar amounts of time. The trendlines reflect the relative differences between sample sets for the mean and maximum D/L-ratios.

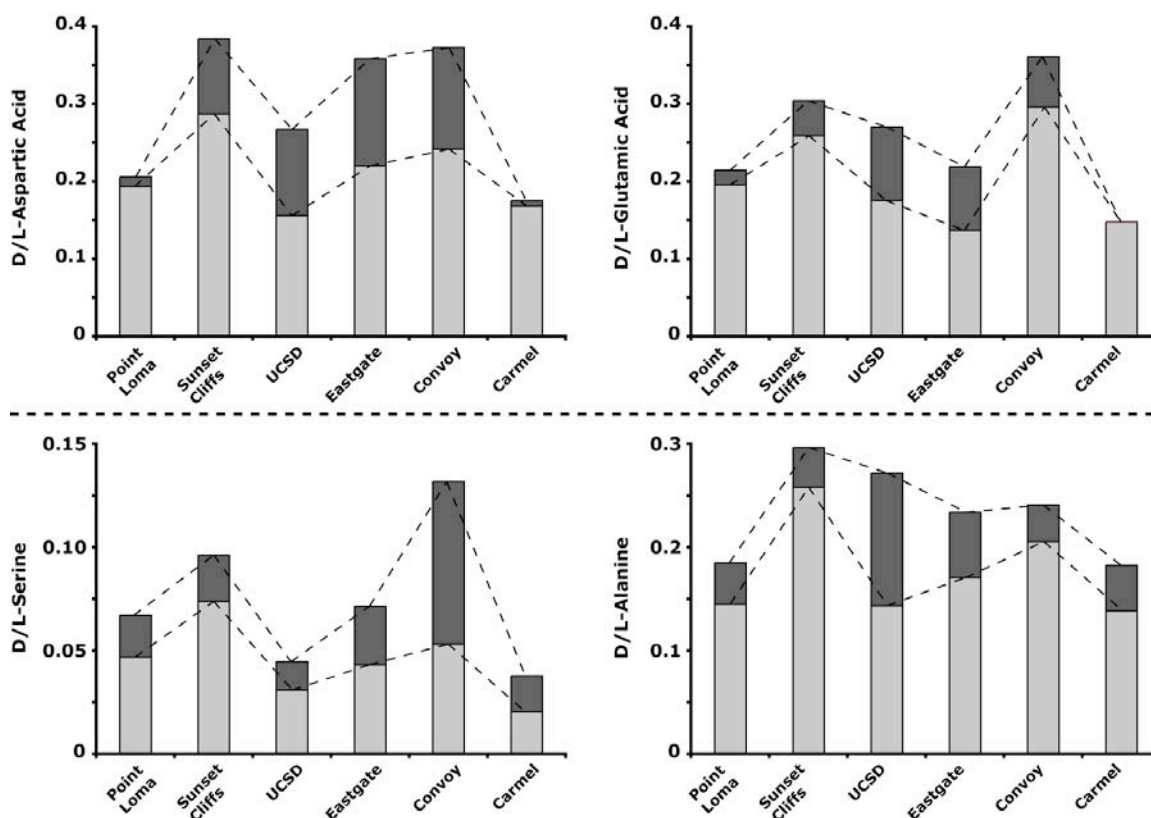


Figure 5.11 Summary of measured median (light gray) and high (dark gray) enantiomeric ratios for amino acids (asp, ser, glu, ala) from ironstone core analyses from various locations. The same relative enantiomeric excess trends are visible in the median and high sample sets for each amino acid evidenced by the trendlines (---). All amino acids are from the highest measured amino acid enantiomeric ratios and reflect the oldest biological material sampled from an extinct microbial life. Analysis of the median and high amino acid enantiomeric ratio screens for the sampling bias that is intrinsic in extracting the older core section from the bulk ironstone material.

In order to determine if the inner core sample enantiomeric abundances (Figure 5.11) are representative of the oldest material, the D/L-enantiomeric abundances were determined for the inner scrapings fractions for UCSD Canyon samples and compared to the bulk core measurements (Figure 5.12).

The UCSD canyon inner core scrapings showed a marked difference between the large and small size fractions. The small size fraction is enriched in total amino acids by a factor of ~ 5 , however while the large size fraction showed lower total amino acids, the D/L ratios were higher than the small size fraction, $\sim 0.30 \pm 0.02$ compared to $\sim 0.19 \pm 0.005$. The difference between the magnetic and non-magnetic ironstone fractions was only in the acidic amino acids (asp, glu), however, the other amino acids showed similar distributions while enantiomeric ratios were only slightly elevated ($\sim 25\%$) in the non-magnetic fraction for serine (0.07-0.09), alanine (0.21-0.26), and valine (~ 0.05). These data show that the oldest amino acid pool is located in the large size distribution from the innermost core, possibly occurring near large iron nodules or deposits that may be associated with extinct microbial communities.

These enantiomeric measurements on the innermost core ironstone scrapings and comparison to bulk measurements (mean and maximum) show that the core sample analyses closely approximate the enantiomeric ratio of the amino acid-rich small size fraction. The samples that showed the highest amino acid D/L-ratios, the large inner core scraping fraction, are generally identical to the highest measured core amino acid racemization levels. Because the UCSD canyon samples show highly similar enantiomeric abundances in the different analyzed fractions (Figure 5.12), the data from the inner core scrapings is assumed to be representative of the ironstone samples at the time of formation.

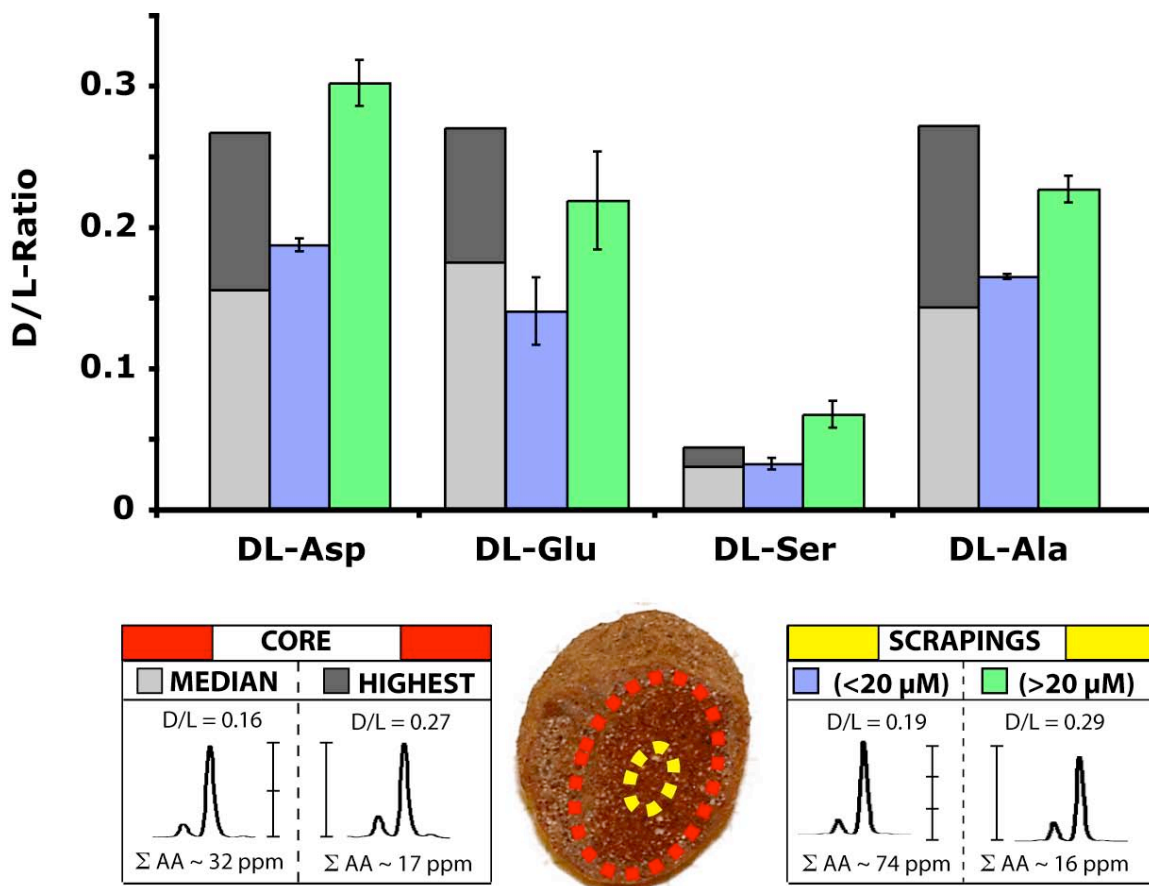


Figure 5.12 Average amino acid DL-ratios of small (< 20 μM) and large size (> 20 μM) fractions from interior ironstone scrapings from UCSD Canyon ironstones compared to median and highest enantiomer ratios from core fraction analyses. Traces of D/L-aspartic acid are shown along with a key of the ironstone target sampling areas. The highest D/L amino acid ratios are from the large fraction (>20 μM) from the inner core scrapings (green; D/L-asp ~ 0.29) although the total amino acid levels are ~5x lower than the small fraction (<20 μM). The highest inner core amino acid enantiomeric ratios (dark gray; D/L-asp ~ 0.27) show good homogeneity compared to the inner core scrapings for all amino acids and is higher in the case of D/L-glu and D/L-ala. The median ironstone core sample enantiomer ratios (light gray) are approximately the average of the large (green) and small (blue) inner ironstone core scrapings for all amino acids. However, the core samples represent the average age of the innermost core in its entirety.

5.3.3 Calibration Method Racemization Rate Determination

The ages of the amino acids within the ironstones can be determined based on racemization kinetics using a calibration method. This age can be interpreted as the length of time since the microbial communities have become extinct and the major assumption of racemization age dating are that a microbial community existed coincidentally in the past and became extinct coincidentally. In order to estimate the racemization rate constants within the

ironstone matrix, a calibration method for amino acid racemization is used and has been applied to previous experimental studies to date similar cliffs within which the ironstones are found (Karrow & Bada, 1980).

Both racemization and degradation are modeled as pseudo-1st order reactions, in agreement with previous studies (Bada, 1991; Aubrey et al., 2006) using Equation 6.1. If it is assumed that the degree of racemization in Sunset Cliffs samples occurred over an average lifetime of 120ka, the age of the Lower Nestor terrace (Kern and Rockwell, 1992), the racemization rates of amino acids may be determined. The major assumptions of this model are that the entire microbial community expired coincidentally after the formation of the ironstone core and that the average exposure temperature for the San Diego ironstones was assumed to be 17°C, based on previous racemization studies of local marine terraces (Wehmiller, 1977). Using Equation 6.1, the racemization rate constants can be determined for various amino acids which reported in Table 5.2.

Equation 5.1

$$\ln\left(\frac{1 + D/L}{1 - D/L}\right) = 2 \cdot k_i \cdot t$$

Table 5.2 Racemization rate constants determined by the calibration method using the median enantiomer ratios for Sunset Cliffs ironstone samples which is the most well studied marine terrace. Ironstones were assumed to have formed early in the history of the host marine terrace (~120ka) at ambient temperature (~17°C). Ages of ironstones from the youngest marine terrace, the Point Loma locale, were determined using the calculated rate constants and found to agree well with the age of the host terrace, the Bird Rock terrace (~80ka). Serine was not used in these calculations as it is particularly sensitive to contamination.

	Sunset Cliffs (120ka)		Point Loma Terrace	
	D/L-ratio*	Racemization rate (yr ⁻¹)	D/L-ratio*	Predicted Age
Aspartic Acid	0.287	2.46 x 10 ⁻⁶	0.194	80 ± 12
Glutamic Acid	0.259	2.21 x 10 ⁻⁶	0.196	90 ± 15
Alanine	0.258	2.20 x 10 ⁻⁶	0.146	66 ± 12

*Median values used to calculate racemization rate constants.

The age of the youngest marine terrace, the Bird Rock terrace, is dated at ~80ka. Using the rates of racemization determined by the calibration sample method on Sunset Cliffs ironstones, the age of the Point Loma terrace ironstones is ~80ka. Using the derived rate constants from the Sunset Cliffs ironstones, the Point Loma research location matches the terrace

age fairly well, so the rates of racemization appear to be accurate. This implies that the ironstones located in the youngest two marine terraces formed very soon after the deposition of these marine terraces.

It is possible to check whether the model assumptions are reasonable using literature values for amino acid racemization determined for other matrices. The aspartic acid racemization kinetics can be determined if the half-life is approximated as that observed in the non-soluble portion of carbonate sediments, ~1 Ma (Bada & Mann, 1980). This calculated to a racemization rate of $6.93 \times 10^{-7} \text{ yr}^{-1}$, slightly slower than the derived rate for aspartic acid racemization. However, the extrapolation of this rate to higher temperatures typical of San Diego County would increase this rate to a value closer to the one derived in this study. Thus, timescales of approximately 100,000 years are necessary for the amino acids to reach their observed enantiomeric ratios using published rate constants, in agreement with our calibration sample.

Using the racemization rates derived from the calibration method of amino acid dating (Table 5.2), the relative ages of the ironstones can be derived (Figure 5.13). Aspartic acid was used because the racemization kinetics are suitable for dating up to approximately million-year timescales. Sample ages calculated by the calibration method using the highest measured D/L-ratios are shown by the hatched bars and represent the oldest analyzed material. The ironstone ages calculated using the mean D/L-ratios are shown by the solid bars. Racemization dating using D/L-glutamic acid, D/L-serine, and D/L-alanine show similar results to the aspartic acid data. The mean and maximum sample ages were used to deduce the ages of the ironstones because these remove any sampling bias from inadequate separation of the inner core from the bulk ironstone during sample preparation.

The ranges of ages from the analyses of various ironstone deposits are shown to be independent of the geological terrace formation ages. This is evident because ironstones from the older terraces, such as the Convoy, Eastgate, and Carmel Mountain sites (farther from the current San Diego coastline and formed at times of higher sea level), do not show older ironstone ages. Instead, samples from Sunset Cliffs show the highest overall mean and maximum inferred ironstone ages, very close to the average age of all ironstone deposits.

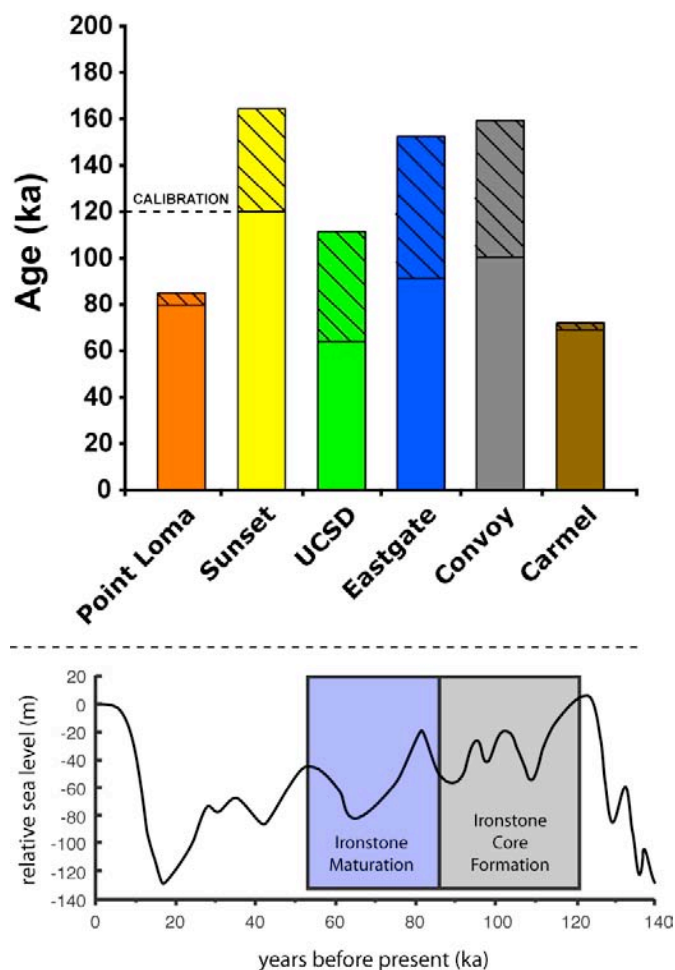


Figure 5.13 Approximate ages of San Diego county ironstones inferred from ironstone core aspartic acid enantiomeric ratios using median (solid) and maximum (hatched) values. The Sunset Cliffs median enantiomer ratio was used as the calibration sample for the determination of racemization rate constants for the amino acids at all sites. Racemization dating using glutamic acid and alanine yielded similar ages and show good overall agreement. Inset shows the sea level history over the last 140ka (Choi, 2005) along with the estimated range of ironstone formation and maturation. The inferred ages of ironstone formation show a general correlation with precipitation history.

If the ironstones truly represent closed systems and contamination is assumed to be negligible, then it appears that all of the ironstones formed coincidentally within the last 100,000 years based on this model. A model of precipitation history modified from Choi (2005), based on data from previous oxygen isotope studies (Shackleton, 1987; Chappell et al., 1996), can be roughly to infer the precipitation history over the last 140ka. The modeled ages of formation coincide with earlier periods of high sea levels and enhanced precipitation, and this wetter climate

may have been responsible for the ubiquitous formation of ironstones in San Diego county as well as other Pacific coastline marine terraces and may be intimately tied to their formation constraints. The deviation of the highest inferred ages compared to the average ages shows that the ironstone inner cores themselves could have taken tens of thousands of years to mature. Based on the fact that these ironstones are younger than the older host terraces, this could be explained by the deposition of an iron-rich surface soil layer across all of the marine terraces at a given geological time. Subsequent water activity could then allow for the ubiquitous formation of ironstones within all of the marine terraces. This is consistent with the deposition of the ironstones at relatively shallow soil horizons across San Diego County that have been recently exposed due to weathering.

5.3.4 IRONSTONE FORMATION

It is not difficult to form spherules in nature given a homogeneous matrix, as it is the least energy formation for crystallization. This has been shown in studies where high-purity crystalline hematite micrometer-scale spherules were formed in an iron solution after high-temperature exposure with the specific aim to explain the Martian blueberries (Golden et al., 2007). However, with a geologically more complicated matrix composition, it becomes more difficult to form spherules naturally. This is because there are more factors involved than simple crystal propagation, physically and chemically. It is therefore probable that these concretions were the result of a more difficult formation process.

A proposed formation model for the ironstones in San Diego County requires high levels of precipitation and subsequent water availability (Figure 5.14). The marine terraces formed as wave-cut platforms during intervals of high sea levels over the last ~1 Ma (Ku & Kern, 1974). Upon withdrawal of the sea, beach ridges accumulated on these platforms from aeolian materials (Figure 5.14A). After accumulation of sediments upon the beach ridges, wet Pleistocene climates and associated increased precipitation events produced iron and manganese-rich leachates from a common soil horizon that led to the formation of a silt and clay-rich subsurface horizon within which ironstone concretions formed. The host soils are enriched in iron and acidic at a pH of around 6 (Abbott, 1981). In order to better mobilize iron from the surface paleosol, it is assumed that oxygen was leached out of the water in the uppermost layers due to microbial activity or soil reactivity (Figure 5.14B). This anoxic water could then mobilize ferric iron (Fe^{2+}) from the

surface soils and carry it vertically through the beach ridges. The silt and clay rich hardpan underlying the concretion layer would have allowed for long drainage times and allowed water to remain for longer durations. The ironstones were then formed by nucleation, perhaps around large sand grains, and subsequent cementation by iron oxides (Figure 5.14C). This was allowed through the transport of ferric iron by acidic rainwater and subsequent oxidation and deposition of ferrous iron (Fe^{3+}).

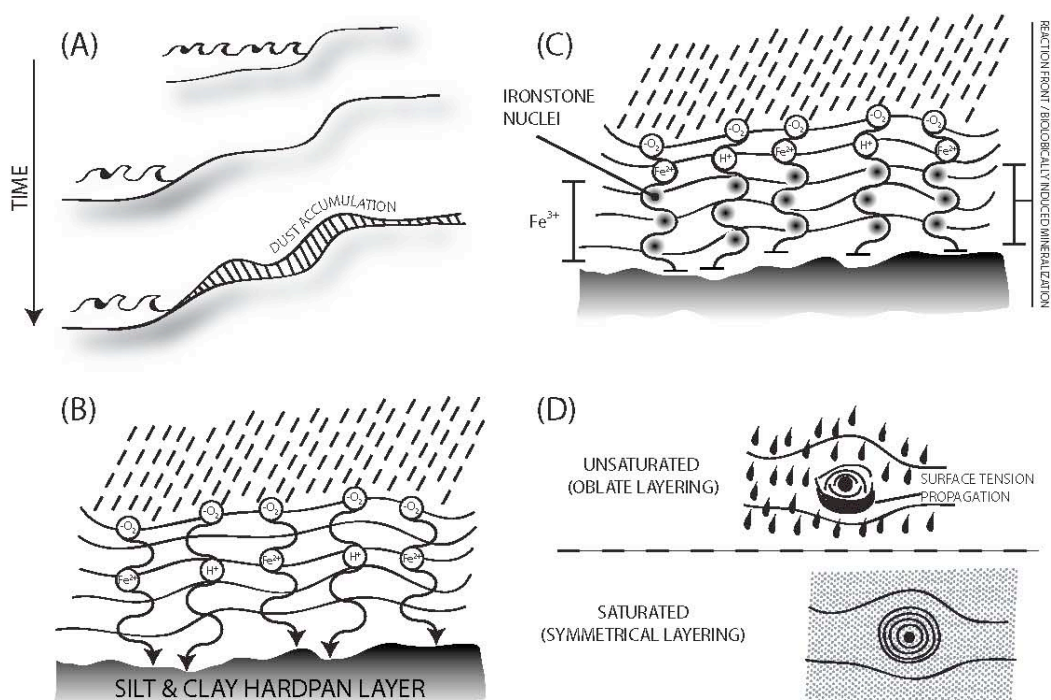


Figure 5.14 Ironstone formation model showing (A), the evolution of San Diego's coastal marine terraces (Kern & Rockwell, 1992), (B) the evolution of the host matrix and formation of the silt and clay-rich hardpan, (C) anoxic percolating water allowing the formation of the ironstones over thousand-year timescales from Fe^{2+} in acidic solution and oxidation of Fe^{3+} at a shallow reaction front, and (D) relation of water-availability to the formation and layering of the ironstones.

A reaction front at the concretion horizon must have been responsible for this change in oxidation state, or the possibility exists that the formation of these ironstones was mediated by microbial action on the iron-rich fluids. If the concretions were formed abiotically, the reaction front could have been caused by an oxygenated water horizon just above the clay-rich layer or different mineralogy. However, given an abiotic reaction front, there would be no reason that this would produce spherical concretions in situ.

Biological life could have mediated the formation of these ironstones by easing the transition of the dissolved ferric (Fe^{2+}) to oxidized ferrous (Fe^{3+}) iron through a variety of microbial pathways, or microbial life could have been directly responsible for precipitating the iron (Tebo et al., 1997). The presence of iron-stained colonial microfossils (Figure 5.7A) implies that these microbes were present at the time of the ironstone formation. Furthermore, the abundance of the organic carbon pool, degraded microbial protein amino acids, and visual evidence of both carbon and bacterial microfossils contends that these concretions are likely to have formed with biological mediation.

Depending on water availability, the layering of the concretions may show some degree of asymmetry (Figure 5.14D). During the transport of ferric iron to the ironstone horizon, water limiting conditions would have allowed for percolating water to collect at the base of a growing ironstone nodule by surface tension. This would have allowed for layering of the ironstones as they grew larger around the nucleus with heavier layers occurring on the bottom. This effect is expected to be less pronounced during saturated periods or if water is highly available. Oblate layering would be more pronounced given extreme unsaturated conditions or periodic water flow during sporadic precipitation events. Most of the ironstone cores appear only to have a small degree of oblate layering, presumably because Pleistocene climates during the ironstone formation were likely wetter than today (Choi, 2005) and formation occurred during times of heavy rainfall, or standing water. The ironstones that do show some oblate layering have heavier layers located on the bottom of the concretions, presumably due to a surface tension effect. The source of water could have been from precipitation events and slow percolation due to the underlying hardpan layer, or extensive lateral anoxic groundwater flow could have mobilized elements, intruded into the concretion layer, and precipitated iron oxides due to microbial activity. Either fluid source could have also formed slightly oblate ironstones because there would still be periods of unsaturated flow allowing for surface tension-controlled propagation.

The fact that the model inferred ironstone ages (Figure 5.13) date coincidentally close to the end of the last interglacial cycle around 100ka strongly implies the necessity of high water availability during the ironstone formation. These deposits are hypothesized to have formed within the host sedimentary cliffs during one or more wet/dry hydrological cycles during which dust would accumulate and become wetted by subsequent rain. The iron-rich leachates involved

in the formation of these spherules could have been derived from aqueous weathering of a thick iron-rich dust layer accumulated during the preceding dry glacial period.

5.3.5 Extrapolation to racemization kinetics expected on Mars

The ironstones found within the sedimentary marine terraces of San Diego county indeed show a high degree of visual (Figure 5.1) and chemical similarity (Figure 5.5) to the concretions imaged on Mars. These similarities imply that a similar formation process may have played a role in the Martian hematite concretions that have been imaged in situ by the MER Opportunity. If these terrestrial concretions are indicative of a similar formation process on Mars, then any biomolecules captured within these concretions may show similar rates of degradation within the respective iron-rich matrices. The rates of racemization used to date the San Diego county ironstones can therefore be extrapolated to colder temperatures in order to estimate the rates that amino acids might racemize over geological timescales on Mars.

The racemization half-lives at temperatures similar to those characteristic of Mars' surface can be extrapolated using Equations 6 and 7. The average surface temperature was assumed to be -20°C to estimate the timescales that amino acids would retain their chirality in a similar geochemical environment.

$$\text{Equation 6.} \quad t_{1/2} = \frac{0.693}{k_{RAC,ASP}}$$

$$\text{Equation 7.} \quad \ln\left(\frac{t_{1/2,T_1}}{t_{1/2,T_2}}\right) = \frac{E_A \cdot \Delta T}{R \cdot T_1 \cdot T_2}$$

Table 5.3 Sunset Cliffs amino acid racemization rates and extrapolation to Mars conditions.

	D/L-ratio	k_{RAC} (yr ⁻¹) ¹	Mars $t_{1/2}$ (Ma) ²	Mars k_{RAC} (yr ⁻¹) ²
Aspartic Acid	0.287	2.46×10^{-6}	30.1	2.30×10^{-8}
Glutamic Acid	0.259	2.21×10^{-6}	33.5	2.07×10^{-8}
Alanine ¹	0.258	2.20×10^{-6}	33.7	2.06×10^{-8}

¹ k_{RAC} was calculated with Equation 6.1 using the average enantiomeric ratios from 11 Sunset Cliffs samples assuming a starting D/L~0.

²The Mars half-lives were calculated using Equation 3 estimating an average activation energy (E_A) of ~ 31 kcal/mole (Bada and Schroeder, 1972) at -60°C , characteristic of Mars' average surface temperature.

The racemization half-lives characteristic of Mars' temperatures fall around 30 Ma (Table 5.3). This is not unreasonable given the fact that the amino acids seem to be stable in terrestrial ironstone matrices for hundreds of thousands of years while the stability would be increased at much colder temperatures to half-lives in the millions of years. The predicted rates of racemization ($\sim 2 \times 10^{-8} \text{ yr}^{-1}$) fall close to those predicted by Bada & McDonald (1995) for rates of racemization on Mars in wet environments at similar temperatures. Drier conditions such as those on Mars would tend to better preserve any chiral signature and decrease the racemization rate constant by a factor of around 1000 (Bada & McDonald, 1995). Assuming a modest decrease of one order of magnitude in the rate constant because of dry conditions characteristic of Mars would make the rate constants $\sim 2 \times 10^{-9} \text{ yr}^{-1}$. This difference would make the half-lives of amino acid racemization in the hundreds of millions of year range and might be more applicable to actual Mars in situ rates.

Other terrestrial Mars blueberry analogs have been analyzed for biomarkers and none were detected by GCMS analyses (Souza-Egipsy et al., 2006). The presence of amino acids, elemental enrichments, and the microfossils within the Sunset Cliff ironstones provide evidence of microbial mediation. It would also have been possible that bacteria persisted within the ironstone matrices using abundant iron and manganese as energy sources, however, the fact that the microbial remnants show evidence of diagenesis over long geological timescales imply that these bacteria have been extinct for a long time. Whatever the process of the iron deposition may be, microbial mediation of the ironstone formation cannot be dismissed.

Enrichment of iron within the Martian concretions may have resulted from a similar process to the terrestrial ironstone formation. Acidified groundwater, high in aqueous Fe^{2+} could have deposited hematite (Fe_2O_3) as it mobilized through the interior of sedimentary deposits. The Sunset Cliffs ironstones are rigid concretions within a softer sedimentary material. On Mars, similar sedimentary material could have become more indurated by atmospheric desiccation, possibly enhanced by the presence of large amounts of salt. This process may be similar to the terrestrial processes of silicification (Thiry et al., 1988) or formation of desiccated desert pavements (Cooke, 1970). After the formation and desiccation of blueberries, the concretions would subsequently erode from the rock due to weathering and cover the ground around bedrock outcrops.

The formation of the enigmatic Martian ‘blueberries’ has been unequivocally viewed as strong evidence of aqueous activity during the time of their formation. The consensus of the ‘blueberry’ formation model on Mars is that the spherules form via groundwater flow within the host matrix and subsequent precipitation of solids due to a reaction front. A mechanism similar to our terrestrial model may have formed ‘blueberry’ concretions on early Mars. Their visual similarity, occurrence in sedimentary deposits, and compositional likeness to the Martian spherules makes a strong case for similar formation processes. There most likely was a defined hydrological cycle historically on Mars, possibly ending as early as 3.5 Ga (Bibring et al., 2006). Mars may have had an ice age as recently as 0.4 Ma (Head et al., 2003), and it may have been possible for the accumulation of massive dust layers during these dry epochs. There may have been extensive formation of concretions during this time within or below an acidic, iron-rich soil matrix. There is now suggestive evidence for spatially limited near surface episodic surface aqueous activity within the last decade (Malin et al., 2006), so the range for the formation of iron-rich spherules on Mars may extend to modern times. The potential exists for ironstone formation not only on early Mars, but also in the eras closely following the wet, early Mars.

5.4 CONCLUSION

The San Diego ironstone formations represent a putative organic-rich terrestrial analog to the blueberries observed on Mars. The detection of biochemical remnants and bacterial microfossils that are perhaps as old as the cliffs themselves suggest that microbial life was abundant within the terrestrial ironstone matrices and may have mediated their formation. Even if the detected microbial remnants are not derived from microbes responsible for the ironstone formation, these concretions represent geological formations rich in organic matter from more recent biological life that was sustained for some period in their history. Similar concretions on Mars could have formed by similar pathways and may contain organics from extinct or extant microbes or from inclusion during their sedimentary formation.

The fact that the San Diego sedimentary concretions are iron-rich may offer some degree of protection to organic compounds against harmful UV-radiation and other degradative mechanisms such as ionizing radiation, which has been suggested to be the limiting factor on the survival of amino acids within the Martian regolith (Kminek and Bada, 2006). Enhanced degradation of amino acids due to Fenton chemistry or other degradative pathways (Sumner,

2004) is observed in this study at high-temperature exposure during heating experiments, however the influence would be smaller at ambient temperatures. Extrapolation of Mars racemization rates to those expected in drier conditions give half-lives of hundreds of millions of years and might be expected to preserve chirality on Mars for billions of years. This implies that the blueberry spherules represent a potentially attractive target for the search for evidence of life on Mars because their racemization half-lives, and longer degradation half-lives, are significantly long for the preservation of chirality over geological timescales.

The proposed formation model requires vertical aqueous activity through a host matrix and cementation by iron oxides. We further interpret the ironstone concretions as having formed over tens of thousands of years within terrestrial sedimentary formations with the strong possibility of mediation by microbes. Similarly, the Martian blueberries may represent similar concretions that require aqueous activity and nucleation during flow through a sedimentary matrix. This model is compatible with the recently suggested hydrology of Meridiani Planum (Andrews-Hannah et al., 2007) and the formation model proposed by McLennan et al. (2005).

Mars blueberries are a potentially attractive target for the search for evidence of life on Mars due to the presence of organic material and potential for preserving biomarkers and chirality on geological timescales. Blueberry concretions on Mars should be considered as potential targets in the search for chemical biosignatures on future missions to Mars. The 2009 NASA Mars Science Lander will lack drilling capabilities, so it is of utmost importance to find surficial deposits that offer a high degree of stability. The 2013 ExoMars rover should also examine these blueberry deposits for evidence of well-preserved organic remnants including amino acids.

ACKNOWLEDGEMENTS

I would like to thank Prof. Devendra Lal for his commitment to this project, Eric Parker for his dedicated analytical expertise and Dr. Bruce Deck for his expertise in the Scripps institution of Oceanography Unified Laboratory Facility (SIO-ULF) which provided us with the TOC, TON, and stable isotope data used to characterize the iron concretion samples. Evelyn York was very helpful while her expertise allowed for a thorough investigation of the ironstones using the SEM. Prof. William Schopf analyzed nanoscale microfossils with the ironstones using SEM for visual evidence of bacteria microfossils. I would like to thank Evan Solomon for helpful discussions about ironstone formation processes and Dr. Loic Vacher for his XRD analyses.

REFERENCES

- Abbott, P.L. (1981) Cenozoic Paleosols San Diego Area, California. *Catena* 8, 223-237.
- Amelung, W. & Zhang, X. (2001) Determination of Amino Acid Enantiomers in Soil. *Soil Biology and Biochemistry* 33, 553-562.
- Andrews-Hanna, J.C., Phillips, R.J., and Zuber, M.T. (2007) Meridiani Planum and the global hydrology of Mars. *Nature* 446, 163-166.
- Aubrey, A., Cleaves, H.J., Chalmers, J.H., Skelley, A.M., Mathies, R.A., Grunthaner, F.J., Ehrenfreund, P., & Bada, J.L. (2006) Sulfate minerals and organic compounds on Mars. *Geology* 34, 357-360.
- Bada, J.L. (1991) Amino acid cosmogeochemistry. *Phil. Trans. R. Soc. Lond. B* 333, 349-358.
- Bada, J.L., & Mann, E.H. (1980) Amino Acid Diagenesis in Deep Sea Drilling Project Cores: Kinetics and Mechanisms of Some Reactions and Their Application in Geochronology and in Paleotemperature and Heat Flow Determinations. *Earth-Science Reviews* 16, 21-55.
- Bada, J.L., and McDonald, G.D. (1995) Amino Acid Racemization on Mars: Implications for the Preservation of Biomolecules from an Extinct Martian Biota. *Icarus* 114, 139-143.
- Bada, J.L., and Schroeder, R.A. (1972) Racemization of Isoleucine in Calcareous Marine Sediments: Kinetics and Mechanism. *EPSL* 15, 1-11.
- Bazylinski D.A., and Frankel, R.B. (2003) Biologically controlled mineralization in prokaryotes. *Rev. Mineral Geochem.* 54, 217-247.
- Bibring, J.P., Langevin, Y. Mustard, J.F., Poulet, F., Arvidson, R., Gendrin, A., Gondet, B., Mangold, N., Pinet, P., Forget, F., & the OMEGA team (2006) Global Mineralogical and Aqueous Mars History Derived from OMEGA/Mars Express Data. *Science* 312, 400-404.
- Chan M. A., Beitler B., Parry W. T., Ormö, J., & Komatsu, G. (2004) A possibly terrestrial analogue for haematite concretions on Mars. *Nature* 429, p731-734.
- Chappel, J., Omura, A., Esat, T., McCulloch, M., Pandolfi, J., Ota, Y., and Pillans, B. (1996) Reconciliation of late Quaternary sea levels derived from coral terraces at Huon Peninsula with deep sea oxygen isotope records. *Earth Planetary Sci. Lett.* 141, 227-236.
- Choi, K. (2005) Pedogenesis of late Quaternary deposits, northern Kyonggi Bay, Korea: Implications for relative sea-level change and regional stratigraphic correlation. *Palaeogeography, Palaeoclimatology, Palaeoecology* 220, 387-404.
- Christensen, P.R., Bandfield, J.L., Clark, R.N., Edgett, K.S., Hamilton, V.E., Hoefen, T., Kieffer, H.H., Kuzmin, R.O., Lane, M.D., Malin, M.C., Morris, R.V., Pearl, J.C., Pearson, R., Roush, T.L., Ruff, S.W., & Smith, M.D. (2000) Detection of crystalline hematite mineralization on Mars by the Thermal Emission Spectrometer: Evidence for near-surface water. *J. Geophys. Res.* 105, 9623-9642.

- Christensen, P.R. & Ruff, S.W. (2004) Formation of the hematite-bearing unit in Meridiani Planum: Evidence for deposition in standing water. *J. Geophys. Res.* 109, E08003.
- Cooke, R.U. (1970) Stone Pavements in Deserts. *Annals of the Association of American Geographers* 60, 560-577.
- Craig, H. (1953) The geochemistry of stable carbon isotopes. *Geochim. Cosmochim. Acta* 3, 53-92.
- Emery, K.O. (1950) Ironstone concretions and beach ridges of San Diego County, California. *California Journal of Mines and Geology* 46, 213-221.
- Ertel, R.E., and Hedges, J.I. (1983) Aquatic & Terrestrial Humic Materials, 143-163.
- Gendrin, A., Mangold, N., Bibring, J.P., Langevin, Y., Gondet, B., Poulet, F., Bonello, G., Quantin, C., Mustard, J., Arvidson, R., & LeMouélic, S. (2005) Sulfates in Martian Layered Terrains: The OMEGA/Mars Express View. *Science* 307, 1587-1591.
- Glavin, D.P., Schubert, M., Botta, O., Kminek, G., & Bada, J.L. (2001) Detecting pyrolysis products from bacteria on Mars. *Earth and Planetary Science Letters* 185, 1-5.
- Glavin, D.P., Cleaves, H.J., Schubert, M., Aubrey, A.D., & Bada, J.L. (2004) New Method for Estimating Bacterial Cell Abundances in Natural Samples by Use of Sublimation. *Applied and Environmental Microbiology* 70, 5923-5928.
- Golden, D.C., Ming, D.W., Morris, R.V., and Graff, T.G. (2007) Hydrothermal synthesis of hematite-rich spherules: Implications for diagenesis and hematite spherule formation in outcrops at Meridiani Planum, Mars. 38th annual LPSC 2007. abstract #2257.
- Golombek, M.P., Grant, J.A., Parker, T.J., Kass, D.M., Crisp, J.A., Squyres, S.W., Haldemann, A.F.C., Adler, M., Lee, W.J., Bridges, N.T., Arvidson, R.E., Carr, M.H., Kirk, R.L., Knocke, P.C., Roncoli, R.B., Weitz, C.M., Schofield, J.T., Zurek, R.W., Christensen, P.R., Fergason, R.L., Anderson, F.S., & Rice Jr., J.W. (2003) Selection of the Mars Exploration Rover landing sites. *J. Geophys. Res.* 108, 8072.
- Head, J.W., Mustard, J.F., Kreslavsky, M.A., Milliken, R.E., and Marchant, D.R. (2003) Recent ice ages on Mars. *Nature* 426, 797-802.
- Karrow, P.F., and Bada, J.L. (1980) Amino acid racemization dating of Quaternary raised marine terraces in San Diego County, California. *Geology* 8, 200-204.
- Kern, J.P. & Rockwell, T.K. (1992) Chronology and deformation of Quaternary marine shorelines, San Diego County, California: in *Quaternary Coasts of the United States: Marine and Lacustrine Systems: Society of Economic Paleontologists and Mineralogists Special Publication* 48, 377-382.

- Kieft, T.L., Amy, P.S., Brockman, F.J., Fredrickson, J.K., Bjornstad, B.N., and Rosacker, L.L. (1993) Microbial Abundance and Activities in Relation to Water Potential in the Vadose Zones of Arid and Semiarid Sites. *Microb. Ecol.* 26, 59-78.
- Klingelhöfer, G., Morris, R.V., Bernhardt, B., Schröder, C., Rodionov, D.S., de Souza Jr., P.A., Yen, A., Gellert, R., Evlanov, E.N., Zubkov, B., Foh, J., Bonnes, U., Kankeleit, E., Gütlich, P., Ming, D.W., Renz, F., Wdowiak, T., Squyres, S.W., & Arvidson, R.E. (2004) Jarosite and Hematite at Meridiani Planum from Opportunity's Mössbauer Spectrometer. *Science* 306, 1740-1745.
- Kminek, G., and Bada, J.L. (2006) The effect of ionizing radiation on the preservation of amino acids on Mars. *EPSL* 245, 1-5.
- Ku, T.L. & Kern, J.P. (1974) Uranium-Series Age of Upper Pleistocene Nestor Terrace, San-Diego, California. *Geological Society of America Bulletin* 85, 1713-1716.
- Lal, D. (2004) Assessing past climate changes from proxy records: an iterative process between discovery and observations. *Quaternary International* 117(1), 5-16.
- Lal, D., Abbott, P.L., Schopf, J.W., Vacher, L., & Jull, A.J.T. Nuclear, chemical and biological characterization of formation histories of ironstones from several sties in S. California: dominant role of bacterial activity. Submitted.
- Malin, M.C., Edgett, K.S., Posiolova, L.V., McColley, S.M., & Dobrea, E.Z.N. (2006) Present-Day Impact Cratering Rate and Contemporary Gully Activity on Mars. *Science* 314, 1573-1577.
- McLennan, S.M., Bell III, J.F., Calvin, W.M., Christensen, P.R., Blank, B.C., de Souza, P.A., Farmer, J., Farrand, W.H., Fike, D.A., Gellert, R., Ghosh, A., Glotch, T.D., Grotzinger, J.P., Hahn, B., Herkenhoff, K.E., Hurowitz, J.A., Johnson, J.R., Johnson, S.S., Jolliff, B., Klingelhöfer, G., Knoll, A.H., Learner, Z., Malin, M.C., McSween Jr., H.Y., Pockock, J., Ruff, S.W., Soderblom, L.A., Squyres, S.W., Tosca, N.J., Watters, W.A., Wyatt, M.B., and Yen, A. (2005) Provenance and diagenesis of the evaporite-bearing Burns formation, Meridiani Planum, Mars. *EPSL* 240, 95-121.
- Miller, S.L., & Bada, J.L. (1988) Submarine hot springs and the origin of life. *Nature* 334, 609-611.
- Morris, R.V., Ming, D.W., Graff, T.G., Arvidson, R.E., Bell III, J.F., Squyres, S.W., Mertzman, S.A., Gruener, J.E., Golden, D.C., Le, L., and Robinson, G.A. (2005) Hematite spherules in basaltic tephra altered under aqueous acid-sulfate conditions on Mauna Kea volcano, Hawaii: Possible clues for the occurrence of hematite-rich spherules in the Burns formation at Meridiani Planum, Mars. *EPSL* 240, 168-178.
- Neidhardt, F.C., Ingraham, J.L., & Schaechter, M. (1990) *Physiology of the bacterial cell: a molecular approach*. Sinauer Associates, Inc., Sunderland, Mass.
- Rieder, R., Gellert, R., Anderson, R.C., Brückner, J., Clark, B.C., Dreibus, G., Economou, T., Klingelhöfer, G., Lugmair, G.W., Ming, D.W., Squyres, S.W., d'Uston, C., Wänke, H., Yen, A.,

& Zipfel, J. (2004) Chemistry of Rocks and Soils at Meridiani Planum from the Alpha Particle X-ray Spectrometer. *Science* 306, 1746-1749.

Shackleton, N.J. (1987) Oxygen Isotopes, Ice Volume and Sea Level. *Quaternary Science Reviews* 6, 183-190.

Soderblom, L.A., Anderson, R.C., Arvidson, R.E., Bell III, J.F., Cabrol, N.A., Calvin, W., Christensen, P.R., Clark, B.C., Economou, T., Ehlmann, B.L., Farrand, W.H., Fike, D., Gellert, R., Clotch, T.D., Golombek, M.P., Greeley, R., Grotzinger, J.P., Herkenhoff, K.E., Jerolmack, D.J., Johnson, J.R., Jolliff, B., Klingelhöfer, G., Knoll, A.H., Learner, Z.A., Li, R., Malin, M.C., McLennan, S.M., McSween, H.Y., Ming, D.W., Morris, R.V., Rice Jr., J.W., Richter, L., Rieder, R., Rodionov, D., Schröder, C., Seelos IV, F.P., Soderblom, J.M., Squyres, S.W., Sullivan, R., Watters, W.A., Weitz, C.M., Wyatt, M.B., Yen, A., & Zipfel, J. (2004) Soils of Eagle Crater and Meridiani Planum at the Opportunity Rover Landing Site. *Science* 306, 1723-1726.

Souza-Egipsy, V., Ormö, J., Beitle, B.B., Chan, M.A., & Komatsu, G. (2006) Ultrastructural Study of Iron Oxide Precipitates: Implications for the Search for Biosignatures in the Meridiani Hematite Concretions, Mars. *Astrobiology* 6, 527-545.

Squyres, S.W., Arvidson, R.E., Bell III, J.F., Brückner, J., Cabrol, N.A., Calvin, W., Carr, M.H., Christensen, P.R., Clark, B.C., Crumpler, L., Des Marais, D.J., d'Uston, C., Economou, T., Farmer, J., Farrand, W., Folkner, W., Golombek, M., Gorevan, S., Grant, J.A., Greeley, R., Grotzinger, J., Haskin, L., Herkenhoff, K.E., Hviid, S., Johnson, J., Klingelhöfer, G., Knoll, A.H., Landis, G., Lemmon, M., Li, R., Madsen, M.B., Malin, M.C., McLennan, S.M., McSween, H.Y., Ming, D.W., Moersch, J., Morris, R.V., Parker, T., Rice Jr., J.W., Richter, L., Rieder, R., Sims, M., Smith, M., Smith, P., Soderblom, L.A., Sullivan, R., Wänke, H., Wdowiak, T., Wolff, M. & Yen, A. (2004a) The Opportunity Rover's Athena Science Investigation at Meridiani Planum, Mars. *Science* 306, 1698-1703.

Squyres, S.W., Grotzinger, J.P., Arvidson, R.E., Bell III, J.F., Calvin, W., Christensen, P.R., Clark, B.C., Crisp, J.A., Farrand, W.H., Herkenhoff, K.E., Johnson, J.R., Klingelhöfer, G., Knoll, A.H., McLennan, S.M., McSween Jr., H.Y., Morris, R.V., Rice Jr., J.W., Rieder, R., & Soderblom, L.A. (2004b) In Situ Evidence for an Ancient Aqueous Environment at Meridiani Planum, Mars. *Science* 306, 1709-1714.

Sumner, D.Y. (2004) Poor preservation potential of organics in Meridiani Planum hematite-bearing sedimentary rocks. *JGR* 109, E12007.

Tebo B. M., Ghiorse W. C., van Waasbergen L. G., Siering P. L., & Caspi R. (1997) Bacterially mediated mineral formation: Insights into manganese(II) oxidation from molecular genetic and biochemical studies. In *Geomicrobiology: Interactions Between Microbes and Minerals*, Vol. 35 (eds. J. F. Banfield and K. H. Nealson), pp. 225-266. Mineralogical Society of America.

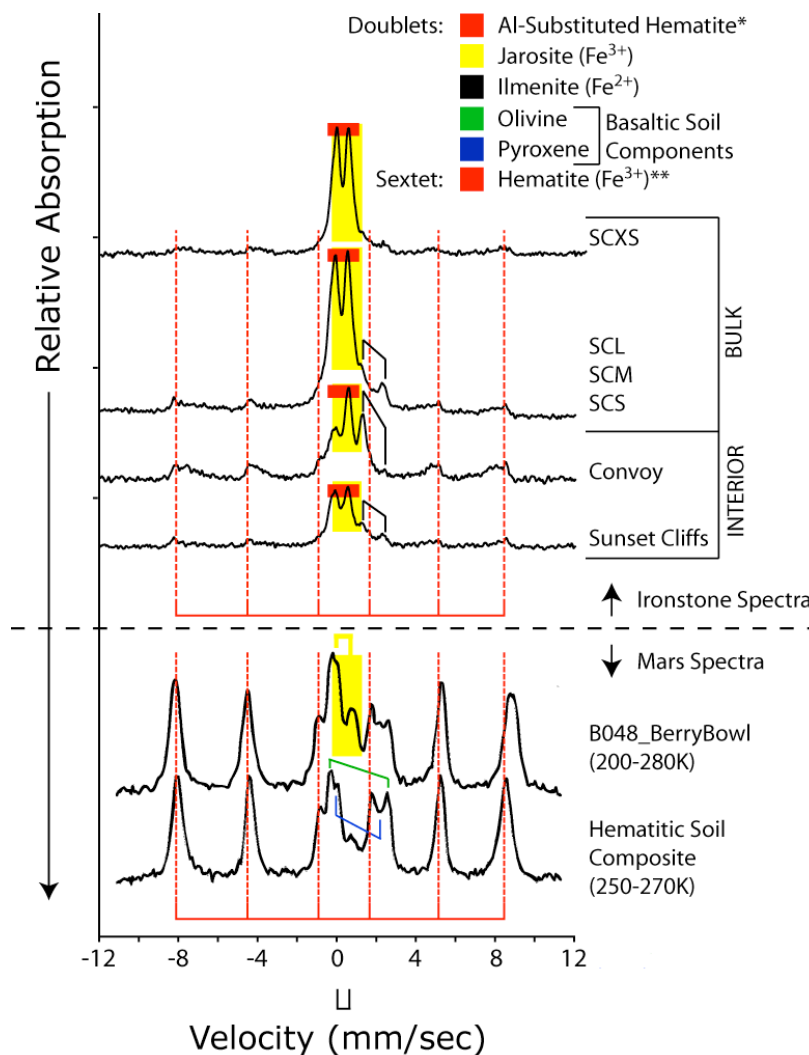
Thiry, M., Ayrault, M.R., & Grisoni, J.C. (1988) Ground-water silicification and leaching in sands: Example of the Fontainebleau Sand (Oligocene) in the Paris Basin. *Geological Society of America Bulletin* 100, 1283-1290.

Wehmiller, J.F. (1977) Amino Acid Studies of the Del Mar, California, Midden Site: Apparent Rate Constants, Ground Temperature Models, and Chronological Implications. *EPSL* 37, 184-196.

Weiner, S., and Dove, P.M. (2003) in *Biom mineralization*. Mineralogical Society of America Geochemical Society, eds. Dove, P.M., De Yoreo, J.J., and Weiner, S. Washington, D.C., pp. 5.

Zhao, M., & Bada, J.L. (1995) Determination of α -dialkylamino acids and their enantiomers in geological samples by high-performance liquid chromatography after derivatization with a chiral adduct of o-phthalaldehyde. *Journal of Chromatography A* 690, 55-63.

SUPPLEMENTARY INFORMATION 5.A Mossbauer spectrometer data showing the analyzed samples compared to Mars Spectra collected by the MER Opportunity. All 6 analyzed ironstone samples show a sextet associated with hematite Fe^{3+} and peaks that may correspond to jarosite and goethite may also be present.



* Also close to doublet for nanophase palagonite, ferrihydrite, goethite, schwertmannite, and akaganeite.

** Also could represent maghemite, magnetite.

Methods. Mossbauer spectrometry data analyzed by M. Darby Dyar at Mount Holyoke College and expanded results & discussion available by request. Sample mounts were prepared by gently crushing 10-14 mg of sample under acetone, then mixing with a sugar-acetone solution designed to form sugar coatings around each grain and prevent preferred orientation. Grains were gently heaped in a sample holder confined by Kapton tape. Mössbauer spectra were acquired at 295K using a source of ~ 50 mCi ^{57}Co in Rh on a WEB Research Co. model WT302 spectrometer (Mount Holyoke College).

CHAPTER VI. South African Gold Mines – Low Biodensity Microbial Communities

ABSTRACT

Studies on water samples from the Witwatersrand Basin, South Africa, contain thermophilic sulfate reducing bacteria (SRB) that show incredibly slow turnover times ($\sim 10^3$ years) and low biomass densities ($< 10^5$ cells/mL). The methods used to estimate turnover times in previous studies may reflect errors associated with sulfate reduction rate calculations. Amino acid abundance data from water filtrate samples and a steady-state model of the microbial community structure is extrapolated to bacterial densities and turnover times from five fracture waters at 3 different mine locations in South Africa. These results are found to be consistent with previous estimates and reflect a unique biological community with low metabolic rates and large turnover time most likely limited by nutrient availability in these deep and isolated extreme environments.

6.1 INTRODUCTION

The Witwatersrand Basin in South Africa currently provides the best access to deep fracture waters in the continental subsurface (Figure 6.1). It is set within a large Archean intracratonic basin composed of volcanosedimentary sequences divided chronologically into the schist basement, the sedimentary quartzite and shale layers of the Witwatersrand Supergroup, and the andesitic lava sequence of the Ventersdorp Supergroup (Coward et al., 1995). The Witwatersrand Supergroup (~ 3000 to 2800 Ma) overlies the schist basement (~ 3070 Ma) and is the main focus for gold mining in the basin. The Witwatersrand Supergroup has been metamorphosed to lower greenschist facies and divided into two groups based on depositional characteristics. The lower part of the Witwatersrand Supergroup (the West Rand Group) is composed of marine distal shelf facies with a minor intertidal component. They are characterized as sands, greywacke, shales, and argillites with minor-banded ironstones and can reach a maximum thickness of 7500m (Coward et al., 1995). The upper part of the Witwatersrand Supergroup (Central Rand Group) is composed of fragments derived from the eroded basement. It is characterized by an upwards-coarsening depositional pattern of fluvial sands, quartzites, and conglomerates with minor shale layers that reach a maximum thickness of 2900m. Overlying the

Central Rand Group is the thick sequence of andesitic lavas that comprises the Ventersdorp Supergroup (2700 Ma). This layer is comprised of up to 1840m of bimodal volcanics, thinner layers of sandstone and conglomerate, and a layer of tholeiitic flood basalt (Coward et al., 1995). The organic-rich Black Reef quartzite deposit marks the transition between the Ventersdorp Supergroup and the Transvaal Supergroup (2000–2500 Ma) (Coward et al., 1995). The Transvaal sediments consist of a thick dolomitic unit overlain by terrigenous sediments. Uplift of the Vredefort Dome at the centre of the Witwatersrand basin (2025 Ma) resulted in deformation of the Transvaal sediments, the Ventersdorp, and the Witwatersrand Supergroups (Coward et al., 1995).

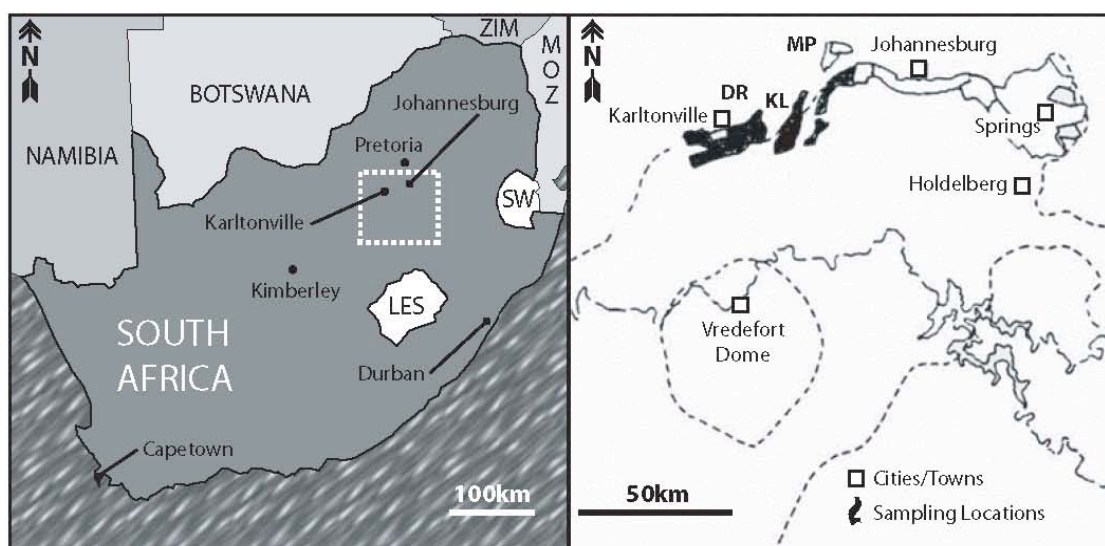


Figure 6.1 Location of South African sampling sites (modified from Slater et al., 2006).

The geochemistry and ages of waters from the Witwatersrand Basin mines have been well documented in previous studies (Onstott et al., 2006). Microbiological studies on these samples has helped extend the biosphere's known depth limit of groundwater environments that contain diverse sulfate reducing microbial communities (Takai et al., 2001a, 2001b; Kieft et al., 1999, 2005; Baker et al., 2003; Moser et al., 2003, 2005; Onstott et al., 2003, 2006; Lin et al., 2002, 2005, 2006; Gihring et al., 2006; Pfiffner et al., 2006). The metabolic activities of these microbes are intimately tied to the geochemical and mineralogical processes occurring in the subsurface. It has even been suggested that subsurface reservoirs contain the majority of the Earth's prokaryotic cells (Whitman et al., 1998; Onstott et al., 1999).

The majority of subsurface ecosystems studied to date have been dominantly heterotrophic, with microbes metabolizing photosynthetically generated organic carbon that has been buried or transported to the subsurface by groundwater flow. Given the long burial times of deep sediments and slow rates of groundwater flow (Murphy et al., 1992), these systems appear to be nutrient limited. The bacteria found deep in the remote Witwatersrand mines are chemoautotrophic sulfate reducers. They metabolize radiolytically generated H_2 along with sulfate generated from oxidation of buried pyrite by radiolytically generated O_2 and H_2O_2 (Lin et al., 2006). These findings expand the concept of subsurface chemoautotrophic microbial ecosystems (Stevens & McKinley, 1995; Pedersen, 1997; Chapelle et al. 2002) to a deeper geologic setting and a novel mechanism. Determining the age of these microbes, their carbon turnover rates, and their potential for metabolic activity is a next logical step in understanding their biogeochemistry.

Geochemical modeling of microbially mediated reactions has repeatedly shown that subsurface microorganisms function at rates of metabolism that are orders of magnitude slower than those of their surface counterparts (Chapelle and Lovley, 1990; Murphy et al., 1992; Phelps et al., 1994; Kieft et al., 1997). These extremely slow rates correspond to generation times of hundreds to thousands of years (Phelps et al., 1994). If cells are to survive for these long intervals, they must maintain cellular integrity and a minimum of necessary cellular macromolecules via endogenous metabolism (Kieft, 2002). The physiological condition of deeply sequestered cells in the subsurface is not well understood. The slow rates of metabolism and long generation times suggest that they are in a condition of long-term starvation and that a significant proportion may be dead. As described above, a similar situation exists in deep ocean sediments, where large numbers of cells have been detected despite low nutrient fluxes. A recent study showed that a surprisingly high proportion of these cells are metabolically active, as indicated by fluorescent in situ hybridization (FISH), which detects cells containing a sufficiently high number of ribosomes (Schippers et al., 2005). In this study, 1/10 to 1/3 of the cells were active by this definition, despite the apparent paucity of energy. For deep terrestrial groundwater, even less is known of how many cells are active or alive.

The importance of cell viability, activity, and C turnover time in subsurface environments cannot be over-emphasized. The rates of metabolic activities, reproduction, and C turnover in these systems have a direct bearing on the rates of microbially mediated geochemical processes in

deep fracture waters, e.g., the rates of mineral weathering and dissolution, and also the extent to which subsurface biomass participates in biogeochemical cycling in communication with the surface world. A similar uncertainty exists for sub-seafloor sediments, which represent another remote and difficult to sample but globally important part of the biosphere. D'Hondt et al. (2002) reported extremely low rates of metabolic activity in deep sea sediments, especially when considered on a per cell basis. Such low rates of metabolism correspond to extremely long microbial generation times (>1000 yrs, Jorgensen and D'Hondt, 2006). However, when the rates of activity are calculated on the basis of metabolically active cells only, then the cellular turnover times are much shorter. Schippers et al. (2005) estimated C turnover times of 0.25-22 yrs for metabolically active (ribosome-rich) bacteria in deep-sea sediments. However, these rates do not take into account what may be a "starving majority" of cells.

Five fracture water samples from three different South African gold mines were investigated in this study: the Mponeng (MP), Driefontein (DR), and Kloof (KL) mines. Biosignatures that indicate dead cells, in some cases cells that have been dead for geologically significant time periods, include diglyceride fatty acids that result from dephosphorylation of membrane lipids (Kieft et al., 1998); and depurination of DNA and racemization of amino acids (Poinar et al., 1996). The latter is an especially telling signal of long-term damage to cells; formation of a completely racemic mixture from a biological source is estimated to occur in 10^5 - 10^6 years in most environments (Bada et al., 1999). Amino acid analyses of these fracture waters can verify the biodensities in these fracture waters and turnover times can be estimated by simple modeling. Amino acid chirality can provide a good comparison of bacterial abundances and turnover times to compare to the numbers estimated by other methods.

6.2 MATERIALS & METHODS

Fracture water sampling. The filtrate samples were obtained from the sample locations (Figure 6.1) by the Princeton Geosciences group in 2002-2003 as described in a previous study (Moser et al., 2003). A subset of 5 filters was sent to Scripps for amino acid analyses in order to corroborate the biodensity estimates.

Table 6.1 Filter samples sent to SIO for analyses.

Filter Sample	Depth (kmbls.)	T (°C)	pH	TOC ¹ (M)	Salinity (ppt)	Age (Ma)	V (L)
DR4 IPC 060902	0.945	27	7.2	6.83×10^{-4}	0.0148	0.013	29,898
MP104 E65XC H1 091902	2.825	52	9.3	4.33×10^{-4}	3.51	30	2,271
KL739 081903	3.100	54	9.5	4.92×10^{-4}	2.67	100	1,000*
KL441 FW 051702	3.300	56	9.1	1.00×10^{-4}	1.74	3-13	155.2
XC56 HWDS H2							
DR938 H2 071602	3.350	54	9.1	3.50×10^{-4}	1.00	3-13	5,178

NOTE: pH and temperature were measured at the time of sampling with a portable meter.

*Volume estimated (Dirk Opperman, written communication).

¹TOC reported for identical boreholes from Onstott et al. (2006).

²Noble gas derived ages reported from Lippman et al. (2003).

The mines regularly drill cover boreholes hundreds of meters into unmined rock to locate water-filled fractures, and these allow for access to the samples evaluated in this study. A sterile expanding packer/manifold assembly was placed into the opening of the borehole and sealed to the inner rock walls below water level to seal the borehole. Water was allowed to flow through the apparatus long enough to displace any air remaining in the borehole or the apparatus before sampling. Thousands of liters of each fracture water sample was concentrated using 1µm pore size Cole Parmer submicronic polypropylene filter cartridge (Model #A-06479-32). The filtration area is specified as 4.00 ft² and was autoclaved at 121°C prior to use. The filters were directly attached by quick-connects to the sampling apparatus, allowing for aseptic in situ filtering without exposure to the mine atmosphere. Approximately ¼ of each of the 5 filter samples was shipped frozen to SIO for amino acid analyses.

Amino acid analyses. The filter samples were received at Scripps Institution of Oceanography stored in a -20°C freezer prior to analysis. Strips of the filter samples, approximately 2 cm wide and 15 cm long (~1.5 grams each), were taken for analysis. The raw filter pieces were first cut into small strips with sterile surgical blades. Extraction was performed in 4mL of double-distilled water for 24 hours at 100°C followed by vapor-phase hydrolysis on the supernatant of the dry filter water extract (~2/3 of the water extract) in 6N HCl at 100°C for 24 hours. The remaining water (~1/3 of the total volume) was adsorbed by the filter and attempts at full recovery of the 4mL original water volume was unsuccessful. Following the extractions, the residues were desalted with AG 50W-X8 resin in order to isolate the amino acids and amines according to a microscale adaptation of the procedure of Amelung & Zhang (2001). The desalting fraction was concentrated into 100µL from which 10µL of each sample was analyzed by

HPLC with pre-column OPA/NAC derivatization (Zhao & Bada, 1995). Samples were quantified against known standards for the amino acids aspartic acid (D/L), serine (D/L), glutamic acid (D/L), glycine, alanine (D/L), and valine (D/L).

In order to quantify the amount of filtered water each analyzed fraction represented, a new filter was weighed out to determine the filter area per unit mass. The new filter (95.3g) was specified to have an equivalent filter surface area of 0.4 m² and each gram was found to represent 0.041973 ft². This number was used to normalize the mass of each analyzed filter portion (vacuum dried mass, after extraction) to an equivalent filtered water volume using the total liters filtered.

6.3 RESULTS & DISCUSSION

Filtered fracture water samples were obtained from 0.945 to 3.350 km depth, ranging in salinity from 0.0148-3.51 ppt at temperatures up to 56°C (Table 6.1). The deeper boreholes (2-3.2 kmbls) have the most saline water (due to prolonged water-rock interaction), $\delta^2\text{H}/\delta^{18}\text{O}$ values that lie off the meteoric water line (Onstott et al., 2006), and He-Xe ages of 40-160 Myr (Lippmann et al., 2003). S isotope data indicate biological sulfate reduction, and $\delta^2\text{H}/\delta^{13}\text{C}$ data indicate abiotic C1-C4 hydrocarbon formation in these deep waters (Kieft et al., 2005; Moser et al., 2005; Ward et al., 2004; Lin et al., 2006; Sherwood Lollar et al., 2006). Some of these deep waters contain surprisingly high concentrations (1-10 mM) of potential microbial carbon and energy sources such as H₂, CH₄, and acetate (Kieft et al., 2005; Lin et al., 2006). The H₂ is explained by radiolysis of water from U and Th decay; this abiogenic H₂ supports a chemoautotrophic ecosystem of dominantly sulfate reducing bacteria (Lin et al., 2006).

Shallower, less saline waters (≤ 1.6 kmbls) are younger with $\delta^2\text{H}/\delta^{18}\text{O}$ values that lie on the meteoric water line, and $\delta^2\text{H}/\delta^{13}\text{C}$ evidence of biological methanogenesis (Slater et al., 2006). Membrane phospholipid fatty acid (PLFA) quantities and flow cytometric analyses indicate cell densities in the 10³-10⁴ cells ml⁻¹ range at most depths (Pfiffner et al., 2006). Methanogens have been detected in fracture fluids from depths ≤ 1.6 kmbls and in service water used for mining, but appear to be absent or insignificant in the deeper, hotter, more saline fracture fluids.

The amino acid compositions of five filter samples were determined for the biological L-amino acids and non-biological D-amino acids. Terrestrial life is composed almost exclusively of L-amino acids which racemize with time after the death of the organism to form D-amino acids.

The relative amounts of these two amino acid configurations can be used for chronological dating of geological samples (Bada et al., 1999) and provide a useful means to evaluate the effect of time on the stability of these key biomolecules.

The chromatograms from the filter extractions are shown in Figure 6.2 and the data reported for the 5 filter samples in Table 6.2. The amino acid concentrations (ng/mL) and aspartic acid D/L ratios for all four of the fracture water samples is reported in Table 6.2 and Figure 6.3. Triplicate sample extracts were similar in distribution, composition, and chirality. It is thus assumed that the extraction procedures on the filter samples were efficient in removing most of the cellular proteins which were hydrolyzed to monomeric amino acids. The low D/L-amino acid enantiomeric ratios show that the original chirality signal has been preserved despite the elevated temperatures (~50°C) and that the bulk of the amino acids are likely from extant cells. The slightly higher D/L-alanine ratio is expected for bacterial communities because of the D-alanine contribution of peptidoglycan, a component of bacterial cell walls (Beveridge, 1989).

Table 6.2 Amino acid concentrations reported in ng/L based on volume of water filtered from South African mine samples. Biodensities were estimated assuming the quantified amino acids represent 70% of the total bacterial protein (Chapter 2), a microbial cell protein content of 55% (Brock, 1970), and that the mass of each cell is 20 fg (Lin et al., 2006).

Sample	DR4	DR938	MP104	KL739	KL441
D-Asp	0.00792	0.0431	0.0651	0.332	1.27
L-Asp	0.179	0.805	1.31	5.09	12.9
L-Glu	0.00839	0.0436	0.0532	0.150	0.934
L-Glu	0.134	0.521	0.813	2.49	11.1
D-Ser	0.0198	0.0998	0.182	0.564	2.35
L-Ser	0.377	2.10	3.69	12.4	27.5
Gly	0.326	1.16	2.32	11.1	21.3
D-Ala	0.0716	0.551	0.556	2.71	8.27
L-Ala	0.203	1.02	2.23	5.51	19.3
D-Val	0.00239	0.100	0.0182	0.0840	0.341
L-Val	0.113	0.490	0.728	11.9	12.5
TOTAL¹	1.44	6.93	12.0	52.3	118
C.E. (cells/mL)²	2.0 x 10²	9.5 x 10²	1.6 x 10³	7.2 x 10³	1.6 x 10⁴

¹Σ = Asp, Glu, Ser, Gly, Ala, Val.
²Assumed a cell mass of 20 fg per cell (Lin et al., 2006) and 55% protein by mass (Brock, 1970).

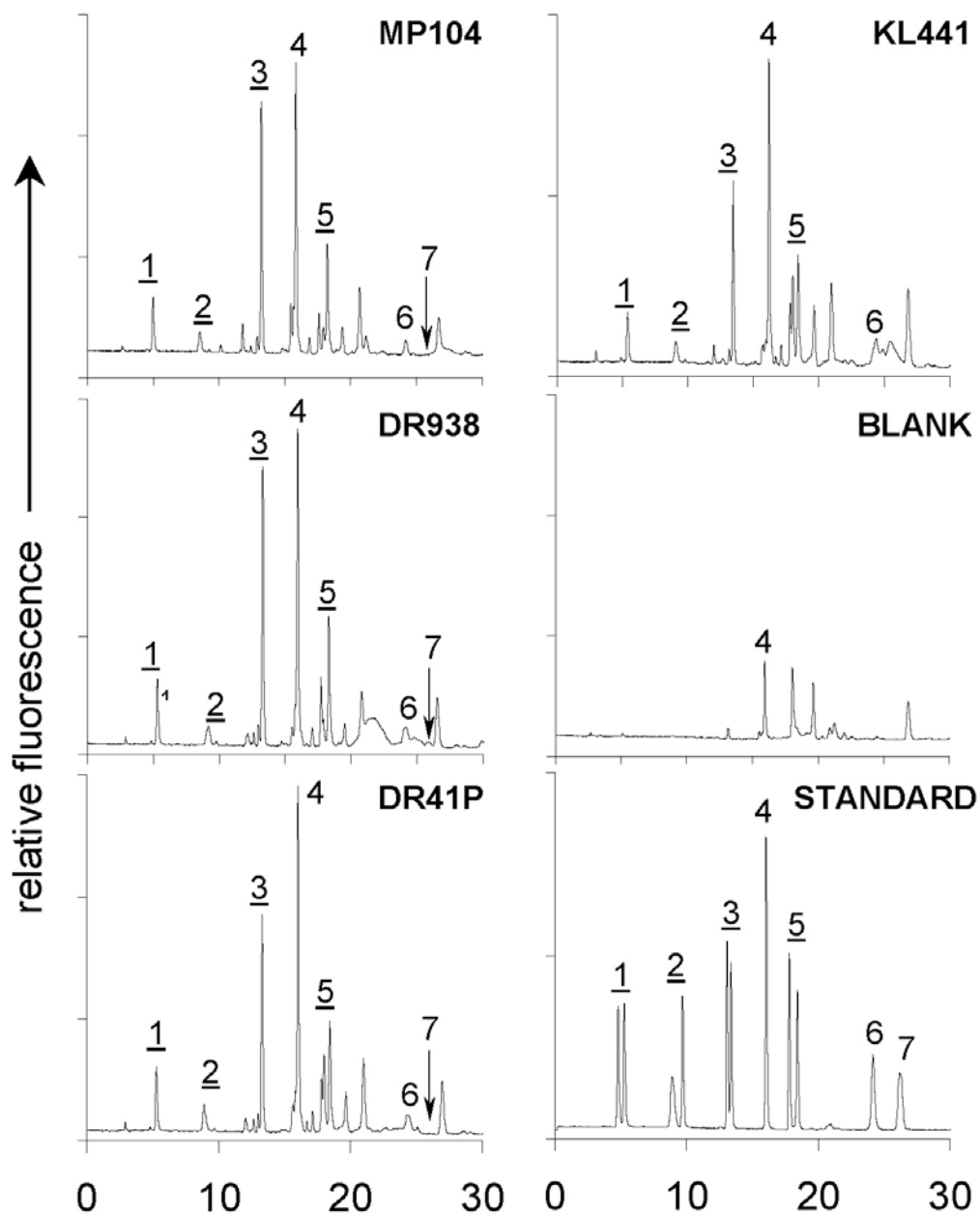


Figure 6.2 Amino acid chromatograms of the low-level filtrate samples, an extract of which was derivatized using OPA/NAC and compared to the blank and a racemic standard. Backgrounds of glycine and two unidentified peaks can be seen and are due to trace concentrations carried through the sample extraction. 1=D/L-Asp, 2=L/D-Glu, 3=D/L-Ser, 4=Gly, 5=D/L-Ala, 6=L-Val, 7=D-Val.

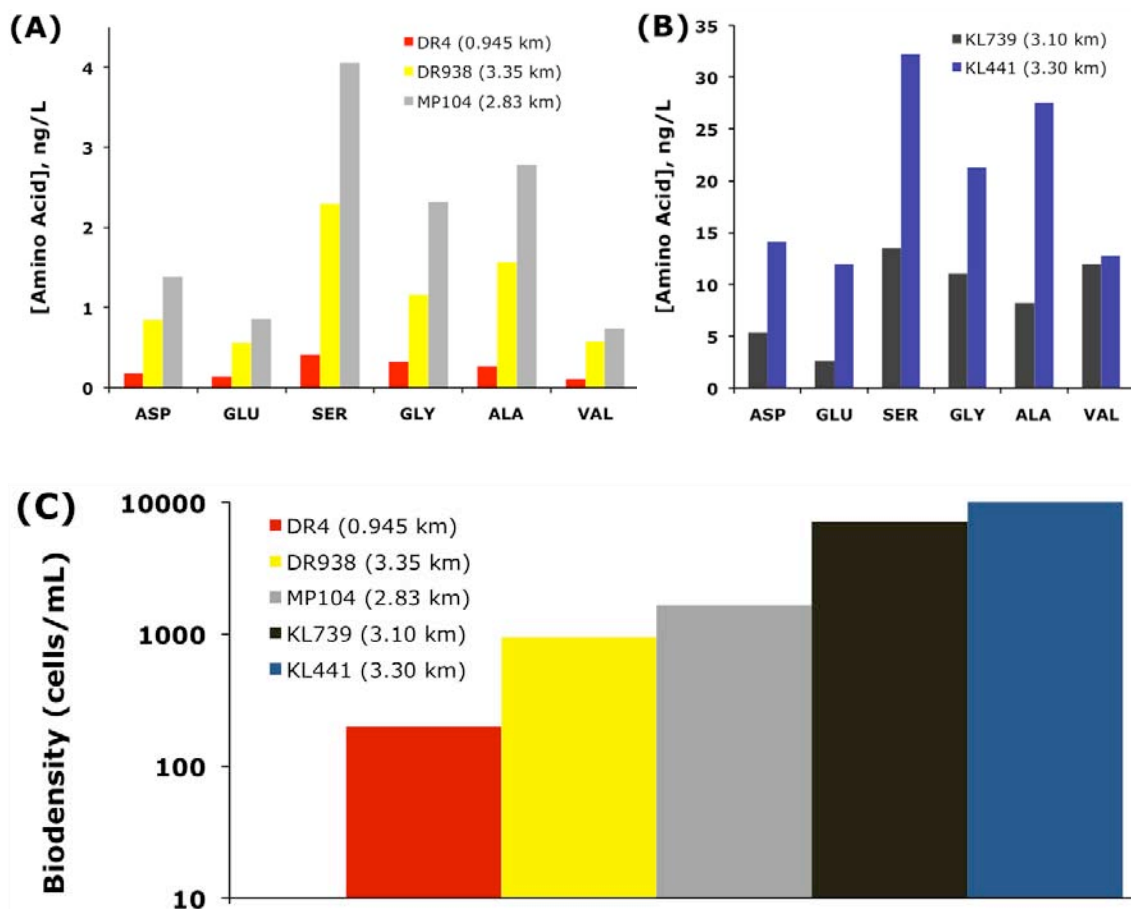


Figure 6.3 Amino acid concentrations measured from deep fracture sample filtrates. Samples are grouped generally into low concentration filtrates (A) and high concentration filtrates (B) and the calculated equivalent cell densities are shown (C).

The most interesting aspect of these plots are the extremely low D/L-ratios which are indicative of only trace quantities of the abiological amino acids. Hydrolyzing samples of pure *E.coli* still causes a little bit of racemization during sample workup. For most amino acids, this is only equal to 0.02, however for alanine, this is equal to 0.05. Therefore, to deduce the actual signal that is coming from racemization within the microbial community, we can subtract these numbers off of the total to get the actual D/L for use in our model.

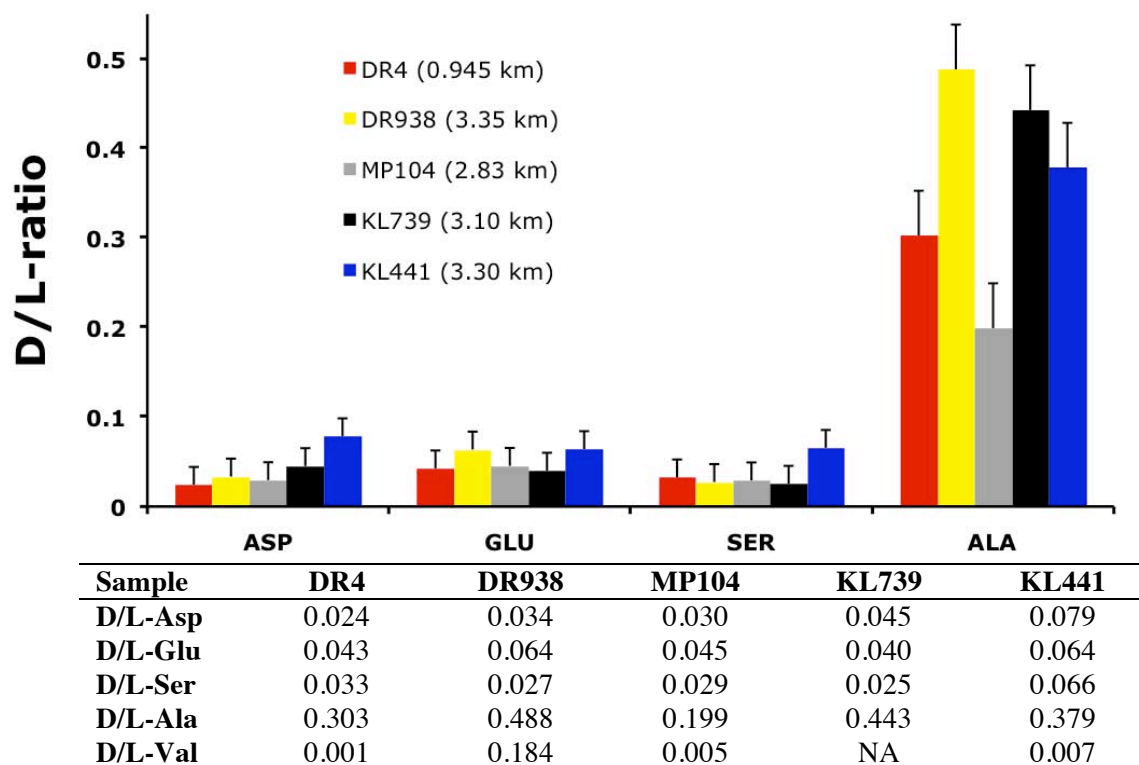


Figure 6.4 Filter sample amino acid D/L-enantiomeric ratios. Reported values are corrected assuming that the induced racemization during acid hydrolysis was 0.02 for all amino acids except for alanine which is 0.05 (Chapter 2). The error bars reflect these corrections. Valine enantiomeric ratios not reported due to interference by coeluting peaks (Figure 6.2).

If it is assumed that the bacterial community is at a steady-state composition with respect to bacterial density, composition, and D/L ratios, then we can infer bacterial cell counts based on total protein amino acids. The amino acids can be extrapolated to bacterial cell counts based on the known composition of a bacterial cell. The total amino acids quantified from the filter can be assumed to represent ~70% of the total amino acids (Chapter 2) and the total protein per cell estimated at 55% (Brock, 1970). Using the average mass of a sulfate reducing bacterial cell, ~20 fg (Lin et al., 2006), the bacterial density can be extrapolated to yield cells/mL. These cell enumeration results are shown in Table 6.2 and Figure 6.3. The amino acids represent from 10^2 - 10^4 bacterial cells per mL in each of the fracture waters. These data are in good agreement with the cell counts previously reported for the site MP104 estimated using sulfate reduction rates (Lin et al., 2006).

Some conclusions can be made regarding turnover rates of the bacterial communities based on the presence of D-amino acids. The presence of only protein amino acids and L-enantiomers show that the majority of the amino acids are from living cells, or cells that have not degraded with time. This could also be a signal from dormant bacteria that is still alive. The trace D-amino acids detected must be derived from extinct bacteria that has been subject to racemization with time. The presence of D-amino acids reveals that the degradation of inactive proteins and component amino acids is slow enough to allow their accumulation as an essentially 'dead' reservoir. The living cells provide new biological amino acids through bacterial turnover while the amino acids from dead cells racemize and subsequently degrade. The relative amounts of D and L amino acids can be used to determine turnover time by using a simple enantiomeric mass balance model of the dynamics of a bacterial community (Figure 6.5). This model assumes that these deep subsurface microbes exist in a steady-state condition of long-term nutrient limitation. Some of these cells remain viable for hundreds to thousands of years in prolonged maintenance mode. If we assume that the colonies are at a steady state condition, then we must analyze sources of the amino acid enantiomers versus sinks.

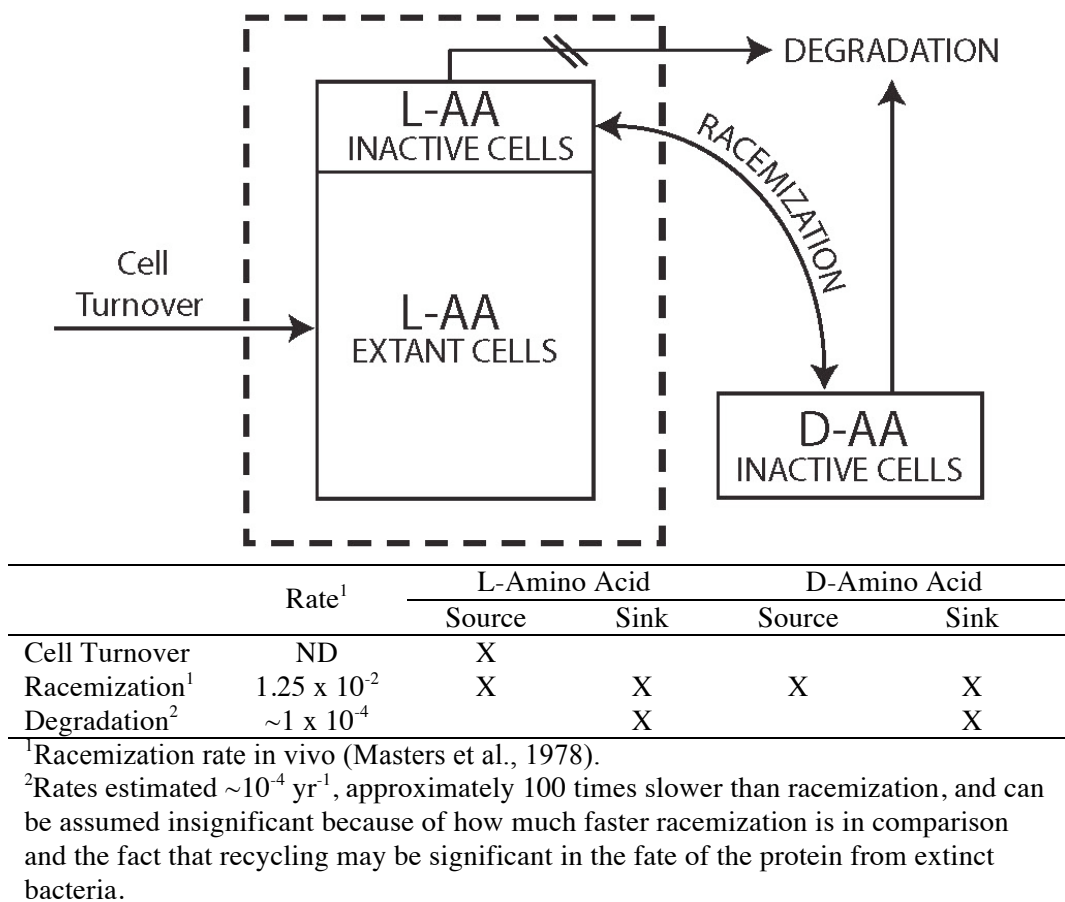


Figure 6.5 Schematic for steady-state amino acid racemization box model.

The sources of biological L-amino acids are the current living pool of bacteria along with the new bacteria that forms at a rate equivalent to the turnover time (t_{TO}). The turnover time is the times that it takes for a bacterial community to double in number, that is, the time required for each cell to divide (Turnover time = Cell Pool Size / Addition Rate = years). D-amino acids are formed by the racemization of proteinaceous L-amino acids from extinct microorganisms (k_{RAC}). The *in vivo* racemization rate is estimated to be the fastest in the literature (Masters et al., 1978). Racemization also serves as a sink for L-amino acids. Both configurations of amino acids are destroyed by degradation, primarily decarboxylation for amino acids such as glycine and primarily deamination for amino acids such as aspartic acid (Li & Brill, 2003). These rates are typically 100-1000 times slower than racemization kinetics and are therefore viewed as insignificant to the overall mass balance (Figure 6.5). Another reason that the amino acid degradation kinetics are omitted is that the bacterial remnants from dead microbes are most likely

recycled on faster timescales than the degradation kinetics show. Therefore, because of the unknown fates of the extinct amino acids, these rates are not included in our model.

First the two amino acid reservoirs must be quantified. There is a general cell pool from the total amino acid data quantified with both D- and L-enantiomers. This pool represents the total cells, both living (viable) and dead (inactivated). The major unknown is the fraction of the bacterial community that is subject to racemization, that is the fraction of cells that are dead, or inactivated, and experiences *in vivo* racemization. This major unknown in this model is solved for assuming the D/L ratio of 1 for dead, or inactivated, bacterial cells. This assumption allows for an upper limit on viable cells to be determined because the smallest number of dead cells can account for the observed D-enantiomeric abundance, assuming that detected D-amino acids are from extinct bacteria which have racemized with time since death. Equations 1 and 2 are amino acid mass balances based on known D/L ratios of the total and inactivated (assumed) enantiomeric ratios. The two equations solve for the fraction of amino acids from extant life ($DASP_E$) and deactivated cells ($LASP_{DA}$) that are subject to racemization. This model is applied to aspartic acid, which shows the fastest amino acid racemization kinetics and should be the most sensitive for our purposes.

$$\text{Equation 6.1} \quad \frac{DASP_{DA}}{LASP_{DA}} = 0.25 \quad (\text{Based on Masters et al., 1978})$$

$$\text{Equation 6.2} \quad \frac{DASP_{DA}}{LASP_D + LASP_{DA}} = \frac{DASP}{LASP}$$

Using these equations, the fraction of viable and inactivated cells may be determined. As mentioned above, the major assumption is that the D/L ratio of inactivated bacterial proteins is equal to 0.25, an assumption based on a previous study which found that cells were effectively inactivated at a D/L \sim 0.2 (Masters et al., 1978), so we assumed the bulk dead fraction to be slightly higher.

The next procedure is to use the kinetics of racemization to determine the turnover time of the bacterial community, a steady-state mass balance modeling approach (Figure 6.5). In order to estimate the relevant kinetics of aspartic acid racemization, it is necessary to extrapolate the *in vivo* aspartic acid racemization rate constant to relevant temperatures. Aspartic acid racemizes the

fastest of the 20 proteinaceous amino acids and show D-amino acid enantiomers in every sample. The rate of aspartic acid racemization *in vivo* has been measured at $1.25 \times 10^{-3} \text{ yr}^{-1}$ in the water soluble fraction of human eye lens proteins (Masters et al., 1978). We can extrapolate this rate from 37°C to 52°C using Equation 6.3 and the activation energy for the racemization of aspartic acid, approximately $38 \pm 3 \text{ kcal/mole}$ (Bada, 1985).

Equation 6.3
$$\ln\left(\frac{k_{T_2}}{k_{T_1}}\right) = \frac{E_A \cdot \Delta T}{R \cdot T_1 \cdot T_2}$$

The rate of Aspartic acid *in vivo* racemization at 52°C is equal to $2.15 \times 10^{-2} \text{ yr}^{-1}$. Within the bacterial communities, the cells are dividing at the cell turnover rate. Therefore, the minimum cell turnover rate is the amount of time it would take for the deactivated cells (extinct life) to have their L-aspartic acid residues racemize *in vivo* to create the observed D/L ratio. We will assume for this model that any racemization is due to extinct bacterial cells to simplify things. In reality there may be minor amounts of racemization before a cell actually deactivates at a D/L ratio of <0.2 .

If we model amino acid concentrations as a function of time, this is shown in Equations 6.4 and 6.5.

Equation 6.4
$$\frac{dAA_T}{dt} = D_0 + L_0 + AA_{NEW} dt - AA_{DEG} dt$$

Equation 6.5
$$\frac{dAA_T}{dt} = D_{ASP,0} + L_{ASP,0} + k_{TO} \cdot CELLS \cdot \frac{L_{ASP}}{CELL} \cdot dt - k_{DC,ASP} \cdot (AA_T \cdot X) \cdot dt$$

If we assume that the biological system is at steady-state, the derivatives disappear giving a simple relationship shown in equation 3 which can be used to calculate the turnover time associated with these bacterial communities.

Equation 6.6
$$\left(k_{TO} \cdot CELLS \cdot \frac{L_{ASP}}{CELL}\right) + (D_{ASP} \cdot k_{RAC}) = k_{RAC} \cdot (AA_T \cdot X)$$

Equation 6.7

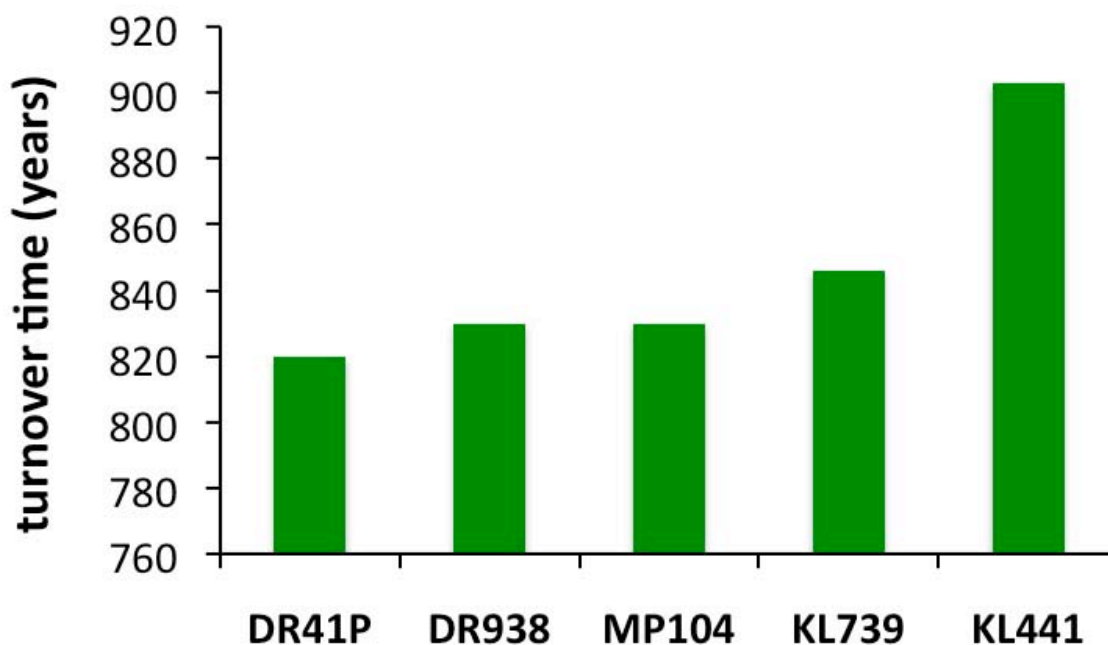
$$\frac{\text{Cells}/\text{mL}}{k_{TO}} \cdot \frac{[L-ASP]_E}{\text{Cells}/\text{mL}} + k_{RAC} \cdot [D-ASP] = k_{RAC} \cdot [L-ASP]_{DA}$$

The steady-state racemization model assumes two reservoirs of L-amino acids from extant cells, $[L-ASP]_E$, and inactive cells, $[L-ASP]_{DA}$. The D-amino acids, $[D-ASP]$, are formed from racemization of the inactive L-amino acids. The degradation rate of the D- and L-amino acids is assumed to be negligible because the rates associated with racemization are so much faster. The sources of L-amino acids are bacterial turnover and racemization. The only unknown in Equation 3 is the turnover rate, k_{TO} . The total cells have been determined based on total amino acids (Table 6.2) and the composition of aspartic acid to total cellular mass (L_{ASP}/cell) is known. It must be estimated that the fraction of lysed cells is equal to 10%. This allows for the correct relationship between the two cell reservoirs, alive and dead, to be specified.

The amino acid concentrations are in ng/mL and the rate constants are in yr^{-1} . The *in vivo* racemization rate constant at 50°C was estimated using data from Bada (1984) as $1.13 \times 10^{-2} \text{ yr}^{-1}$ and is similar to those reported in Masters et al. (1978). The cell density is taken from the amino acid cell enumeration, and the ratio of D-aspartic acid, $[D-ASP]$, to inactivated L-aspartic acid, $[L-ASP]_{DA}$, is estimated to be 0.2 (Masters et al., 1978).

The model turnover time range for the 5 filter samples is ~800 to ~900 years with an average of ~800 years. This agrees with turnover times calculated from alanine D/L-ratios of hundreds of years and the estimates from Lin et al. (2006), however this is a preliminary estimate and might not be an ideal model for this type of environment.

Amino acid turnover times for the 4 analyzed filter samples are reported in Figure 6.6. The MP104 filter samples has turnover times between 200-419 years with an average of 306 years. This agrees with turnover times calculated from alanine D/L-ratios of hundreds of years and the estimates from Lin et al. (2006).



Sample	Σ Amino acids (ng/mL)	Biodensity (cells/mL)	Fraction Living	Turnover Time (years)
DR41P	1.44	2.0×10^2	0.797	~820
DR938	6.93	9.5×10^2	0.758	~830
MP104	12.0	1.6×10^3	0.775	~830
KL739	52.3	7.2×10^3	0.712	~846
KL441	118	1.6×10^4	0.588	~903

Note: Total amino acids and inferred biodensities from Table 6.2. Turnover times and microbial reservoirs (fraction living) calculated using the steady-state model with aspartic acid assuming that inactive cells have a D/L ratio of 0.25 (Masters et al., 1978).

Figure 6.6 Amino acid derived cell counts and turnover times from fracture water communities.

The assumption of a DL-ratio of 0.25 shows that the deactivated amino acid pool has significant contribution to the L-amino acid pool as well. This implies that there is not very fast recycling of detrital bacterial remains, which may be reasonable based on the nutrient limited slow-metabolic sulfate reducing community present in these Witwatersrand mines. This may be an inaccurate assumption, but Figures 6.7-A and 6.7-B show the sensitivities of the fraction of cells alive (f) and turnover time versus assumed DL-ratio for filter MP104. As is evident from these curves, the fraction of viable cells is much more sensitive to this original assumption than the turnover times. Therefore, the turnover times show relatively high confidence rather than the absolute living fraction of cells. However, both are exponential curves, therefore, they show

relatively consistent results for D/L-ratio assumptions between 0.5 and 1.0 for the living fractions and 0.2 and 1.0 for turnover times.

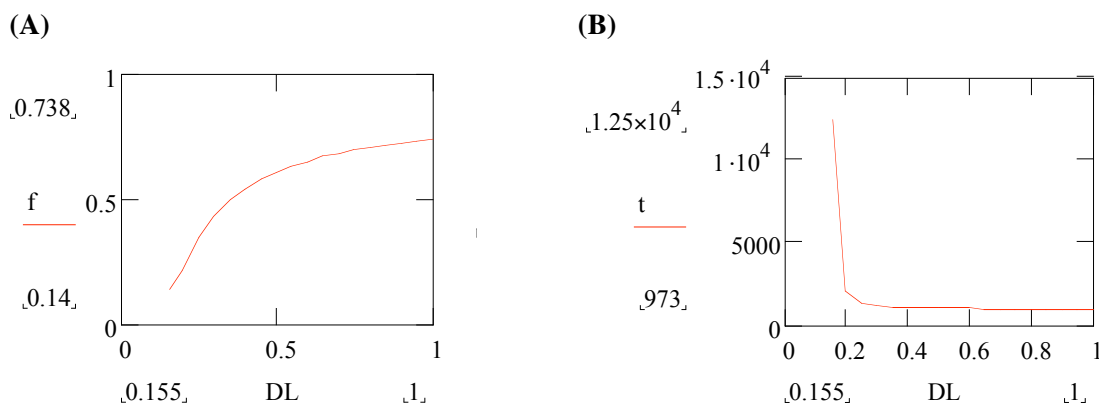


Figure 6.7 Model sensitivity of fraction of viable cells (*f*) compared to total cells (A) and turnover time (*t*) based on assumed D/L ratio associated with inactivated bacterial protein. Sensitivity analysis based on filter MP104.

Relatively little is known of the starvation survival capabilities of chemoautotrophs, especially anaerobic ones like the methanogens and sulfate reducers. There is knowledge of stress genes and proteins (e.g., heat shock proteins) in the archaea, including methanogens, but these are usually studied in response to acute physical or chemical stress, e.g., heat or osmotic stress (Macario et al., 1999). Similarly, HSPs are known to occur in sulfate reducers, including the Firmicutes that is common in the Witwatersrand basin, but little is known of how they survive chronic nutrient limitation. We can surmise that because CO₂ fixation is energetically costly, starved cells are unlikely to assimilate new carbon to replace or to repair damaged macromolecules. Instead, as with better studied heterotrophs, the cells rely on endogenous carbon and energy stores for survival. The importance of this is that autotrophic cells in maintenance or starvation mode are unlikely to be assimilating new inorganic carbon.

Using the age of the fracture water and the concentration of biogenic CH₄, the estimated rate of methanogenesis in shallow fracture waters was estimated to be $2 \times 10^{-8} \text{ M yr}^{-1}$ and $< 2 \times 10^{-10} \text{ M yr}^{-1}$ at deeper sites (Onstott et al., 2006). These activities were used to determine turnover times if 200–300 years associated with the bacterial colonies at the Mponeng mine. The turnover times that this model obtains for the Mponeng site agree fairly well with this previous study. The other mine sites also yield similar estimated turnover times.

The deep (2.8 km), alkaline, saline fracture water accessed in the Mponeng Mine near Carletonville, where radiolysis of water generates H₂ and sulfate (indirectly, by oxidation of buried pyrite) providing an electron donor and electron acceptor to the autotrophic “DLO” sulfate-reducing bacteria (Lin et al., 2006). The rate of substrate utilization (5.9×10^6 to 1.8×10^7 $\mu\text{M yr}^{-1}$, Lin et al., 2006) and the yield control the total population density.

At Mponeng mine, the water is derived strictly from local unconfined aquifers and reservoirs. Clone libraries have shown diverse communities of dominantly aerobic heterotrophic microbes, but also some anaerobes, e.g. methanogens (Onstott et al., 2003; Gihring et al., 2006), with cell densities $\sim 10^3$ cells ml⁻¹ (Onstott et al., 2003). Here, the age of the cells should equal the age of both the DOC, which is the source for most heterotrophs and also the DIC, which can be a source for autotrophs, e.g., methanogens. This makes a useful end-member control for testing the validity of the model.

6.4 CONCLUSION

The amino acids represent approximately 2×10^5 – 2×10^6 bacterial cells per mL. These values are in good agreement with the cell counts determined by staining methods (Lin et al., 2006). Any disagreement may show an overestimation of cell density based on staining methods due to background fluorescence (Glavin et al., 2004). The turnover times calculated from the amino acid data are consistent with previous estimates (Lin et al., 2006) and show values clustered around a turnover time of 800 years, a very long period. This could be consistent with an extreme nutrient-limited bacterial community. The most surprising model result was the large fraction of cells that were actually viable. Although the models show greater uncertainties in this parameter, the range of the fraction of alive cells is always less than one. This may reflect the fact that this community is composed largely of dormant cells, or a factor that is unknown at this time.

Future studies should continue to provide complementary and corroborating turnover times, cell ages, fraction of cells alive, and bacterial sulfate reduction rates. These communities show that bacteria can live with extremely slow metabolism and similarly amazingly slow turnover rates that are indicative of nutrient starvation. It can be assumed that these bacteria, inhabiting an extreme terrestrial environment, may be indicative of the types of life on Mars in

some ways. For instance, similar nutrient limitation based on unavailability of carbon or nitrogen would lead to similar communities of sulfate reducers.

Our detection limits in the search for life on Mars must be adequate to detect these low-levels of microbial life on the order of $<10^2$ cells per mL or $<10^3$ cells per gram. Only if these detection limits are exceeded can the community come to a reasonable conclusion of the presence of life on Mars.

ACKNOWLEDGEMENTS

Primarily we would like to thank Prof. Tullis Onstott, Dr. Tom L. Kieft, and Dr. Bianca Jane Silver for generously providing us with these filter samples for analysis. We would like to thank the South African mine workers and groups with whom Princeton has collaborated with since 1996. In particular, Dirk J. Offerman and other colleagues at the University of the Free State have helped us maintain close relationships with the mine personnel and also offer nearby laboratory facilities as a staging area and for processing of samples.

REFERENCES

- Amelung, W., and Zhang, X. (2001) Determination of amino acid enantiomers in soils. *Soil Biology & Biochemistry* 33, 553-562.
- Bada J.L., Wang, X.Y.S., Hamilton, H. (1999) Preservation of key biomolecules in the fossil record: current knowledge and future challenges. *Phil. Trans. Royal Soc. London Series B Biol. Sci.* 354, 77-86.
- Bada, J.L. (1984) In Vivo Racemization in Mammalian Proteins. *Methods in Enzymology* 106, 98-115.
- Bada, J.L. (1985) Amino acid racemization dating of fossil bones. *Ann. Rev. Earth Planet. Sci.* 13, 241-68.
- Baker, B.J., Moser, D.B., MacGregor, B.J., Fishbain, S., Wagner, M., Fry, N.K., Jackson, B., Speolstra, N., Loos, S., Takai, K., Sherwood Lollar, B., Fredrickson, J., Balkwill, D., Onstott, T.C., Wimpee, C.F., and Stahl, D.A. (2003) Related assemblages of sulphate-reducing bacteria associated with ultradeep gold mines of South Africa and deep basalt aquifers of Washington State. *Environ. Microbiol.* 5, 1168-1191.
- Beveridge, T.J. (1989) Role of cellular design in bacterial metal accumulation and mineralization. *Annual Rev Microbiol* 43, 47-71.
- Brock, T.D. (1970) *Biology of Microorganisms*. Prentice Hall, Englewood Cliffs, N.J. 737p.
- Chapelle, F.H., O'Neill, K., Bradley, P.M., Methe, B.A, Ciuffo SA, Knobel LL, Lovley D.R. (2002) A hydrogen-based subsurface microbial community dominated by methanogens. *Nature* 415, 312-315.
- Chapelle, F.H., and Lovley, D.R. (1990) Rates of Microbial Metabolism in Deep Coastal Plain Aquifers. *Appl. Environ. Microbiol.* 56(6), 1865-1874.
- Coward, M.P., Spencer, R.M., and Spencer, C.E. (1995) Development of the Witwatersrand basin, South Africa. *Early Precambrian Processes* 95, 243-269.
- D'Hondt, S., Rutherford, S., and Spivack, A.J. (2002) Metabolic activity of subsurface life in deep-sea sediments. *Science* 295, 2067-2070.
- Gihring, T., Moser, D.P., Lin, L-H., Davidson, M., Onstott, T.C., Morgan, L., Milleson, M., Kieft, T.L., Trimarco, E., Balkwill, D.L., and Dollhopf, M.E. (2006) The distribution of microbial taxa in the subsurface water of the Kalahari Shield, South Africa. *Geomicrobiol J.* 23, 415-430.
- Glavin, D.P., Cleaves, H.J., Schubert, M., Aubrey, A., and Bada, J.L. (2004) New method for estimating bacterial cell abundances in Natural Samples using sublimation. *Appl. Environ. Microbio.* 70(10), 5923-5928.
- Jorgensen, B.B., and D'Hondt, S. (2006) A Starving Majority Deep Beneath the Seafloor. *Science* 314, 932-934.

- Kieft, T.L., Fredrickson, J.K., Onstott, T.C., Gorby, Y.A., Kostandarithes, H.M., Bailey, T.J., Kennedy, D.W., Li, S.W., Plymale, A.E., Spadoni, C.M., and Gray, M.S. (1999) Dissimilatory reduction of Fe(III) and other electron acceptors by a *Thermus* isolate. *Appl. Environ. Microbiol.* 65, 1214-1221.
- Kieft, T.L., Kovacik, W.P. Jr., Ringelberg, D.B., White, D.C., Haldeman, D.L., Amy, P.S., and Hersman, L.E. (1997) Factors limiting to microbial growth and activity at a proposed high-level nuclear repository, Yucca Mountain, Nevada. *Appl. Environ. Microbiol.* 63, 3128-3133.
- Kieft, T.L., McCuddy, S.M., Onstott, T.C., Davidson, M., Lin, L-H., Mislouack, B., Pratt, L., Boice, E., Sherwood Lollar, B., Lippmann-Pipke, J., Pfiffner, S.M., Phelps, T.J., Gihring, T., Moser, D., and van Heerden, A. (2005) Geochemically generated, energy-rich substrates and indigenous microorganisms in deep, ancient groundwater. *Geomicrobiol. J.* 22, 325-335.
- Kieft, T.L., Murphy, E.M., Haldeman, D.L., Amy, P.S., Bjornstadt, B.N., McDonald, E.V., Ringelberg, D.B., White, D.C., Stair, J.O., Griffiths, R.P., Gsell, T.C., Holben, W.E., and Boone, D.R. (1998) Microbial transport, survival, and succession in a sequence of buried sediments. *Microb. Ecol.* 36, 336-348.
- Kieft, T.L. (2002) Microbial Starvation Survival in Subsurface Environments. pp. 2019-2028. In: *Encyclopedia of Environmental Microbiology*, G. Bitton (Ed.) John Wiley, NY.
- Li, J., Brill, T.B. (2003) Spectroscopy of hydrothermal reactions, part 26: Kinetics of decarboxylation of aliphatic amino acids and comparison with the rates of racemization. *Int. J. Chem. Kinetics* 35(11), 602-610.
- Lin, L-H., Onstott, T.C., Lippmann, J., Ward, J.A., Hall, J.A., and Sherwood Lollar, B. (2002) Radiolytic H₂ in the continental crust: a potential energy source for microbial metabolism in deep biosphere. *Geochim. Cosmochim. Acta* 66, A457.
- Lin, L-H., Slater, G.F., Lollar, B.S., Lacrampe-Couloume, G., and Onstott, T.C. (2005) The yield and isotopic composition of radiolytic H₂, a potential energy source for the deep subsurface biosphere. *Geochim. Cosmochim. Acta* 69, 893-903.
- Lin, L-H., Wang, P-L., Rumble, D., Lippmann-Pipke, J., Boice, E., Pratt, L.M., Sherwood Lollar, B., Brodie, E.L., Hazen, T.C., Anderson, G.L., DeSantis, T.Z., Moser, D.P., Kershaew, D., and Onstott, T.C. (2006) Long-term sustainability of a high-energy, low-diversity crustal biome. *Science* 314, 479-482.
- Lippmann, J., Stute, M., Torgersen, T., Moser, D.P., Hall, J., Lin, L., Borcsik, M., Bellamy, R.E.S., and Onstott, T.C. (2003) Dating ultra-deep mine waters with noble gases and ³⁶Cl, Witwatersrand Basin, South Africa. *Geochim. Cosmochim. Acta* 67, 4597-4619.
- Macario, A.J.L., Lange, M., Ahring, B.K., and De Macario E.C. (1999) Stress genes and proteins in the archaea. *Microbiol Molec Biol Rev* 63, 923-967.

Masters, P.M., Bada, J.L., and Zigler, S.M. (1978) Aspartic acid racemization in heavy molecular weight crystallins and water-soluble protein from normal human lenses and cataracts. Proc. Natl. Acad. Sci. U.S.A. 75, 1204-1208.

Moser, D.P., Gihring, T.M., Brockman, F.J., Fredrickson, J.K., Balkwill, D.L., Dollhopf, M.E., Sherwood Lollar, B., Pratt, L.M., Boice, E., Southam, G., Wanger, G., Baker, B.J., Pfiffner, S.M., Lin, L-H., and Onstott, T.C. (2005) *Desulfotomaculum* and *Methanobacterium* spp. dominate a 4- to 5- kilometer-deep fault. Appl. Environ. Microbiol. 71, 8773-8783.

Moser, D.P., Onstott, T.C., Fredrickson, J.K., Brockman, F.J., Balkwill, D.L., Drake, G.R., Pfiffner, S., White, D.C., Takai, K., Pratt, L.M., Fong, J., Sherwood Lollar, B., Slater, G., Phelps, T.J., Spoelstra, N., Deflaun, M., Southam, G., Welty, A.T., Baker, B.J., Hoek, J. (2003) Temporal shifts in microbial community structure and geochemistry of an ultradeep South African gold mine borehole. Geomicrobiol. J. 20, 1-32.

Murphy, E.M., Schramke, J.A., Fredrickson, J.K., Bledsoe, H.W., Francis, A.J., Sklarew, D.S., and Linehan, J.C. (1992) The influence of microbial activity and sedimentary organic carbon on the isotope geochemistry of the Middendorf aquifer. Water Resour. Res. 28, 723-740.

Onstott, T.C., Lin, L-H., Davidson, M., Mislowack, B., Borcsik, M., Hall, J., Slater, G., Ward, J., Sherwood Lollar, B., Lippmann-Pipke, J., Boice, E., Pratt, L.M., Pfiffner, S., Moser, D., Gihring, T., Kieft, T.L., Phelps, T.J., van Heerden, E., Litthauer, D., Deflaun, M., and Rothmel, R. (2006) Geohydrological constraints on the origin, age, and biogeochemical trends of deep fracture water in the Witwatersrand Basin, S. Africa. Geomicrobiol. J. 23, 369-414.

Onstott, T.C., Moser, D.P., Pfiffner, S.M., Fredrickson, J.K., Brockman, F.J., Phelps, T.J., White, D.C., Peacock, A., Balkwill, D., Hoover, R., Krumholz, L.R., Borscik, M., Kieft, T.L., and Wilson, R. (2003) Indigenous and contaminant microbes in ultradeep mines. Environ. Microbiol. 5, 1168-1191.

Onstott, T.C., Phelps, T.J., Kieft, T.L., Colwell, F.S., Balkwill, D.L., Fredrickson, J.K., and Brockman, F.J. (1999) A global perspective on the microbial abundance and activity in the deep subsurface. Ch. 38 pp. 489-500. In: Enigmatic Microorganisms and Life in Extreme Environments. J. Seckbach (Ed.), Kluwer Publications.

Pedersen, K. (1997) Microbial life in deep granitic rock. FEMS Microbiol. Rev. 20, 399-414.

Pfiffner, S.M., Cantu, J.M., Smithgall, A., Peacock, A.D., White, D.C., Moser, D.M., Onstott, T.C., and van Heerden, E. (2006) Phospholipid fatty acid profiles and biodensity estimates for water, rock, and air samples recovered from Witwatersrand Basin mines. Geomicrobiol. J. 23, 431-442.

Phelps, T.J., Murphy, E.M., Pfiffner, S.M., and White, D.C. (1994) Comparison between geochemical and biological estimates of subsurface microbial activities. Microb. Ecol. 28, 335-349.

Schippers, A., Neretin, L.N., Kallmeyer, J., Ferdelman, T.G., Cragg, B.A., Parkes, R.J., and Jorgensen, B.B. (2005) Prokaryotic cells of the deep sub-seafloor biosphere identified as living bacteria. Nature 433, 861-864.

Poinar, H.N., Höss, M., Bada, J.L., and Pääbo, S. (1996) Amino Acid Racemization and the Preservation of Ancient DNA. *Science* 272, 864-866.

Sherwood Lollar, B., Lacrampe-Couloume, G., Slater, G.F., Ward, J., Gihring, T.M., Lin, L-H., and Onstott T.C. (2006) Unravelling abiogenic and biogenic sources of methane in the Earth's deep subsurface. *Chem. Geol.* 226, 328-339.

Slater, G.F., Lippmann-Pipke, J., Moser, D.P., Reddy, C.R., Onstott, T.C., Lacrampe-Couloume, G., and Sherwood Lollar, B. (2006) ^{14}C in methane and DIC in the deep terrestrial subsurface: implications for microbial methanogenesis. *Geomicrobiol. J.* 23, 453-462.

Stevens, T.O., McKinley, J.P. (1995) Lithoautotrophic microbial ecosystems in deep basalt aquifers. *Science* 270, 450-454.

Takai, K., Moser, D.P., Onstott, T.C., Spoelstra, N., Pfiffner, S.M., Dohnalkova, A., and Fredrickson, J.K. (2001a) *Alkaliphilus transvaalensis* gen. nov., sp. nov., an extremely alkaliphilic bacterium isolated from a deep South African gold mine. *Int. J. Syst. Evol. Microbiol.* 51, 1245-1256.

Takai, K., Moser, D.P., DeFlaun, M.F., Onstott, T.C., and Fredrickson, J.K. (2001b) Archaeal diversity in waters from deep South African gold mines. *Appl. Environ. Microbiol.* 67, 5750-5760.

Ward, J.A., Slater, G.F., Moser, D.P., Lin, L-H., Lacrampe-Couloume, G., Bonin, A.S., Davidson, M., Hall, J.A., Mislowack, B., Bellamy, R.E.S., Onstott, T.C., and Sherwood Lollar, B. (2004) Microbial hydrocarbon gases in the Witwatersrand Basin, South Africa: implications for the deep biosphere. *Geochim. Cosmochim. Acta* 68, 3239-3250.

Whitman, W.B., Coleman, D.C., and Wiebe, W.J. (1998) Prokaryotes: the unseen majority. *Proc. Natl. Acad. Sci. U.S.A.* 95, 6578-6583.

Zhao, M., and Bada, J.L. (1995). Determination of α -dialkylamino acids and their enantiomers in geological samples by high-performance liquid chromatography after derivatization with a chiral adduct of o-phthalaldehyde. *J. Chromatogr. A* 690, 55-63.

CHAPTER VII. Chemical Biosignatures from Antarctic Dry Valley Microbial Life

ABSTRACT

The Antarctic dry valley deserts have been recognized since the 1970s as a Mars analog because of the prevailing cold and dry climate. Despite these harsh climates, microbial communities persist in some of these regions using sunlight as the primary source of energy. Evidence of extinct and extant microbial communities can be found both within the surface and subsurface ice and rock. Amino acid analyses of surficial sandstone and limestone rock samples reveal strong evidence of extant microbial communities with equivalent biodensities on the order of 10^6 - 10^{10} cells/gram. Most samples show evidence of cryptoendolithic microbial life in a rich subsurface organic pool. The samples that revealed no extant microbial life via SEM analyses show excellent preservation of microbial remnants revealing that the Antarctic dry valleys offer good locations for biosignature preservation because organic degradation is very slow in these environments. Samples that show only microfossils can be distinguished from the samples that harbor cryptoendolithic microorganisms by amino acid diagenetic indicators. These studies show the persistence of microbial biomarkers on geological timescales under cold, dry conditions and provide ideal host settings to search for evidence of life on Mars.

7.1 INTRODUCTION

Despite the extreme conditions of the Antarctic dry valleys, microbial communities still exist. The average temperature of the Antarctic dry valleys is -20°C (Clow et al., 1988). Two major microbial reservoirs exist in the Antarctic dry valleys (McKay, 1997), seasonal communities that exist beneath lake ice (Parker et al., 1982), and within the porous subsurface of sandstone rocks (Friedman, 1982). The latter communities, the cryptoendolithic microbial ecosystems, are usually found at elevations greater than 1500m (McKay, 1997), where temperatures are cooler than the valley floor. In fact, all elevations above $\sim 1000\text{m}$ experience extreme hyperarid, frigid climates (Denton et al., 1993), which is where microbial life is the most rare.

Physical and chemical evidence of microbial life within Antarctic sandstone has been well studied and although some of these communities have been long extinct, many continue to

thrive within the subsurface rocks with characteristically long turnover times and low biodensities. Most of these communities are dominated by cyanobacteria or lichen (de la Torre et al., 2003), both of which utilize sunlight as an energy source. The primary strains of life are bacteria, fungi, alga (Siebert et al., 1996), and two different archaea have been identified (Brambilla et al., 2001). Availability of sunlight as a function of depth within the subsurface has been shown to exert major control over lichen biological respiration in these regions (Friedman et al., 1993). Their growth turnover times are typically on the order of 10^3 - 10^4 years, coincident with the timescale of geological weathering (Sun and Friedman, 1999). The extant microbial communities typically have low cell counts around 10^3 - 10^6 cells per gram while some locations are completely devoid of microbial life and all that exists is the traces of an extinct biota. Many of these communities became extinct around 10-15 Ma when the Antarctic climate became similar to what persists today.

Biomarkers have been detected previously in sandstone and limestone rock samples from the Antarctic dry valleys (Figure 7.1) using various techniques. Cell staining and transmission electron microscopy (TEM) analyses of calcite, granite, and sandstone from the McMurdo dry valleys have been used to detect both living and dead microorganisms within the host rocks (de los Ríos et al., 2004; Wierzchos et al., 2004). Similar studies have detected biosignatures in rocks from the Ross Desert (Wierzchos and Ascaso, 2001; de los Ríos et al., 2003; Ascaso and Wierzchos, 2003) and Taylor Valley (de los Ríos et al., 2005). Biosignatures have also been detected by proton-induced x-ray emission (PIXE) from the Antarctic dry valleys (Wierzchos et al., 2006). The formation of iron-rich diagenetic products from extinct microbial remnants is recognized as another method of biomarker investigation from these coincident iron oxides (Wierzchos et al., 2003). These studies show that the biosignatures from extinct and extant life are ubiquitous in the rocks of Antarctica. Previous studies have focused primarily on visual evidence of microbial life within these Antarctic microenvironments rather than detecting specific classes of biomarkers.

The Antarctic Dry Valleys have drawn attention as a Mars analog since the 1970s (Horowitz et al., 1972). The conditions of the Dry Valley Deserts of Antarctica offer many potential similarities, especially to the Polar regions of Mars. The physical processes studied in the valleys were first suggested as a potential explanation for non-aqueous weathering on the Martian surface (Anderson et al., 1972). The current prevailing climatological conditions have

been suggested to provide a formation process for certain Martian minerals and potential phases in the polar regions (Dickinson & Rosen, 2003).

Rock samples from the Antarctic dry valleys offer ideal environments in which to observe and quantify extant cryptoendolithic microbial life. One important biosignature to assess are the amino acid concentrations and distributions within these environments, corresponding to the amount of biomass within these communities and a rough estimate of biodensities (Glavin et al., 2004). Many of these rocks show no evidence of biological life according to previous studies (Wierzchos et al., 2006) and offer a unique opportunity to contrast the amino acid compositions of rock samples with extant and extinct microbial communities.

7.2 EXPERIMENTAL SECTION

Five sandstone and one limestone rock samples were collected from various regions of the Dry Valley Deserts in Antarctica (76.5°-78.5°S, 160°-164°E), shown in Figure 7.1. Pieces of sandstone rock were gathered by E.I. Friedmann in 1983-1984 from two zones of the Ross Desert in the McMurdo Dry Valleys. These included samples A834 and A577 from the Mount Fleming area (77°33'S, 160°06'E, 2200 m altitude) and sample A867-110-R from the Linnaeus Terrace region. The rocks were air-dried and stored in sterile glass vials within air-conditioned rooms (-20°C) until use. A rock from the milder region of Taylor Valley (77°58'S, 160°63'E), sample A945, was collected over a 1994-1995 expedition and shipped frozen and stored in a cold room (-23°C) at the Antarctic Research Facility at Florida State University until use. Two rock samples were collected from the Northeast Commonwealth Glacier, a quartz sandstone sample 120-G (77°35'S, 163°24'E, 120 m elevation), and a carbonate rock sample GG-680 (77°41'S, 162°55'E, 680 m elevation). These samples were shipped and stored dry at -20°C until prepared for analyses. The climatological conditions and mineralogical compositions have been reported previously (Wierzchos & Ascaso, 2002; Wierzchos et al., 2005).

The samples were initially prepared by separating and homogenizing 0.100 grams of each rock sample using an agate ball mill. All of the rocks (except for sample 867-110-R) were sampled at 3-4 different depth horizons. The powdered samples were then pressed under 3 tons of pressure into a pellet 11 mm in diameter on a 0.5 gram boric acid substrate. A blank pressed boric acid pellet was also included for background correction.

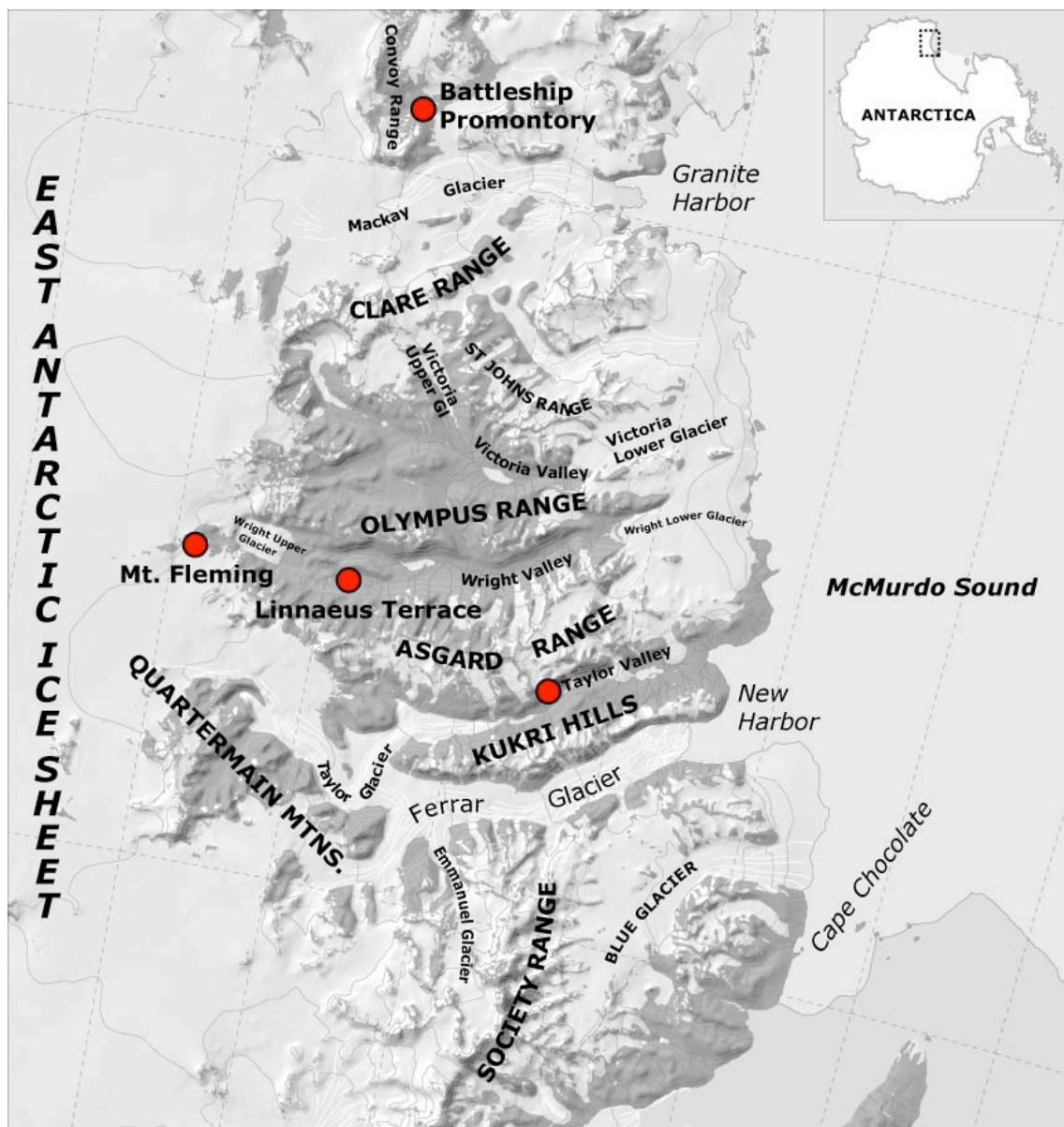


Figure 7.1 Sampling locations (•) of Antarctic dry valley rock samples (figure data provided by the Antarctic Digital Database, ADD).

The labeled sample set was delivered to Scripps Institution of Oceanography (SIO) from the Universitat de Lleida in sterile mini-petri dishes for amino acid analysis after the PIXE and SEM biosignature analyses were completed (Table 7.1).

Table 7.1 Descriptions and locations of samples investigated in this study and previously detected microbial remnants (detailed in Wierzchos et al., 2006).

Rock Type	Locale	Sample	color	depth (mm)	Microbes*
Sandstone	Taylor Valley	COM-120-Sup	gray	0-1	-cyanobacteria
		COM-120-G ¹	green	1-2	
		COM-120-W	white	12-15	
	Battleship Promontory	945-36-Sup	yellow	0-1	-fungi -algae -cyanobacteria -lichens
		945-36-C1 ²	white	2-4	
		945-36-F2	red	5-8	
		945-36-Y	light red	12-15	
		834-560-Y	yellow	0-1	
	Linnaeus Terrace	834-560-W	white	3-5	-fungi -cyanobacteria -algae, lichens
		834-560-R	red	12-15	
		867-110-R	red	XX-XX	
	Mount Fleming	834-577-B ³	black	0-1	(Extinct) -fossils detected
		834-577-W ⁴	white	1-5	
		834-577-R	red	10-15	
Limestone	Taylor Valley (Goldman Glacier)	GG-680-Sup	gray	0-1	-cyanobacteria
		GG-680-B	black	1-5	
		GG-680-W	white	10-15	

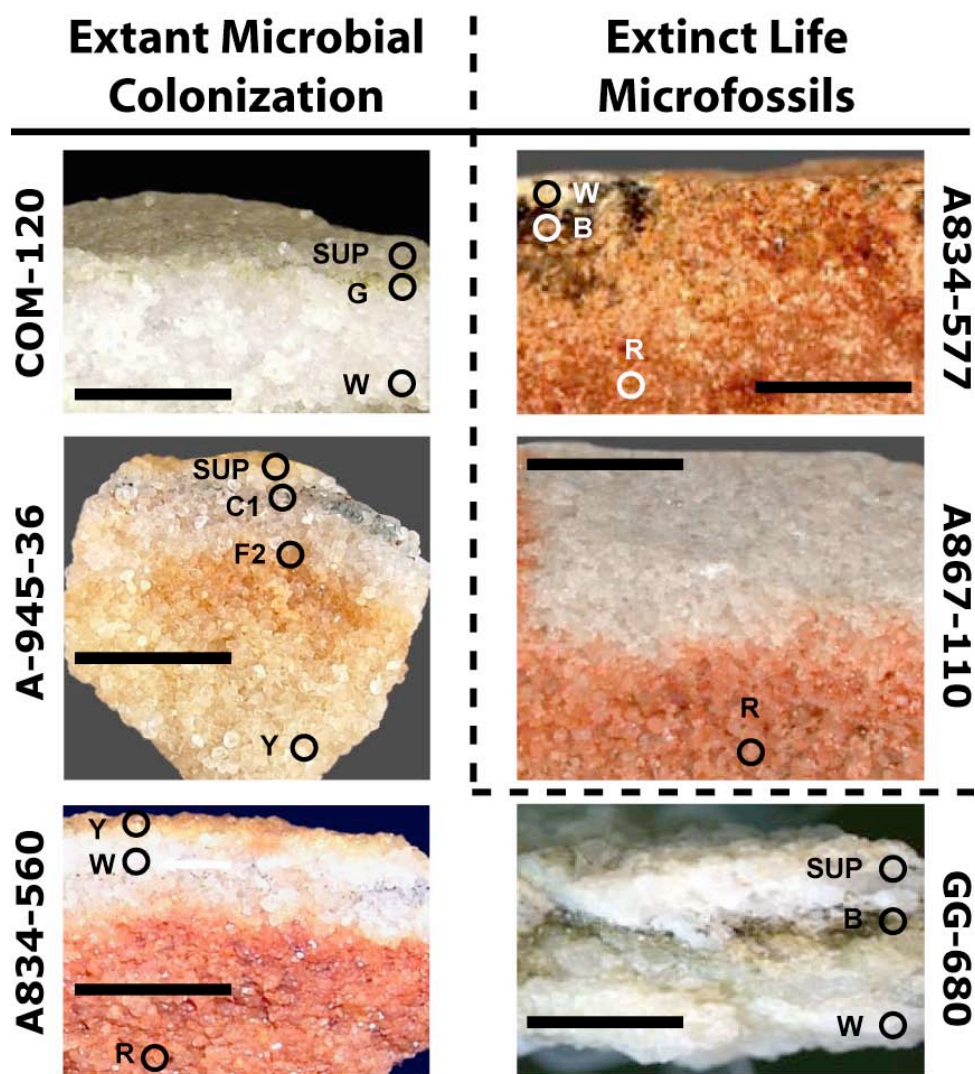
Key: = endolithic microorganism colonization; = microfossils detected; Sup = upper crust
G = green; W = white; B = black; R = red.

*Evidence of these types of microbial communities were detected in subsurface fractions from four rock samples by visual SEM evidence and may represent different classes of cryptoendoliths that are harbored in each respective sample (Wierzchos, personal communication).

¹Wierzchos et al. (2004)
²Wierzchos & Ascaso (2001)
³Wierzchos & Ascaso (2002)
⁴Wierzchos et al. (2005)

The sample identification labels on the underside of each pellet were first scraped off with sterile surgical blades to remove any residue. The pellets were then weighed out into 20 x 150 mm Pyrex test tubes (sterilized at 500°C for >12 hours) in order to record the total mass of the boric acid substrate that may have been removed by scraping. 1mL of 6N doubly-distilled hydrochloric acid (ddHCl) was added to each test tube (20 x 150 mm), evacuated with nitrogen, and flame sealed. The flame-sealed tubes were exposed to heat for 24 hours at 100°C in order to liberate free amino acids from the bound state and hydrolyze intact protein remnants. After hydrolysis, the samples were removed from heat, cracked, and the 6N HCl supernatant was transferred into a 12 x 100 mm test tube. The acid was evaporated on a vacuum centrifuge under mild heat (45°C) to dryness. This residue was loaded onto equilibrated desalting columns with 3

x 1 mL of ddH₂O and at this time, a norleucine internal standard was also added the column (5 μ L of 10⁻⁴ M racemic D/L-norleucine solution). The columns were rinsed with 5 column volumes of water to elute the anions and neutral species, then amino acid residues were eluted with 3 mL of 3.5 M ddNH₄OH. These fractions were brought to complete dryness in 1.5 mL mini-ependorf vials and resuspended in 100 μ L of doubly-distilled water (ddH₂O). 10 μ L of the 100 μ L total extract was combined with 10 μ L of 0.4M sodium borate buffer (natural pH ~ 9.4), and dried down to remove any residual ammonia carried through the desalting stage.



All samples are sandstone except GG-680 (Limestone)

Figure 7.2 Images of rock samples with sampling depths designated.

The dried samples were resuspended in 20 μL of ddH₂O and derivatized with 5 μL of 0.15 M *o*-phthaldialdehyde/*N*-acetyl-L-cysteine (OPA/NAC). After 1-minute of reaction time, the solution was quenched with 475 μL of 50mM sodium acetate buffer (pH adjusted to 5.5). 50 μL of the 500 μL total derivatized sample was injected and analyzed by reverse-phase HPLC (RP-HPLC). The peak areas were compared to standards of known concentration including a hydrolyzed protein Pierce-H standard (Figure 7.3) dried down with borate buffer and resuspended before derivatization. D/L-enantiomers of aspartic acid, glutamic acid, serine, alanine, and valine were quantified against racemic mixtures made from pure standards purchased from Sigma.

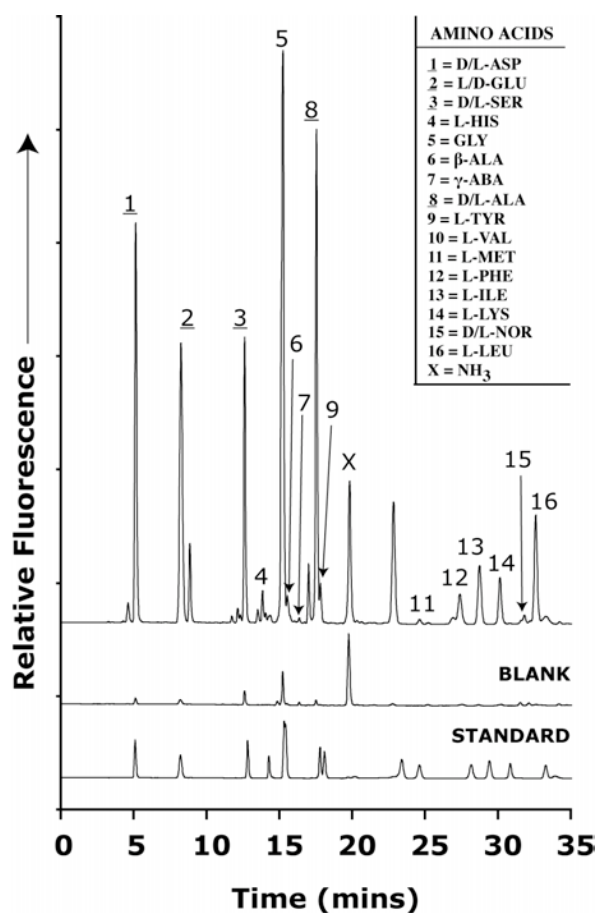


Figure 7.3 Representative chromatogram (0-35 mins) of an analyzed Antarctic subsurface sample colonized by cryptoendolithic microorganisms (COM-120-G) plotted against a borate pellet procedural blank (middle) and the Pierce-H protein standard (bottom). This trace shows the separation and identification of 13 protein amino using a Luna C-18(2) column. Detected non-protein amino acids, β -alanine and γ -aba, are also labeled in the figure. The internal standard is in between peaks 12 and 13 and represents the average which was $\sim 90\%$ recovery.

The analytical RP-HPLC system consists of an Hitachi L-6200 intelligent pump coupled with a Phenomenex Luna-C18(2) 5 μ M 100A and a Shimadzu RF-535 fluorescent detector. The buffer system was a 50mM sodium acetate buffer with 8% methanol and a gradient was run in order to achieve optimal separation of the amino acids (Program 9, Chapter 2). Fluorescently tagged amino acids were detected at an excitation wavelength of 340 nm and an emission wavelength of 450 nm. Data acquisition was provided by ThermoScientific Grams/AI and all peak areas were integrated using Grams 8.0. Quantification of the internal standard (D+L-norleucine) was made difficult by interfering peaks downfield, especially with leucine, however, in all cases, the samples showed defined peaks for both D- and L-norleucine that integrated to be at least 90% of the peak areas of the internal standard run alone. The average recovery is assumed to be between 90-100% and did not factor into the amino acid calculations.

7.3 RESULTS & DISCUSSION

The acid-hydrolyzed sample extracts were light yellow before desalting except for the boric acid blank, possibly indicating the extraction of complex organic molecules. 13 of 20 protein amino acids were detected and quantified in the Antarctic dry valley samples, including 4 pairs of D/L enantiomers (asp, glu, ser, gly, ala). Proline is not detected by these methods (unreactive 2° amine), and asparagine and glutamine are converted to aspartic acid and glutamic acid, respectively, during acid hydrolysis. No appreciable amounts of threonine (shoulder of glycine), histidine, or arginine were detected, however these are minor amino acid components of bacteria (<5% total) and are not expected to be present in high abundances (Chapter 2). Non-protein amino acids, β -alanine (β -ala) and γ -aminobutyric acid (γ -ABA), were present in most of the samples which is discussed below.

Amino acid concentrations (Table 7.2) showed relatively homogenous distributions between samples, however the absolute concentrations were highly variable (Figure 7.4). The concentrations of the abiological D-amino acid enantiomers were very low, indicating the presence of extant microbial communities and/or excellent preservation of microbial proteins from extinct communities within these samples.

Table 7.2 Major amino acid concentrations in Antarctic Dry Valley samples. Values are in ppm and represent the average of 3 runs each. Actual chromatograms are located in Supplementary Information A & B.

Sample	Asp*		Glu*		Ser*		Gly	β -ala	γ -aba	Ala*		Total
	D-	L-	D-	L-	D-	L-				D-	L-	
COM-120-Sup	0.0840	1.49	2.44	0.195	0.0340	1.26	1.87	0.0314	BB	0.0854	0.992	8.48
COM-120-G ¹	1.23	18.8	22.8	4.16	0.453	8.73	17.5	0.332	0.1454	1.49	16.8	92.44
COM-120-W	0.0962	1.26	2.13	0.198	0.0243	1.00	1.94	0.0228	BB	0.0892	0.667	7.43
945-36-Sup	0.161	2.50	4.10	0.146	0.0458	2.75	4.24	0.136	0.0838	0.0860	1.62	15.87
945-36-C1 ²	0.453	6.48	7.81	0.309	0.0736	6.44	7.88	0.0577	1.14	0.206	6.37	37.22
945-36-F2	0.270	5.61	6.53	2.11	0.386	4.55	7.25	0.376	0.443	0.975	6.51	35.01
945-36-Y	0.0573	1.12	1.49	0.577	0.0914	0.884	1.16	0.0551	0.119	0.258	1.06	6.87
834-560-Y	0.0928	1.80	2.98	0.0847	0.0124	1.74	2.50	0.0256	BB	0.0316	0.930	10.20
834-560-W	0.0398	0.461	0.768	0.0317	0.00539	0.484	0.802	0.0388	BB	0.0134	0.246	2.89
834-560-R	0.0861	1.08	1.55	0.236	0.0286	0.934	1.81	0.0822	BB	0.339	0.701	6.85
867-110-R	0.0397	0.705	1.08	0.0877	0.0150	0.587	1.08	0.0851	BB	0.0314	0.306	4.02
834-577-B ³	0.476	10.0	8.90	0.736	0.0964	3.44	6.49	0.298	0.0715	0.429	4.68	35.62
834-577-W ⁴	0.0513	0.779	0.711	0.116	0.0144	0.343	0.888	0.0753	BB	0.0632	0.416	3.46
834-577-R	0.0602	0.805	1.43	0.0531	0.0233	0.703	1.86	0.106	0.1235	0.0421	0.499	5.71
GG-680-Sup	0.330	6.56	12.63	0.360	0.119	8.62	11.4	0.0069	BB	0.173	4.13	44.33
GG-680-B ⁵	0.0187	0.201	0.340	0.0231	0.00634	0.268	0.208	0.0269	BB	0.0114	0.0937	1.20
GG-680-W	0.0458	0.856	1.50	0.0487	0.00845	1.07	1.79	0.0312	BB	0.0139	0.368	5.73

Note: his, tyr, and met present in low concentrations in all samples.

*enantiomeric abundances quantified.

Many Antarctic Dry Valley Desert rocks have been shown to harbor extant cryptoendolithic microbial communities. These microbes persist in the cold and dry Antarctic climates despite the harsh climatological conditions. The biodensities of these communities have been previously determined for similar algal and bacterial communities to range between 10^2 and 10^4 cfu/gram (Vishnivetskaya et al., 2003). It is assumed that the majority of these samples harbor extant microbial communities at variable biodensities. This assumption has been verified by Wierchos (2006) for a number of these samples by SEM analyses (Table 7.1).

The individual and total amino acid concentrations showed high variability not only between sample sets, but also with depth for each individual rock sample. Because the source of the amino acids is assumed to be primarily extant biological life, an estimation of biomass can be made based on the total amino acid concentration in terms of *E. coli* equivalent (ECE) cell counts. The total amino acids are assumed to constitute 55% of the mass of a bacterial cell and an average mass per cell is assumed to be similar to *E. coli*, that is 1.55×10^{-13} g protein/cell (Neidhardt, 1990), identical to the methods of Glavin et al. (2001). In this calculation, it is assumed that the 6 quantified amino acids represent ~66.1% of the total amino acids within a cell (Chapter 2). The total amino acids and ECE cell counts can be plotted to show where the bulk of the amino acids are as a function of depth, presumably corresponding to the majority of the extant cryptoendoliths (Figure 7.4).

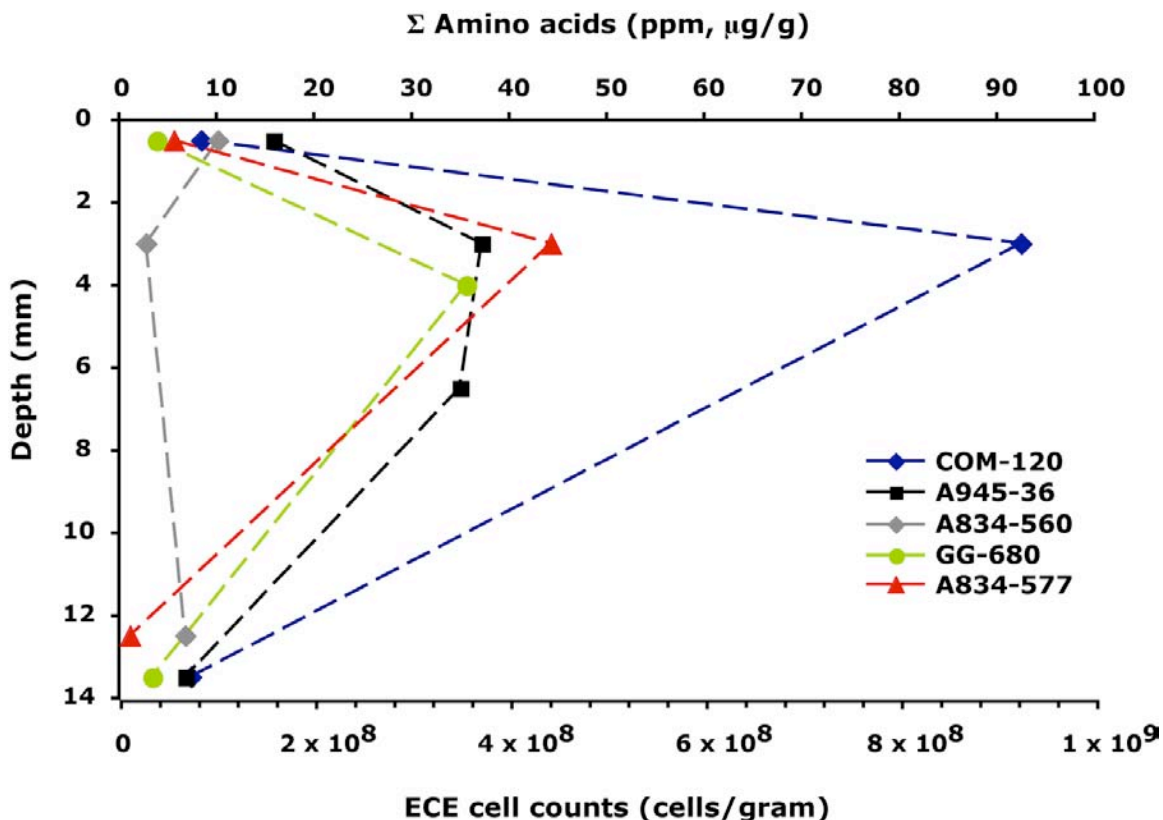


Figure 7.4 Plot of total amino acids (Σ asp, glu, ser, gly, ala) as a function of sample depth for the various sample sites. Individual amino acids show the identical trends with all but one sample (A834-560) showing elevated subsurface amino acid concentrations (~ 4 mm depth), indicative of cryptoendolithic microbial colonization. Estimated *E. coli* equivalent (ECE) cell counts are plotted on the y-axis assuming that the total protein mass of a cell is equivalent to 1.55×10^{-13} grams/cell (Neidhardt et al., 1990) and that the quantified amino acids make up 66.1% of the total protein dry weight of the cell (Chapter 2). The samples from A834-560 shows a relatively constant depth profile with low total amino acids while the rest of the samples show profiles consistent with the presence of cryptoendolithic microbial communities within the rocks at depths of 3-7 mm.

Clearly these samples all show evidence of high concentrations of amino acids within the subsurface layer, which may correspond to extinct or extant cryptoendolithic microbial life. The bulk of the cryptoendolithic microbial biomass is observed as amino acid spikes at depths, consistent with the SEM images within these exact samples showing evidence of extant cells (Wierchos et al., 2006). These SEM analyses show visual evidence of extant cryptoendoliths imaged at depths of ~ 3 mm for samples COM-120-G, A945-36-C1, A834560W, and GG-680B. Evidence of these photosynthetic microbial communities is observed in all of the samples except for sample A834-560, which instead shows elevated amino acids in the surface layer (A834-560-

Y). Possibly in this sample, an appreciable amount of the biomass is concentrated closer to the surface in the 0-1mm region instead of the 3-5mm region, but this cannot be deduced from these analyses.

It is unknown why sample A867-560 shows a different trend than the majority in Figure 7.4. The immediate subsurface sample, A834-560-W has been shown to contain endolithic microbial communities. Therefore, it is assumed that this sample would show the highest total amino acids and therefore ECE cell counts. However, the trend from sample A834-560 looks more similar to sample A834-577, the sample in which only microfossils have been imaged without any extant microbial communities. The only similarity in the samples A834-577 and A834-560 were that they were sampled from higher elevations and the increased radiation may have had something to do with this trend.

The numbers of viable bacterial cells have been previously determined for similar algal and bacterial communities to range between 10^2 and 10^6 cells/gram (Vishnivetskaya et al., 2003). The numbers derived in this study place the upper limit range of cells counts, based on amino acid composition, at 10^8 cells/gram, much higher than previously determined. However, these may be highly productive cryptoendoliths and represent an upper limit of microbial cell counts because the amino acid extrapolations also include dead organic matter and not only viable cells.

The D/L-ratios of each sample can be used to evaluate the diagenetic state of the amino acids, and is an indicator of how much degraded organic matter might coexist in these extant communities. The higher the D/L-ratio, the more degraded the amino acids are. This could be indicative of extinct ecosystems within the rock that has since become extinct.

D-enantiomers are present in very low concentrations with average D/L ratios for asp, glu, ser, and ala equal to 0.05, 0.08, 0.03, and 0.1, respectively. The high abundances of L-amino acids implies that these detected biosignatures are from extant communities or very well preserved extinct microbial life. The sample that shows the strongest variation of enantiomeric ratios with depth is sample A-945-36. Similarly, sample A834-560 shows elevated D/L-amino acid ratios and at lower depths, these samples in particular show highly racemized amino acids and do not adequately approximate the D/L-ratios of extant communities because of the highly racemized amino acids with depth. It is interesting to note that the amino acids with the highest D/L ratios are alanine and glutamic acid for all samples. If we assume that these enantiomeric ratios all started low when the communities thrived, then the relative racemization rates would

tend to follow the order: glu > ala > ser > asp. The amino acid distributions in the other samples generally agree with this relative trend. The enantiomeric ratios measured for alanine might reflect some degree of bacterial cell wall amino acids, which often have high concentrations of D-alanine (Hecky et al., 1973).

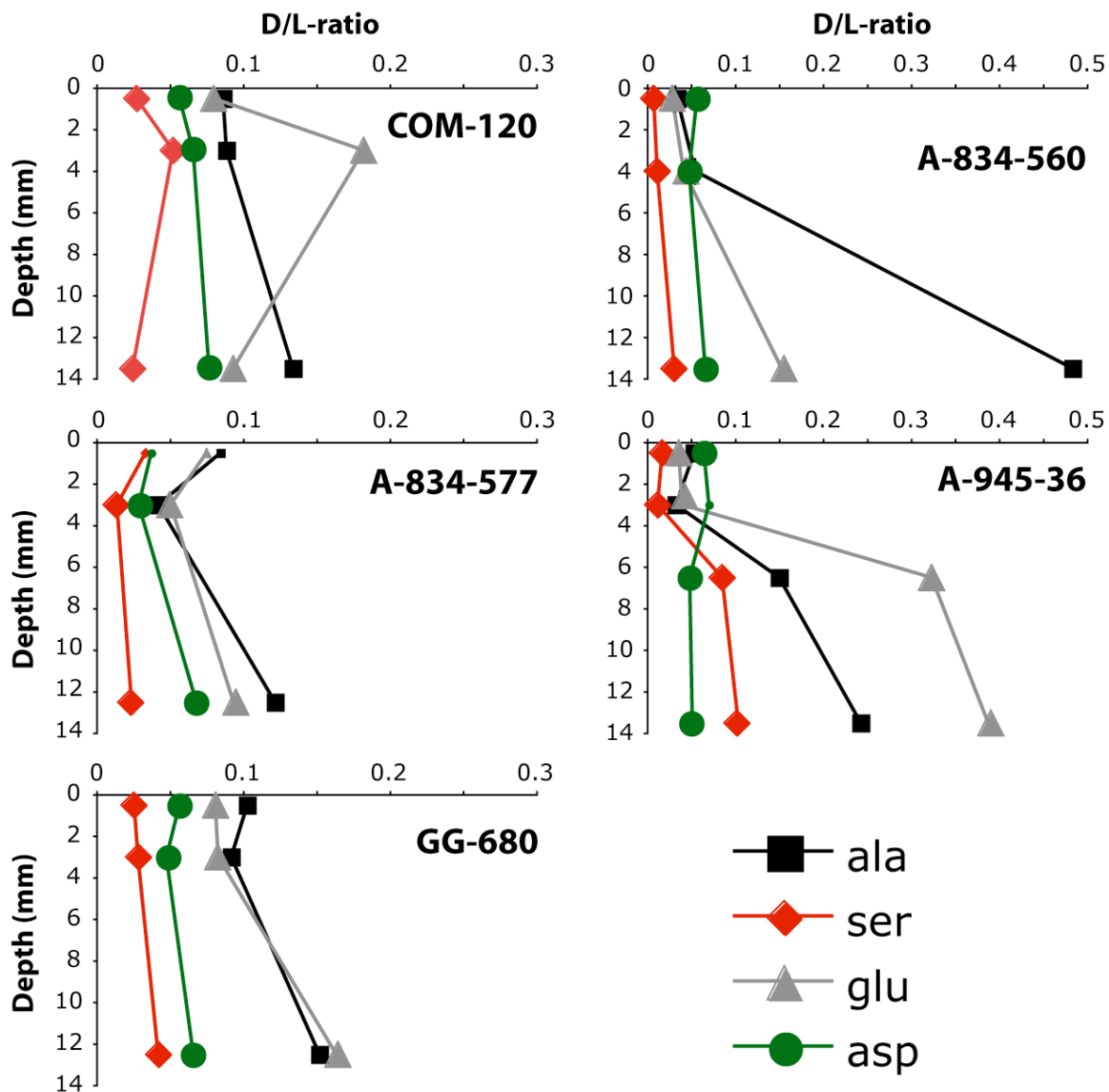


Figure 7.5 Amino acid enantiomeric ratios representative of various rock samples for D/L-aspartic acid, D/L-glutamic acid, D/L-serine, and D/L-alanine. Some of the D-alanine enantiomer is from peptidoglycan within cell wall material. Samples COM-120 and GG-680 show the most homogeneous amino acid enantiomeric ratios with little racemization ($D/L < 0.1$).

Although most of the samples show a high degree of variation with depth, sample COM-120 shows the most consistent profile of low D/L-ratios, showing D/L-ratios below 0.1 for all amino acids except glutamic acid within the layer where the bulk of the cryptoendoliths are located. These low D/L-ratios suggest that the sample is well colonized with extant biological life, or that the sample is very well preserved because the enantiomeric ratios show little racemization. The relative levels of amino acids therefore should well represent an extant microbial community and can be compared to other samples that might show changes in composition over time due to degradation.

The amino acid determination is much more sensitive than the imaging technologies utilized in previous studies. In order to determine the stability of amino acids within these matrices, it is essential to compare samples that harbor cryptoendolithic microbes to those that do not have any extant microbial life, rather, it is all extinct microbial life in the form of microfossils. Only microfossils have been imaged in samples from the rock A834-577 ($<10^3$ cells/g) while not even microfossils have been imaged in sample A867-110-R. A plot of the amino acids for a sample rich in cryptoendoliths (120-COM) compared to a plot of the samples within which only microfossils were detected (Table 7.1) show different trends, possibly related to very slow degradation over time (Figure 7.6).

It appears that these trends for alanine, glutamic acid, glycine, and serine (compared to aspartic acid) all show strong deviations from the extant community in sample 120-COM (Figure 7.6). This could be due to degradation over time from ratios of amino acids present in extant communities to those measured in sample A834-577 and A867-110R. If this is indeed the case, then the relative decarboxylation rates of the individual amino acids can be determined. Based on these analyses, the data suggest that alanine and glutamic acid are more stable than aspartic acid and that glycine and serine show lower stabilities than aspartic acid. Using similar methods, the actual rates of decarboxylation might be able to be estimated if it is assumed that this degradation has been occurring for millions of years since the bacterial community became deceased.

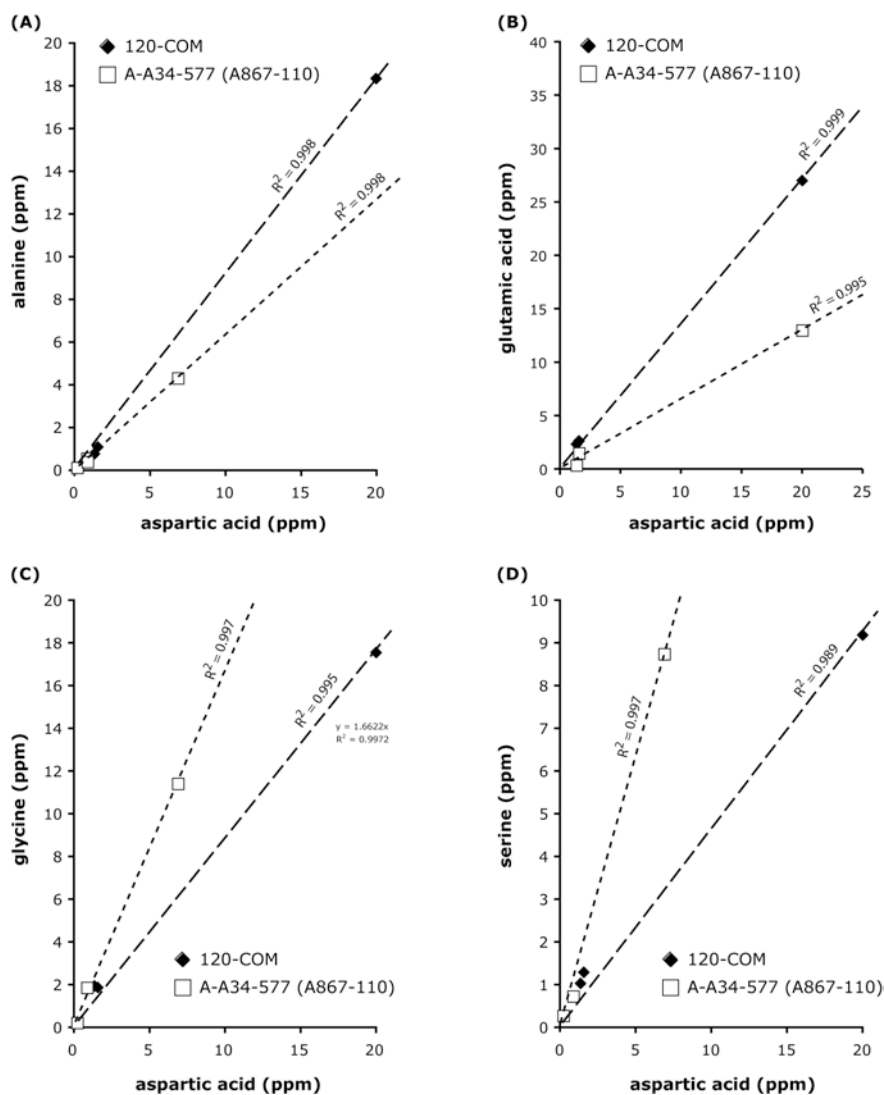


Figure 7.6 Amino acids measured in sample COM-120 (live endolithic microorganism colonization) compared to the samples with no extant microbes detected (only microfossils) for (A) alanine vs. aspartic acid, (B) glutamic acid vs. aspartic acid, (C) glycine vs. aspartic acid, and (D) serine vs. aspartic acid. Linear trends show strong correlations ($R^2 > 0.98$).

7.3.1 Amino Acid Diagenetic Indicators

Other indicators exist that can be used to infer the relative diagenetic state of the organic matter with depth besides the D/L-ratios are amino acid amine degradation products. Although these compounds are decarboxylation products of aspartic acid and glutamic acid (Figure 7.7), respectively, they are not liberated during standard heating experiments and are assumed to be products of biological amino acid degradation (Bada, 1991). These compounds may indicate some relative degree of biological activity between samples, and have also been used as a

diagenetic indicator in marine sediments (Cowie & Hedges, 1994) and their implications are discussed below.

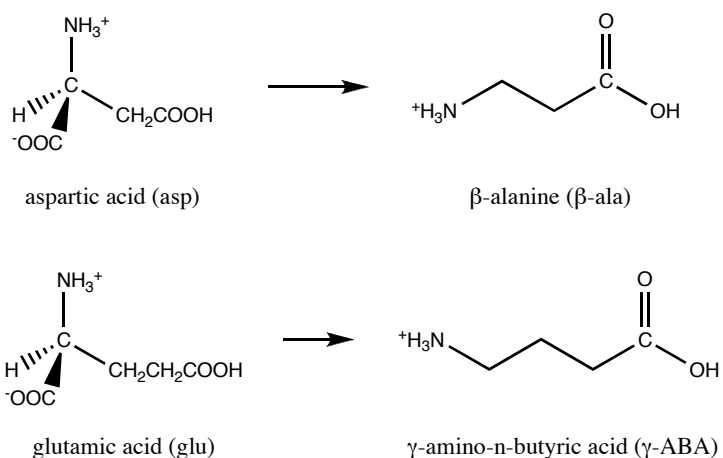


Figure 7.7 Degradation of glutamic and aspartic acids to γ -amino-n-butyric acid (γ -ABA) and β -alanine (β -ala), respectively.

A plot of aspartic acid and β -alanine with depth for each sample should show an inverse correlation based on the diagenetic state of the amino acids (Cowie & Hedges, 1994). Likewise, a plot of γ -aba compared to glutamic acid should indicate the same trend. β -ala and γ -aba are well known to be formed by microbially catalyzed amino acid decarboxylation, so the relative abundances of the parent amino acids and daughter degradation products can give a relative idea of the amount of diagenesis and nature of the amino acids. With extant microbial communities, the levels of amino acids should be high while the degradation products likewise will be high. Over time, it is observed that the amount of the parent amino acid and the amine degradation products show an inverse correlation (Cowie & Hedges, 1994). The plots of degradation products versus amino acids show two distinct trend groupings (Figure 7.8).

Sample A834-577 show inverse correlations with depth of the amount of aspartic acid compared to β -ala and of glutamic acid compared to γ -aba. An extant microbial community should show a different trend that shows higher degradation products (γ -aba and β -ala) corresponding to higher amino acid concentrations. Indeed all of the samples seem to show this except the aforementioned sample A834-577, the sample within which no life was detected by SEM methods. This appears to show a marked difference between extinct and extant biological communities present in these Antarctic rock samples.

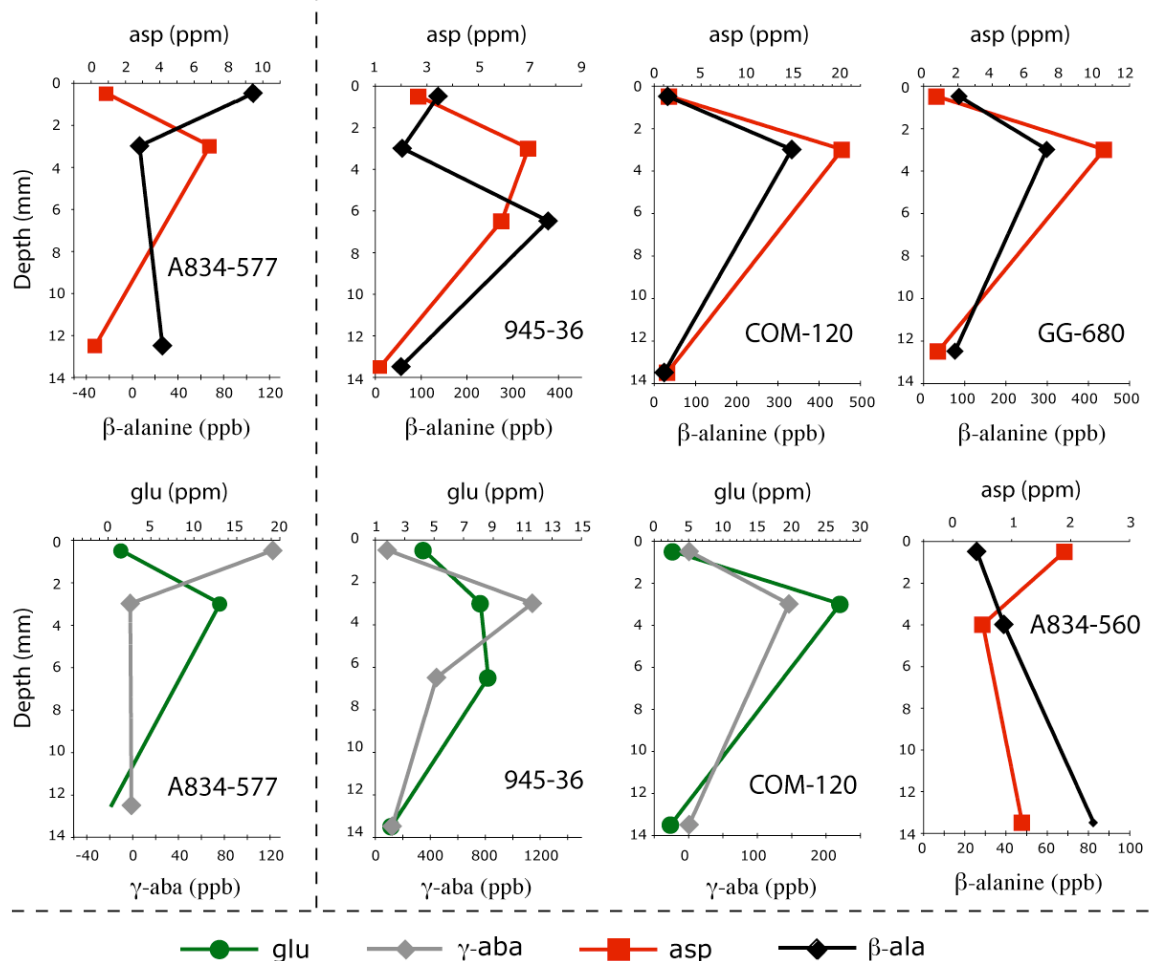


Figure 7.8 Plots of diagenetic indicators aspartic acid compared to β -ala and γ -aba compared to glutamic acid with depth for each sample. Plots of γ -aba are not shown for samples GG-680 and A834-560 but they showed the same trends. Notice some of the γ -aba values plotted are equal to zero.

7.4 CONCLUSION

This study represents another analysis for biosignatures on samples that have previously been analyzed by other methods. However, the analyses in this study provide the first chemical biosignature evidence that has been collected on these dry valley samples. The marked bacterial distribution present in these sandstone samples (Glavin et al., 2001) show evidence that these amino acids are derived from biological sources. The relatively low amino acids D/L-enantiomeric ratios reveal that microbial remnants are very well preserved in these extremely cold locations after becoming extinct in the recent geological past (~million year timescales). Certain diagenetic indicators suggest that there is a way to differentiate between extinct and

extant biological communities based on relative amounts of amino acids and/or the abundance of their amine degradation products. However, despite these differences, the amino acids derived from microbial life show good preservation overall and should persist for millions of years in these extremely cold and dry climates. Similar preservation might be expected on Mars if the amino acids are protected from radiative degradation which would destroy them on the surface in thousands of years. Sufficient layers of ice could provide this shelter, as could iron-rich minerals, or perhaps sulfate minerals (Aubrey et al., 2006).

It is important that future life detection missions to Mars focus on biomarkers that would be well preserved for hundreds of millions of years in order to detect evidence of an extinct Martian biota. The technique must be adequately sensitive to determine trace amounts of organic compounds within the regolith or rock record. Instruments have demonstrated the detection of spectral biosignatures within Antarctic rock samples using Raman spectrometers (Edwards et al., 2005), however these methods may be insufficiently sensitive and may not detect definitive biosignatures. Instrumentation that focuses on the detection of amino acids, the largest molecular biological reservoir by mass, offers superior sensitivity and through chirality determination may unequivocally determine the biological source of amino acids. Here we have shown that subtle differences in the amino acid compositions can reveal much about the microbial community in terms of diagenetic state. These such issues must be evaluated when interpreting biosignatures detected on Mars.

ACKNOWLEDGEMENTS

I would like to thank Dr. Jacek Wierzchos and his colleagues for providing the sandstone samples from the Antarctic Dry Valley Deserts. This study would not have been possible without the dedicated work of the late Prof. Imre Friedman whose studies helped conclusively determine the presence of extremophilic cryptoendolithic microbial colonization in the Antarctic Dry Valley Deserts.

REFERENCES

Anderson, D.M., Gatto, L.W., and Ugolini, F.C. (1972) An Antarctic analog of Martian permafrost terrain. *Antarctic Journal of the United States* 7, 114-116.

Ascaso, C., and Wierzchos, J. (2003) The Search for Biomarkers and Microbial Fossils in Antarctic Rock Microhabitats. *Geomicrobiology Journal* 20, 439-450.

Aubrey, A.D., Cleaves, H.J., Chalmers, J.H., Skelley, A.M., Mathies, R.A., Grunthaner, F.J., Ehrenfreund, P., and Bada, J.L. (2006) Sulfate minerals and organic compounds on Mars. *Geology* 34, 357-360.

Bada, J.L. (1991) Amino acid cosmochemistry, *Phil. Trans. R. Soc. Lond. B* 333, 349-358.

Brambilla, E., Hippe, H., Hagelstein, A., Tindall, B.J., and Stackebrandt, E. (2001) 16S rDNA diversity of cultured and uncultured prokaryotes of a mat sample from Lake Fryxell, McMurdo Dry Valleys, Antarctica. *Extremophiles* 5, 23-33.

Clow, G.D., McKay, C.P., Simmons, Jr., G.M., and Wharton, Jr., R.A. (1988) Climatological Observations and Predicted Sublimation Rates at Lake Hoare, Antarctica. *J. Climate* 1, 715.

Cowie, G.L., and Hedges, J.I. (1994) Biochemical indicators of diagenetic alteration in natural organic matter mixtures. *Nature* 369, 304-307.

De la Torre, J.R., Goebel, B.M., Friedman, E.I., and Pace, N.R. (2003) Microbial Diversity of Cryptoendolithic Communities from the McMurdo Dry Valleys, Antarctica. *Appl. Environ. Microbiol.* 69(7), 3858-3867.

de los Ríos, A., Wierzchos, J., Sancho, L.G., and Ascaso, C. (2003) Acid microenvironments in microbial biofilms of antarctic endolithic microecosystems. *Environ. Microbiol.* 5, 231-237.

de los Ríos, A., Wierzchos, J., Sancho, L.G., Green, T.G.A., and Ascaso, C. (2005) Ecology of endolithic lichens colonizing granite in continental Antarctica. *The Lichenologist* 37, 383-395.

de los Ríos, A., Wierzchos, J., Sancho, L.G., and Ascaso, C. (2004) Exploring the physiological state of continental Antarctic endolithic microorganisms by microscopy. *Microbial Ecology* 50, 143-152.

Denton, G.H., Sugden, D.E., Marchant, D.R., Hall, B.L., and Wilch, T.I. (1993) East Antarctic ice sheet sensitivity to Pliocene climate change from a Dry Valleys perspective. *Geografiska Annaler* 75A, 155-204.

Dickinson, W.W., and Rosen, M.R. (2003) Antarctic permafrost: An analogue for water and diagenetic minerals on Mars. *Geology* 31, 199-202.

Edwards, H.G.M., Moody, C.D., Jorge Villar, S.E., and Wynn-Williams, D.D. (2005) Raman spectroscopic detection of key biomarkers of cyanobacteria and lichen symbiosis in extreme Antarctic habitats: Evaluation for Mars Lander missions. *Icarus* 174, 560-571.

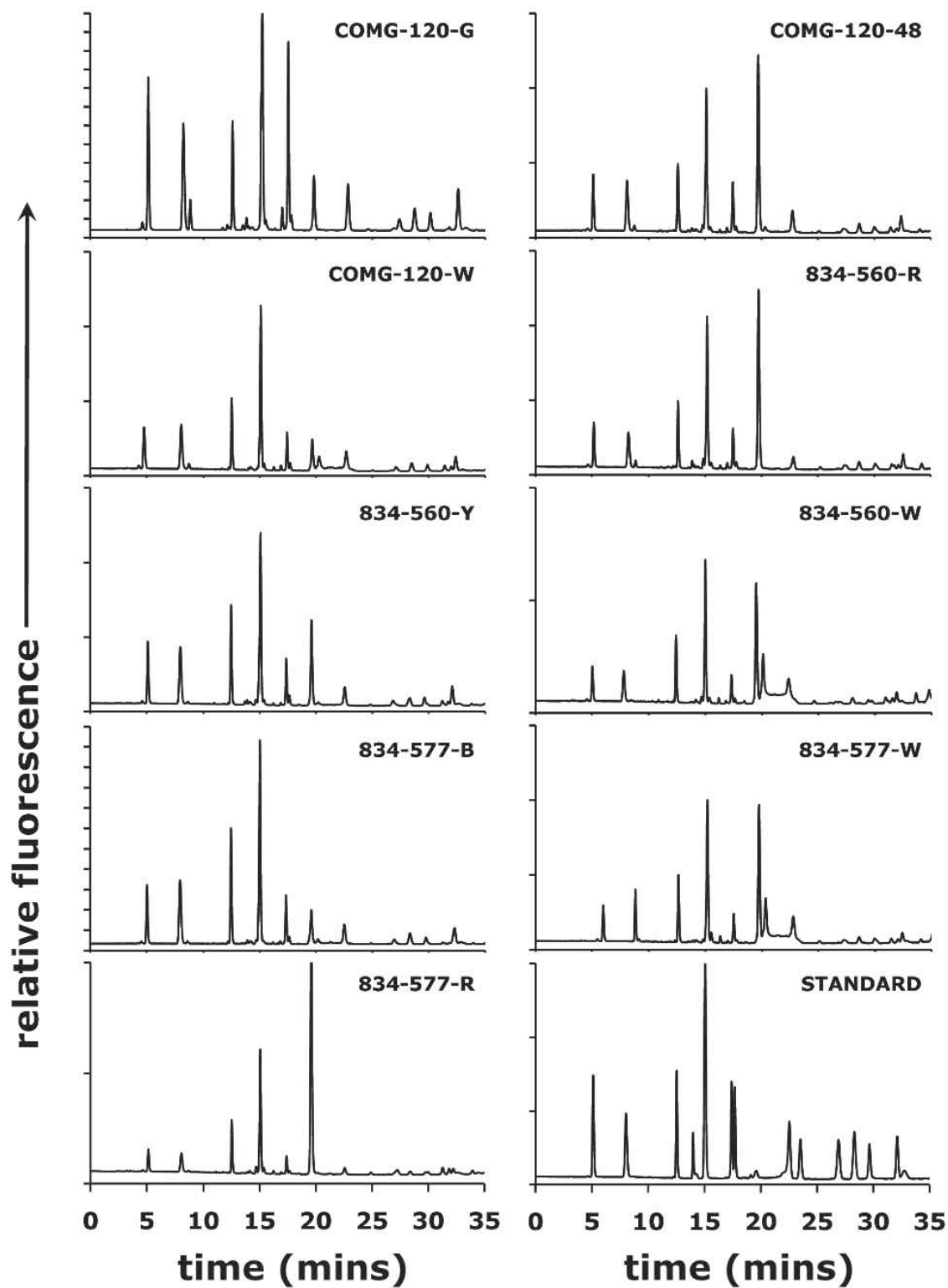
- Friedman, E.I. (1982) Endolithic Microorganisms in the Antarctic Cold Desert. *Science* 215, 1045-1053.
- Friedman, E.I., Kappen, L., Meyer, M.A., and Nienow, J.A. (1993) Long-term Productivity in the Cryptoendolithic Microbial Community of the Ross Desert, Antarctica. *Microb. Ecol.* 25, 51-69.
- Glavin, D.P., Schubert, M., Botta, O., Kminek, G., and Bada, J. L. (2001) Detecting Pyrolysis Products from Bacteria on Mars. *Earth Planet. Sci. Lett.* 185, 1-5.
- Glavin, D.P., Cleaves, H.J., Schubert, M., Aubrey, A., and Bada, J.L. (2004) New method for estimating bacterial cell abundances in Natural Samples using sublimation. *Appl. Environ. Microbio.* 70(10), 5923-5928.
- Hecky, R.E.K., Mopper, K., Kilham, P., and Degens, E.T. (1973) The amino acid and sugar composition of diatom cell-walls. *Mar. Biol.* 19, 323-331.
- Horowitz, N.H., Cameron, R.E., and Hubbard (1972) Microbiology of the Dry Valleys of Antarctica. *Science* 176(4032), 242-245.
- McKay, C.P. (1997) The search for life on Mars. *Origins of Life and Evolution of the Biosphere* 27, 263-289.
- Neidhardt, F.C., Ingraham, J.L., and Schaechter, M. (1990) *In Physiology of the bacterial cell: a molecular approach*. Sunderland, Massachusetts: Sinauer Associates, 506 pp.
- Parker, B.C., Simmons, Jr., G.M., Seaburg, K.G., Cathey, D.D., and Allnut, F.T.C. (1982) *J. Plank. Res.* 4, 271-286.
- Siebert, J., Hirsch, P., Hoffman, B., Gliesche, C.G., Peissl, K., and Jendrach, M. (1996) Cryptoendolithic microorganisms from Antarctic sandstone of Linnaeus Terrace (Asgard Range): diversity, properties, and interactions. *Biodiversity and conservation* 5, 1337-1363.
- Sun, H.J., and Friedman, E.I. (1999) Growth on Geological Time Scales in the Antarctic Cryptoendolithic Microbial Community. *Geomicrobiology Journal* 16, 193-202.
- Vishnivetskaya, T.A., Spirina, E.V., Shatilovich, A.V., Erokhina, L.G., Vorobyova, E.A., and Gilichinsky, D.A. (2003) The resistance of viable permafrost algae to simulated environmental stresses: implications for astrobiology. *International Journal of Astrobiology* 2(3): 171-177.
- Wierzchos, J., and Ascaso, C. (2002) Microbial fossil record of rocks from the Ross Desert, Antarctica: implications in the search for past life on Mars. *Int. J. Astrobiology* 1, 51-59.
- Wierzchos, J., Sancho, L.G., and Ascaso, C. (2005) Biomineralization of endolithic microbes in rocks from the McMurdo Dry Valleys of Antarctica: implications for microbial fossil formation and their detection. *Environ. Microbiol.* 7, 566-575.
- Wierzchos, J., Ascaso, C., Ager, F.J., García-Orellana, I., Carmona-Luque, A., and Respaldiza, M.A. (2006) Identifying elements in rocks from the Dry Valleys desert (Antarctica) by ion beam

proton induced X-ray emission. *Nuclear Instruments and Methods in Physics Research B* 249, 571-574.

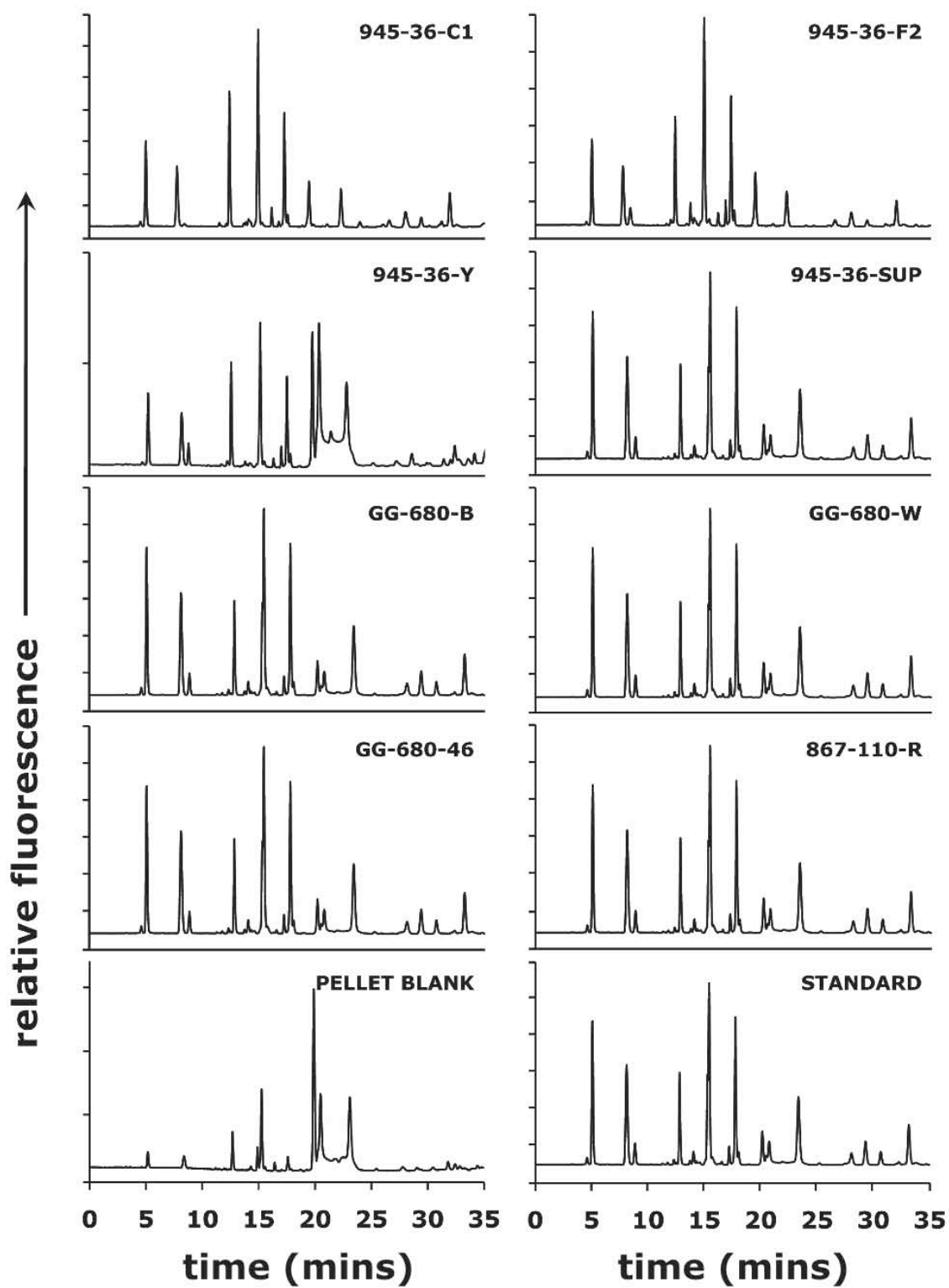
Wierzchos, J., Ascaso, C., Sancho, L.G., and Green, A. (2003) Iron-Rich Diagenetic Minerals are Biomarkers of Microbial Activity in Antarctic Rocks. *Geomicrobiology Journal* 20, 15-24.

Wierzchos, J., de los Ríos, A., Sancho, L.G., and Ascaso, C. (2004) *Journal of Microscopy* 216, 57-61.

Supplementary Information 7.A HPLC-RP Chromatograms (0-35 mins) of half of the samples stacked against a Pierce-H standard sample.



Supplementary Information 7.B RP-HPLC-RP Chromatograms (0-35 mins) of the second half of the analyzed samples against a standard and blank.



CHAPTER VIII. Atacama Desert Surface Soils as Mars Analogs

ABSTRACT

The Atacama Desert, Chile, is one of the driest and oldest deserts in the world. It has been suggested to be a good analog to the Martian regolith based on the soil mineralogy, oxidizing surface soils, and arid climate. Analyses of surface soil samples from a North-South transect of the Atacama Desert showed distributions of amino acids correlated with aridity. A more thorough investigation into the effect of surface and immediate subsurface sample depth on organic content, specifically amino acids, was investigated using samples collected from the Yungay research station in the hyperarid core of the Atacama Desert, Chile. These investigations were specifically targeted towards examining the small-scale microenvironment sensitivity to organic distribution and preservation with depth. Only small differences in total carbon and nitrogen were observed vertically, however, amino acids and their degradation products were strongly correlated with depth in the subsurface. High lateral variability in surface sample composition was observed suggesting that the small-scale microenvironment characterization largely controls organic preservation. These are important considerations in the search for extraterrestrial life as samples from this analog location show strong variability with depth and the same might be expected on Mars. Future Mars missions must take these factors into consideration in deciding what key factors are critical for life-detection mission success (i.e. mineralogy, sampling depths) and must necessarily include a method to probe and sample the Martian subsurface.

8.1 INTRODUCTION

The Atacama Desert is located near the coast of Chile stretching for over 1000 km and covering an area over 180,000 km². The desert is positioned between the Pacific Ocean and the Andes. The Atacama Desert is among the most arid (McKay et al., 2003) and oldest deserts in the world with climatic stability suggested to have persisted over ~150 Ma (Hartley et al., 2005). Because of these extreme conditions, these areas represent challenging environments in which to detect biosignatures (Navarro-Gonzalez et al., 2003; Warren-Rhodes et al., 2006). The Atacama Desert soils have been suggested to be the best terrestrial analog to Mars (Banin, 2005) due to their mineralogy (i.e. high concentration of gypsum and iron oxides) and high concentrations of

surface oxidants (Quinn et al., 2005). These general characteristics suggest that the Atacama Desert is an ideal research site for interpretation of both remotely sensed and *in situ* direct measurements from Mars (Sutter et al., 2007).

Samples from a North-South transect (Figure 8.1) were examined for amino acids in order to investigate large scale variability of organic content. A small subset from samples collected from one of the driest areas in the Atacama Desert within the hyperarid core was subsequently investigated to focus on small-scale variabilities and dependence on various types of microenvironments. The Yungay research site in the central hyperarid core of the Atacama Desert region (Figure 8.1) and is an established research station in the remote areas of this vast desert approximately 50 km east of the Pacific Ocean, close to the city of Antofagasta. This site was chosen because it is within the driest area of the Atacama Desert (McKay et al., 2003) and offers an important opportunity to study a terrestrial analog to Mars with characteristically low biodensities.

8.2 MATERIALS AND METHODS

Samples from the Atacama Desert, Chile, were collected from a North to South transect by Rafael Navarro-Gonzalez in 2002 and delivered to Scripps in the Fall of 2003. Samples from the Atacama Desert Yungay field research site were personally collected during a field campaign in June of 2005. The collection procedure started at the top of the remote sterile hill (YUN1122) and circled downward for a total of 22 sampling locations from which 5 representative sites (See Figure 8.1) were chosen as our sample subset. The subset was chosen to represent a variety of different microenvironments at various heights on the hill. All of the samples were collected with sanitary sampling procedures and stored in sterile whirlpak or fisherbrand bags upon collection. These were later transferred to sterilized polypropylene or glass vials for storage. A subset of these samples representing a diversity of microenvironment was selected from 5 different locations distributed across the whole hill (Table 8.1).

All samples were analyzed in the laboratory for total hydrolyzable amino acids (THAA). For the analyses of the 2002 samples, ~250 mg of samples were weighed out for analyses into 10 x 100mm test tubes. These were sealed in 16 x 1500mm test tubes and vapor phase hydrolyzed with 1mL of 6N HCl for 24 hours at 100°C. The soil samples were transferred onto equilibrated desalting columns (Amelung & Zhang, 2001), rinsed with 3 column volumes of water, and eluted

with 3mL of 2.5M NH_4OH . These residues were concentrated using a vacuum centrifuge and resuspended in 100uL of ddH₂O before analyses. 10uL fractions were run on the HPLC after drydown with 10uL of 0.4M sodium borate buffer.

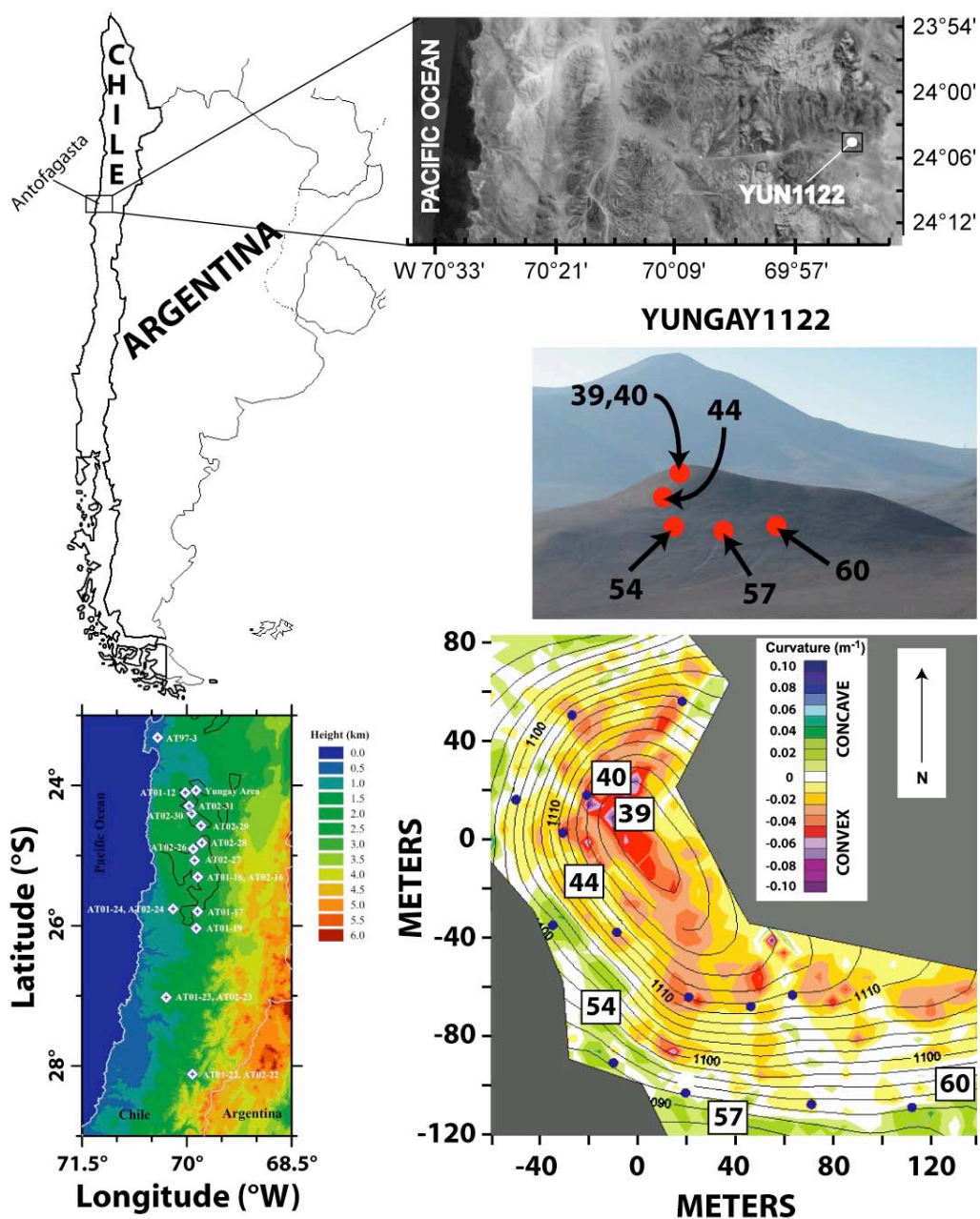


Figure 8.1 Location of Atacama Desert sampling locations. Shown are the locations of the 2002 North-South transect samples (A), and the geographic location of the Yungay research station location in the Atacama Desert, Chile (B). A photograph of the pristine hill sampled from in the Atacama Desert (YUNGAY1122) is also shown along with an aerial topographic map showing the sample subset collection sites (Figure modified from Skelley et al., 2007).

In order to assay for amino acids in the extremely low-level Yungay samples (Table 8.1), ~500 mg samples were weighed out into sterilized pyrex 16 x 150 mm test tubes. These were liquid-phase hydrolyzed in 6M HCl for 24 hours at 100°C. After hydrolysis ~750uL of 1mL of the hydrolyzed acid was transferred to 10 x 100 mm test tubes and evaporated to dryness on a vacuum centrifuge to remove the HCl. These residues were resuspended in 1mL of ddH₂O, and desalted according to the methods outlined above. The 3mL sample desalting extracts were concentrated into a final volume of 100uL, of which 10uL and 30uL fractions were run on the HPLC according to traditional methods (Zhao & Bada, 1995).

Table 8.1 Descriptions of Atacama soil samples collected from YUN1122 in June 2005.

Site	Latitude (South)	Longitude (West)	Elevation (meters)	Sample	Characterization
40 ¹	24°03.63'	69°52.09'	1081	AB1	Exposed Duracrust
				A2	Sub-Duracrust
				B2	Sub-Duracrust
				C1	Subsurface Gypsum/Anhydrite
44 ¹	24°03.65'	69°52.10'	1075	A1	Desert Pavement
				A2	Sub-Desert Pavement
				B1	Exposed Duracrust
				B2	Sub-Exposed Duracrust
				C1	Subsurface Gypsum/Anhydrite
54 ²	24°03.68'	69°52.10'	1055	A1	Duracrust
				A2	Sub-Duracrust
				A3	Dark Salts
				A4	Dark Salts
57 ³	24°03.71'	69°52.07'	1046	A1	Duracrust Fines
				A2	Fines, up to gypsum layer
				A3	Fines, Gypsum layer
60 ⁴	24°03.69'	69°52.01'	1054	A1	Center, gypsum from wall
				B1	Surface gypsum, top 5cm
				B2	Homogeneous porous rock
				C1	duracrust/gypsum

1 – Weathered Soils with duracrust coating
2 – Diffuse Mud Flow Site, within flow regime
3 – Duracrust Soil over gypsum layer
4 – Gypsum-rich aquaduct outcrop

The Yungay sample subset was analyzed total carbon content before and after treatment with excess 3N HCl. The HCl treated samples quantify the total organic carbon (TOC) and total organic nitrogen reservoirs as the carbonate dissolves and is lost as CO₂ during this step. The

analyses for total carbon were each run on duplicate samples of ~60mg while the TOC samples were run once on ~30mg samples.

This sample set was also analyzed by vapor-phase transfer experiments identical to previous methods (Aubrey et al., 2006) in order to investigate the presence of volatile amines such as methylamine and ethylamine which may be present in these samples as decarboxylation products of glycine and alanine, respectively. The high salt and gypsum content of these soils and the fact that they are acidic may allow for the retention of these amines as hydrochloride salts after their formation due to amino acid degradation.

8.3 RESULTS

The samples from Navarro-Gonzalez et al. (2003) showed a strong correlation of amino acid concentration with sample collection latitude. The higher concentrations of amino acids (and presumably total biomass) were detected in the more northern sample latitudes where precipitation is higher on average (Figure 8.2). These results were in agreement with previous studies on these identical samples (Navarro-Gonzalez et al., 2003) and were expected based on the drastic climate differences in high latitudes (usually more precipitation and cooler temperatures) compared to lower latitudes (much drier climates and almost zero annual precipitation).

The extrapolation of the total amino acids to an *E. coli* equivalent cell count (ECE) has been used previously to express bacterial density (Glavin et al., 2004) and offers an approximation as to the order of magnitude of bacterial cell concentrations (Chapter 2). The extrapolated cell counts for the latitudinal profile samples (Figure 8.2) agree with measurements of colony forming units per gram (CFU/g) previously published (Navarro-Gonzalez et al., 2003).

The large-scale distribution of biosignatures in the Atacama Desert therefore looks to be highly dependent upon climate, specifically precipitation and temperature. The lowest amounts of amino acids, and inferred cell counts, occur in the lower latitudes where the temperatures are highest and the precipitation lowest. Many areas in the Atacama Desert offer these harsh climates, and the Yungay area of the Atacama Desert is one of these remote and extremely dry areas within the hyperarid core of the Atacama Desert.

In order to examine the small-scale amino acid concentration and distribution variabilities of a specific area in the hyperarid core of the Atacama Desert, a pristine sampling location was

chosen to study (Figure 8.1). The soil samples collected from the Yungay area show very low carbon contents, ranging from 0.25-2.5 mg carbon per gram of soil. The organic carbon contents of these samples is much lower, not greater than 0.3 mg organic carbon per gram of soil (Figure 8.3).

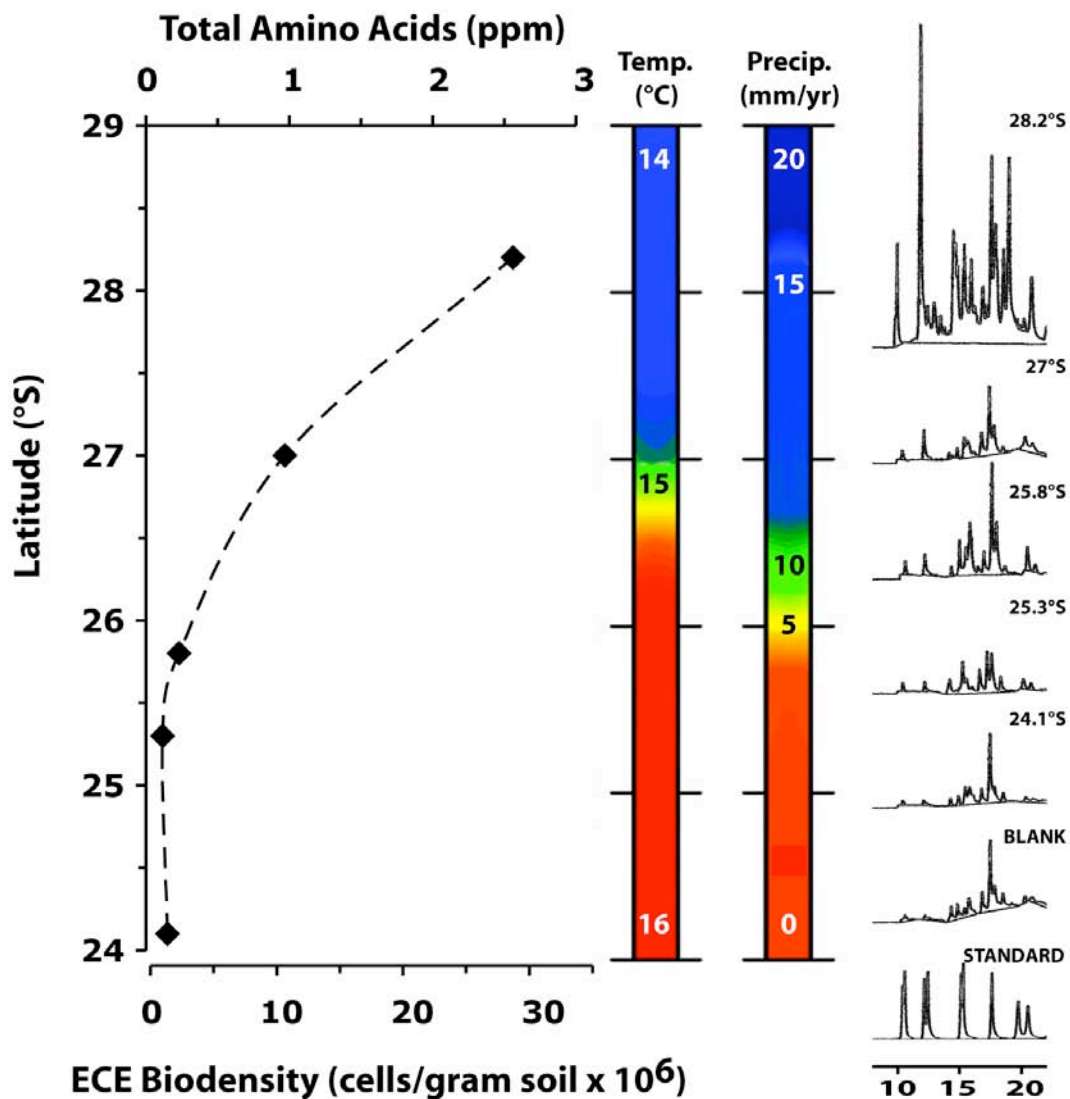


Figure 8.2 HPLC chromatograms of total amino acid concentrations (x_1) and estimated E.C.E. cell counts (x_2) versus latitude (y_1), precipitation, and temperature (y_2). The general trend is elevated total amino acids (and inferred cell counts) in areas with higher water content, in agreement with previous studies (Navarro Gonzalez et al., 2003).

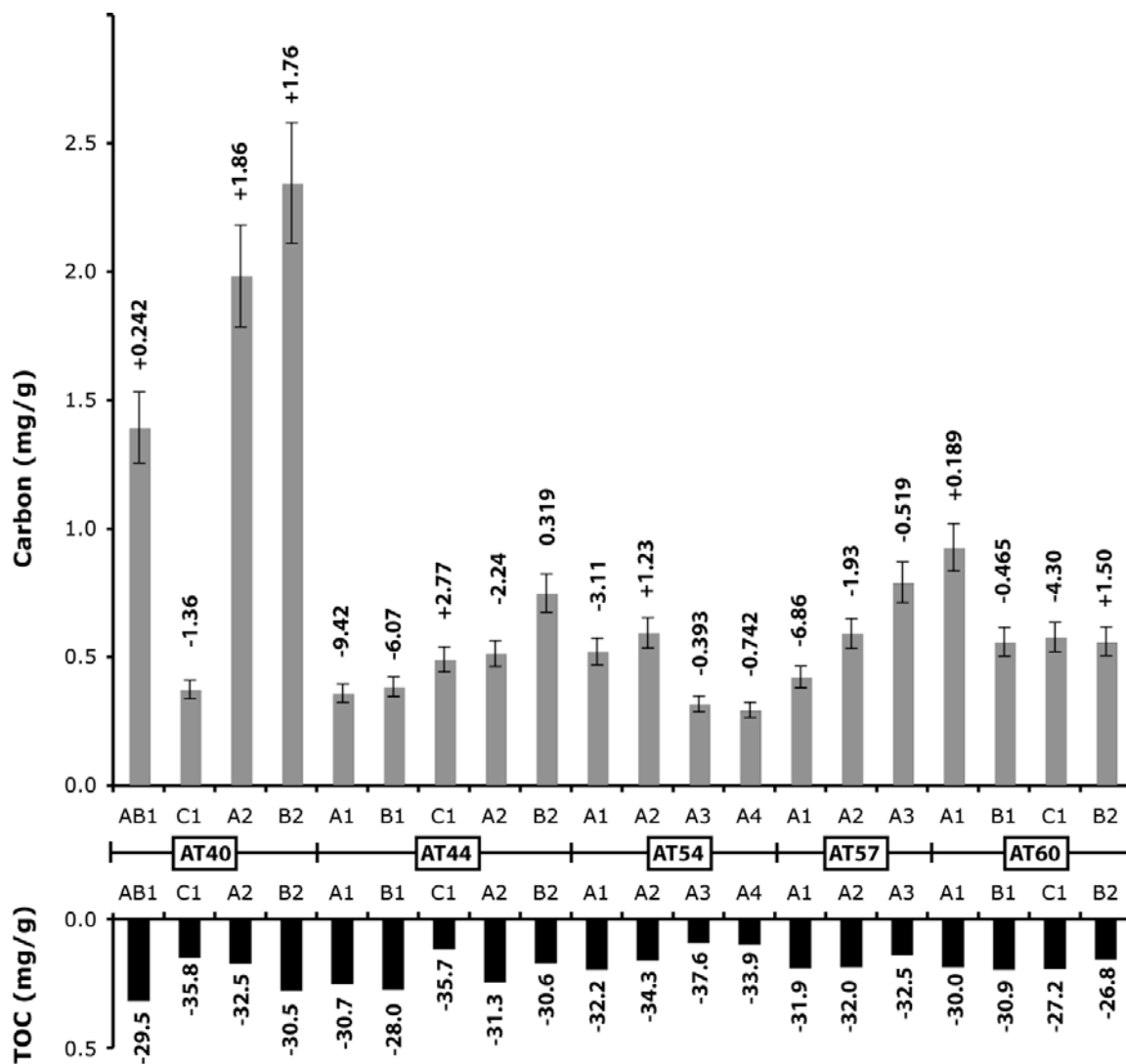


Figure 8.3 TOC and stable isotope labels for the Atacama Desert sample subset run untreated (gray) and after treatment with excess acid to remove carbonate (black). The labels reflect the $\delta^{13}\text{C}$ values for the respective fraction. The percentage of TOC (acid treated) compared to total carbon (untreated) varies between 8% and 65%. The acid-treated samples showed $\delta^{13}\text{C}$ values between -26.8 and -37.6 while the untreated samples all fell in the range of +2.8 to -9.4. Error bars represent $\pm 10\%$ for the untreated samples.

The difference in the total carbon and acid-treated total carbon measurements (TOC) give a general idea of the relative amounts of carbonate present in these samples as this is the fraction dissolved during acid pre-treatment. The TOC percents range from 8% to 65% of total carbon with the highest percentages generally in the surface samples. Isotopic measurements on the bulk carbon (+2.8 – -9.4 ‰) may reflect the derivation of the carbonate from atmospheric sources.

The absolute TOC levels increase slightly from the immediate surface to the subsurface in the depth profiles for samples 40, 44, 54, and 57 while they stay relatively constant for sample 60. The deeper depth profiles show variable results where sample 54 has less TOC below the subsurface while sample 57 increases slightly. Regardless, these differences are rather slight. The untreated total carbon values show less variation at depth while high variability is observed at the surface.

The amino acid measurements from the Atacama Desert soils (Table 8.2) showed two distinct amino acid distributions. There were samples that appeared to look completely devoid of microbial life biosignatures and were instead dominated by β -alanine, a degradation product of aspartic acid. These samples are indicative of highly degraded organic matter and appear to be from inhospitable microenvironments which show no sign of extant microbial life. The second common amino acid distribution was similar to a typical extant microbial life biosignature, however large concentrations of β -alanine and the occurrence of γ -amino-n-butyric acid (γ -ABA) were observed in these samples as well. These measurements most likely reflect the detection of low levels of extant microbial life in the Atacama Desert surface and subsurface, however, the coincidence of large amounts of β -alanine, equal to or exceeding the glycine concentrations, seems to be a unique feature of these samples. These may be explained by an organic-poor microbial community that necessitates the processing and reworking of amino acids in order to access organic molecules. The high levels of β -alanine are presumably derived bacterial protein degradation and show the effects of bacterially induced amino acid decarboxylation, in accord with previous studies (Bada, 1991).

Table 8.2 Hydrolyzed and desalted blank-corrected amino acid concentrations for all samples (ppb).

Site	Sample	Asp		Glu		Ser		Gly	β -Ala	γ -ABA	Ala		Total
		D-	L-	D-	L-	D-	L-				D-	L-	
40	AB1	BD	BD	1.80	2.59	1.04	4.41	BD	1,710	34.9	18.9	26.0	1,799.6
	A2	BD	BD	1.66	4.30	<1	4.53	BD	273	9.44	9.01	49.2	351.1
	B2	BD	BD	3.19	1.04	BD	BD	BD	191	BD	BD	BD	195.2
	C1	BD	BD	BD	BD	<1	3.27	BD	3.09	BD	BD	BD	6.36
44	A1	37.7	629	528	2010	77.9	356	1,050	2,310	30.7	200	1660	8,889
	A2	29.5	385	322	1200	31.6	159	456	1,130	16.9	116	901	4,747
	B1	BD	BD	11.6	40.0	9.61	13.1	BD	903	7.34	27.9	193	1,205.6
	B2	1.44	22.9	58.8	193	18.8	25.4	193	1240	25.7	75.9	444	2,298.9
54	C1	BD	BD	BD	BD	4.86	21.0	BD	54.5	<1	BD	<1	80.36
	A1	20.6	193	238	686	37.2	111	289	1,162	9.84	103	650	3,499.6
	A2	38.9	308	196	677	26.4	147	352	569	6.40	79.4	517	2,917.1
	A3	13.4	246	50.5	259	6.16	134	294	25.2	BD	25.3	283	1,336.6
57	A4	20.1	401	76.5	433	8.54	221	502	35.2	2.19	45.3	514	2,258.8
	A1	8.45	75.0	146	389	10.3	37.4	137	642	6.96	68.3	345	1,865.4
	A2	15.2	153	159	470	19.8	82.3	109	335	5.30	60.0	360	1,768.6
	A3	31.2	195	28.3	381	15.1	53.6	145	116	1.16	60.8	237	1,264.2
60	A1	BD	BD	<1	BD	BD	<1	BD	14.5	1.62	BD	1.84	17.96
	B1	BD	BD	<1	1.60	<1	1.66	BD	384	18.6	2.59	BD	408.5
	B2	5.54	29.7	27.8	81.1	8.62	15.2	69.5	78.8	11.5	25.3	107	460.1
	C1	BD	<1	2.52	10.5	<1	2.55	BD	360	28.2	7.70	4.99	416.5
GY	01	BD	1.32	3.62	19.3	3.73	5.45	8.76	1,180	44.3	13.4	54.7	1,334.6
	02	16.3	123	105	309	10.3	36.5	19.4	93.4	4.20	62.5	230	1,009.6
SP	000	BD	5.96	21.2	76.9	7.22	8.56	57.5	106	2.84	20.8	148	455.0
	088	BD	BD	BD	BD	<1	<1	BD	BD	BD	BD	BD	0
136	<1	2.07	BD	1.26	BD	<1	6.21	5.04	BD	BD	BD	BD	14.58

Note: Errors not reported but average error calculated by the standard deviation of 6 standards was $\pm 2\%$.

BD = Below detection limit of 1 ppb.

Microbial cell enumerations via PLFA and culturing experiments in similar samples from the Atacama Desert have resulted in cell counts of $2.0 \times 10^6 - 1.0 \times 10^7$ cells/gram and $1.6 \times 10^3 - 4.6 \times 10^3$ cells/gram, respectively (Lester et al., 2007). This marked difference in the culturable and total cell enumerations are expected based on the uncertainties associated with cell culturing studies (Janssen et al., 2002). Other cell culture studies on Atacama Desert soil samples from similar regions around Yungay have detected similar biodensities and lower (Navárrro-Gonzalez et al., 2003; Maier et al., 2004).

Similar to PLFA analyses, the total amino acid compositions can give an estimate of the total biomass of bacterial cells from extinct and extant life combined. Because there is a portion of degraded organic matter present in these Atacama soil samples besides the low level extant biodensities, these estimates represent an upper limit of total cell concentrations. The observed biodensity range in all the samples analyzed (Table 8.2) fall between 1.7×10^4 and 6.0×10^7 cells/gram and are in the range of previous estimates.

The general assumption of using D/L-ratios as diagenetic indicators is that the higher the D/L amino acid ratio, the lesser the bacterial biomass. Amino acids from extant microbial communities dilute this signal (essentially pure L-amino acids), which represents some fraction of the total amino acids. The fact that these samples show combination of living and dead communities compromises the meaningful analyses of enantiomeric ratios for age determination, however they can still be used to assess the relative diagenetic state of the organic matter.

8.3.1 *Amino acid distributions and microenvironments – A Qualitative assessment*

The amounts of β -Alanine in the surface samples are especially high for the majority of the samples, both in those that show little or no evidence of extant microbial life and in the samples with bacterial distributions of amino acids. Analyses of desert varnishes from the Sonoran Desert show concentrations of the non-protein amino acids β -ala and γ -aba, which were interpreted of evidence of biological enzymatic decarboxylation (Perry et al., 2003). It is interesting that in both environments these degradation products are present in high concentrations, indicating that some type of environmental factor may be responsible for its formation. However, the protein and non-protein amino acids detected in this previous study were parts-per-million concentrations for β -ala (~44 ppm), γ -aba (14 ppm), and glycine (319 ppm). Although the absolute amounts are greater in the Sonoran Desert samples, the relative

amounts of these degradation products compared to glycine are much less than observed in the Atacama Desert samples. The ratio of glycine to β -Alanine for the Sonoran Desert are ~ 0.14 while the ratios observed in the Atacama are much greater than 1.

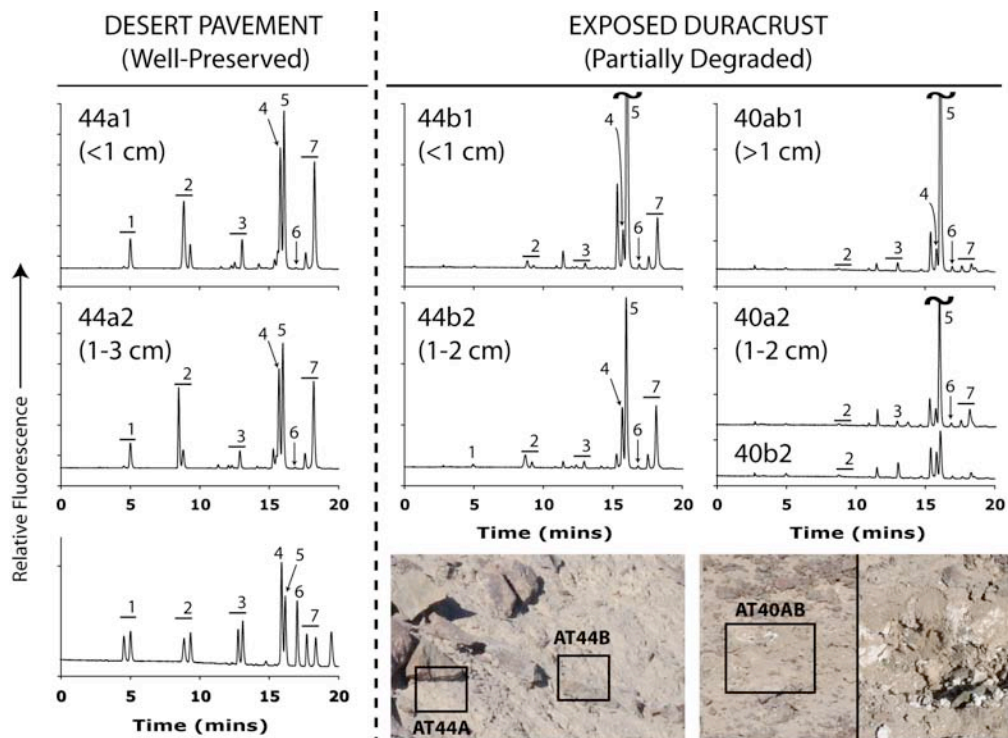


Figure 8.4 RP-HPLC chromatograms (0-20 mins) of 10 μ L concentrated Atacama sample extracts from sites 40 and 44 showing the amino acids measured in different microenvironments. Note the difference in amino acid distributions between a desert pavement sample (sample 44a, shielded duracrust) and exposed duracrust samples (44b, 40ab). Note the exaggerated scales of the exposed duracrust samples.

Samples analyzed from three different sites (40ab, 44a, 44b) characterize differences in amino acid compositions of two surface duracrusts and a desert pavement microenvironment (Figure 8.4). Duracrust is a very dry, consolidated surface soil which forms a type of crust in the uppermost surface soils of the Atacama Desert while desert pavement is a more refractory consolidated matrix which might provide more protection from the elements. The desert pavement samples from the surface and immediate subsurface show much higher levels of amino acids and are not dominated only by β -Alanine, as the exposed duracrust samples show, rather they show microbial distributions of amino acids. Similar amino acid concentrations and distributions are observed in the desert pavement surface (<1 cm, 44a1) and immediate

subsurface samples (1-3 cm, 44a2) indicate a homogeneous vertical concentration in the upper 3 cm.

The surface and immediate subsurface samples from site 40 (exposed duracrust) show little difference in amino acid concentration with depth. They show compositions strongly dominated by trace amounts of glycine and high concentrations of β -Alanine and even in a gypsum sample from the upper 10 cm of soil, amino acids are undetectable except for traces of glycine and β -Alanine. The surface duracrust and immediate subsurface samples at site 44 (44b1, 44b2) show the identical distribution to site 40 except for the preservation of low concentrations of D/L-alanine, an amino acid highly stable to decarboxylation (Li & Brill, 2003).

These β -Alanine dominated duracrust samples are indicative of highly degraded organic matter without any contribution from extant microbes. The Atacama soils are unique in the fact that they show highly oxidizing properties, so the chemistry of these surface soils combined with the high UV-radiation flux may be responsible for these high levels of observed degradation. The relative concentrations measured in samples from site 44 are similar to those in Skelley et al. (2007) for the shielded duracrust (44a) compared to an exposed environment (44b). The observed high lateral variability in amino acids and inferred microbial abundance appears to be a function of the specific microenvironment.

In highly degraded surface environments with extremely low biodensities, bacterial remnants are often the source of amino acid biosignatures because refractory cell wall molecular components tend to persist for longer timescales than free amino acids. Glycine-dominated compositions have been observed before in heavily degraded marine organic matter (Dauwe et al., 1999) and are suggested to result from high glycine concentrations within refractory bacterial cell walls (Hecky et al., 1973). Glycine also tends to dominate amino acid distributions in nearshore anoxic sediments (Rosenfeld, 1979) and ancient shells (Robbins & Ostrom, 1995). Previous analyses of a core section for total hydrolyzable amino acids (THAA) has shown that the dominant amino acid glycine increases in mole fraction at greater depths (Pedersen et al., 2001), suggesting that diagenetic processes create a greater fraction of glycine as what is observed in extant bacterial communities. Also of interest is the dominance of glycine in THAA amino acid distributions from hydrothermal vent fluids, which originate from the degradation of extant bacterial communities (Takano et al., 2004). Although glycine is present as a large part of microbial proteins, the glycine dominance suggests that it persists over long geological timescales

because of its relatively high stability and the fact that it is formed diagenetically from other amino acid precursors.

Sites 40 and 44 were near the top of the sampled hill and represent areas that are not associated with water. The relative slopes of the hill at the sampling locations are shown in Figure 8.1, and analysis of the concavity at these sites might give a rough estimate of the amount of water that would persist during infrequent precipitation events. Sites 54, 57, and 60 are located at lower elevations (~1050 m) than sites 40 and 44 (~1080 m). Also, they show convex curvature (Figure 8.1) and would allow for water accumulation and flow along these paths. The higher elevation sites show concave curvature and it is clear that precipitation that might stimulate biological activity would not be effective at persisting in such areas. Site 60 shows a variety of microenvironments within a small area and shows evidence of recent water activity because of the surface gypsum deposits directly on the surface (Figure 8.5). It appears that a type of flow system was present at one time that upwelled or exited from this region, based on the geology and physical appearance of this area.

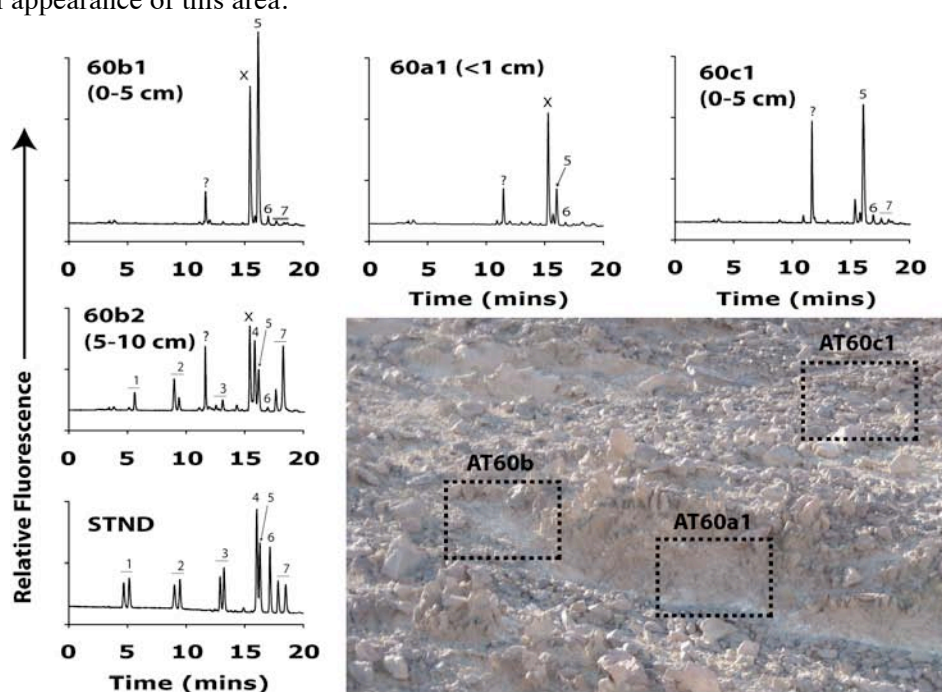


Figure 8.5 RP-HPLC chromatograms (0-20 minutes) of 30 μ L concentrated Atacama sample surface extracts collected from site 60. Different sites reflect unique microenvironments and bacterial distributions are observed in the samples that show evidence of recent water activity, evident by surface deposits of gypsum. 1 = D/L-asp, 2=L/D-glu, 3=D/L-ser, 4=gly, 5= β -ala, 6= γ -aba, 7=D/L-ala. Peak X comes directly in front of glycine and elutes at the exact retention time of threonine (X~thr). The peak between glutamic acid and serine (labeled ?) is unknown.

Samples were taken from within the region indicating water activity (AT60a) and at two background sites on the side of the mound at the surface and subsurface (AT60b) and ~2 feet above the mound at the surface within local duracrust. None of the surface sites showed microbial amino acid distributions, and instead their distributions were dominated by β -ala and a peak that is tentatively identified as threonine (Figure 8.5, peak X). The preferential accumulation of threonine and glycine can be explained by their high concentrations in refractory cell wall material (Hecky et al., 1973) and may persist in highly degraded environments. A subsurface sample beneath the degraded surface sample at site 60b showed a microbial distribution associated with low levels of biodensity. This was in a sample 5-10 cm deep that was directly beneath the subsurface gypsum layer (~5-10 cm). This subsurface site may show evidence of enhanced preservation of amino acids at depth, however there were still high levels of β -alanine in this sample indicating amino acid decarboxylation by microbial life.

Two small depth profiles were taken at sites 54 and 57 in order to investigate the vertical distribution of amino acids in two neighboring areas. Sample site 57 was sampled up to 6 cm depth at a surface duracrust deposit (<1 cm) and two immediate subsurface sites which probed the subsurface gypsum-rich layer located at a depth of ~5 cm. The amino acid concentrations are extremely consistent over this threshold and indicate an extant microbial community at low biodensities ($\sim 10^7$ cells/gram) at all sampling depths. The fact that high concentrations of β -alanine are coincident with the amino acids at this site shows clear evidence of extant (or well preserved extinct) microbial life indicates that the bacterial activity may be responsible for its occurrence. However, the relative amount of the decarboxylation product of aspartic acid decreases with depth and at 3-6 cm depths is lower than the concentration of glycine. This may suggest that the generation of β -alanine is due to surface processes, however, this has never been observed before and is more likely due to bacterial degradation in an energy-limited extreme environment.

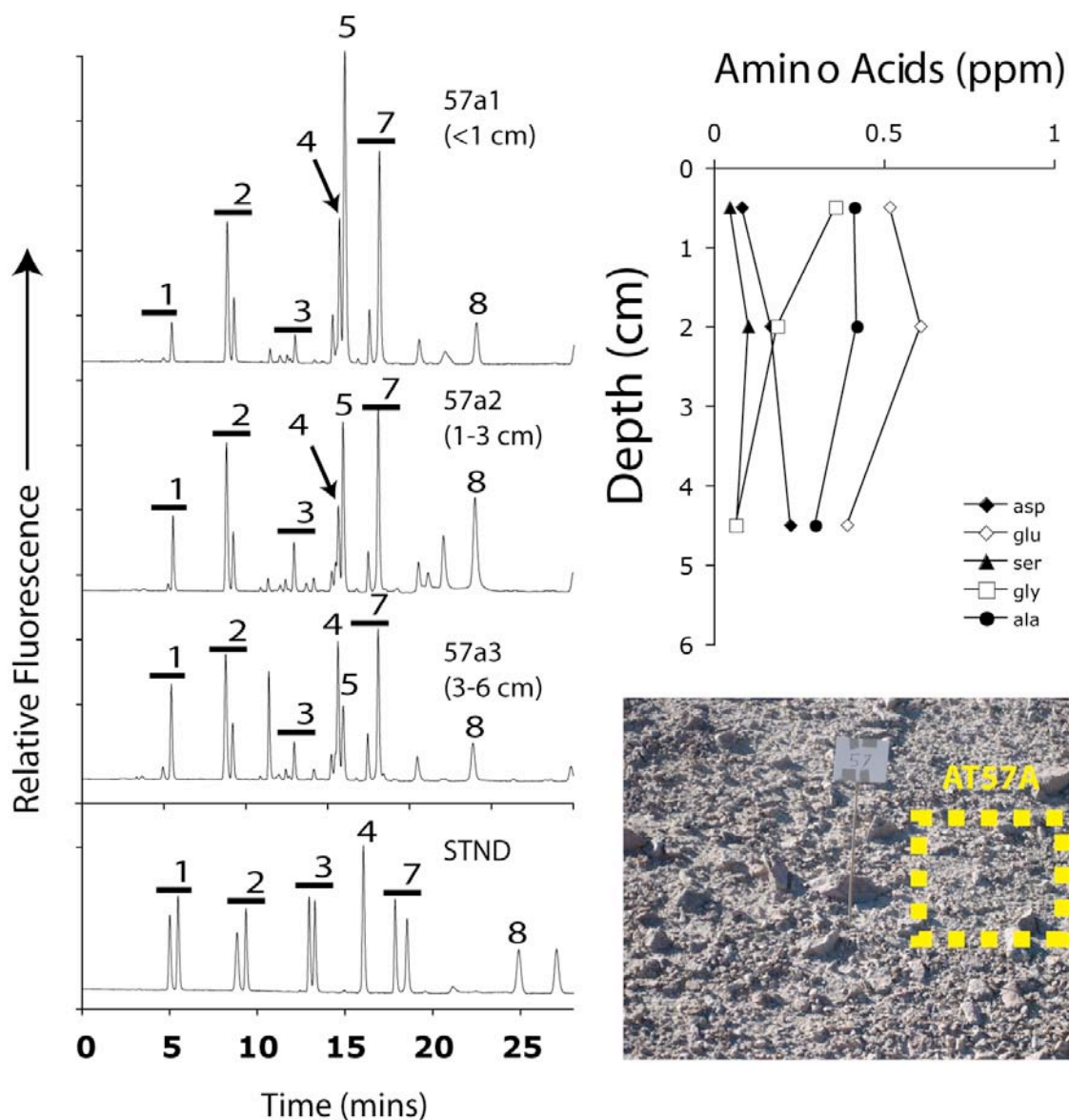


Figure 8.6 RP-HPLC chromatograms (0-27 minutes) of 30 μ L concentrated Atacama sample extract collected from site 57, showing a depth profile in the upper ~5 cm for amino acid abundances. The profile shows consistent concentrations of amino acids with depth, however, the presence of high concentrations of β -Ala indicate that the organic matter has been degraded over time.

The second depth profile at site 54 was chosen because there was a water flow line within the surface soil indicating past water activity (Figure 8.7). 4 different depths were sampled within the surface duracrust and subsurface and at two deeper depths within subsurface dark salt deposits. All of these sites show evidence of extant microbial life, again coincident with the

presence of high concentrations of β -alanine, higher in the surface than at depth. The amino acid abundances decrease with depth to approximately half the surface value for glu, gly, and ala while asp and serine show a more consistent depth profile (Figure 8.7). This indicates that the surface samples are more degraded with respect to relative amino acids because their concentrations are so highly dissimilar.

In all sites surveyed, β -alanine appears in surprisingly high concentrations. The relative abundance of decreases with depth in the subsurface, but the highly degraded surface samples show compositions dominated by this degradation product. At all locations where evidence of water activity is observed, via surface gypsum precipitates (AT60a) and subsurface deposits (AT54A), or beneath evidence of previous water flows (AT54a), amino acids consistent with microbial distributions are observed. It is not difficult to detect amino acids within these low-level areas, however, the relative concentrations and preservation appear to be strongly influenced by the prevailing microenvironment.

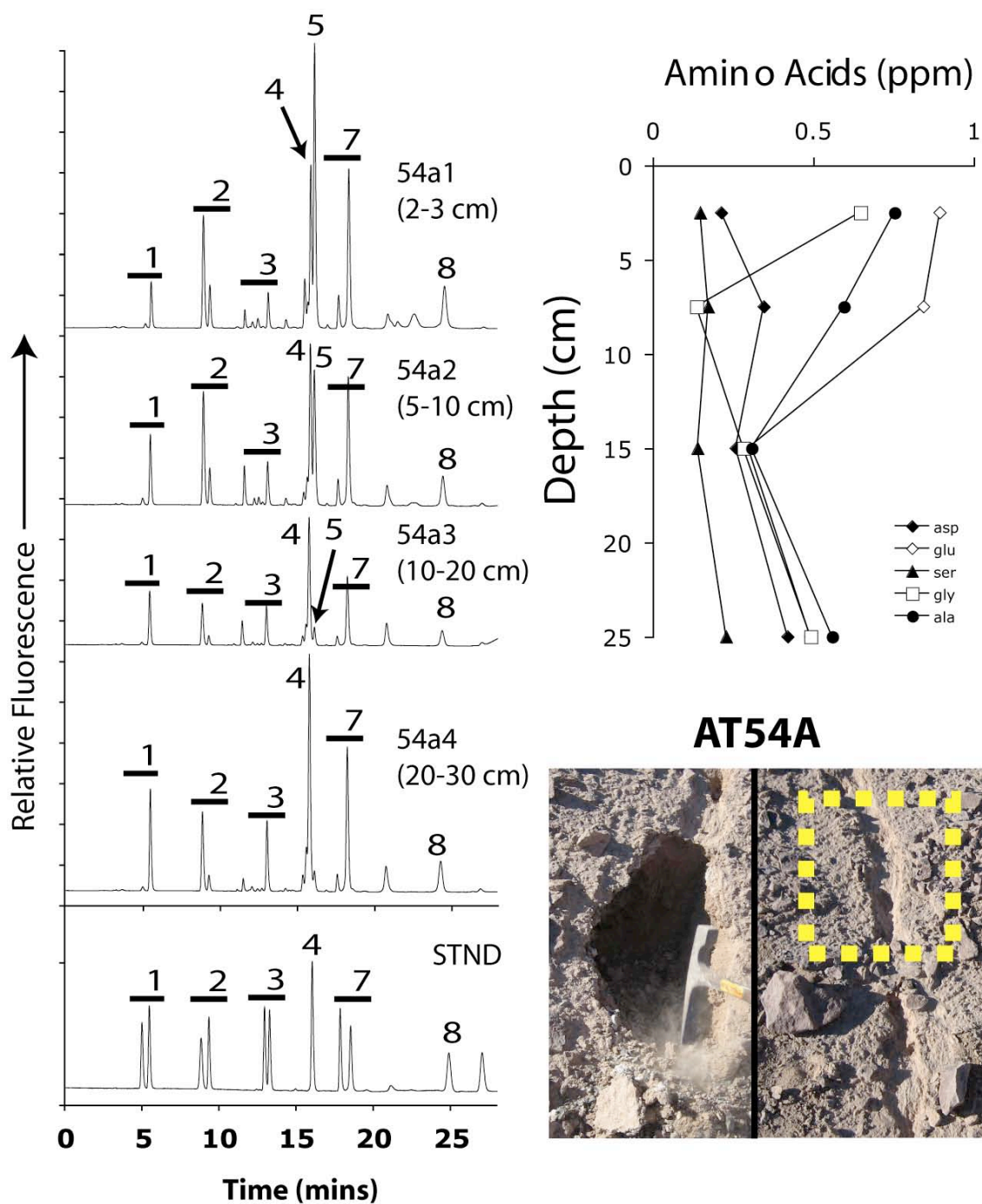


Figure 8.7 RP-HPLC chromatograms (0-30 minutes) of 30uL concentrated Atacama sample extract collected from site 54, showing a depth profile in the upper ~30 cm for amino acid abundances. High concentrations of β -Ala indicate that there has been extensive bacterial degradation over time.

8.4 BIOCHEMICAL INDICATORS OF DIAGENETIC ALTERATION

There are a variety of methods to determine the relative diagenetic state of the proteins and amino acids in the Atacama Desert samples. The sulfate present in Atacama Desert soils has been suggested to be from volcanic sources (Berger & Cooke, 1997), but more recent results suggest that the nitrate salts were derived from atmospheric sources (Böhlke et al., 1997) and sulfate salts as well are derived from the atmosphere (Rech et al., 2003; Bao et al., 2004; Michalski et al., 2004). The evaporitic gypsum present in the uppermost Atacama Desert soils date from the Pliocene to Pleistocene (Pueyo et al., 2001), and more specific constraints have characterized the bulk of the originally deposited gypsum as ~2 Ma (Hartley & Chong, 2002; Ewing et al., 2007), although this is an upper limit and subsequent atmospheric deposition of sulfates or nitrates could dilute this signal (Ewing et al., 2006).

The top 5 cm at site 57 look to be relatively homogeneous in terms of amino acid D/L-ratios for all amino acids (Figure 8.8). Surface samples from site 54 show elevated surface D/L-ratios compared to the subsurface sites (Figure 8.8), especially for glutamic acid and serine while the effect for aspartic acid and alanine is less pronounced. All of the amino acids show a general decline with depth in D/L-ratio and at a 15 cm depth, the ratios are all fairly low, indicative of better-preserved organic matter which show the same enantiomeric abundances down to 20 cm depth. The highest surface enantiomeric ratios at site 54 (glutamic acid and serine) can be explained by the low stability of serine is very unstable and prone to racemization over short geological timescales. Similarly, glutamic acid is one of the more unstable protein amino acids and degrades much faster than alanine which shows the least effect of depth on D/L-ratio. These trends with depth imply that there is generally more racemized amino acids within the upper soil layers and might be due to UV-radiation induced racemization.

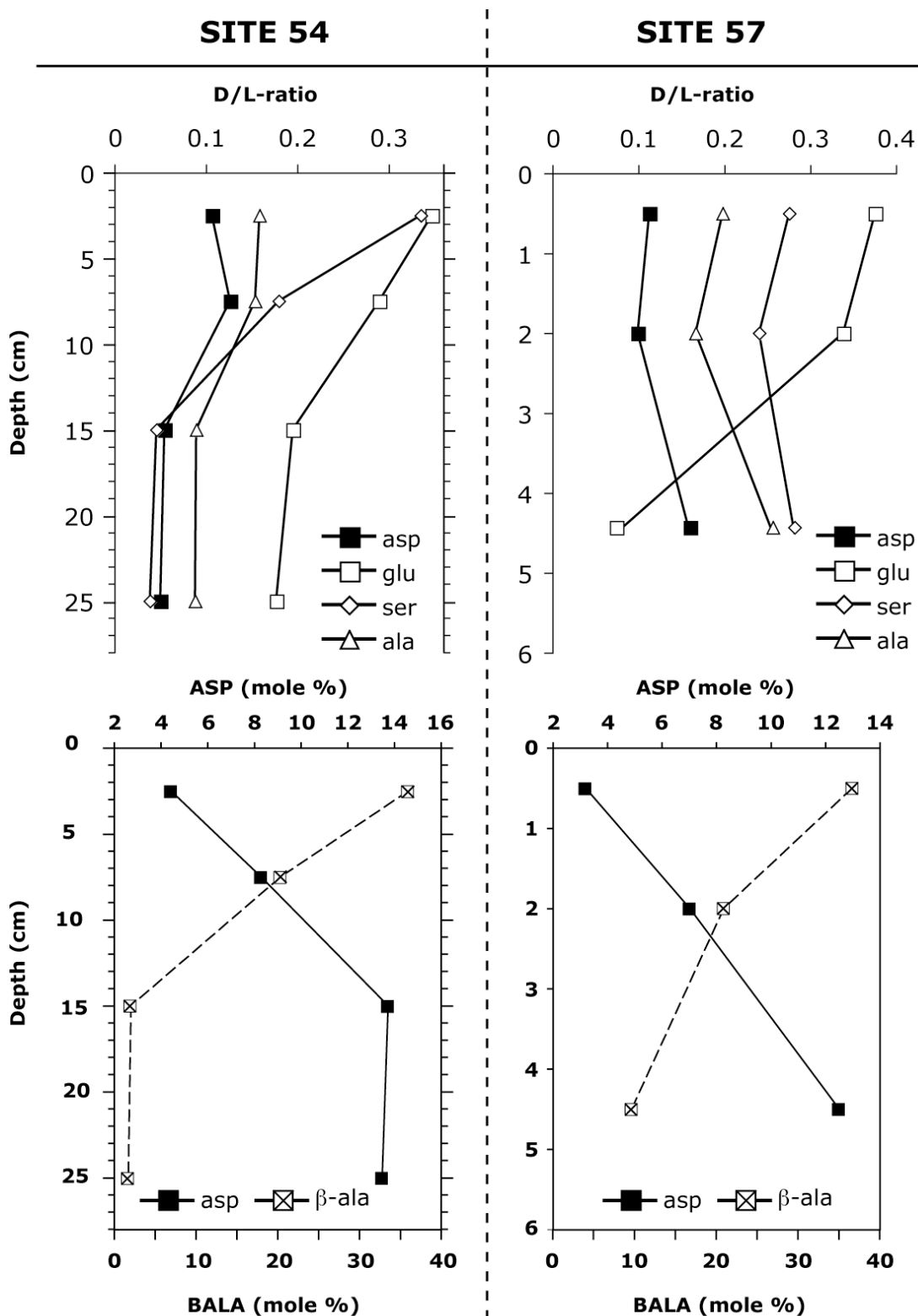


Figure 8.8 Depth profiles of diagenetic indicators for sample sites 54 and 57 of amino acid D/L-ratio variations and variations of β -alanine and aspartic acid with depth.

The presence of amino acid degradation products, such as β -alanine and γ -aba, has been used previously as a diagenetic indicator for organic matter within sediments (Cowie & Hedges, 1994; Dauwe et al., 1999; Kudo et al., 2006). In particular, these studies tend to show the increase of β -alanine and γ -aba with increasing depth (corresponding to deposition age) within the sediments (Cowie & Hedges, 1994), presumably through the microbial decarboxylation of amino acids with time. Likewise, these trends are observed to be the reverse of the variation of aspartic acid and glutamic acid, which show decreases over time. Similar diagenetic indicators can be used within the Atacama Desert soils for the two sample sites with a depth series (sites 54 and 57), although there may not be a correlation of sample age with depth. Instead, this correlation may be the distance away from the harsh surface conditions where high levels of UV-radiation tend to promote degradation and oxidation of organics.

With marine sediments, the mole fraction of β -alanine tends to increase with depth (\sim age), however, these samples show the reverse trend with the degradation product β -alanine higher in surface samples while it is lower in the subsurface. This may be indicative of the effects of the harsh surface conditions in the Atacama Desert as the cause of enhanced degradation, possibly due to degradation by UV-radiation, an inorganic pathway, or more likely, the degradation of old refractory organics by bacteria in the upper soils.

In general, the degree of diagenesis in these samples is much higher in the top 2-5 cm of soil. This is evident by the fact that the highest D/L-amino acid ratios are observed in this horizon and are relatively consistent in the top 5 cm (Figure 8.8, Site 57). This could possibly be due to surface physical mixing processes, however this is unlikely due to the relatively benign climate that this region experiences. More probable is that this reflects an upper limit of the UV-radiation effects in the surface soils. Any solar radiation input could cause rapid racemization over geological timescales, altering the enantiomeric composition of the organic matter. Also indicative of advanced diagenesis is the high mole fraction of B-ala present in the uppermost surface samples and rapid decline in the top 10 cm. Surface processes in this region therefore clearly influence not only amino acid racemization rates but distributions as well.

Enantiomeric excesses of amino acids in Atacama Desert soils (specifically serine and alanine) have previously been suggested to results for in situ amino acid synthesis facilitated by UV light (Tsapin, 2005), however this is an untested theory and unlikely. More probably is the

explanation that there is enhanced diagenesis and accumulation of refractory organic material that has been undergoing racemization for long timescales.

Another proxy for the diagenetic state of the organic matter in the Atacama sulfates is the detection of amine degradation products of various amino acids. Alanine and glycine degrade primarily by decarboxylation while serine also undergoes decarboxylation as well as competitive degradation mechanisms (Figure 8.9).

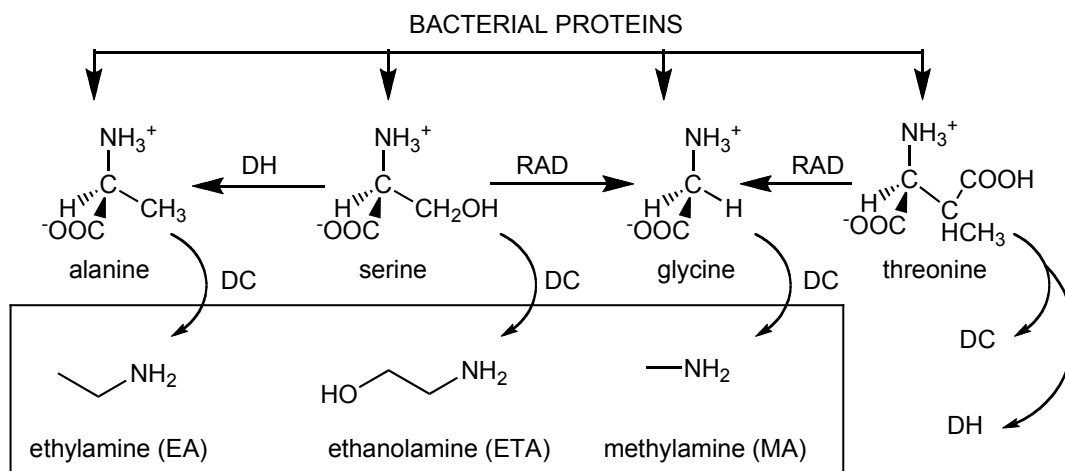


Figure 8.9 Potential diagenetic pathways of amino acid interconversion by reverse aldol cleavage (RAD) and dehydration (DH) and decarboxylation (DC) degradation reactions into detectable amine compounds. Serine, glycine, and alanine are among the most abundant bacterial protein amino acids. Racemization is not included in these pathways, but is another diagenetic process whereby D-enantiomers are formed from bacterial amino acids.

Serine also undergoes other degradation pathways besides decarboxylation to form other amino acids. For instance, serine can dehydrate to produce racemic alanine or undergo reverse aldol cleavage to form glycine (Bada, 1991). Degradation of methionine can produce glycine (Kvenvolden, 1975), although this amino acid is not present in bacteria in significant concentrations so must be a minor pathway for glycine accumulation. In order to simplify this model, the amino acids that degrade primarily by decarboxylation, glycine and alanine, and the detection of their decarboxylation products are the focus of the rest of this study. The other pathways to glycine and alanine formation are considered to be insignificant compared to their decarboxylation destruction pathways.

Methylamine and ethylamine are volatile products and as such (Figure 8.10), they are perhaps not fully retained by the mineral matrix after amino acid decarboxylation. Previous studies have shown high concentrations of amines in old geological sulfate samples (Aubrey et al., 2006). However similar high levels of methylamine and ethylamine have not been reported because their quantification is so problematic. Even within samples that might be expected to have high concentrations of these degradation products, such as studies on irradiated amino acids (Kminek & Bada, 2006) and geological samples where they might be expected to be present (Walton, 1998). In fact, the Atacama Desert soils may not show efficient preservation of the absolute levels of amino acid amine degradation products based on the fact that they are a mixed mineral matrix. However, the samples from the subsurface gypsum horizon should be rich enough in gypsum that these might be accurate in identifying the decarboxylation products methylamine and ethylamine and inferring relative trends with depth. Indeed the concentrations of methylamine and ethylamine are well above blank levels and most likely reflect a retained signal of past amino acid decarboxylation to form these products.

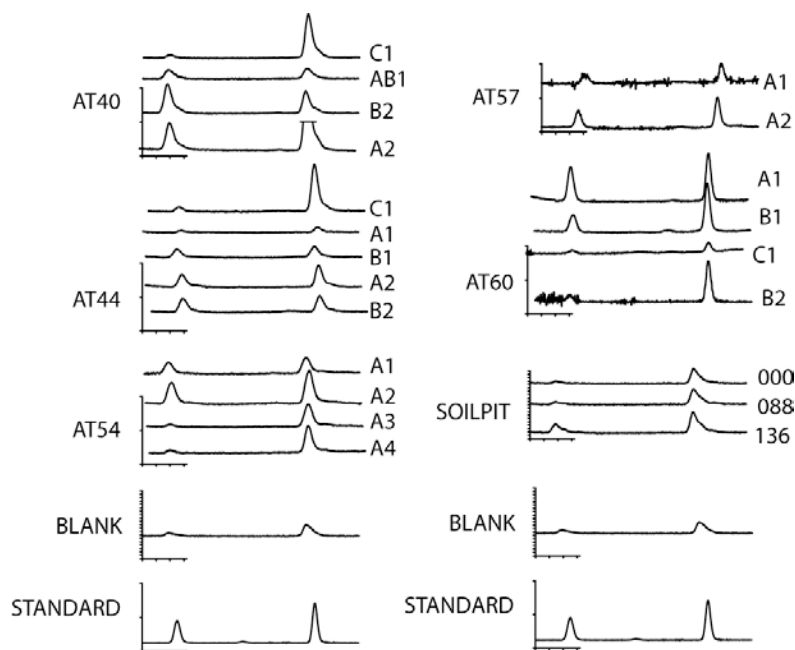


Figure 8.10 RP-HPLC chromatograms of amino acid degradation products from amine transfer experiments shown for methylamine and ethylamine (22-31 minutes) for all samples with depth. These products are used to assess the relative amino acid degradation over time to form methylamine from glycine and ethylamine from alanine. Blank levels of methylamine and ethylamine were approximately 10 ppb, presumably derived from background concentrations from the air.

The Z-ratio used to characterize the relative amounts of amine degradation product to parent amino acid (Aubrey et al., 2006) can be defined for individual amino acid degradation products as follows:

$$\text{Equation 8.1} \quad Z_{MA} = \frac{[MA]}{[gly]} \quad \text{glycine} \rightarrow \text{methylamine (MA)}$$

$$\text{Equation 8.2} \quad Z_{EA} = \frac{[EA]}{[alanine]} \quad \text{alanine} \rightarrow \text{ethylamine (EA)}$$

Then the relative ages of these samples may be determined using Equation 8.3:

$$\text{Equation 8.3} \quad \ln\left(\frac{AA_t}{AA_0}\right) = -k_{DC} \cdot t$$

Where the amino acid concentration at time zero (AA_0) is expressed as:

$$\text{Equation 8.4} \quad AA_0 = AA_t + AMINES_t$$

Therefore, the expression becomes:

$$\text{Equation 8.5} \quad \ln\left(\frac{AA_t}{AA_t + AMINES_t}\right) = -k_{DC} \cdot t$$

$$\text{Equation 8.6} \quad \ln(1 + Z) = k_{DC} \cdot t$$

These data may be used to estimate the ages of the depth sample sites 54 and 57. Because the majority of samples lack glycine, most of these data will use the kinetic system of alanine and ethylamine to estimate the sample ages. The rate constant for glycine conversion to methylamine is estimated at $6.4 \times 10^{-8} \text{ yr}^{-1}$ and the rate constant for alanine conversion to ethylamine is estimated at $1.7 \times 10^{-7} \text{ yr}^{-1}$. These rates were calculated using sulfate

decarboxylation data from Aubrey et al. (2006) for the ~4 Ma year old Anza-Borrego gypsum sample at 20°C and the temperature of the Atacama was assumed to be similar.

Table 8.3 Concentrations of amino acid decarboxylation products for depth profile sites 54 and 57 determined by reverse-phase HPLC after vapor-phase transfer for methylamine (MA) and ethylamine (EA), and calculations of Z-ratios.

		MA (gly)		EA (ala)	
		ppb	Z-ratio	ppb	Z-ratio
54	a1	19.1	0.066	7.9	0.011
	a2	49.1	0.140	48.3	0.081
	a3	BB	NA	21.6	0.070
	a4	BB	NA	26.1	0.047
57	a1	10.6	0.078	3.9	0.0095
	a2	15.7	0.144	9.8	0.0232
	a3	4.4	0.030	41.6	0.1395

BB = Below Blank levels.
 NA = Not Applicable.
 Note: Uncertainties for MA = 7.8 % and EA = 4.8 %.

Plot of amine chronometer parent versus daughters for the glycine/methylamine and alanine/ethylamine should plot linearly for all samples or within the sample sets if the Atacama soils were all the same ages. However, they do not plot linearly, indicating that there are differences in the ages of the soils within each sample set and between sample sets. This variation was investigated for sample sets 54 and 57 in order to deduce the relative ages with depth for sample sets 54 and 57 (Figure 8.11).

The gypsum deposits all date <2 Ma according to these methods, in agreement with previous studies which define the subsurface Atacama desert gypsum deposits as having formed at ~2 Ma (Hartley & Chong, 2002). The only discrepancy in the amino acid decarboxylation dating method appears to be the deepest sample at site 57. The age of the sample computed using the ratio of methylamine to glycine shows much younger organic matter than the ethylamine/alanine system predicts. Realistically, the samples are a mixture of the older gypsum material and the more recent surface soils due to gardening effects and vertical salt mobility within surface soil layers, so some discrepancies are expected.

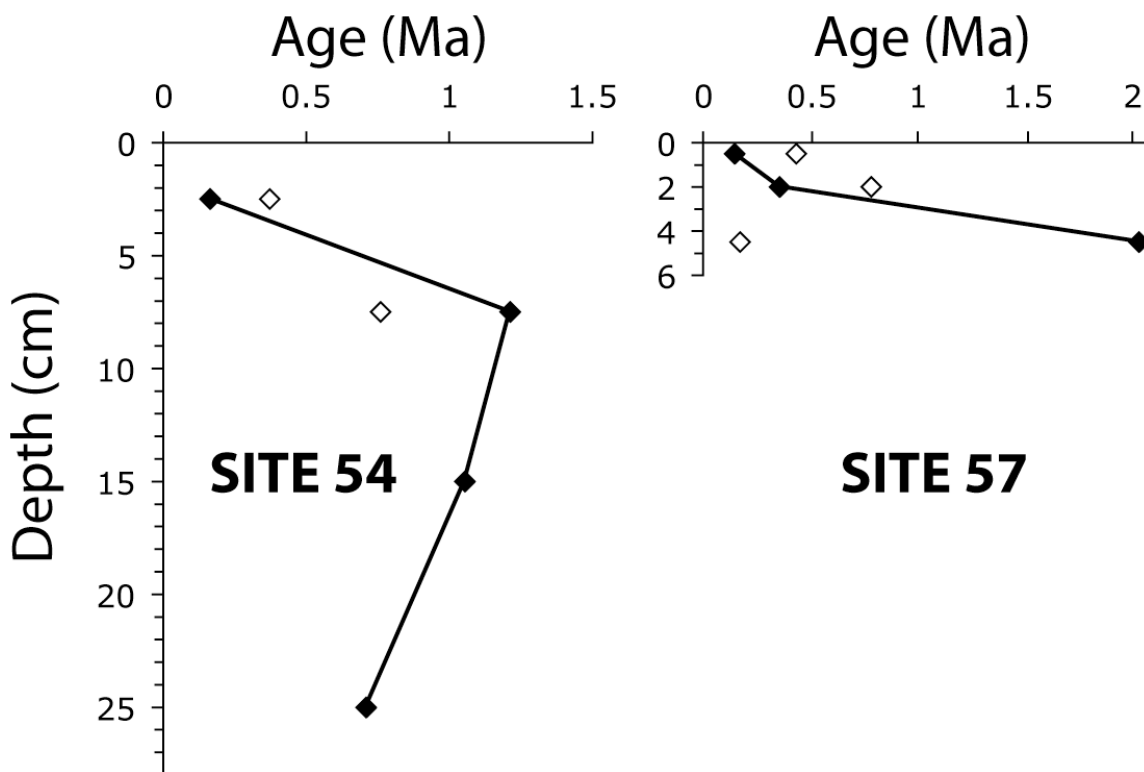


Figure 8.11 Plot of amino acid decarboxylation age dating for sites 54 (~28 cm) and 57 (~5 cm) using the kinetics associated with alanine decarboxylation to form ethylamine (◆). Single points for the ages calculated using the glycine decarboxylation to form methylamine are shown by open points (◇).

The overall composite picture of the diagenetic state of the Atacama Desert amino acid distributions with depth appear to show highly degraded organic matter in the surface soils, most likely by biological activity (Bada, 1991). These degraded amino acids are in fact younger than the soils beneath, but the small amount of shelter from the harsh surface conditions gained at shallow depths (2-3 cm) is enough to show better preservation in the subsurface materials. The deeper samples show lower D/L-enantiomer ratios (Figure 8.7, Figure 8.8) and lower mole fractions of β -alanine. Likewise, the initial increase in estimated age with sample depth over the top ~5 cm (Figure 8.11) is consistent with a typical sediment environment. At depths below this, the age difference is complicated by higher biodensities which complicate the decarboxylation dating method.

8.5 CONCLUSION

Amino acids are detected in concentrations similar to extant bacterial communities from $10^4 - 10^7$ cells/gram. The prevailing distributions are a degradation product dominated reservoir and a microbial dominated reservoir. Even the microbial amino acid biosignatures are observed coincident with large concentrations of amino acid degradation products including methylamine, ethylamine, and β -alanine, presumably derived in similar environments because of the harsh surface conditions.

The immediate surface soils from the Yungay region of the Atacama Desert consistently show only degraded levels of amino acids often with high amounts of β -alanine. However, if adequately protected or sheltered from the harsh conditions, such as under desert pavement or in subsurface locations, amino acid biosignatures can persist in these harsh conditions. This variation with microenvironment seems to be the cause of the high spatial variability in surface amino acid compositions and deserves further attention. Bacterial distributions may exist close to the surface if adequately protected in such microenvironments.

REFERENCES

- Amelung, W., and Zhang, X. (2001) Determination of amino acid enantiomers in soils. *Soil Biology & Biochemistry* 33, 553-562.
- Aubrey, A.D., Cleaves, H.J., Chalmers, J.H., Skelley, A.M., Mathies, R.A., Grunthaner, F.J., Ehrenfreund, P., and Bada, J.L. (2006) Sulfate minerals and organic compounds on Mars. *Geology* 34, 357-360.
- Bada, J.L. (1991) Amino acid cosmochemistry. *Phil. Trans. R. Soc. Lond. B* 333, 349-358.
- Banin, A. (2005) The Enigma of the Martian Soil. *Science* 309, 888-890.
- Bao, H., Jenkins, K.A., Khachatryan, M., Díaz, G.C. (2004) Different sulfate sources and their post-depositional migration in Atacama soils. *Earth and Planetary Science Letters* 224, 577-587.
- Berger, I.A., and Cooke, R.U. (1997) The Origin and Distribution of Salts on Alluvial Fans in the Atacama Desert, Northern Chile. *Earth Surface Processes and Landforms* 22, 581-600.
- Böhlke JK, Erickson, GE, and Revesz, K. (1997) Stable isotope evidence for an atmospheric origin of desert nitrate deposits in northern Chile and southern California, U.S.A. *Chemical Geology* 136, 135-152.
- Cowie, G.L., and Hedges, J.I. (1994) Biochemical indicators of diagenetic alteration in natural organic matter mixtures. *Nature* 369, 304-307.
- Dauwe, B., Middelburg, J.J., Herman, P.M.J., and Heip, C.H.R. (1999) Linking Diagenetic Alteration of Amino Acids and Bulk Organic Matter Reactivity. *Limnology and Oceanography* 44(7), 1809-1814.
- Ewing, S.A., Sutter, B., Owen, J., Nishiizumi, K., Sharp, W., Cliffs, S.S., Perry, K., Dietrich, W., McKay, C.P., and Amundson, R. (2006) A threshold in soil formation at Earth's arid-hyperarid transition. *Geochimica et Cosmochimica Acta* 70, 5293-5322.
- Ewing, S.A., Michalski, G., Thiemens, M., Quinn, R.C., Macalady, J.L., Kohl, S., Wankel, S.D., Kendall, C., McKay, C.P., and Amundson, R. (2007) Rainfall limit of the N cycle on Earth. *Global Biogeochemical Cycles* 21, GB3009.
- Glavin, D.P., Cleaves, H.J., Schubert, M., Aubrey, A., and Bada, J.L. (2004) New Method for Estimating Bacterial Cell Abundances in Natural Samples by Use of Sublimation. *Appl. Environ. Microbiol.* 70, 5923-5928.
- Hartley, A.J., and Chong, G. (2002) Late Pliocene age for the Atacama Desert: Implications for the desertification of western South America. *Geology* 30(1), 43-46.
- Hartley, A.J., Chong, G., Houston, J., and Mather, A.E. (2005) 150 million years of climatic stability: evidence from the Atacama Desert, Northern Chile. *Journal of the Geological Society of London* 162, 421-424.

Hecky, R.E.K., Mopper, K., Kilham, P., and Degens, E.T. (1973) The amino acid and sugar composition of diatom cell-walls. *Mar. Biol.* 19, 323-331.

Janssen, P.H., Yates, P.S., Grinton, B.E., Taylor, P.M., and Sait, M. (2002) Improved Culturability of Soil Bacteria and Isolation in Pure Culture of Novel Members of the Divisions Acidobacteria, Actinobacteria, Proteobacteria, and Verrucomicrobia. *Appl. Environ. Microbiol.* 68(5), 2391-2396.

Kminek, G., and Bada, J.L. (2006) The effect of ionizing radiator on the preservation of amino acids on Mars. *Earth Planetary Sci. Lett.* 245, 1-5.

Kudo, J., Kobayashi, K., Marumo, K., and Takano, Y. (2006) Fluctuation in proteinaceous labile organic matter verified with degradation rate constants of terrestrial biochemical indicators. *Organic Geochemistry* 37, 1655-1663.

Kvenvolden, K.A. (1975) Advances in the Geochemistry of Amino Acids. *Annual Review of Earth and Planetary Sciences* 3, 183-212.

Lester, E.D., Satomi, M., and Ponce, A. (2007) Microflora of extreme arid Atacama Desert soils. *Soil Biology & Biochemistry* 39, 704-708.

Li, J., and Brill, T.B. (2003) Spectroscopy of Hydrothermal Reactions, Part 26: Kinetics of Decarboxylation of Aliphatic Amino Acids and Comparison with the Rates of Racemization. *International Journal of Chemical Kinetics* 35(11), 602-610.

Maier, R.M., Drees, K.P., Neilson, J.W., Henderson, D.A., Quade, J., Betancourt, J.L., Navarro-Gonzalez, R., Rainey, F.A., McKay, C.P. (2004) Microbial life in the Atacama Desert. *Science* 306, 1289-1290.

McKay, C.P., Friedmann, E.I., Gómez-Silva, B., Cáceres-Villanueva, L., Andersen, D.T., and Landheim, R. (2003) Temperature and Moisture Conditions for Life in the Extreme Region of the Atacama Desert: Four Years of Observations Including the El Niño of 1997-1998. *Astrobiology* 3(2), 393-406.

Michalski, G., Böhlke, J.K., and Thiemens, M. (2004) Long term atmospheric deposition as the source of nitrate and other salts in the Atacama Desert, Chile: New evidence from mass-independent oxygen isotopic compositions. *Geochimica et Cosmochimica Acta* 68(20), 4023-4038.

Navarro-González, R., Rainey, F.A., Molina, P., Bagaley, D.R., Hollen, B.J., de la Rosa, J., Small, A.M., Quinn, R.C., Gunthner, F.J., Cáceres, L., Gomez-Silva, B., and McKay, C.P. (2003) Mars-Like Soils in the Atacama Desert, Chile, and the Dry Limit of Microbial Life. *Science* 302, 1018-1021.

Pedersen, A-G.U., Thomsen, T.R., Lomstein, B.A., and Jorgensen, N.O.G. (2001) Bacterial Influence on Amino Acid Enantiomerization in a Coastal Marine Sediment. *Limnology and Oceanography* 46(6), 1358-1369.

Perry, R.S., Engel, M.H., Botta, O., and Staley, J.T. (2003) Amino Acid Analyses of Desert Varnish from the Sonoran and Mojave Deserts. *Geomicrobiology Journal* 20(5), 427-438.

Pueyo, J.J., Chong, G., and Jensen, A. (2001) Neogene evaporites in desert volcanic environments: Atacama Desert, northern Chile. *Sedimentology* 48, 1411-1431.

Quinn, R.C., Zent, A.P., Grunthaner, F.J., Ehrenfreund, P., Taylor, C.L., and Garry, J.R.C. (2005) Detection and characterization of oxidizing acids in the Atacama Desert using the Mars Oxidation Instrument. *Planetary and Space Science* 53, 1376-1388.

Rech, J.A., Quade, J., and Hart, W.S. (2003) Isotopic evidence for the source of Ca and S in soil gypsum, anhydrite and calcite in the Atacama Desert, Chile. *Geochimica et Cosmochimica Acta* 67(4), 575-586.

Robbins, L.L., and Ostrom, P.H. (1995) Molecular isotopic and biochemical evidence of the origin and diagenesis of shell organic matter. *Geology* 23(4), 345-348.

Rosenfeld, J.K. (1979) Amino Acid Diagenesis and Adsorption in Nearshore Anoxic Sediments. *Limnology and Oceanography* 24(6), 1014-1021.

Skelley, A.M., Aubrey, A.D., Willis, P.A., Amashukeli, X., Ehrenfreund, P., Bada, J.L., Grunthaner, F.J., and Mathies, R.A. (2007) Organic amine biomarker detection in the Yungay region of the Atacama Desert with the Urey Instrument. *Journal of Geophysical Research* 112, G04S11.

Sutter, B., Dalton, J.B., Ewing, S.A., Amundson, R., and McKay, C.P. (2007) Terrestrial analogs for interpretation of infrared spectra from the Martian surface and subsurface: Sulfate, nitrate, carbonate, and phyllosilicate-bearing Atacama Desert soils. *Journal of Geophysical Research* 112:g4, G04S10.

Takano, Y., Horiuchi, T., Marumo, K., Nakashima, M., Urabe, T., and Kobayashi, K. (2004) Vertical distribution of amino acids and chiral ratios in deep sea hydrothermal sub-vents of the Suiyo Seamount, Izu-Bonin Arc, Pacific Ocean. *Organic Geochemistry* 35, 1105-1120.

Tsapin, A.I. (2005), Amino Acids distribution in Atacama Desert soil. De novo Amino Acid Synthesis, *Eos Trans. AGU*, 86(52), Fall Meet. Suppl., Abstract P51D-0944.

Walton, D. (1998) Degradation of intracrystalline proteins and amino acids in fossil brachiopods. *Org. Geochem.* 28(6), 389-410.

Warren-Rhodes, K., Rhodes, K.L., Pointing, S.B., Ewing, S.A., Lacap, D.C., Gómez-Silva, B., Amundson, R., Friedmann, E.I., and McKay, C.P. (2006) Hypolithic Cyanobacteria, Dry Limit of Photosynthesis, and Microbial Ecology in the Hyperarid Atacama Desert. *Microbial Ecology* 52, 389-398.

Zhao, M., and Bada, J.L. (1995) Determination of α -dialkylamino acids and their enantiomers in geological samples by high-performance liquid chromatography after derivatization with a chiral adduct of o-phthalaldehyde. *J. Chromatogr. A* 690, 55-63.

CHAPTER IX. Instrumentation to Detect Life on Mars – The *Urey* Instrument

ABSTRACT

One of the most advanced remote organic detection apparatus being considered for future missions to Mars is the *Urey* instrument suite. This instrument has been developed in collaboration with Scripps Institution of Oceanography, University of California at Berkeley, NASA Ames, and the NASA Jet Propulsion Laboratory and represents a highly advanced instrument suite for life detection (Aubrey et al., 2008). The *Urey* instrument package efficiently extracts and characterizes extremely low levels of organic compounds from the Martian regolith by utilizing efficient extraction methods and highly-sensitive quantification via micro-capillary electrophoresis channel separation and detection via laser-fluorometry. The fluorescent label used for the *Urey* instrument, fluorescamine, specifically targets primary amines and separates them via u-capillary electrophoresis (Skelley & Mathies, 2003; Skelley et al., 2005). This lab-on-a-chip design integrates very well with the *Urey* extraction apparatus and can detect amino acids, amino sugars, the nucleobases adenine and cytosine, and amino acid degradation products such as ethanolamine (from serine, ETA), methylamine (from glycine, MA) and ethylamine (from alanine, EA). These are the compounds that we are currently optimizing the extraction system around. Other temperature ramp profiles may be developed in the future to allow for optimization of any molecular class. This instrument is a lab-on-a-chip for life detection and coupled with the 2-stage extraction system, it will provide end-to-end capabilities for flight instrumentation. This extraction system shows preliminary results that it is ideal for low-level detection of biomolecules during planetary exploration and could serve as a front-end extractor for a variety of advanced instrumentation. This is evident from the testing on Atacama soil samples where evidence of life and biosignatures are often elusive (Navarro-Gonzalez et al., 2003).

Scientific characterization of the organic components of a variety of geological samples is shared using HPLC quantification of raw SCWE extracts and sublimed extracts. Some data from samples that have been run through the whole system are also shown, although this optimization of the entire extraction system is a work in progress. Recent testing on samples from the Atacama Desert, Chile, has validated the extraction system and further optimization is a

continuing work in progress. This optimization includes specific protocols for a variety of different sample mineralogies so that no matter what sample is analyzed (gypsum, clay, jarosite, etc.), a good result is assured with these different sample types. The extraction system represents an essential part of the *Urey* instrument suite which must function to deliver high-quality pure extracts to the CE in order to achieve good separation with this highly advanced analytical instrument. Scientific characterization of the organic components of these Atacama Desert samples is shared as well as the scientific ramifications of the organic levels in this Mars analog location.

9.1 INTRODUCTION - INSTRUMENTATION

The front-end extraction system of the *Urey* instrument suite consists of the subcritical water extractor (SCWE). This instrument has been developed to extract organics directly from pulverized rocks or soils and provides the first stage extraction of organic biomolecules which may be present in low levels in the Martian minerals or surface regolith. The second extraction stage, the Mars Organic Detector (MOD), utilizes sublimation to isolate and concentrate organics from the raw SCWE extract. This will eliminate any interference of salts or other impurities that could potentially compromise the analytical instrumentation and will deliver a pure organic extract to the CE for analysis. Following the extraction protocol, the *Urey* instrument can analyze extremely low levels of target molecules by fluorescence detection including amino acids, amines, amino sugars, and nucleobases (cytosine, guanine, adenine) after derivatization with fluorescamine, and naturally fluorescent PAHs.

The two extraction systems are intimately coupled and offer an efficient and comprehensive approach to sample handling. One of *Urey's* central target molecular classes are amino acids, so this study focuses primarily on characterization of this organic reservoir. Amino acids are such a ubiquitous component to terrestrial life (55% by mass as protein) and they can be detected and separated well using state-of-the-art technology. The intrinsic amino acid chirality also can unequivocally determine the origin of detected organic compounds because their distributions are so different (Kvenvolden, 1973), and they have been suggested to be prime targets for the search for extant or extinct biological life for these reasons (Bada et al, 2005). Herein the viability of the SCWE apparatus is evaluated as a front-end sample extractor for use during *in situ* mission to Mars and the coupling with the MOD sublimator is also discussed. The

system is validated using both highly included samples and extremely low-level Atacama Desert soils to show the capabilities of such a system and demonstrate its vital integration as part of the *Urey* instrument suite.

9.2 ANALYTICAL PROCEDURES

All of the SCWE extractions were performed with the identical method at NASA JPL using the bench top unit (Figure 9.1). 0.5-1.0 g of soil sample was loaded into the sample cell and sealed inline with the pump. Water at ambient temperature (20°C) was pumped into the cell and the cell and 800 psi water (~5.5 MPa) was passed through the cell for 10 sec to insure that there were no leaks or trapped air bubbles. The extraction parameters were set according to the desired conditions. The extract was collected in one 8mL fraction after the extraction conditions were reached after the desired exposure time was achieved. The 8 ml of extract was collected and shipped frozen to Scripps Institution of Oceanography. In order to flush the sample chamber between runs, the chamber was cooled down to 20°C (2.5-3 min) and the blank water cell was inserted to flush out (10 ml) any residue left from the soil sample. The samples were shipped on ice to Scripps.

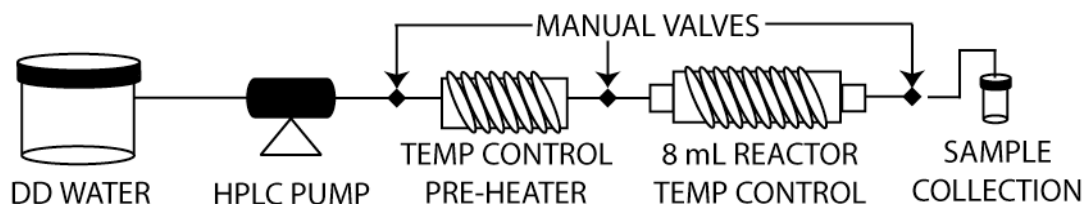


Figure 9.1 SCWE Batch-type reactor used in these extractions.

Laboratory HPLC analyses performed at Scripps Institution of Oceanography (SIO) involve pre-column derivatization with O-phthaldialdehyde/N-Acetyl L-Cysteine (OPA/NAC) according to the procedures of Zhao & Bada (1995). This reagent reacts with any primary amines, including amino acids. Following derivatization with this chiral adduct, the compounds were separated via reverse-phase HPLC and fluorescence detection using a Shimadzu RF-530 fluorescence detector (340nm excitation, 450nm emission wavelengths) and a Phenomenex Synergi Hydro-RP column (250 x 4.6 mm). These analyses allowed for the optimization of

SCWE condition and extraction efficiencies of the sub-critical water to be determined for various temperatures and extraction times.

All sublimation extractions were performed under vacuum at the approximate ambient pressure of Mars (5 torr) for at 450°C for 5 minutes or at 1100°C for 30 seconds using the laboratory sublimation apparatus (Figure 9.5). Both of these sublimation treatments have been shown to sublime amino acid standards with high efficiency. The sublimation apparatus is shown in Figure 9.5 along with the extraction protocol for sample analysis and comparison to the hydrolyzed/desalted amino acid concentrations.

9.3 SCWE INSTRUMENT

The SCWE instrument provides three main purposes during its extraction process. The first contact with the soil is provides with a low-temperature (~25°C) rinse of the soil in order to remove some of the inorganic salts which are highly soluble at low temperatures. Then after the cell is locked and sealed, it is brought up to 2000 psi (~13.8 MPa) and water is forced through the cell assembly in order to start the organic extraction. At this point, the energy provided by the SCWE instrument translates into 2 different pathways. As figure 9.2 demonstrates conceptually, the proteins from extinct or extant microbial life must first be released from the “bound” stage (Activation barrier A), then these proteins must be hydrolyzed into component amino acids (Activation barrier B) before the analysis of these fractions for organic extraction efficiency.

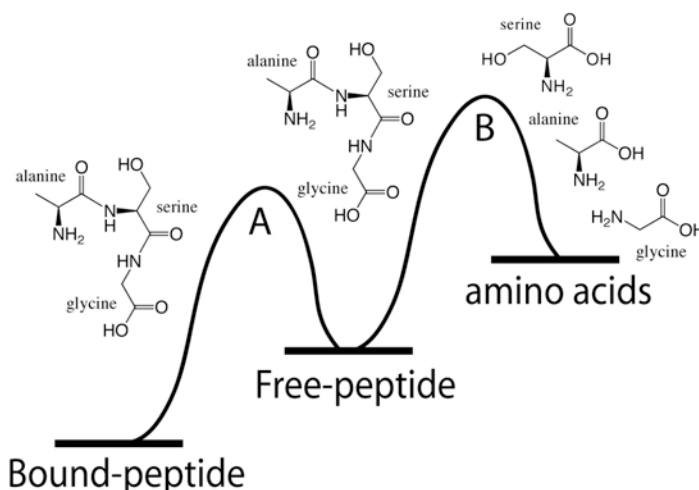


Figure 9.2 Conceptual schematic of energy associated with sub-critical water treatment of proteins: (A) the liberation of organics from the bound state and (B) the hydrolysis of peptides to Urey’s target molecules.

Although high efficiencies of both extraction and hydrolysis have been observed using the SCWE, any incomplete degree of hydrolysis will be completed during the second stage sublimation extraction which effectively hydrolyzes all proteins during the high temperature treatment.

A unique property of water is that its dielectric constant decreases with increasing temperature and pressure (Josephson, 1982), making it exhibit properties chemically similar to organic solvents under these conditions (Figure 9.2). Subcritical water has been previously demonstrated to efficiently extract organics from botanicals (Ong et al., 2006; Ibañez, 2003), fish meat (Yoshida et al., 1999), and soils (Hartonen, 1997). The advantages of subcritical water extraction include the ability to simultaneously extract a variety of organic compounds, the use of a relatively benign solvent, and the ability to extract organics quickly and efficiently.

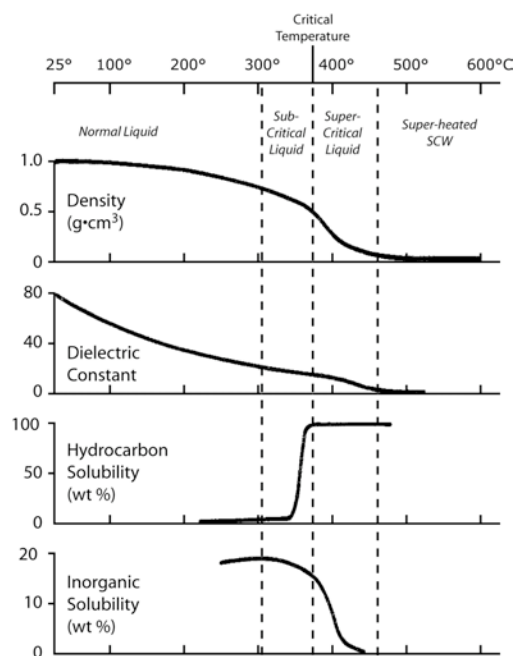


Figure 9.3 Properties of water at 200-300 bar pressure as a function of temperature (adapted from Josephson, 1982).

Extraction of organics from any soil with the SCWE becomes a simple task of passing water through a sample of Martian soil at high temperatures and pressures in order to liberate the organics from the matrix (Figure 9.3). It is of primary importance that this technique occurs

quickly enough so that the organic materials are not significantly degraded while not compromising the overall extraction efficiency. This is a primary concern because one benefit of analyzing for amino acids is that it shows not only concentration and distribution, their chirality can provide very strong evidence of biological processes. Therefore, retention of chirality through the whole extraction process is very important.

The first optimized extraction conditions were determined based on the preliminary extraction series on the South Bay gypsum at temperatures of 150, 200, and 250°C for 1, 10, 30, 60, and 180 minutes. The results are summarized in Figure 9.4. The calibration extraction runs (150° and 200°C) clearly showed that the hotter temperature provided the best efficiencies.

Based on a temperature series and extractions run on the South Bay San Diego sample, the optimized SCWE exposure was determined to be 250°C for somewhere between 1 and 10-minutes. Figure 9.4 shows the observations used to develop this optimized protocol. Although the longer SCWE treatment (10 minutes) showed higher total amino acid recoveries, the distribution was completely dominated by glycine and alanine instead of a wide distribution of amino acids, possibly showing some type of high temperature effect on the South Bay gypsum sample..

Even more important than the overall extraction efficiency is the sample chirality. The plot of D/L-ala with time and temperature shows the optimized extraction conditions with a red dot (Figure 9.4). This was chosen based on the fact that this exposure showed identical concentrations to the hydrolyzed and desalted laboratory fraction and exhibited the same distribution of amino acids. The really long sample treatments greater than 10 minutes of extraction time resulted in unusually high relative amounts of glycine and alanine for unknown reasons. This may be some kind of matrix effect or interconversion of some amino acids, for instance the increases of gly and ala can be attributed to the sharp decrease in serine these samples. Clearly if the distribution of amino acids is changing drastically, the amino acids would be highly racemized with no preservation of chirality under such conditions while the optimized 1-minute run only showed ~20% racemization.

Optimization for amino acid extraction from Atacama Desert surface soils was carried out at JPL using a temperature series between 30 and 250°C for times between 1 and 30 minutes. These data have been published and the end result for the Atacama samples was 200°C exposure for 10 minutes as optimal (Amashukeli et al., 2007). The South Bay gypsum must sequester

organics better or be more difficult to extract amino acids from because it required harsher optimized conditions (250°C for ~3 minutes) than the Atacama soils. Surprisingly, these conditions were very similar due to the fact that these samples are two fairly different media. The South Bay gypsum is a highly included coastal evaporitic deposit which showed high purity after XRD analysis. The Atacama Desert soil sample represents a mixed matrix with some small percentage of gypsum, but also heavily included with iron oxides and carbonate. More testing on a variety of mineral matrices will allow for a better understanding of the efficiencies and major controls on the organic extraction with the SCWE.

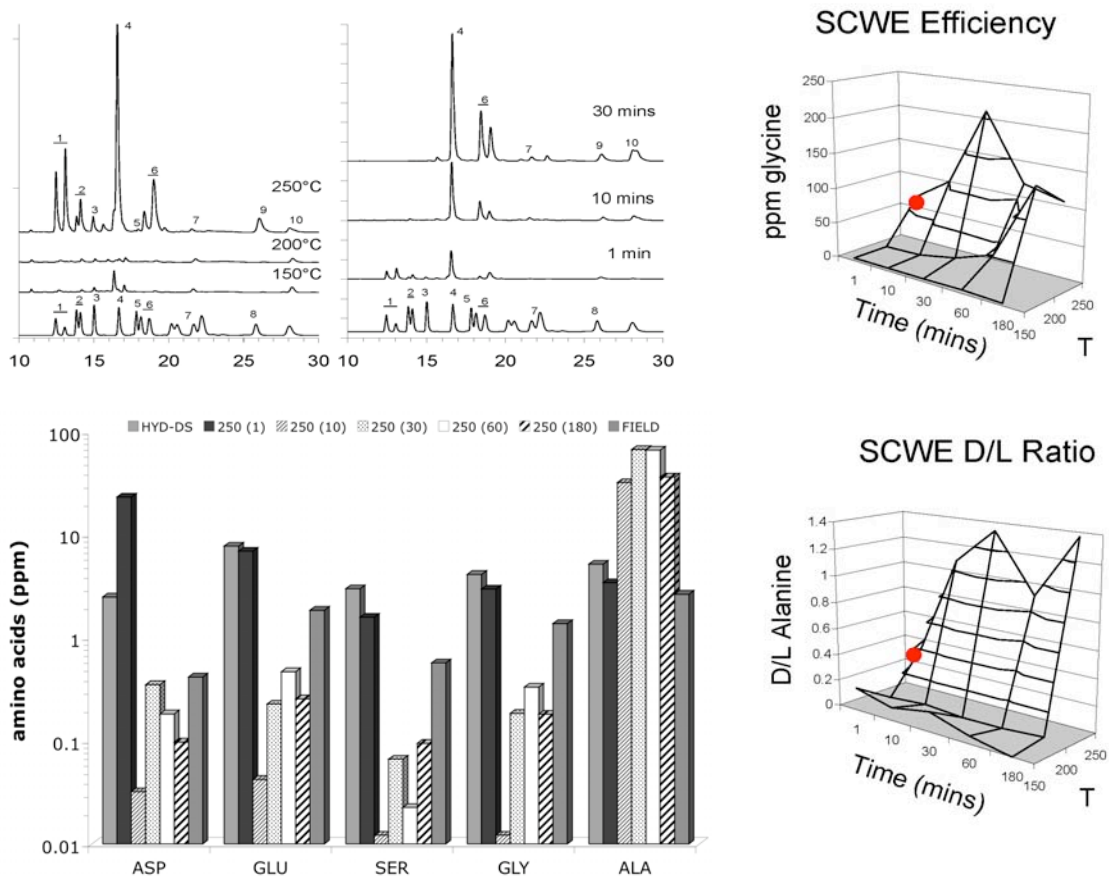


Figure 9.4 Graphical representation of the optimization of the South Bay SCWE extraction, for temperature series of 1-minute exposure and a 250°C time series. 1=D/L-aspartic acid, 2=D/L-glutamic acid, 3=D+L-serine, 4=glycine, 5=β-alanine, 6=D/L-alanine, 7=L-valine, 8=D-valine, 9=methylamine, 10=ethylamine. Below this is a plot of glycine ppm observed from each extract compared to D/L-alanine ratio. The red points show where the optimized conditions lie, 250°C for 3 minutes. The gypsum is shown at the bottom for the time series at 250°C which shows the benefit of the 1-10 minute extractions at 250°C because the distributions of amino acids are so much better while chirality is still preserve within these samples.

9.4 MOD INSTRUMENT

Although first recommended as a stand-alone sample extraction apparatus for in situ missions over a decade ago (Kminek et al., 2000), the MOD is now a secondary extraction system for Urey used to isolate and concentrate target organic compounds from a bulk water extract after freeze drying the liquid from the aliquot. Efficiencies of direct sublimation are often only around 30-50%, however it with the SCWE feed solution, the effect of catalytic degradation should be minimal.

Sublimation extraction has been shown to be an efficient method of extraction and isolation of organic compounds in many studies. The first comprehensive overview of work on the sublimation of amino acids and peptides was published by Gross & Grodsky (1955), whose work showed very high recoveries of amino acid standards by their methods. More recently, sublimation has been demonstrated to effectively isolate amino acids (Glavin & Bada, 1998), nucleobases (Glavin et al., 2002), amines (Glavin et al., 2001), and PAHs from natural samples (Kminek et al., 2000) at low pressures (~5 torr). The sublimation recovery of adenine from bacterial colonies is a method of cell enumeration (Glavin et al., 2004), and similar biodensity estimates are possible based on amino acid recoveries after sublimation. Sublimation studies have suggested to offer a method of amino acid preservation during atmospheric entry in micrometeorites (Glavin & Bada, 2001) as well as other extraterrestrial objects entering our atmosphere (Basiuk & Navarro-González, 1998).

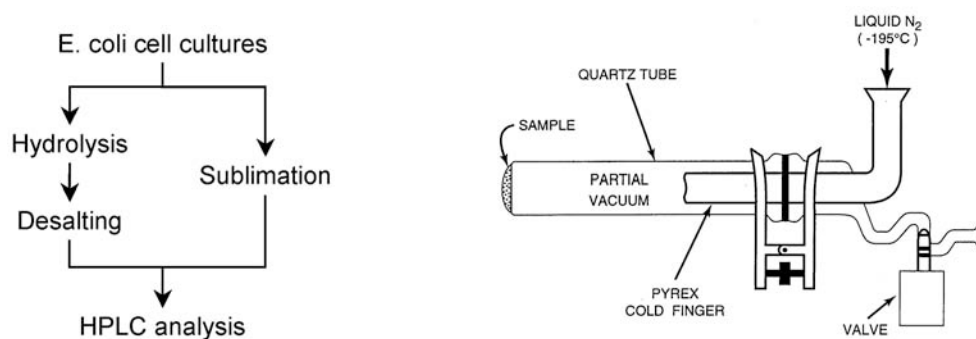


Figure 9.5 Analytical protocol and sublimation apparatus schematic (Glavin et al., 2001).

Samples inoculated with *E. coli* were used to investigate the efficiency of recovery associated with direct sublimation extraction. The cultures were prepared in the identical

methods detailed previously (Chapter 2). 0.1914 grams of *E. coli* inoculated serpentine medium ($\sim 1 \times 10^{10}$ cells/gram; Glavin et al., 2004) was sublimed for 30 seconds at 1100°C. Given these sublimation conditions, the amino acids are expected to be sublimed between 150° and 200°C during the temperature profile up to $\sim 500^\circ\text{C}$ described in detail elsewhere (Glavin & Bada, 2001). This sample was eluted from the sublimation cold finger in 1mL of ddH₂O and stored frozen until analysis. 10uL of a total of 1mL sublimate was run on the HPLC via reverse-phase liquid chromatography (RP-HPLC) according to traditional methods (Zhao & Bada, 1995). The concentrations of the sublimed *E. coli* cells were between biodensities from 10^3 - 10^7 cells/gram. These were compared to the total amino acid recoveries as a function of cell concentration.

Amino acid standards alone have been shown to sublime with very high efficiencies (Glavin et al., 2001; Glavin & Bada, 1998), however natural samples show low recoveries because of interference with the mineralogy of the samples (Glavin & Bada, 1998).

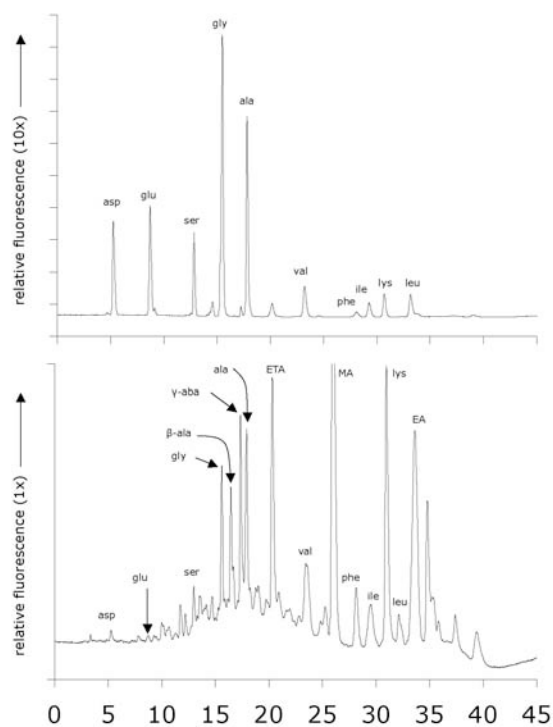


Figure 9.6 HPLC results and tabulated sublimation recoveries from sublimed *E. coli* samples (10x fluorescence exaggeration) compared to a hydrolyzed and desalted sample (each chromatogram represents $\sim 1 \times 10^{-6}$ injected cells). Recoveries only reported for 5 most abundant amino acids; peaks downfield may coelute with various amine degradation products. Recoveries for asp = 0.47%, glu = 0.60%, ser = 4.4%, gly = 6.3%, and ala = 8.6%.

The *E. coli* sublimations showed low recoveries of amino acids. The amino acid recoveries are all below 10% and the highest recovery is from alanine followed by glycine and serine. The major products included high concentrations of ethanolamine, methylamine, and ethylamine. These are the degradation products of primary amino acids present in bacterial colonies (Figure 9.7).

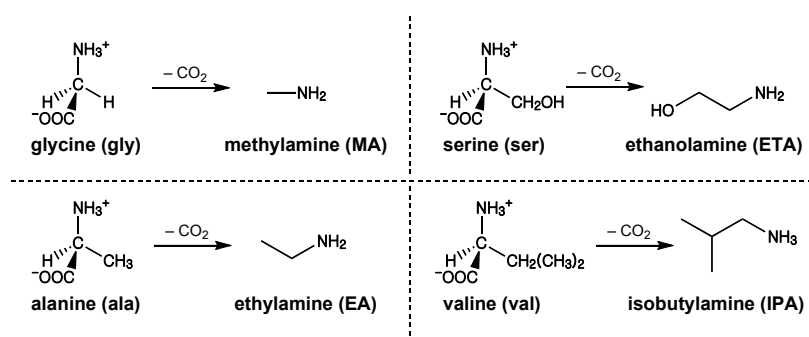


Figure 9.7 Formation of degradation products from decarboxylation of common amino acids.

It must be noted that β -alanine and γ -ABA were also detected in trace amounts, however, it is very unlikely that they were formed from direct heating of the sample. These low amino acid sublimation recoveries are very similar to previous results of similar studies of sublimed *E. coli* bacterial communities (Glavin et al., 2001) and natural samples (Glavin et al., 1998). Although amino acid standards sublime with very high efficiencies (Glavin et al., 1998), these recoveries from *E. coli* cells (on the order of <5%) show the poor yields of amino acids associated with the sublimation process. Poor recoveries have also been observed through the sublimation of natural samples. Any instrument using sublimation as its primary sample extraction method, such as the MOD, would result in a decrease in sensitivity of approximately 2 orders of magnitude (100x).

The results from the sublimation of a variety of different bacterial biodensities show similar low recoveries of amino acids. The individual and total amino acids recovered after sublimation show linear trends (Figure 9.8, A-F) plotted against biodensity represented by the sublimed analyzed aliquot on a logarithmic scale.

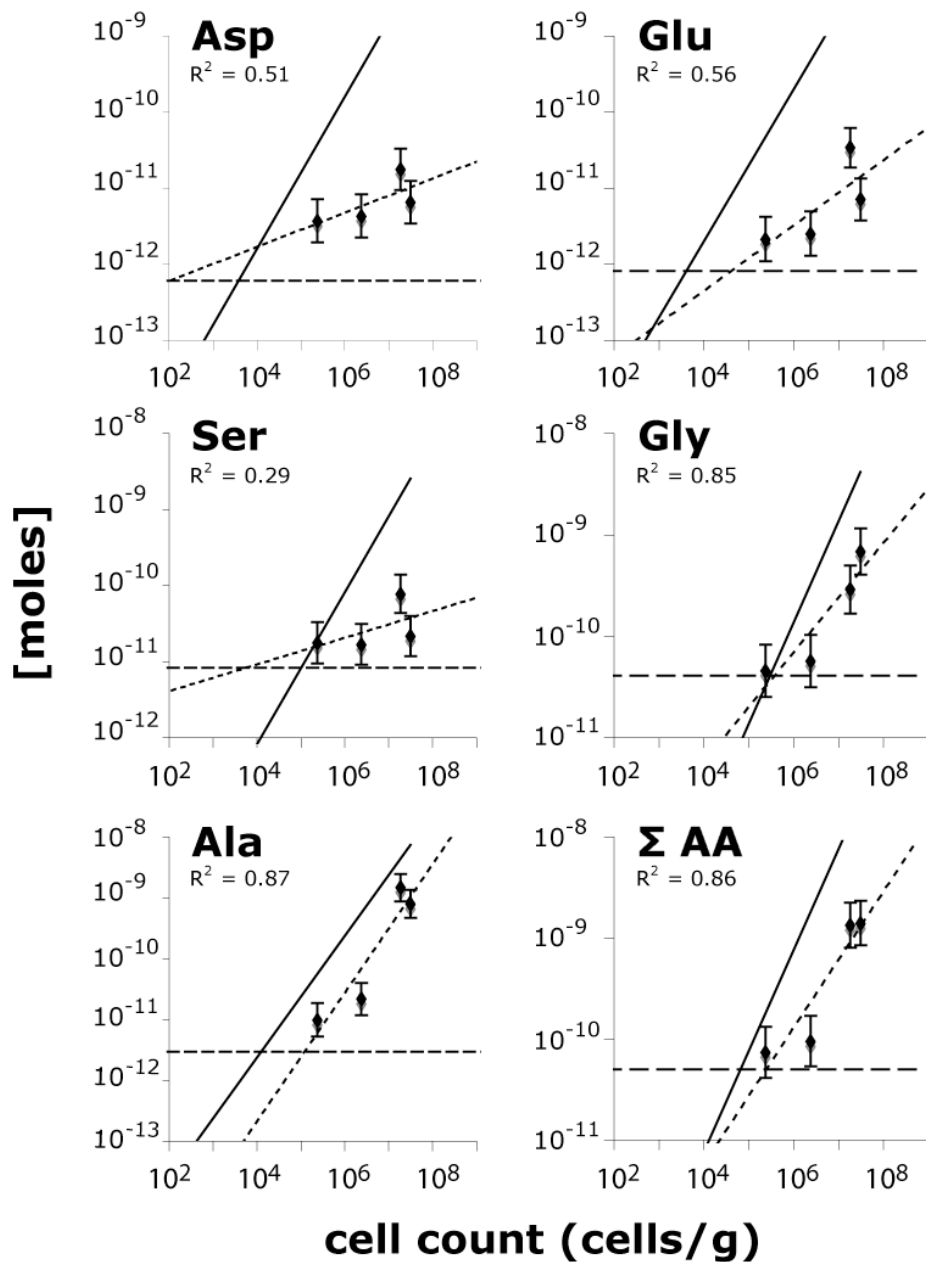


Figure 9.8 Methods of cell enumeration via sublimation (1100°C for 30 seconds) based on amino acid sublimation recoveries of (A) aspartic acid, (B) glutamic acid, (C) serine, (D) glycine, (E) alanine, and (F) total amino acids (Σ asp, glu, ser, gly, ala), (B) methylamine, and (C) ethylamine. The black lines show the expected yields from 100% sublimation recoveries. The dashed line represents the limit of detection for these methods based on background concentrations. Uncertainties were based on standard deviations of multiple standards ($\pm 5\%$). Integrations were difficult based on a skewed baseline (similar to the trace, Figure 9.6), so better separation and less interference would result in better linear correlation.

It has been mentioned before that sublimation of bacterial remnants present in natural samples also show low yields of amino acid sublimation recoveries. The variety of samples that were sublimed exhibit similar poor amino acid recoveries. Plots of sublimed natural samples compared to the traditional hydrolyzed/desalted samples analyses also show poor sublimation recoveries when sublimed directly as a solid sample

Although sublimation extraction of these samples resulted in poor yield from the extinct or extant bacterial communities due to catalyzed degradation during heating, chirality is preserved through the sublimation extraction method which makes it a viable method for the detection of terrestrial life. If the organics were purified before sublimation, this extraction method should work well to isolate organics from bacteria as has previously been suggested.

9.5 SCWE AND MOD COUPLING

The Atacama soil sample subset collected from the Atacama Desert in June of 2005 was extracted in the laboratory with the batch-type SCWE. 1 gram of each sample was extracted at a constant pressure of 2000 psi (~13.8 MPa) and 250°C for 3 minutes, the optimized conditions as determined by previous extraction experiments. The pre-heater and heater were ramped up to 250°C with the solid sample inside. After the temperature set points were reached (after approximately 1.5 minutes), the water supply valve was opened and the preheated 250°C fluid entered the reactor. The constant 2000 psi (~13.8 MPa) was achieved approximately ½ second after the fluid had entered the reactor. It was allowed to equilibrate for 3 minutes, and then the analyte valve was opened and 8mL of extract was collected in one fraction. These samples were analyzed by HPLC with OPA/NAC pre-column derivatization.

All of the Atacama Desert subset samples were analyzed for total organic carbon and nitrogen using a Costech elemental combustion C-N analyzer. Carbon and nitrogen isotopic ratios were determined with a Thermofinnigan Delta-XP Plus stable isotope ratio mass spectrometer. In order to remove any inorganic carbon (carbonate), samples were pre-treated with an excess of 3N doubly-distilled HCl before analyses for total organic carbon (TOC) and nitrogen (TON).

All of the samples from the sites that we chose to investigate with the SCWE and a sublimed fraction of this extract were analyzed for organic carbon (TOC), total organic nitrogen

(TON), and stable isotope concentrations ($\delta^{13}\text{C}$, $\delta^{15}\text{N}$). 1.25 mL of the total 8 mL of SCWE extracted liquid sample were dried down and also analyzed for TOC and TON. These results, along with the approximate percentages of TOC and TON of the acid pre-treated solid were calculated (Figure 9.9).

The recoveries look really good for the bulk organic carbon. The isotope values of these samples were all very light, and the values for the pre-treated sample set are reported in Chapter VIII and the values for the SCWE were an average of 5-10 per mille lighter than the bulk TOC.

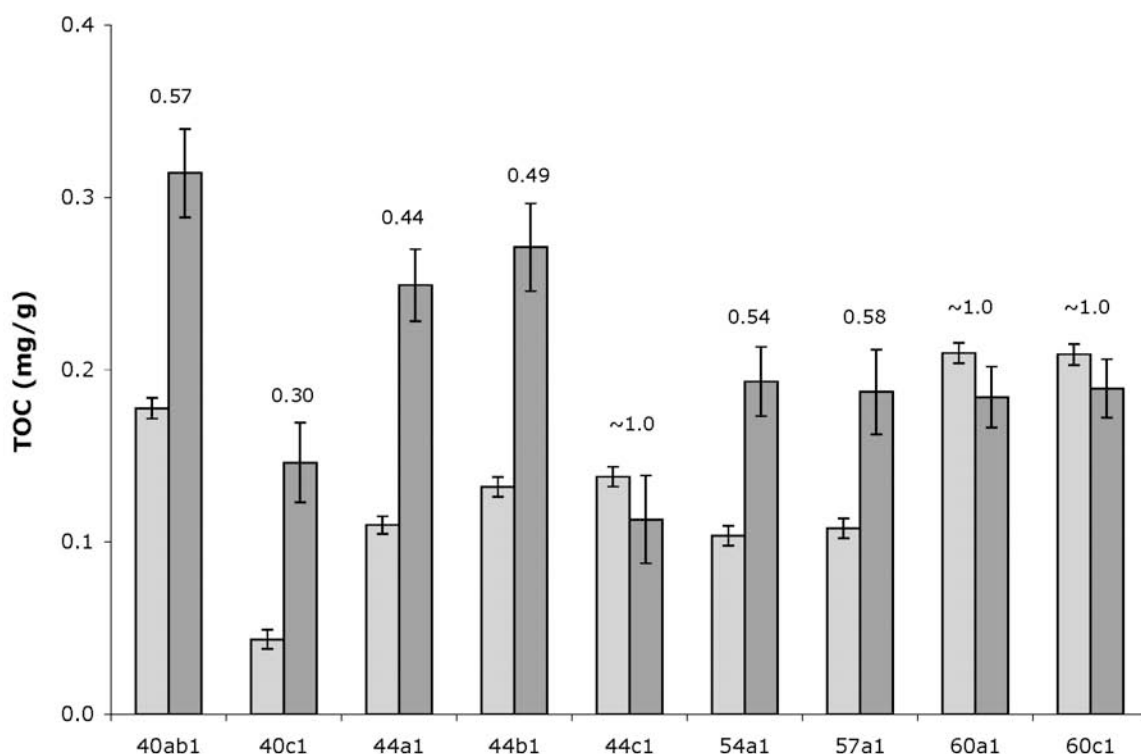


Figure 9.9 Total organic carbon (TOC) measurements of SCWE-extracted Atacama soil samples (light gray) compared to TOC in the acid-treated solid samples (dark gray) with percent comparisons above samples.

The investigation of the *Urey* sample extraction system on amino acids was tested using the SCWE-extracts from the Atacama Desert samples which have been previously characterized for total organic carbon, total nitrogen, and amino acid concentrations (Figure 9.9, TOC; Chapter VIII). Three samples were first extracted with the sub-critical water extractor (SCWE) and 4mL of a total of 8mL extract (1/2 the total SCWE extract) was sublimed after stripping the water from

the samples via freeze drying. These dried residue samples were sublimed at 450°C for 5 minutes. They were removed from the cold finger with 1mL of ddH₂O and 100uL aliquots (1/10th) were analyzed by RP-HPLC.

Table 9.1 Amino acid concentrations (ppb) determined by reverse-phase HPLC analyses of laboratory SCWE extracted Atacama soil samples. * = enantiomers detected and quantified.

Sample	Asp*	Glu*	Ser*	Gly	β-Ala	γ-ABA	Ala*	ΣAA
40AB1	252	49.1	194	308	1.31	10.8	29.6	844
40A2	257	53.6	171	268	2.65	16.2	148	915
40C1	ND	ND	<1	105	ND	8.22	66.2	180
44A1	52.0	8.32	18.0	59.9	13.4	8.71	78.9	239
44B1	134	11.2	20.1	104	21.8	19.3	125	435
57A1	63.7	8.56	15.3	39.1	4.39	2.06	53.2	186

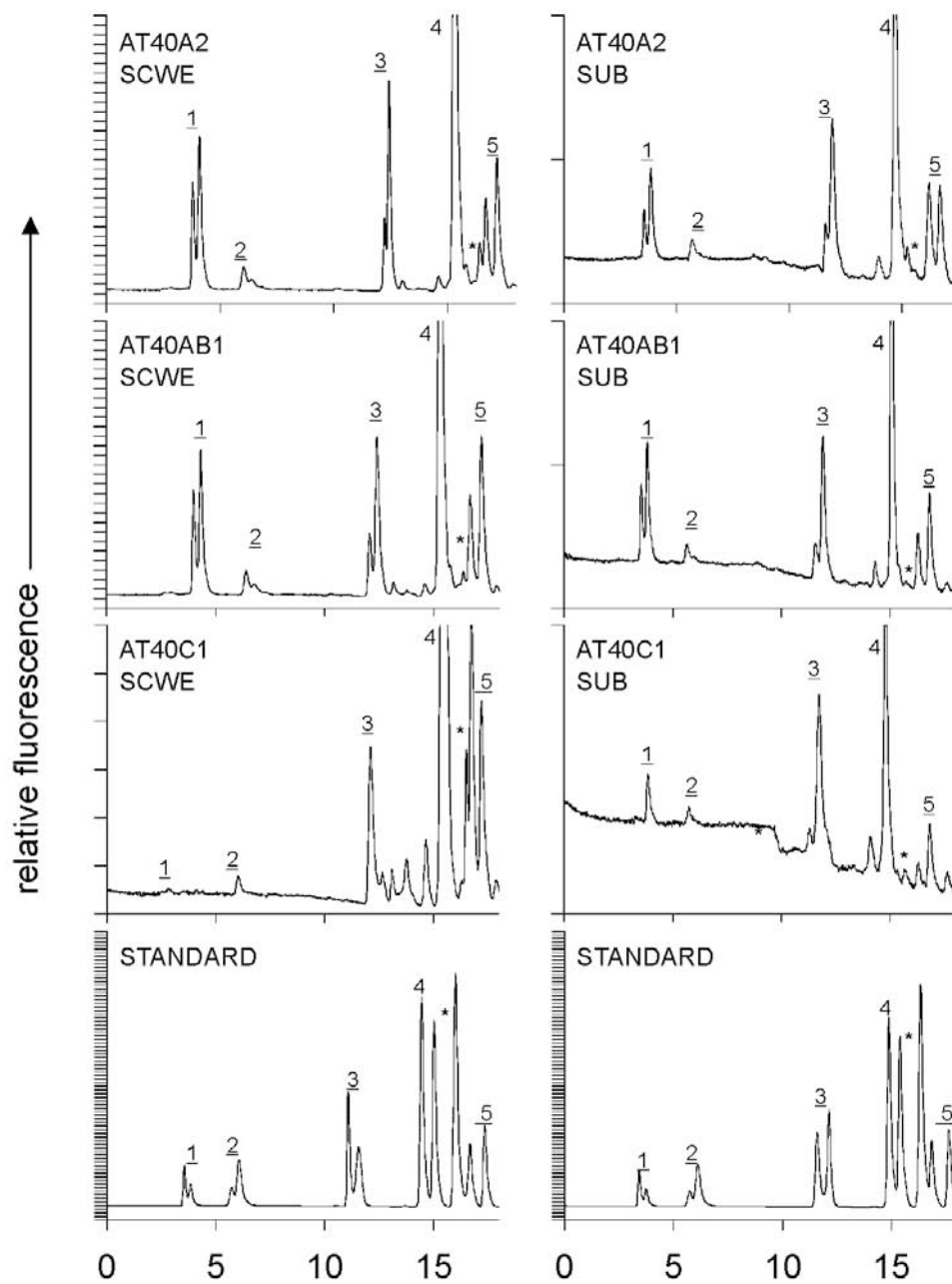
Table 9.2 Amino acid D/L ratios determined by reverse-phase HPLC analyses of laboratory SCWE extracted Atacama soil samples.

	D/L-Asp	D/L-Glu	D/L-Ser	D/L-Ala
40AB1	0.67	0.053	0.16	0.35
40A2	0.64	0.19	0.079	0.63
40C1	NA	NA	NA	>1
44A1	0.63	0.059	0.12	0.59
44B1	0.77	0.094	0.22	0.79
57A1	0.61	0.057	0.17	0.96

The amino acid distribution looks similar from one site to the next. The positive sample sites yield surprisingly high amino acid levels ranging from low to mid-ppb levels. These levels of amino acids correspond to cell counts in the range of 10⁴-10⁵ cells per gram assuming an average cellular mass of 20fg, 55% protein content by mass, and that the quantified amino acids account for 75% of the total amino acids.

The sublimed fraction HPLC analyses are shown in Figure 9.10 compared to the traces reported in Table 9.1 and enantiomeric excesses in Table 9.2. The peaks are all detectable and show decent separation for these low level samples. The percent recoveries are reported at the bottom of Figure 9.10 for asp, glu, ser, gly, and ala. These recoveries are all slightly higher than the solid *E. coli* sublimation, however this isn't a good comparison because the *E. coli* is extant life while the Atacama bulk organic matter is likely more degraded. The best comparison would be a sublimed solid soil sample from the Atacama Desert. There were never any defined peaks in

the directly sublimed Atacama samples from the Yungay area, where these are located, especially not in this type of wide distribution with clear peaks for aspartic acid (one of the more unstable amino acids) and consistent recoveries for all of the amino acids (all around 5%). So the statement could be made that we see the direct effects of the SCWE pre-extraction in terms of overall recovery of amino acids and better distribution of these recoveries. The total recoveries for the surface SCWE-sublimed sample (AT40AB1) and the subsurface SCWE-sublimed sample (AT40A2) are equal to 4.4 and 5.2, indicating that the subsurface sample might show a slightly better recovery, but more than that, it shows consistency in the replicate data. Sample AT40C1 was not quantified because the peaks were so small. The D/L ratios were difficult to accurately calculate for these low level samples, especially for the sublimed SCWE fraction. Clearly aspartic acid (1) and glutamic acid (2) show retention of chirality during sublimation while alanine looks to be highly racemized in both the SCWE direct analysis and the SCWE-sublimed analysis. This tentatively demonstrates that the Urey extraction system as a whole is demonstrated to preserve chirality.



RECOVERY	Asp (1)	Glu (2)	Ser (3)	Gly (4)	Ala (5)
AT40A2	3.4 %	5.1 %	7.5 %	4.0 %	6.2 %
AT40AB1	4.6 %	4.7 %	5.4 %	3.9 %	3.6 %

Figure 9.10 HPLC chromatograms from sublimed SCWE Atacama Desert extracts from subsurface sample AT40A2 and surface samples AT40AB1 and AT40C1 compared to direct HPLC analysis of the fractions before sublimation. 1=D/L-aspartic acid, 2=L/D-glutamic acid, 3=D/L-serine, 4=glycine, *=β-alanine/γ-aminobutyric acid, 5=D/L-alanine. Y-axis graduations represent 0.5 fluorescence units.

9.6 DISCUSSION AND EVALUATION OF RESULTS

The largest problem with sublimation is the inherent degradation associated with treatment of natural samples at the high temperatures (>150°C) necessary for amino acid sublimation, although pure standards offer very high recoveries (Glavin et al., 2001). The coupling of the sub-critical water extraction (SCWE) with the MOD will allow for the most efficient extraction of target organics from the Mars regolith.

Coupled with SCWE extraction, the degradation of amino acids to amines during sublimation is minimized although any amino acid decarboxylation products will also be detected by Urey. Pure amino acid standards have always been observed to yield from 90-99% recoveries (Glavin & Bada, 1998) while direct sublimation shows recoveries often less than these reported in Figure 9.10, or approximately the same levels but without as good of distribution of all the amino acids (Figure 9.8; Figure 9.6). The poor recoveries are mainly attributed to the presence of divalent cations during sublimation that causes increased degradation during the 150-200°C exposure for under 5 minutes (Glavin & Bada, 1998). It is difficult to determine whether these samples are showing any effect of the SCWE extraction before sublimation unless the identical sample were sublimed as a solid in comparison. However, the pre-extraction using the SCWE instrument will undoubtedly allow for a purified extract to be sublimed. This should show more of an effect on recoveries with a little more tweaking of the instrument. After all, the salt pre-rinse will allow for at least a fraction of the interfering compounds to be removed. The SCWE will eventually be optimized for the salt pre-rinse (which is not part of the current protocol) for a more purified water extract will definitely show better efficiencies of sublimations and if an organic extract is delivered to MOD with very low backgrounds of salts, the recoveries should approach those of amino acid standards (>90%).

The SCWE method also shows promising results for the extraction of total organic carbon from Atacama soil samples with an average recovery of greater than 50% and maximum recoveries of around 100% (Figure 9.9). This shows that Urey is truly accessing the bulk organic carbon which shows extremely light stable carbon isotopes (<-25 per mille) which is important at this stage before the runs are optimized on a molecular class level.

9.7 CONCLUSION

Sublimation alone does not result in adequate amino acid recoveries from natural samples (~5-10 % total recovery). The interaction of the organics with the mineral matrix results in enhanced degradation of amino acids and the formation of large amounts of ammonia and the decarboxylation products methylamine and ethylamine. Despite this amino acid degradation associated with the sublimation of natural samples, the best sublimation efficiencies occurred with glycine and alanine in all sample matrices. In order to decrease the amount of degradation associated with natural sample sublimation, it is necessary to extract the organic fraction with high-pressure, high-temperature water (Yoshida et al., 1999). Sublimation of the dried SCWE liquid fraction results show similar overall recoveries (5-10%), but show the benefits of a cleaner baseline and better overall recoveries of all of the target amino acids.

It should be possible to optimize the SCWE to extract salts with a low-temperature rinse of the natural sample followed by the extraction of bound organics with a higher temperature rinse. This will result in recoveries >90%, similar to those reported in previous studies for pure standards (Glavin & Bada, 1998). The optimization of the two sample extraction instruments is essential for the success of Urey in detecting life on Mars in future missions and should be further examined as functions of SCWE and MOD temperature treatment protocols and sample mineralogy.

SCWE extraction represents a relatively new method of liberating organics from bulk soils and minerals (Skelley et al., 2007; Amashukeli et al., 2007). This method takes advantage of the optimal properties of water to dissolve organics at elevated temperatures and pressures and should be considered to be a prime extraction method for analytical organic geochemistry. The fact that this method is relatively fast in liberating amino acids and hydrolyzing intact proteins while minimizing degradation and racemization makes it a prime candidate for pre-processing of Martian soil samples on future missions to Mars.

The *Urey* instrument suite includes an SCWE sample extractor with the capabilities to operate over wide temperature and pressure ranges. We have demonstrated that sub-critical water exposure at 250°C for 3 minutes will free bound bulk organics (TOC, TON) and liberate amino acids from Atacama near-surface soils at approximately 50% efficiency. Further optimization of the SCWE treatment conditions might bring the extraction fraction to unity. Different molecular compound classes should be liberated from a soil or mineral media at different optimized

temperatures. Therefore, future development of the SCWE conditions will result in a temperature ramp protocol that results in various sequential fractions containing different compounds. This is currently being developed specific to each type of mineralogy (e.g. gypsum, anhydrite, jarosite, bulk soil).

ACKNOWLEDGEMENTS

This paper includes collaborative efforts between Scripps Institution of Oceanography, University of California at Berkeley, and the NASA Jet Propulsion laboratory. Credit is given to the Urey team members, especially our P.I. Jeffrey L. Bada, and the following people: Alison M. Skelley and Richard Mathies, Peter Willis and Frank J. Grunthaner and Xenia Amashukeli. We would like to thank JPL and ESA for their support and endorsement of the *Urey* instrument concept and NASA for their continuous support.

REFERENCES

- Amashukeli, X., Pelletier, C.C., Kirby, J.P., and Grunthaner, F.J. (2007) Subcritical water extraction of amino acids from Atacama Desert soils. *J. Geophys. Res* 112, G04S16.
- Aubrey, A.D., Chalmers, J.H., Bada, J.L., et al. (2008) The Urey Instrument: An Advanced in situ Organic and Oxidant Detector. *Astrobiology*, in press.
- Bada, J.L., Sephton, M.A., Ehrenfreund, P., Mathies, R.A., Skelley, A.M., Grunthaner, F.J., Zent, A.P., Quinn, R.C., Josset, J.L., Robert, F., Botta, O., Glavin, D.P. (2005) *Astronomy and Geophysics* 46 (6), 6.26-6.27.
- Basiuk, V.A., and Navarro-González, R. (1998) Pyrolytic Behavior of Amino Acids and Nucleic Acid Bases: Implications for Their Survival during Extraterrestrial Delivery. *Icarus* 134, 269-278.
- Glavin, D.P., and Bada, J.L. (1998) Isolation of Amino Acids from Natural Samples Using Sublimation. *Anal. Chem.* 70, 3119-3122.
- Glavin, D.P., Schubert, M., and Bada, J.L. (2002) Direct Isolation of Purines and Pyrimidines from Nucleic Acids Using Sublimation. *Anal. Chem.* 74(24), 6408-6412.
- Glavin, D.P., and Bada, J.L. (2001) Survival of amino acids in micrometeorites during atmospheric entry. *Astrobiology* 1(3), 259-269.
- Glavin, D.P., Cleaves, H.J., Schubert, M., Aubrey, A., and Bada, J.L. (2004) New Method for Estimating Bacterial Cell Abundances in Natural Samples by Use of Sublimation. *Applied Environmental Microbiology* 70, 5923-5928.
- Glavin, D.P., Schubert, M., Botta, O., Kminek, G., and Bada, J.L. (2001) Detecting pyrolysis products from bacteria on Mars. *Earth Planet. Sci. Lett.* 185, 1-5.
- Gross, D., and Grodsky, C. (1955) On the Sublimation of Amino Acids and Peptides. *Journal of the American Chemical Society* 77(6), 1678-1680.
- Hartonen, K., Inkala, K., Kangas, M., and Riekkola, M.L. (1997) Extraction of polychlorinated biphenyls with water under subcritical conditions. *J. Chromatogr. A* 785(1-2), 219-226.
- Ibañez, E., Kubátová, A., Señoráns, F.J., Cavero, S., Reglero, G., and Hawthorne, S.B. (2003) Subcritical water extraction of antioxidant compounds from rosemary plants. *J. Agric. Food Chem.* 51(2), 375-382.
- Josephson, J. (1982) Supercritical fluids. *Environ. Sci. Technol.* 16, 548A-551A.
- Kminek, G., Bada, J.L., Botta, O., Glavin, D.P., and Grunthaner, F.J. (2000) MOD: An Organic Detector for the Future Robotic Exploration of Mars. *Planet. Space Sci.* 48(11), 1087-1091.
- Kvenvolden, K.A. (1973) Criterion for Distinguishing Biogenic and Abiogenic Amino Acids – Preliminary Considerations. *Space Life Sciences* 4, 60-68.

Navarro-González, R., Rainey, F.A., Molina, P., Bagaley, D.R., Hollen, B.J., de la Rosa, J., Small, A.M., Quinn, R.C., Gunthner, F.J., Cáceres, L., Gomez-Silva, B., and McKay, C.P. (2003) Mars-Like Soils in the Atacama Desert, Chile, and the Dry Limit of Microbial Life. *Science* 302, 1018-1021.

Ong, E.S., Cheong, J.S.H., and Goh, D. (2006) Pressurized hot water extraction of bioactive or marker compounds in botanicals and medicinal plant materials. *J. Chromatogr. A* 1112(1-2), 92-102.

Skelley, AM, and Mathies, RA (2003) Chiral separation of fluorescamine-labeled amino acids using microfabricated capillary electrophoresis devices for extraterrestrial exploration. *Journal of Chromatography A* 1021 (1-2):191-9.

Skelley, AM, Scherer, JR, Aubrey, AD, Grover, WH, Isvester, RHC, Ehrenfreund, P., Grunthner, FG, Bada, JL, and Mathies, RA (2005) Development and evaluation of a microdevice for amino acid biomarker detection and analysis on Mars. *Proceedings of the National Academy of Sciences of the United States of America* 102, p1041-1046.

Skelley, A.M., Aubrey, A.D., Willis, P.A., Amashukeli, X., Ehrenfreund, P., Bada, J.L., Grunthner, F.J., and Mathies, R.A. (2007) Biomarker Detection in the Yungay Region of the Atacama Desert with the Urey Instrument. *J. Geophys. Res.* 112, G04S11.

Yoshida, H., Terashima, M., and Takahashi, Y. (1999) Production of Organic Acids and Amino Acids from Fish Meat by Sub-Critical Water Hydrolysis. *Biotechnol. Prog.* 15, 1090–1094.

Zhao, M., and Bada, J.L. (1995) Determination of α -dialkylamino acids and their enantiomers in geological samples by high-performance liquid chromatography after derivatization with a chiral adduct of o-phthalaldehyde: *Journal of Chromatography A*, v. 690, p. 55-63.

CHAPTER X. The Future Search for Evidence of Extinct or Extant Life on Mars

ABSTRACT

In May 2008, the NASA Phoenix lander will begin to return data from the polar regions of Mars and add to our knowledge of these unique regions of the planet. Then, a couple of years later, the next generation of NASA's Mars Exploration Rovers, the Mars Science Laboratory (MSL), will have landed on the planet and will be exploring the surface conducting *in situ* geochemical investigations. The European Space Agency (ESA) is going to contribute to this golden age of Martian exploration with their own rover, ExoMars, which is set to launch in 2013. These future *in situ* investigations include advanced capabilities to look for not only evidence of water, but also evidence of carbon and biomolecules (Des Marais et al., 2003). The success of these endeavors relies heavily upon utilizing the most advanced instrumentation, the search for appropriate biomolecules that will unequivocally determine if life is present, and the expertise to know where to look for these biomolecules. One of these such instruments, the *Urey* Mars Organic Detector, is a central portion of the life-detection payload instrument package that focuses on the detection of evidence of extinct or extant life on Mars. The studies conducted in the preceding chapters have demonstrated a variety of factors which must be considered when evaluating targets for biomolecule detection including the strong dependence on organic preservation as a function of the sample's host mineralogy, exposure (depth), and thermal history. Using these stability criteria to evaluate targets for life detection will allow for the best chances at detecting evidence of life on Mars.

10.1 MARTIAN EXPLORATION

Remote sensing data gathered by orbiting spacecraft have vastly increased our geological and geochemical knowledge of the planet on broad and specific resolutions. The most recent of these spacecraft, the Mars reconnaissance orbiter (MRO), has allowed for detailed mapping of elevation (HiRISE, High Resolution Imaging Science Experiment), subsurface water abundance (SHARAD, Shallow Radar), and mineralogy (CRISM, Compact Reconnaissance Imaging Spectrometer for Mars). There are no specific life detection experiments that can be flown on an orbiter, although the mineralogy and water abundance can provide valuable data to help

determine where extant life may persist and where biomolecular evidence of extinct life may be well preserved.

The Mars exploration rovers (MER) have provided invaluable geological, geochemical, and visual data on two specific regions of Mars, Opportunity's landing site, Meridiani Planum, and Spirit's landing site in Gusev Crater. These areas show two distinctly different geological histories of Mars while Meridiani Planum shows visual and geochemical evidence of past standing bodies of water (Squyres et al., 2004). The Phoenix Scout mission is another current mission to Mars (launched 8/2007, arrival 5/2008) that is geared towards studying another distinctly different region, the polar regions, and assessing the presence of liquid water and the concentrations of carbon in these regions. The thermal and evolved gas analyzer (TEGA) has the capabilities to measure concentrations and isotopic abundances of hydrogen, oxygen, carbon, and nitrogen. These data may show evidence of biological fractionation, especially if depleted bulk isotopic compositions are detected. However, even this would not definitively prove the existence of extinct or extant life on Mars, as there are no specific biomolecular targets in this experiment.

The next Mars mission to launch is the Mars Science Laboratory (MSL) which is scheduled to launch near the end of 2009. Based widely on recent MRO results, including the detection of sulfates and phyllosilicate-rich areas by CRISM, a recent consensus among scientific experts have narrowed the landing sites for the 2009 Mars Science Laboratory down to six potential locations (Morton, 2007). The engineering and scientific packages on MSL represents the latest in technology and offers many benefits over the twin MER rovers. The increased scientific capabilities of the MSL instrument payload allow for the remote determine of soil and rock compositions (ChemCam, Laser-Induced Remote Sensing for Chemistry and Micro-Imaging), mineral identification by powder X-ray diffraction (CheMin, Chemistry & Mineralogy X-Ray Diffraction), and the ability to detect biomolecules via gas chromatography-mass spectrometry (GCMS) and spectrometry methods (SAM, Sample Analysis at Mars Instrument Suite). MSL includes capabilities to specifically addresses the question of habitability and looking for extant or extinct life using the SAM instrument suite. The capabilities of SAM include the ability to detect hydrocarbons, including methane, amino acids, and other important biomolecules which may show evidence of life. The major drawback of these methods are that

trace levels of preserved biomolecules from an extinct biota or extremely low levels of extant microbial life ($<10^5$ cells/gram) may not be detectable by GCMS methods.

Successful technology flown aboard the MER rovers that are included in the MSL configuration are the alpha particle X-ray spectrometer (APXS) for the determination of elemental abundances and similar optical technology as the MER rovers including a mast camera (MastCam), Mars hand lens imager (MAHLI), and a decent imager (MARDI). MSL Sample handling capabilities include the ability to drill into surface rocks in order to sample at depth (~6 inches).

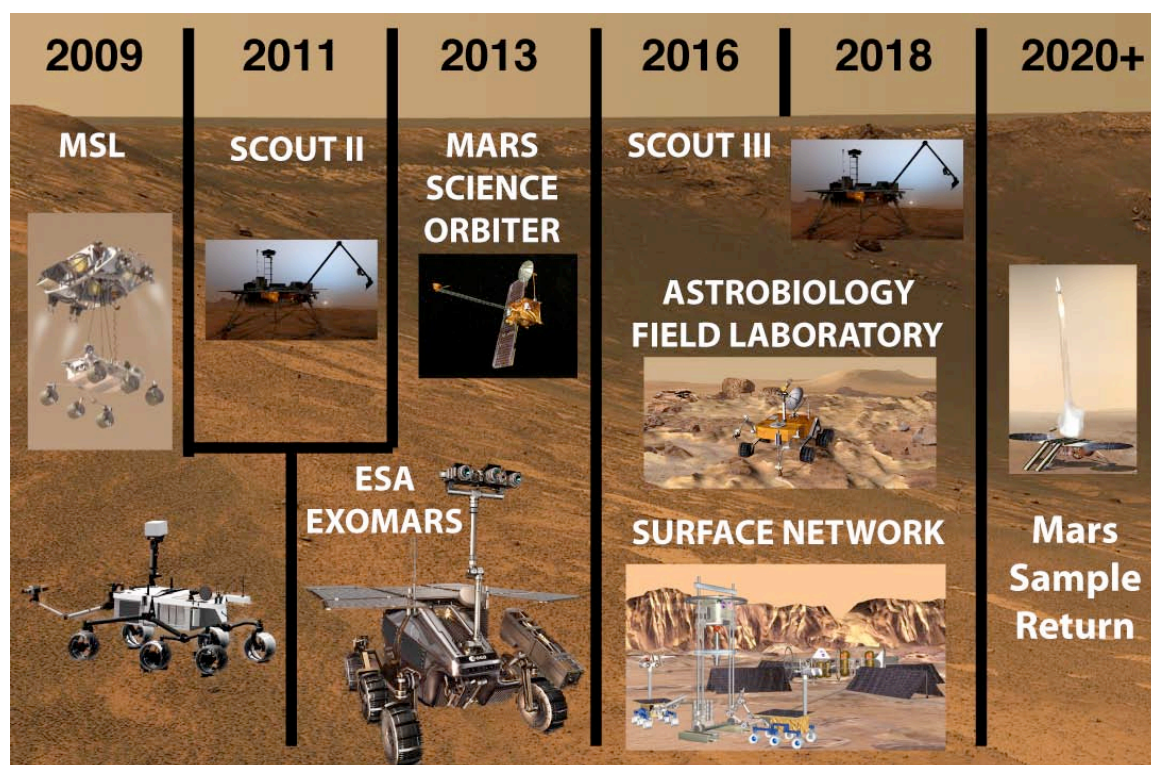


Figure 10.1 Near-future planned missions to Mars (modified from Beegle et al., 2007).

Improvements in instrumentation technology continue to expand the capabilities of robotic exploration of the Martian surface. Future missions to Mars (Figure 10.1) will include the Astrobiology Field Laboratory (AFL) and eventual sample return missions, although the high cost associated with these types of missions make it a problem to address in the next generation of Mars exploration.

Most Mars analog studies to date have specifically focused on the surface analogs to Mars because these are the most accessible regions for *in situ* studies. As technology increases over the next decades, the accessible areas for *in situ* robotic studies will include more remote areas in Mars' subsurface. These advanced methods may lead to the detection of extant microbial communities sheltered from the harsh surface environments, similar to communities detected terrestrially (Chapter 6).

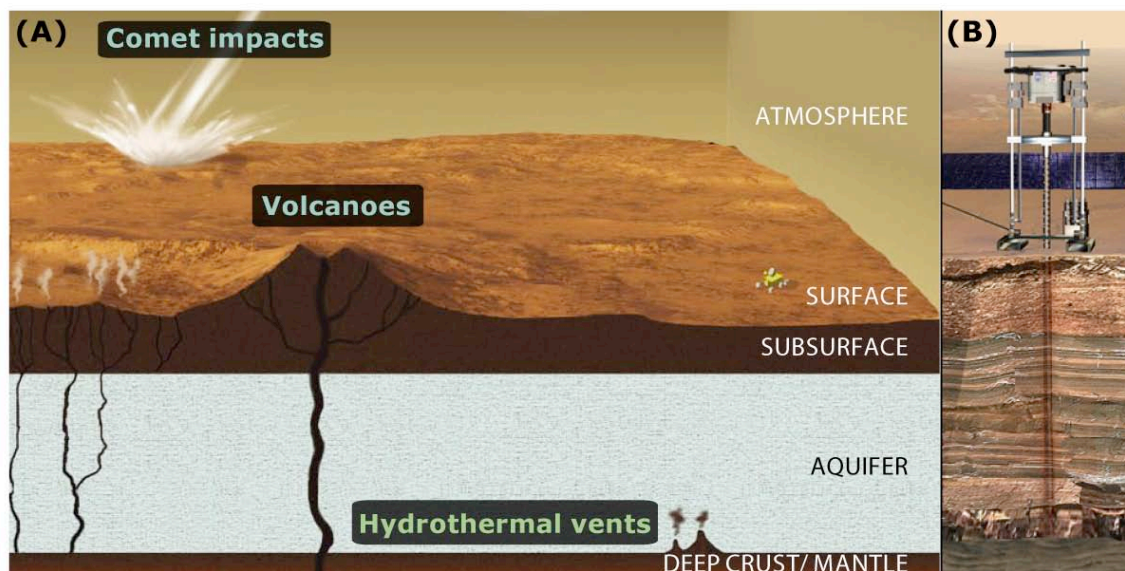


Figure 10.2 Artist rendition of a cross-section of Mars showing active processes that have persisted over the majority of the planet's history (A; modified from Atreya, 2007). The stability zone of water in the Martian subsurface is estimated to be from 2-10 km deep but as shallow as a few hundred meters depth (Malin & Edgett, 2000). Systematic investigations of other pertinent analog environments that will become pertinent during future studies *via* advanced techniques such as subsurface drilling (B; image from NASA).

Urey has been selected as part of the Pasteur payload for the European Space Agency's (ESA) ExoMars rover mission in 2013 (Aubrey et al., 2008). This instrument suite represents the most sensitive analytical approach to finding evidence of extinct or extant life on Mars. Urey's target biomolecules comprise molecular classes that compose greater than 80% of the mass of cellular life (Table 10.1). Urey also offers state-of-the-art detection limits, at parts-per-trillion sensitivity (ppt) for many of these biomolecular classes. The detection limits for bacterial communities have been estimated $\sim 10^3$ cells per gram, which is a factor of 100-1000 times more sensitive than GCMS instruments. *Urey* has the capabilities to examine these specific classes of target biomolecules and discriminate between abiotic and biological amino acids based on the

chirality of these compounds, which is key in determining the source of these amino acids which could be biological life or meteoritic influx.

Table 10.1 List of *Urey* target compounds and mass percentages of *E. coli* cell.

Compound Class	Occurrence	Mass percent ¹
amino acids ²	proteins, peptidoglycan	62.7 %
nucleobases ³	RNA, DNA	19.7 %
ethanolamine	lipids, lipopolysaccharides	0.7 %
amino sugars	lipopolysaccharides	0.3 %
diamines	putrescine, spermidine, peptidoglycan	0.9 %

NOTE: Only primary amines are labeled by fluorescamine. Quantification of compounds possible after complete hydrolysis (e.g. nucleic acids, proteins, lipids)
¹dry weight basis (Neidhardt & Umbarger, 1996)
²amino acid chirality also measured by *Urey*.
³adenine, cytosine, and guanine quantified by *Urey*.

The 2013 ExoMars mission includes capabilities to sample within the Martian regolith (~2 m) instead of just within the immediate subsurface (cm) of rocks as MSL is currently equipped to do. The danger of looking for biomolecules within the surface regolith is that galactic cosmic radiation may have destroyed these compounds in the near-surface (Kminek & Bada, 2006) and converted them to other abiological carbon compounds through diagenetic pathways (Benner et al., 2000). Although some of these possible diagenetic products produced from long-term decomposition of biologically derived organic compounds, PAHs, are targeted by *Urey*, the absence of amino acids would be detrimental to the life detection experiments. The chirality determination allows for the unequivocal determination of evidence of extinct or extant life as biological processes would most likely result in an overwhelming abundance of either the D- or L-enantiomer. Therefore, the ability of ExoMars to sample deep within the regolith offers a much greater chance of success in detecting a wide variety of *Urey*'s target organic compounds and resolving amino acid chirality in these experiments.

During the upcoming generations of in situ rover missions to Mars, the issue of where to look for well-preserved biomolecules is just as important as the advanced instrumentation that is flown there. The success of future life detection studies flown aboard the MSL (2009), ExoMars (2013), and the AFL (2018) should have specific geological targets in mind before the analyses even begin. Because the surface of Mars is so hostile, it is necessary to target physically protected areas that offer protection from galactic cosmic rays, minerals such as calcium sulfates

(gypsum, anhydrite) which can best preserve these molecules, and to stay away from the minerals that do not show good terrestrial preservation of biomolecules.

10.2 THESIS CONCLUSIONS

All of the Mars analog sites examined in this study show detectable concentrations of amino acids and organics (TOC, TON). With the superior detection limits, *Urey* may detect intact amino acids, but amine degradation products may also be sequestered in the mineral record on Mars. If they are present anywhere that was at one time similar to the environments investigated in this study, and especially if they are sequestered within a solid mineral matrix, there is a good chance that these biosignatures might persist.

A number of other suggestions can be made with respect to the search for biomolecules on Mars based on the studies conducted in this thesis. Besides confirming and corroborating previous scientific findings, a number of statements can be made regarding the future search for evidence of extinct or extant life on Mars.

- 1) Amino acids formed biologically compared to those formed abiotically differ both in distribution and chirality and can be discriminated easily through enantiomeric measurements (Chapter 2).
- 2) The preservation of amino acids in terrestrial sulfate minerals suggest that biomolecules from extinct bacterial communities should be well preserved over long geological timescales (Chapters 3-4).
- 3) Analogs to the Martian hematite blueberries show evidence of biological life within them and possibly at the time of their formation. This could be indicative of aqueous formation processes and possible biologically induced mineralization (Chapter 5).
- 4) Nutrient limited sulfate-reducing bacterial communities show extremely low metabolic rates and turnover times and represent an extremely low biodensity bacterial concentration that must be within the detection limits of instrumentation sent to Mars (Chapter 6).
- 5) Samples from the cyptoendolithic inhabited zone within Antarctic surface rocks show excellent preservation of microbial biosignatures and may be indicative of degrees of preservation on Mars over geological timescales (Chapter 7).

- 6) Atacama Desert surface samples from dry microenvironments show high levels of degradation associated with advanced diagenetic processes in extreme environments. The immediate subsurfaces in these environments seem to offer some degree of protection from the surface conditions and show detectable microbial distributions of amino acids suggesting that productive microbial communities persist despite the harsh conditions (Chapter 8).

These consideration all lead to the conclusion that some type of preservation mechanism is necessary to detect biomolecules in the Martian near-surface. This protection may be achieved by sampling in the immediate subsurface at 1-2 meters depth, or mineral matrices may be able to provide the enhanced preservation of biomolecules under these environmental conditions.

Using the racemization results from the studies conducted on San Diego county ironstones, analogs to the Martian blueberries ubiquitous in the Meridiani Planum region, some predictions may be made on the preservation of chirality over geological timescales. Extrapolations of these data to lower temperatures characteristic of Mars' surface concludes that sufficiently cold temperatures are necessary for chirality to be preserved over billions of years (Figure 10.3).

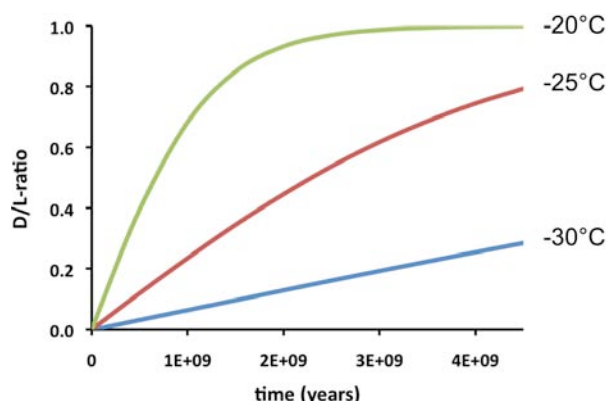


Figure 10.3 Predicted racemization rates of aspartic acid at three different temperatures characteristic of Mars' surface (-20°, -25°, -30°C). Rates derived from the ironstone matrix study (Chapter 5) extrapolated to lower temperatures.

The rates of racemization at -20°C results in a loss of amino acid chirality necessary for unequivocal evidence of biological amino acids in approximately a billion years. This limit is extended at -25° and -30°C, as a definitive biological chiral signature might be preserved for the lifetime of the planet.

If we model amino acid degradation over the geological history of Mars using the data derived previously (Chapter 3), conclusions may be made about the expected lifetimes of amino acids within Martian sulfate minerals (Figure 10.4).

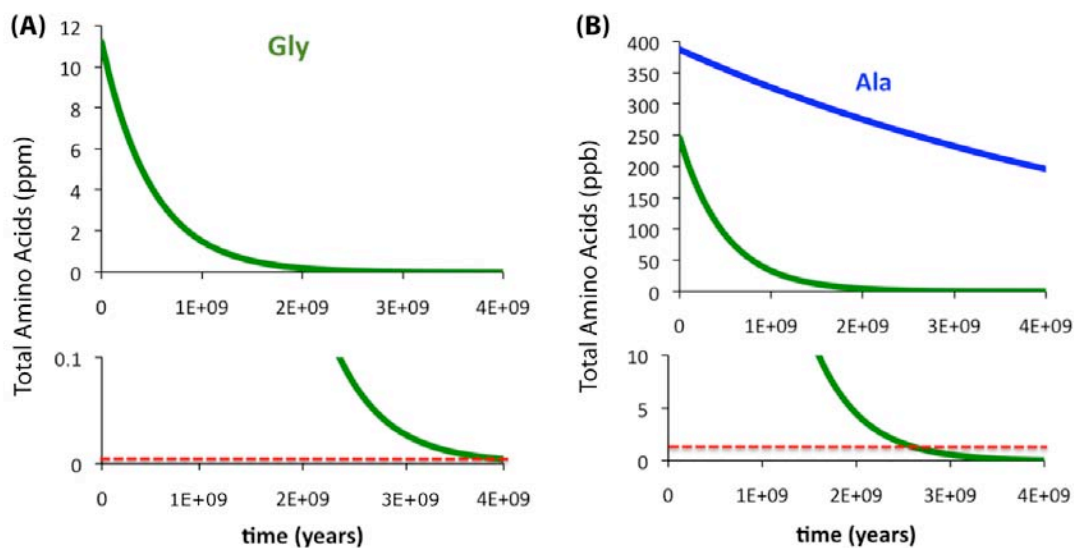


Figure 10.4 Expected lifetimes of glycine (green) and alanine (blue) within sulfate mineral matrices on Mars assuming a conservative surface temperature of 0°C and concentrations of amino acids associated with: (A) high biodiversity microbial communities (ppm levels) similar to those observed in Australian saline lake gypsum, and (B) low biodiversity communities (ppb levels) similar to those observed in the Atacama Desert soils. Rates for glycine and alanine decarboxylation are the average of those from 3 samples calculated in Chapter 3 and alanine is observed to persist much longer due to its higher stability in gypsum matrices. The red lines represent the detection limit of our laboratory methods (~1ppb).

By modeling the decarboxylation of glycine and alanine as a pseudo first-order equation based on the detection of amine degradation products allowed for the rates of decarboxylation to be derived. If it is assumed that the surface of Mars harbored extant microbial life at one time, then these rates can be used to model degradation of glycine and alanine within sulfate minerals assuming a high biodiversity microbial population such as those detected in Australian sulfate minerals (Figure 10.4A) or a low biodiversity community similar to those present in the Atacama Desert (Figure 10.4B). Assuming an average temperature of 0°C for the surface of Mars, concentrations of glycine above our laboratory detection limits are modeled to persist for ~4 billion years. If low levels of microbial life were present initially in the Martian surface, concentrations of glycine above our detection limits are shown to persist for ~2.5 billion years by

this model. The greater stability of other amino acids results in significantly greater predicted lifetimes, such as alanine (Figure 10.4B).

The instrument development portion of this thesis shows the results of ongoing optimization work regarding the extraction of organic compounds from Mars analog samples. Although current work is expanding our knowledge of SCWE and MOD extraction efficiencies as a function of mineralogy, it has been shown that:

- 1) Sub-critical water treatment is an ideal method of organic extraction from mineral matrices and is an integral part of the *Urey* instrument suite.
- 2) The coupling between the SCWE and MOD offers a coherent method of extraction and labeling of primary amine compounds for analysis by capillary electrophoresis.

Urey's primary goal of detecting organic compounds at sub-pptr sensitivity shows the promise of quantifying key organic carbon and nitrogen reservoirs that may indicate the presence of extinct or extant life. Carbonate outcrops on Mars have been strangely absent from remote detection by orbiting spacecraft, detected only within Martian dust primarily as 2-5% MgCO_3 (Bandfield et al., 2003). These may be due to the fact that early acidic oceans may have forced the liberation of carbonates as CO_2 (Fairén et al., 2004), as inadequate carbonate photochemical stability is doubtful (Quinn et al., 2006). A study of chemical weathering of Martian analog minerals provides more evidence that the present soil composition could have been produced by acidic reactions (Banin et al., 1997). A similar problem with the chemistry of the Martian regolith is that the nitrogen abundances are poorly constrained. Processes that could explain the lack of detectable nitrogen reservoirs are escape of nitrogen to space, burial within the regolith as nitrate and ammonium salts, or stabilization within phyllosilicate matrices (Mancinelli & Banin, 2003). In this respect, Clay minerals could also act to sequester amino acids by adsorption, similar to what has been observed terrestrially (Aufdenkampe et al., 2001) and is discussed previously (Chapter 8). The trace detection of organics by Urey could provide an estimate of the organic nitrogen reservoirs within the surface and subsurface regolith. Sulfate salts still remain the most widely detected on Mars, composing up to 30% of soil composition are probably present as hydrated MgSO_4 (Vaniman et al., 2004) or hydrated CaSO_4 (Langevin et al., 2005).

10.3 FINAL DISSERTATION CONCLUSIONS

During the upcoming generations of in situ rover missions to Mars, the issue of where to look for well-preserved biomolecules is just as important as the advanced instrumentation that is flown there. The success of future life detection studies flown aboard the MSL (2009), ExoMars (2013), and the AFL (2018) should have specific geological targets in mind before the analyses even begin. Because the surface of Mars is so hostile, it is necessary to target physically protected areas that offer protection from galactic cosmic rays, minerals such as calcium sulfates (gypsum, anhydrite) which can best preserve these molecules, and to stay away from the minerals that do not show good terrestrial preservation of biomolecules.

All of the Mars analog sites examined in this study show detectable concentrations of amino acids and organics (TOC, TON) by our methods, so Urey will have no trouble detecting amino acids and nucleobases compounds if they are present in similar environments and concentrations. The large reservoirs of sulfate minerals detected via remote sensing and in situ studies coupled with the predicted high stabilities of amino acids within these mineral matrices over billion year timescales make them primary targets in the search for organic compounds on Mars.

Urey has many opportunities to fly aboard future in situ Mars exploration missions (Figure 10.1) and its small size and low mass make it applicable to small payloads. Currently, Urey is included in all of the payload configurations for ExoMars 2013. When sample return missions become a reality sometime after 2020, it will be essential that the utilized sterilization methods do not affect the state of the organic matter. Ionizing radiation has been shown to degrade amino acids at high rates (Kminek & Bada, 2006), so any suggested method of gamma-irradiation (Allen et al., 1999) must be short enough so that the of amino acids is not affected.

REFERENCES

- Allen, C.C., Albert, F.G., Combie, J., Banin, A., Yablekovitch, T., Kan, I., Bodnar, R.J., Hamilton, V.E., Jolliff, B.L., Kuebler, K., Wang, A., Lindstrom, D.J., Morris, P.A., Morris, R.V., Murray, R.W., Nyquist, L.E., Simpson, P.D., Steele, A., and Symes, S.J. (1999) Effects of sterilizing doses of gamma radiation on Mars analog rocks and minerals. *Journal of Geophysical Research* 104(E11), 27,043-27,066.
- Atreya, S.K. (2007) The Mystery of Methane on Mars and Titan. *Sci. Am.* May Issue, 42-51.
- Aubrey, A.D., Chalmers, J.H., Bada, J.L., et al. (2008) The Urey Instrument: An Advanced in situ Organic and Oxidant Detector. *Astrobiology*, in press.
- Aufdenkampe, A.K., Hedges, J.I., Richey, J.E., Krusche, A.V., and Llerena, C.A. (2001) Sorptive Fractionation of Dissolved Organic Nitrogen and Amino Acids onto Fine Sediments within the Amazon Basin. *Limnology and Oceanography* 46(8), 1921-1935.
- Bandfield, J.L., Glotch, T.D., and Christensen, P.R. (2003) Spectroscopic Identification of Carbonate Minerals in the Martian Dust. *Science* 301, 1084-1087.
- Banin, A., Han, R.X., Kan, I., and Cicelsky, A. (1997) Acidic volatiles and the Mars Soil. *Journal of Geophysical Research* 102(E6), 13,341-13,356.
- Beegle, L.W., Wilson, M.G., Abilleira, G., Jorda, J.F., and Wilson, G.R. (2007) A Concept for NASA's Mars 2016 Astrobiology Field Laboratory. *Astrobiology* 7(4), 545-577.
- Benner, S.A., Devine, K.G., Matveeva, L.D., and Powell, D.H. (2000) The missing organic molecules on Mars. *PNAS* 97, 2425-2430.
- Des Marais, D.J., Allamandola, L.J., Benner, S.A., Boss, A.P., Deamer, D., Falkowski, P.G., Farmer, J.D., Blair Hedges, S., Jakosky, B.M., Knoll, A.H., Liskowsky, D.R., Meadows, V.S., Meyer, M.A., Pilcher, C.B., Nealson, K.H., Spormann, A.M., Trent, J.D., Turner, W.W., Woolf, N.J., and Yorke, H.W. (2003) The NASA Astrobiology Roadmap. *Astrobiology*. 2003, 3(2), 219-235.
- Fairén, A.G., Fernández-Remolar, D., Dohm, J.M., Baker, V.R., and Amils, R. (2004) Inhibition of carbonate synthesis in acidic oceans on early Mars. *Nature* 431, 423-426.
- Kminek, G., and Bada J.L. (2006) The effect of ionizing radiation on the preservation of amino acids on Mars. *Earth Planet. Sci. Lett.* 245, 1-5.
- Langevin, Y., Poulet, F., Bibring, J.-P., and Gondet, B. (2005) Sulfates in the North Polar region of Mars detected by OMEGA/Mars Express. *Science* 307, 1584-1586.
- Malin, M.C., and Edgett, K.E. (2000) Evidence for Recent Groundwater Seepage and Surface Runoff on Mars. *Science* 288, 2330-2335.
- Mancinelli, R.L., and Banin, A. (2003) Where is the nitrogen on Mars? *International Journal of Astrobiology* 2(3), 217-225.

Morton, O. (2007) Committee releases shortlist of Mars landing sites. *Nature* 450, 145.

Neidhardt, F.C., and Umbarger, H.E. (1996) Chemical composition of *Escherichia coli*, pp. 13-16. In F.C. Neidhardt, R. Curtiss III, J.L. Ingraham, E.C.C. Lin, K.B. Low, B. Magasanik, W.S. Reznikoff, M. Riley, M. Schaechter, and H.E. Umbarger (ed.), *Escherichia coli* and *Salmonella*: cellular and molecular biology, 2nd ed. ASM Press, Washington, D.C.

Quinn, R., Zent, A.P., and McKay, C.P. (2006) The Photochemical Stability of Carbonates on Mars. *Astrobiology* 6(4), 581-591.

Squyres, S.W., Grotzinger, J.P., Arvidson, R.E., Bell III, J.F., Calvin, W., Christensen, P.R., Blark, B.C., Crisp, J.A., Farrand, W.H., Herkenhoff, K.E., Johnson, J.R., Klingelhöfer, G., Knoll, A.H., McLennan, S.M., McSween Jr., H.Y., Morris, R.V., Rice Jr., J.W., Rieder, R., & Soderblom, L.A. (2004) In Situ Evidence for an Ancient Aqueous Environment at Meridiani Planum, Mars. *Science* 306, 1709-1714.

Vaniman, D.T., Bish, D.L., Chipera, S.J., Fialips, C.I., Carey, J.W., and Feldman, W.C. (2004) Magnesium sulphate salts and the history of water on Mars. *Nature* 431, 663-665.

APPENDIX A.
**Racemization & Degradation Heating Experiments on Southern
Australian Sulfate Samples (Chapter 4)**

HEATING EXPERIMENTS. In order to model the degradation rates of amino acids in these environments and to examine the relative effect of mineral matrix on these rates, heating experiments were conducted on a Southwestern Australia gypsum sample (1C) and jarosite sample (8). The degradation of amino acids at various temperatures, determined by analyzing heated samples compared to the unheated sample, can be used to determine the activation energies associated with amino acid degradation and racemization in different mineral matrices.

Both racemization and degradation are modeled as pseudo-1st order reactions, in agreement with previous studies (Aubrey et al., 2006). The rate constants for degradation of various amino acids were calculated for the 24, 48, and 72-hour exposures at 150°, 200°, and 250°C heating experiments in comparison to an unheated sample according to the first order integrated rate equation (Equation A.1).

$$\text{Equation A.1} \quad \ln[AA]_t - \ln[AA]_0 = -k_{DEG} \cdot t$$

It is well known that reaction rates are a function of temperature and vary according to the Arrhenius equation (Equation A.2). In this relationship, the rate constant (k) is a function of the reaction's activation energy (E_a), absolute temperature (T), and the pre-exponential factor (A).

$$\text{Equation A.2.} \quad k = A \cdot e^{\left(\frac{E_a}{R \cdot T}\right)}$$

Because the heating experiments were conducted at various temperatures, the variation of reaction rate with temperature can be determined by plotting the natural log of the rate constant, $\ln(k)$, versus the inverse absolute temperature. This gives a plot with the slope equal to $-E_a/R$ and a y-intercept equal to the natural log of the pre-exponential factor, $\ln(A)$.

Equation A.3
$$\ln(k) = \ln(A) - \frac{E_a}{R} \cdot \left(\frac{1}{T}\right)$$

Arrhenius plots using heating experiment data for amino acid degradation within gypsum and jarosite matrices are shown in Figure A.1. The rates all look to be too fast as they are ~1000x faster than previously published in situ rates of degradation. The rates of degradation for the amino acids glycine, alanine, and valine are shown compared to serine, aspartic acid, and glutamic acid. The amino acids which degrade primarily by decarboxylation are ~10 times as fast as the amino acids with other degradation pathways.

The activation energies for decarboxylation are a factor of 3 higher than the decarboxylation activation energies previously determined empirically (Li & Brill, 2003).

Table A.1 Calculated activation energies and Arrhenius pre-exponential factors for amino acid degradation within gypsum and jarosite.

		GYPSUM			JAROSITE		
	Species	E _a (kJ/mole)	ln(A) (yr ⁻¹)	k _{DEG(25°C)} (yr ⁻¹)	E _a (kJ/mole)	ln(A) (yr ⁻¹)	k _{DEG(25°C)} (yr ⁻¹)
DC	Gly	28.1	12.7	3.9	41.5	15.1	0.194
	Ala	39.9	15.2	0.42	47.2	16.9	0.116
	Val	26.3	11.5	2.4	25.3	10.7	1.57
DA	Asp	37.9	14.7	0.58	55.2	18.9	0.038
DH	Glu	29.1	12.5	2.2	52.0	18.1	0.060
	Ser	49.3	18.4	0.23	64.4	21.8	0.015

DC = decarboxylation.

DA = deamination.

DH = dehydration.

*slope (-E_a/R) multiplied by 8.314 J·K⁻¹·mol⁻¹ to find value of E_a.

The amino acid degradation rates determined through heating experiments are unrealistically fast and probably do not approximate the natural in situ rates of decomposition. These rates are 100-10,000x similar published values and represent the limits of high-temperature heating experiment extrapolation. The relative order of amino acid racemization rates observed in gypsum are gly > val ~ glu > asp ~ ala > ser while the order observed in jarosite is val > gly ~ ala > glu > asp > ser. These trends agree with the decarboxylation order from various papers (Li & Brill, 2003) for the gypsum matrix although the jarosite matrix shows much more variability.

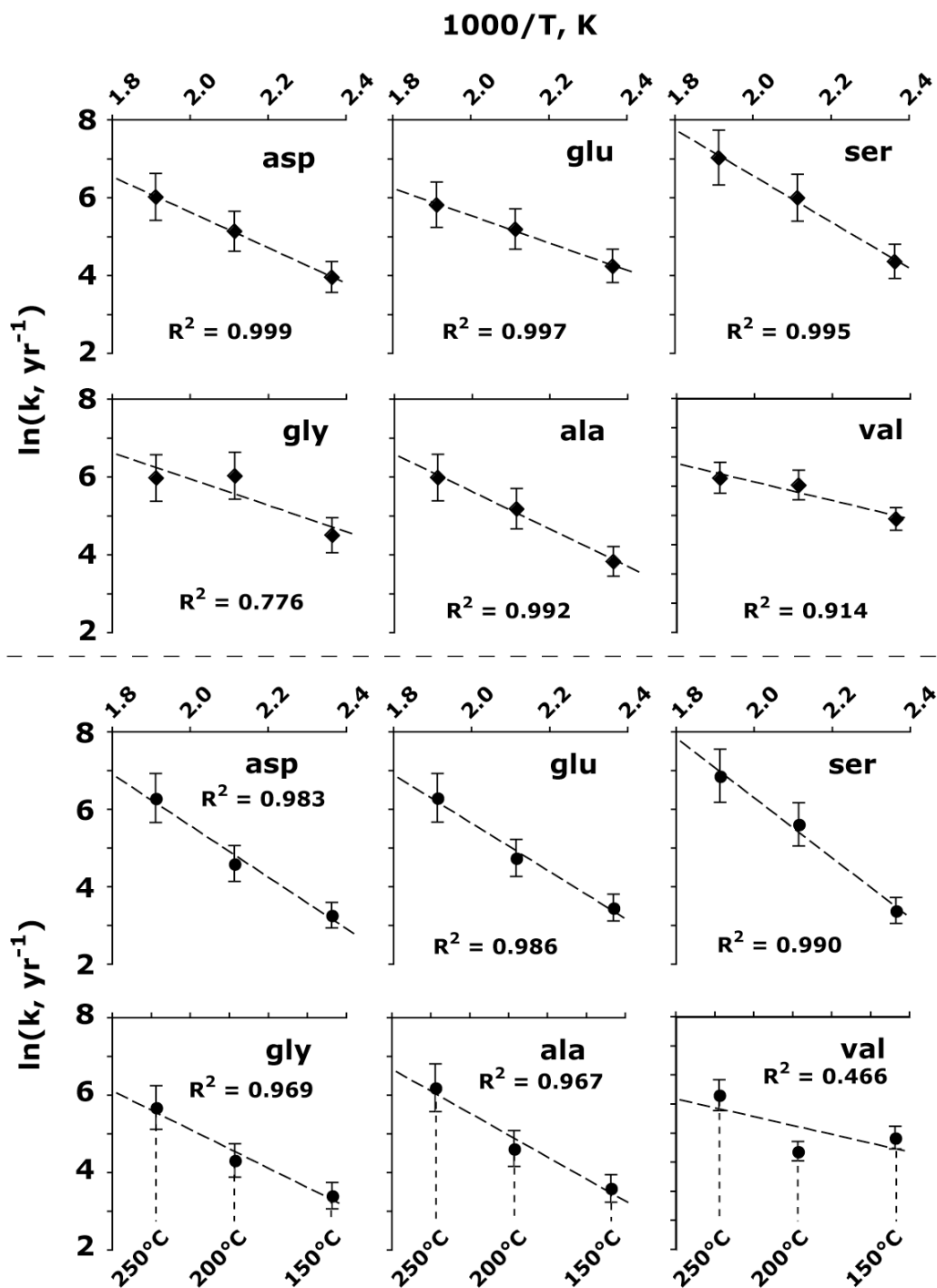


Figure A.1 Pseudo-1st order Arrhenius plots of degradation reactions for total (Σ AA) and individual amino acids (asp, glu, ser, ala) from 72-hour heating experiments at 150°, 200°, and 250°C for a shallow water bottom growth gypsum sample from Aerodrome Lake (◆) and for a jarosite-rich groundwater-precipitated red jarosite sediment from Lake Tyrrell (●). The activation energies (E_a) and Arrhenius coefficients ($\ln A$) are shown below the plots for each amino acids along with extrapolated degradation rates at 25°C ($k_{\text{DEG},25^\circ\text{C}}$).

Determinations of amino acid racemization rate constants are a little more difficult to calculate and vary according to a slightly more difficult relationship (Equation 4).

$$\text{Equation A.4} \quad \ln\left(\frac{1+D/L}{1-D/L}\right) - \ln\left(\frac{1+D/L}{1-D/L}\right)_{t=0} = 2 \cdot k_{RAC} \cdot t$$

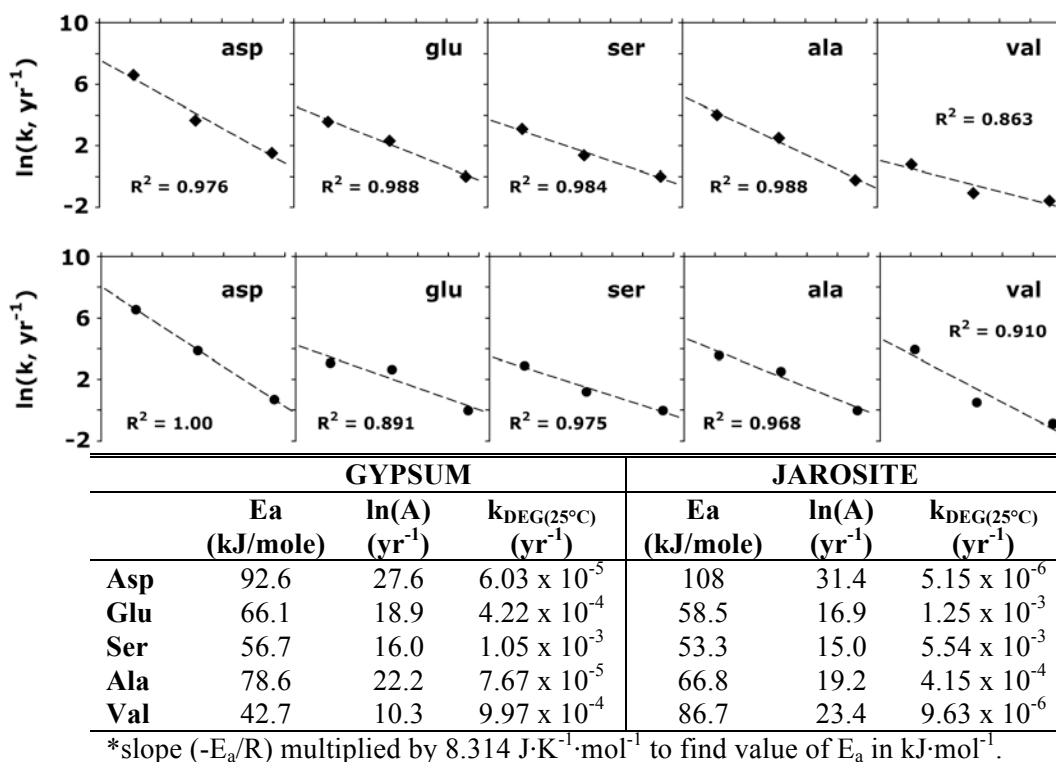


Figure A.2 Pseudo-1st order Arrhenius plots of amino acid racemization (asp, glu, ser, ala, val) from 72-hour heating experiments at 150°, 200°, and 250°C for a shallow water bottom growth gypsum sample from Aerodrome Lake (◆) and for a jarosite-rich groundwater-precipitated red jarosite sediment from Lake Tyrrell (●). The activation energies (E_a) and Arrhenius coefficients (ln A) are shown below the plots for each amino acid along with extrapolated racemization rates at 25°C (k_{RAC,25°C}).

The rates of racemization are more reasonable than the values for amino acid degradation (Figure A.2). Typical amino acid dating mechanisms using biologically derived amino acids assume that a bacterial community died coincidentally and that racemization was occurring since that time. This is a good estimation in many cases, however, it cannot be assumed to be true of these modern samples. The heating experiments show a marked difference in the amino acid degradation and racemization rate data (Figure A.3).

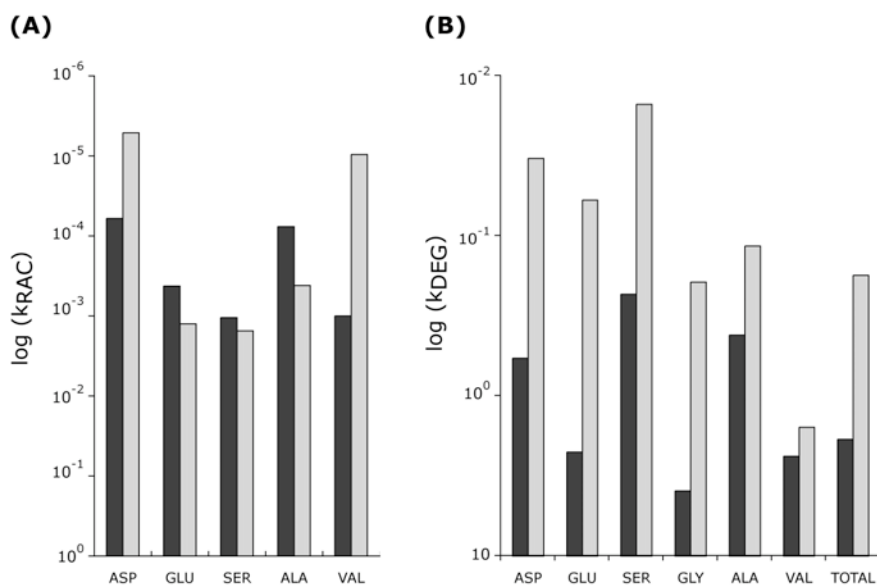


Figure A.3 Plots of Amino acid racemization (A) and degradation (B) rates determined through heating experiments for various amino acids plotted for gypsum (dark gray) and jarosite samples (light gray). Rate data at 25°C are plotted to compare the rates of degradation and racemization.

Using known amino acid degradation rates (glycine or alanine), it would be possible to calculate an approximate age of the gypsum and jarosite samples based on the presence of amine degradation products compared to the total concentrations of their parent amino acids. However, the degradation rates calculated from the heating experiments show evidence of high-temperature catalysis within the gypsum and jarosite matrices in all cases which prohibits their accurate extrapolation to lower temperatures. Alanine shows accelerated decarboxylation rates at 25°C ($\sim 10^{-1} \text{ yr}^{-1}$) and activation energies much too low ($\sim 45 \text{ kJ/mole}$) without a catalyst. Glycine likewise shows rates that are much too fast ($> 10^{-1} \text{ yr}^{-1}$) and low activation energies (20-40 kJ/mole).

REFERENCES

Aubrey, A., Cleaves, H.J., Chalmers, J.H., Skelley, A.M., Mathies, R.A., Grunthaner, F.J., Ehrenfreund, P., & Bada, J.L. (2006) Sulfate minerals and organic compounds on Mars. *Geology* 34, 357-360.

Li, J., and Brill, T.B. (2003) Spectroscopy of hydrothermal reactions, part 26: Kinetics of decarboxylation of aliphatic amino acids and comparison with the rates of racemization. *Int. J., Chem. Kinet.* 35(11), 602-610.

APPENDIX B.

Racemization & Degradation Heating Experiments on San Diego County Ironstone Samples (Chapter 5)

HEATING EXPERIMENTS. In order to estimate the stabilities of amino acids within the ironstone matrices, bulk ironstone and powdered ironstone core samples from Sunset Cliffs, San Diego, were heated for 24, 48, and 72 hours over a temperature series at 150°, 200°, and 250°C. The rates of racemization and degradation in bulk and inner core samples were determined along with pre-exponential factors (A) and activation energies (kcal/mole) for each reaction. These degradation rates should be evaluated carefully as they may not adequately represent degradation of the amino acids in nature (Williams & Smith, 1977) and may not accurately be extrapolated to lower temperatures. However, they should be evaluated based on relative rates between amino acids and compared to values determined for other host matrices.

The ages of the amino acids within the ironstones can be determined based on racemization kinetics. This can be interpreted as an age since the microbial communities have become extinct and the major assumption of racemization age dating are that a microbial community existed coincidentally in the past. There are two different methods of determining the racemization kinetics of amino acids within an ironstone matrix. The first of these is through heating experiments carried out on the ironstone samples and the second is a calibration method (Chapter 6).

Both racemization and degradation are modeled as pseudo-1st order reactions, in agreement with previous studies (Bada, 1991; Aubrey et al., 2006). The rate constants for degradation of various amino acids were calculated for the 24, 48, and 72-hour exposures at 150°, 200°, and 250°C heating experiments in comparison to an unheated sample according to the first order integrated rate equation (Equation B.1).

$$\text{Equation B.1} \quad \ln[AA]_t - \ln[AA]_0 = -k_{DEG} \cdot t$$

It is well known that reaction rates are temperature dependent and vary according to the Arrhenius equation (Equation B.2). In this relationship, the rate constant (k) is a function of the reaction's activation energy (E_a), absolute temperature (T), and the pre-exponential factor (A).

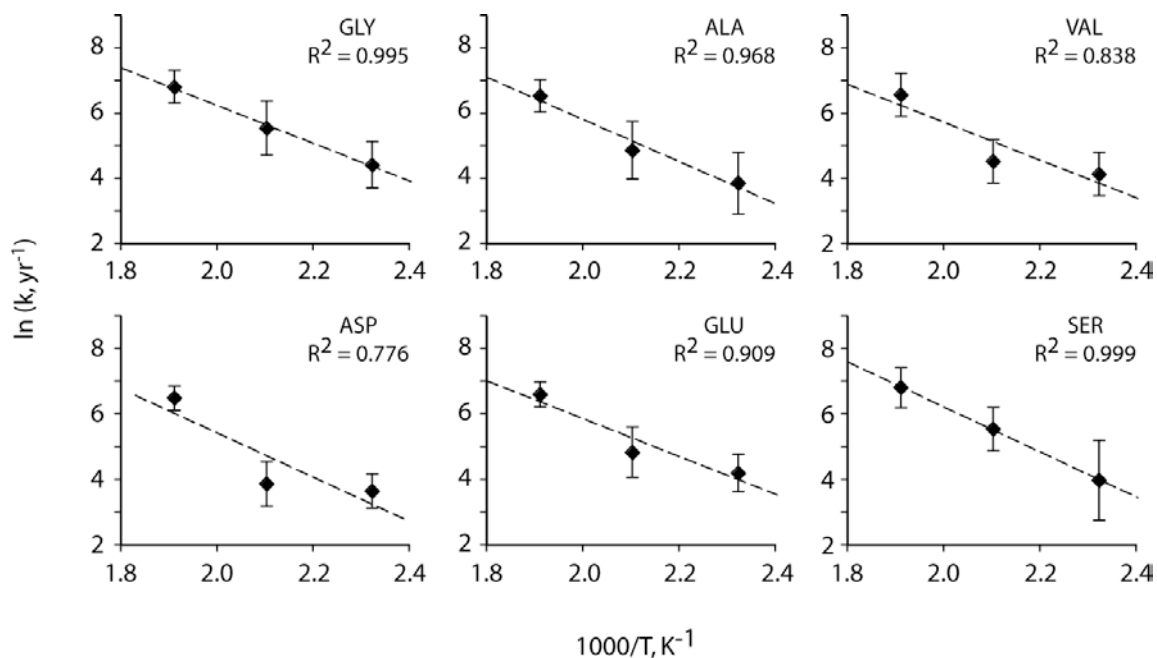
Equation B.2
$$k = A \cdot e^{\left(\frac{E_a}{R \cdot T}\right)}$$

Because the heating experiments were conducted at various temperatures, the variation of reaction rate with temperature can be determined by plotting the natural log of the rate constant, $\ln(k)$, versus the inverse absolute temperature (1000/K). This gives a plot with the slope equal to $-E_a/R$ and a y-intercept equal to the natural log of the pre-exponential factor (Equation B.3).

Equation B.3
$$\ln(k) = \ln(A) - \frac{E_a}{R} \cdot \left(\frac{1}{T}\right)$$

Arrhenius plots for amino acid degradation for a heated bulk ironstone sample (SCL-03) show linear trends with good correlation to the data (Figure B.1).

The relative order of the amino acids that degrade primarily by decarboxylation are the same as those reported previously where glycine > valine > alanine (Li & Brill, 2003). However, these rates of amino acid degradation are probably much too fast to adequately represent the in situ rates of degradation. The activation energies for amino acid decarboxylation derived in this study (~50 kcal/mole), are approximately half those reported in recent literature (Li & Brill, 2003), indicating that these rates calculated from high-temperature heating experiments are not indicative of the in situ rates at lower temperatures. This may be explained by complicated high-temperature chemistry, especially in the presence of high iron concentrations. These rates are even faster than aqueous rates of decarboxylation, similar to those reported previously (Bada, 1991). The most stable amino acid in these heating experiments is aspartic acid which shows degradation rates approximately one order of magnitude slower than glycine.



Primary Mechanism	Amino Acid	$-E_a/R$ (slope)	E_a (kJ/mole)	$\ln(A)$ (yr^{-1})	$k_{\text{DEG}(25^\circ\text{C})}$ (yr^{-1})
Decarboxylation	Gly	-5.78	48.1	17.8	0.204
	Ala	-6.46	53.7	18.7	0.052
	Val	-5.80	48.2	17.3	0.116
Deamination	Asp	-6.75	56.1	18.9	0.024
Dehydration	Glu	-5.77	48.0	17.4	0.142
	Ser	-6.88	57.2	20.0	0.046

*slope ($-E_a/R$) multiplied by $8.314 \text{ J}\cdot\text{K}^{-1}\cdot\text{mol}^{-1}$ to find value of E_a .

Figure B.1 Pseudo 1st-order Arrhenius plots for amino acid degradation obtained through heating experiments at 150°, 200°, and 250°C for 24, 48, and 72-hour exposure on powdered Sunset Cliffs bulk ironstones and degradation rate extrapolations to 25°C. Each point represents the average of at least 3 samples except for the low temperature (150°C) 24-hour degradation for aspartic and glutamic acids, and valine trends represent an average of 2 points. Error bars represent ± 1 standard deviation ($\pm\sigma$). All samples were blank corrected and normalized to D-norleucine internal standard recoveries. The powdered ironstone core sample showed approximately the same amino acid degradation kinetics.

Determination of amino acid racemization rate constants are a little more difficult to calculate and vary according to a slightly more difficult relationship (Equation B.4).

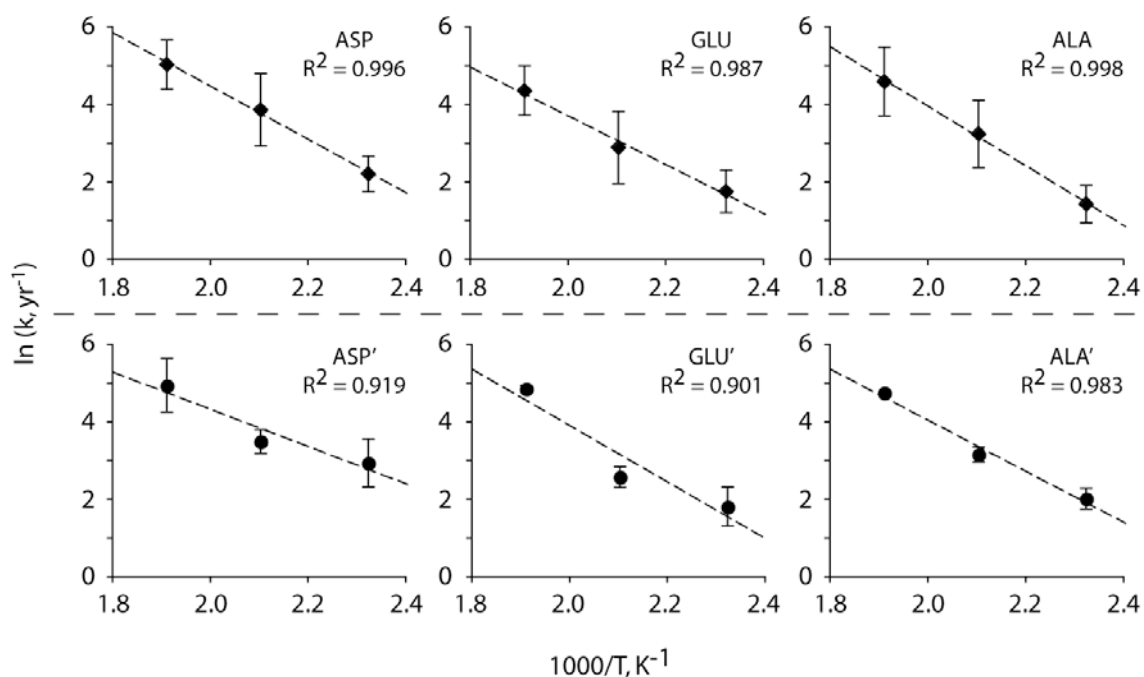
$$\text{Equation B.4} \quad \ln\left(\frac{1 + D/L}{1 - D/L}\right) - \ln\left(\frac{1 + D/L}{1 - D/L}\right)_{t=0} = 2 \cdot k_{RAC} \cdot t$$

Using the enantiomeric ratios and assuming that $D/L=0$ at time zero, Equation 4 simplifies to Equation B.5:

$$\text{Equation B.5} \quad \ln\left(\frac{1 + D/L}{1 - D/L}\right) = 2 \cdot k_{RAC} \cdot t$$

The Arrhenius plots for amino acid racemization can yield values for activation energies and pre-exponential factors (A) for each amino acid for the bulk and core fractions (Figure B.2).

The calculated racemization rates from the heating experiments show fairly good agreement for glutamic acid and alanine, however aspartic acid shows high variability between the bulk and core samples from Sunset Cliffs, differing by approximately one order of magnitude. The fact that these rates are higher than the majority of published racemization rates indicates that the heating experiments do not scale linearly to the in situ racemization rates at ambient temperature ($\sim 25^\circ\text{C}$). The activation energies for these racemization reactions, however, are significantly lower than previously published numbers (31.2 kcal/mole; Bada & Schroeder, 1972), indicating that high temperatures act as a catalyst and prohibit accurate extrapolation to lower temperatures.



Fraction		$-E_a/R^*$	E_a (kJ/mol)	$\ln(A)$ (yr^{-1})	$k_{\text{RAC}(25^\circ\text{C})}$ (yr^{-1})
Ironstone – Bulk	Asp	-6.86	57.0	18.2	8.2×10^{-3}
	Glu	-6.29	52.3	16.3	8.3×10^{-3}
	Ala	-7.69	63.9	19.3	1.5×10^{-3}
Ironstone – Core	Asp	-4.81	39.9	14.0	1.2×10^{-1}
	Glu	-7.29	60.6	18.5	2.6×10^{-3}
	Ala	-6.58	54.7	17.3	8.4×10^{-3}

*slope ($-E_a/R$) multiplied by $8.314 \text{ J}\cdot\text{K}^{-1}\cdot\text{mol}^{-1}$ to find value of E_a .

Figure B.2 Pseudo 1st-order Arrhenius plots for amino acid racemization obtained through heating experiments at 150°, 200°, and 250°C for 24, 48, and 72-hour exposure on powdered Sunset Cliffs bulk ironstones and racemization rate extrapolations to 25°C. Each point represents the average of at least 3 samples and error bars represent ± 1 standard deviation ($\pm\sigma$). All samples were blank corrected and normalized to D-norleucine internal standard recoveries. The kinetics for serine racemization were omitted because of inadequate separation of enantiomers and L-valine coeluted with trace amounts of residual ammonia carried through the desalting stage.

The fast kinetics of racemization and degradation may be explained by metallic ion catalysis which may show elevated rates at high temperatures and prohibit accurate extrapolation to low temperature diagenesis. However, these kinetics are anything but simple and show the effects of a mixed mineral matrix on degradation rates which are seen to be significant in high-temperature degradation and may also be significant over geological timescales. It is interesting to note that the unreasonably fast racemization ($\sim 10^{-3} \text{ yr}^{-1}$) and degradation ($\sim 10^{-2} \text{ yr}^{-1}$) rates at 25°C both correspond to lower activation energies for these reactions compared to what has previously been observed in similar geological samples. This may also be explained by reactions on aged proteins which have undergone advanced diagenesis to humic acid or kerogen-like substances (elevated TOC/TON ratios ~ 9), therefore yielding racemization constants not indicative of the rate of amino acid racemization over the history of the sample.

Even if it is assumed that the racemization rates over geologic time are equivalent to the slowest rates determined from the heating experiments, a D/L-aspartic acid ratio of ~ 0.3 would be equivalent to ironstones only ~ 40 years old if the average temperature of exposure was 25°C and a starting D/L ratio of zero. It is impossible that the ironstones were formed this recently because the ironstones are highly matured geological formations and the host paleosol horizon was buried deep within the sedimentary cliffs. Also, it is unlikely that these ironstones were formed in the present climatic regime (Abbott, 1981) as it is predicted that unique environmental conditions in the past led to the formation of these ironstones. Caveats associated with extrapolation of heating studies to the racemization of amino acids in geological samples have been published before (Collins et al., 1999; Wehmiller et al., 1977). Therefore, we need to use another method to estimate the rates of racemization within these geological samples.

REFERENCES

- Abbott, P.L. (1981) Cenozoic Paleosols San Diego Area, California. *Catena* 8, 223-237.
- Aubrey, A., Cleaves, H.J., Chalmers, J.H., Skelley, A.M., Mathies, R.A., Grunthaner, F.J., Ehrenfreund, P., & Bada, J.L. (2006) Sulfate minerals and organic compounds on Mars. *Geology* 34, 357-360.
- Bada, J.L. (1991) Amino acid cosmogeochemistry. *Phil. Trans. R. Soc. Lond. B* 333, 349-358.
- Bada, J.L., and Schroeder, R.A. (1972) Racemization of Isoleucine in Calcareous Marine Sediments: Kinetics and Mechanism. *EPSL* 15, 1-11.
- Collins, M.J., Waite, E.R., and van Duin, A.C.T. (1999) Predicting protein decomposition: the case of aspartic-acid racemization kinetics. *Phil. Trans. R. Soc. Lond. B* 354, 51-64.
- Li, J., and Brill, T.B. (2003) Spectroscopy of Hydrothermal Reactions, Part 26: Kinetics of Decarboxylation of Aliphatic Amino Acids and Comparison with the Rates of Racemization. *Int. J. Chem. Kinetics* 35(11), 602-610.
- Wehmiller, J.F. (1977) Amino Acid Studies of the Del Mar, California, Midden Site: Apparent Rate Constants, Ground Temperature Models, and Chronological Implications. *EPSL* 37, 184-196.
- Williams, K.M., and Smith, G.G. (1977) A critical evaluation of the application of amino acid racemization to geochronology and geothermometry. *Orig. Life Evol. Biosph.* 8, 91-144.